Reports of the Department of Geodetic Science and Surveying

Report No. 377

Radial Orbit Error Reduction and Sea Surface Topography Determination Using Satellite Altimetry

by

Theodossios Engelis

Prepared for

National Aeronautics and Space Administration
Goddard Space Flight Center
Greenbelt, Maryland 20770

NASA Grant No. NAG5-519
OSURF Project 717044

The Ohio State University
Department of Geodetic Science and Surveying
1958 Neil Avenue
Columbus, Ohio 43210-1247

June 1987

Reports of the Department of Geodetic Science and Surveying

Report No. 377

Radial Orbit Error Reduction and Sea Surface Topography Determination Using Satellite Altimetry

by

Theodossios Engelis

Prepared for

National Aeronautics and Space Administration
Goddard Space Flight Center
Greenbelt, Maryland 20770

NASA Grant No. NAG5-519
OSURF Project 717044

The Ohio State University
Department of Geodetic Science and Surveying
1958 Neil Avenue
Columbus, Ohio 43210-1247

June 1987

ABSTRACT

A method is presented in satellite altimetry that attempts to simultaneously determine the geoid and sea surface topography with minimum wavelengths of about 500 km and to reduce the radial orbit errors caused by geopotential errors.

The modeling of the radial orbit error is made using the linearized Lagrangian perturbation theory. Secular and second order effects are also included. After a rather extensive validation of the linearized equations, alternative expressions of the radial orbit error are derived. A Fourier series formulation allows for easier computations, examination of the frequency content of the error and computation of different statistics. A geographic representation with respect to geocentric latitude and longitude gives a significantly better insight on the spatial variations of the error. Similar expressions are derived for the geoid undulation error and sea surface topography. Numerical estimates for the radial orbit error and geoid undulation error are computed using the differences of two geopotential models as potential coefficient errors, for a Seasat orbit.

To provide statistical estimates of the radial distances and the geoid, a covariance propagation is made based on the full geopotential covariance. Accuracy estimates for the Seasat orbits are given which agree quite well with already published results.

Observation equations are developed using sea surface heights and crossover discrepancies as observables. A minimum variance solution with prior information provides estimates of parameters representing the sea surface topography and corrections to the gravity field that is used for the orbit generation. The potential of the method is demonstrated in a solution where simulated geopotential errors and the Levitus sea surface topography are used to generate the observables for a three day Seasat arc. The simulation results show that the method can be used to effectively reduce the radial orbit error and recover the sea surface topography.

FOREWORD

This report was prepared by Mr. Theodossios Engelis, Graduate Research Associate, Department of Geodetic Science and Surveying, under the supervision of Professor Richard H. Rapp. This study was supported by NASA Grant NAG5-519, The Ohio State University Research Foundation Project No. 717044. This report constitutes the final report of the grant. This grant was administered by the NASA Goddard Space Flight Center, Greenbelt Maryland 20771. The NASA Technical Officer for this grant is Mr. James Marsh, Code 621. Substantial computer support was provided by the Instruction and Research Computer Center.

A slightly modified version of this report was submitted to the Graduate School of The Ohio State University in partial fulfillment of the requirements for the Degree Doctor of Philosophy.

The reproduction and distribution of this report was carried out with funds supplied, in part, by the Department of Geodetic Science and Surveying.

ACKNOWLEDGMENTS

I express my sincere appreciation to my adviser Richard H. Rapp for his guidance, help and support throughout this research work. Working with him during my long student years has been one of the most educating experiences. To him and to Professors Ivan I. Mueller and Clyde C. Goad I am most indebted for their constructive criticism on my work and their suggestions and comments.

Special thanks go to Mr. James Marsh and Mr. Frank Lerch of NASA/Goddard Space Flight Center, to Dr. Demos Christodoulidis of JPL and to Mr. Steve Klosko, Dr. Erricos Pavlis and Dr. Oscar Colombo of EG&G Washington Analytical Services Center, Inc. for their suggestions during discussions and for providing me with all the necessary data sets.

During my studies at The Ohio State University I have had the luck of meeting a number of people around the world. Their friendship interaction and constructive criticism have helped me improve my scientific knowledge and make my stay more enjoyable. Special thanks go to the "Greek delegation" and particularly to Dr. Kostas Katsambalos and Dr. Erricos Pavlis for helping me during the initial and most difficult period of my studies and to Mr. Nikolaos Pavlis for his contribution in clarifying some issues on a variety of topics. Dr. Petros Patias and his family will always be remembered for their friendship.

Last but not least, I am indebted to Mrs. Linda Lentz and to Ms. Tracy Runyon for their excellent typing of this lengthy manuscript and their patience and willingness in making the many corrections that I felt were necessary to bring it to the present form.

TABLE OF CONTENTS

ABSTRACT		ii
FOREWORD		iii
ACKNOWLEDGMENTS		iv
LIST OF TABLES		vii
LIST OF FIGURES		ix
1.	INTRODUCTION	1
2.	DESCRIPTION AND APPLICATIONS OF SATELLITE ALTIMETRY	5
	2.1 Introduction	5
	2.2 Satellite Altimetry	6
	2.3 Existing Solutions of the Combined Altimeter Problem	11
3.	FORMULATION OF THE SOLUTION	14
	3.1 Introduction	14
	3.2 Mathematical Model	14
4.	ANALYSIS OF RADIAL ORBIT ERRORS	19
	4.1 The Satellite Orbit	19
	4.2 Equations of Motion	20
	4.3 The Disturbing Function	22
	4.3.1 Inclination and Eccentricity Functions	24
	4.4 The Radial Orbit Error	25
	4.5 The Radial Orbit Error of Gravitational Origin	27
	4.5.1 Linearized Equations of Motion	27
	4.5.2 The Reference Orbit	28
	4.5.3 First Order Radial Orbit Error	32
	4.5.4 Resonant Effects	36
	4.5.5 Second Order Radial Orbit Error	40
	4.6 The Radial Orbit Error Due to Initial State Vector Error	42
	4.7 Validation of the Theory for Errors of Gravitational Origin	43
5.	ALTERNATIVE EXPRESSIONS OF THE RADIAL ORBIT ERROR	53
	5.1 Introduction	53
	5.2 Fourier Series Formulation	54

5.2.1 Determination of the Fourier Frequencies 54
5.2.2 Determination of the Fourier Coefficients 56
5.2.3 Numerical Results 62
5.3 Approximate Expressions of the Radial Orbit Error for a Near Circular Orbit 69
5.4 Geographic Representation of the Radial Orbit Error 73
5.4.1 First Order Periodic Radial Orbit Error 74
5.4.2 Resonant, Second Order and Initial State Vector Induced Error 81
5.4.3 Observability of the Radial Orbit Error from Crossover Discrepancies 85

6. ANALYSIS OF GEOID UNDULATION ERRORS AND STATIONARY SST 89

7. COVARIANCE ESTIMATION OF RADIAL DISTANCES AND GEOID UNDULATIONS BASED ON A GEOPOTENTIAL COVARIANCE 98

7.1 Introduction 98
7.2 Covariance Propagation Using the Fourier Series Approach 99
7.3 Covariance Propagation Using the Geographic Representation 112

8. IMPROVEMENT OF THE ORBIT AND DETERMINATION OF STATIONARY SST 122

8.1 Introduction 122
8.2 Problems Involved in the Estimation 122
8.3 Conditioning of the System and Solution 123
8.4 A Simulated Solution 126

9. CONCLUSIONS, RECOMMENDATIONS 144

LIST OF REFERENCES 149

APPENDICES

A. Satellite State Vector Transformations 154
B. Perturbations Due to J_2 158
C. Computation of Second Order Radial Orbit Error 164
D. Multiple Angle to Single Angle Trigonometric Transformation 170
E. Determination of Crossover Intersections 173

LIST OF TABLES

TABLE		PAGE
1.	Initial State Vector Used for the GEM10B and GEM9 Numerically Integrated Orbits	44
2.	Mean Elements and Rates Computed by Numerical Averaging and Analytical Methods	45
3.	Combinations between ℓ,p,q that Generate a Frequency k.	55
4.	Phases for p,q from Table 3 that Generate a Frequency k	57
5.	Constant, 1 cy/rev and Total RMS Radial Orbit Error for Seasat Arcs Using the GEM10B - GRIM3L1 Half Differences as Potential Coefficient Errors	65
6.	RMS of Seasat Radial Orbit Error for each Coefficient Degree and Order Using the GEM10B - GRIM3L1 Half Differences as Potential Coeficient Errors. Units are in Centimeters	68
7.	RMS Geoid Undulation Omission Errors for a Gravity Field up to ℓ_{max} = 36 as Computed from the OSU86F Field and its Standard Deviations up to ℓ_{max} = 180	96
8.	Variance Components of Fourier Coefficients of Seasat Radial Distances Based on the Scaled PGSS4 Covariance	106
9.	Constant, 1 cy/rev and Total RMS Radial Distance Standard Deviations for all Seasat Arcs Based on the Scaled PGSS4 Covariance	107
10.	RMS of Seasat Radial Distance Standard Deviations for each Coefficient Degree and Order Based on the Scaled PGSS4 Covariance. Units are in Centimeters	110
11.	RMS Magnitudes and Percentage Discrepancies by Degree Using the Scaled PGSS4 Covariance	128
12.	RMS Magnitudes and Percentage Discrepancies by Order Using the Scaled PGSS4 Covariance	128

TABLE PAGE

13. RMS True Magnitudes and Discrepancies Using the Scaled PGSS4 Covariance 129

14. RMS True Magnitudes and Discrepancies Using the Unscaled PGSS4 Covariance 130

LIST OF FIGURES

FIGURES		PAGE
1.	Semimajor Axis Error Computed by Differencing Two Numerically Integrated Orbits Based on GEM9 and GEM10B to Harmonic Degree 10.	47
2.	Amplitude Spectrum of Semimajor Axis Error.	47
3.	Error in the Non Singular Variable au Computed by Differencing Two Numerically Integrated Orbits Based on GEM9 and GEM10B up to Harmonic Degree 10.	48
4.	Amplitude Spectrum of the Error in the Non Singular Variable au.	48
5.	Radial Orbit Error Computed by Differencing Two Numerically Integrated Orbits Based on GEM9 and GEM10B up to Harmonic Degree 10.	49
6.	Amplitude Spectrum of Radial Orbit Error.	49
7.	Discrepancies in the Computation of the Semimajor Axis Error Using the Numerical and Analytical Methods.	50
8.	Amplitude Spectrum of the Discrepancies in the Computation of the Semimajor Axis Error.	50
9.	Discrepancies in the Computation of the Radial Orbit Error Using the Numerical and Analytical Methods.	51
10.	Amplitude Spectrum of the Discrepancies in the Computation of the Radial Orbit Error.	51
11.	Discrepancies in the Computation of the Radial Orbit Error After Additional Empirical Correction Has Been Applied.	52
12.	Amplitude Spectrum of the Discrepancies in the Computation of the Radial Orbit Error After Additional Empirical Correction has been Applied.	52
13.	Seasat Radial Orbit Error Computed Analytically Using the GEM10B - GRIM3L1 Half Differences as Potential Coefficient Errors.	63

14. Amplitude Spectrum of Seasat Radial Orbit Error Using the GEM10B - GRIM3L1 Half Differences as Potential Coefficient Errors 64

15. Amplitude Spectrum of Seasat Radial Orbit Error Using a Uniform Potential Coefficient Error of $5 \cdot 10^{-9}$. 64

16. RMS Seasat Radial Orbit Error by Harmonic Order Using the GEM10B-GRIM3L1 Half Differences as Potential Coefficient Errors. 66

17. RMS Seasat Radial Orbit Error by Harmonic Order Using a Uniform Potential Coefficient Error of $5 \cdot 10^{-9}$. 66

18. RMS Seasat Radial Orbit Error by Harmonic Degree Using the GEM10B-GRIM3L1 Half Differences as Potential Coefficient Errors. 67

19. RMS Seasat Radial Orbit Error by Harmonic Degree Using a Uniform Potential coefficient Error of $5 \cdot 10^{-9}$. 67

20. Radial Orbit Error of Ascending Seasat Arcs Using the GEM10B-GRIM3L1 Half Differences as Potential Coefficient Errors. C.I. = 50 cm. 82

21. Radial Orbit Error of Descending Seasat Arcs Using the GEM10B-GRIM3L1 Half Differences as Potential Coefficient Errors. C.I. = 50 cm. 82

22. Mean Radial Error of a Seasat Arc Using the GEM10B-GRIM3L1 Half Differences as Potential Coefficient Errors. C.I. = 50 cm. 87

23. Variable Radial Error of a Seasat Arc Using the GEM10B-GRIM3L1 Half Differences as Potential Coefficient Errors. C.I. = 50 cm. 87

24. Along Track Geoid Undulation Error Using the GEM10B - GRIM3L1 Half Differences as Potential Coefficient Errors. 94

25. Amplitude Spectrum of Geoid Undulation Error Using the GEM10B - GRIM3L1 Half Differences as Potential Coefficient Errors. 94

26. RMS Geoid Undulation Error by Harmonic Degree and Cumulative, Using the GEM10B - GRIM3L1 Half Differences as Potential Coefficient Errors. 95

27. RMS Geoid Undulation Error by Harmonic Order Using the GEM10B - GRIM3L1 Half Differences as Potential Coefficient Errors. 95

28. Spectrum of Seasat Radial Distance Standard Deviations Based on the Scaled PGSS4 Covariance. 106

29. RMS of Seasat Radial Distance Standard Deviations by Harmonic Degree Based on the Scaled PGSS4 Covariance. 109

30. RMS of Seasat Radial Distance Standard Deviations by Harmonic Order Based on the Scaled PGSS4 Covariance. 109

31. Seasat Radial Distance Standard Deviations Based on the Scaled PGSS4 Covariance. 111

32. Error Correlations Between Seasat Radial Distances Based on the Scaled PGSS4 Covariance. 111

33. Spectrum of Geoid Undulation Standard Deviations Based on the Scaled PGSS4 Covariance. 113

34. Spectrum of Residual Sea Surface Standard Deviations Based on the Scaled PGSS4 Covariance. 113

35. Standard Deviations of Radial Distances of Seasat Ascending Arcs Based on the Scaled PGSS4 Covariance to Harmonic Degree 20. C.I. = 10 cm. 119

36. Standard Deviations of Radial Distances of Seasat Descending Arcs. Based on the Scaled PGSS4 Covariance to Harmonic Degree 20. C.I. = 10 cm. 120

37. Standard Deviations Reflecting the Geographic Mean Error of Seasat Arcs Based on the Scaled PGSS4 Covariance to Harmonic Degree 20. C.I. = 10 cm. 120

38. Standard Deviations Reflecting the Geographic Variable Error of Radial Distances of Seasat Arcs Based on the Scaled PGSS4 Covariance to Harmonic Degree 20. C.I. = 10 cm. 121

39. Geoid Undulation Standard Deviations Based on the Scaled PGSS4 Covariance to Harmonic Degree 20. C.I. = 10 cm. 121

40. A Priori Radial Error of Seasat Ascending Arcs Based on Simulated Potential Coefficient Errors to Harmonic Degree 10. C.I. = 20 cm. 133

41. A Posteriori Radial Error of Seasat Ascending Arcs Based on the Discrepancies Between Simulated and Recovered Potential Coefficient Errors to Harmonic Degree 10. C.I. = 2 cm. 133

42. A Priori Standard Deviations of Radial Distances of Seasat Ascending Arcs Based on the Scaled PGSS4 Covariance to Harmonic Degree 10 . C.I. = 20 cm. 134

43. A Posteriori Standard Deviations of Radial Distances of Seasat Ascending Arcs Based on the Estimated Geopotential Covariance to Harmonic Degree 10. C.I. = 2 cm. 134

44. A Priori Radial Error of Seasat Descending Arcs Based on Simulated Potential Coefficient Errors to Harmonic Degree 10. C.I. = 20 cm. 135

45. A Posteriori Radial Error of Seasat Descending Arcs Based on the Discrepancies Between Simulated and Recovered Potential Coefficient Errors to Harmonic Degree 10. C.I. = 2 cm. 135

46. A Priori Standard Deviations of Radial Distances of Seasat Descending Arcs Based on the Scaled PGSS4 Covariance to Harmonic Degree 10. C.I. = 20 cm. 136

47. A Posteriori Standard Deviations of Radial Distances of Seasat Descending Arcs Based on the Recovered Geopotential Covariance to Harmonic Degree 10. C.I. = 2 cm. 136

48. A Priori Mean Geographic Radial Error of a Seasat Arc Based on Simulated Potential Coefficient Errors to Harmonic Degree 10. C.I. = 20 cm. 137

49. A Posteriori Mean Geographic Radial Error of a Seasat Arc Based on the Discrepancies Between Simulated and Recovered Potential Coefficient Errors to Harmonic Degree 10. C.I. = 2 cm. 137

50. A Priori Standard Deviations Reflecting the Mean Geographic Radial Error of a Seasat Arc Based on the Scaled PGSS4 Covariance to Harmonic Degree 10. C.I. = 20 cm. 138

51. A Posteriori Standard Deviations Reflecting the Mean Geographic Radial Error of a Seasat Arc Based on the Recovered Geopotential Covariance to Harmonic Degree 10. C.I. = 2 cm. 138

52. A Priori Variable Geographic Radial Error of a Seasat Arc Based on Simulated Potential Coefficient Errors to Harmonic Degree 10. C.I. = 20 cm. 139

53. A Posteriori Variable Geographic Radial Error of a Seasat Arc Based on the Discrepancies Between Simulated and Recovered Potential Coefficient Errors to Harmonic Degree 10. C.I. = 2 cm. 139

54. A Priori Standard Deviations Reflecting the Variable Geographic Radial Error of a Seasat Arc Based on the Scaled PGSS4 Covariance to Harmonic Degree 10. C.I. = 20 cm. 140

55. A Posteriori Standard Deviations Reflecting the Variable Geographic Error of a Seasat Arc Based on the Estimated Geopotential Covariance to Harmonic Degree 10. C.I. = 2 cm. 140

56. A Priori Geoid Undulation Errors Based on Simulated Potential Coefficient Errors to Harmonic Degree 10. C.I. = 10 cm. 141

57. A Posteriori Geoid Undulation Errors Based on the Discrepancies Between Simulated and Recovered Potential Coefficient Errors to Harmonic Degree 10. C.I. = 10 cm. 141

58. A Priori Standard Deviations of Geoid Undulations Based on the Scaled PGSS4 Covariance to Harmonic Degree 10. C.I. = 5 cm. 142

59. A Posteriori Standard Deviations of Geoid Undulations Based on the Estimated Geopotential Covariance to Harmonic Degree 10. C.I. = 2 cm. 142

60. Stationary SST Based on the Harmonic Coefficients of the Levitus SST Model to Harmonic Degree 10. C.I. = 10 cm. 143

61. Stationary SST Based on the Estimated Coefficients to Harmonic Degree 10. C.I. = 10 cm. 143

CHAPTER I

INTRODUCTION

Until the middle of the last decade only about one third of the ocean surface was surveyed by sporadic oceanographic missions. With the advent of satellite altimetry a global observation system was established to provide synoptic observations of the oceans. The usefullness of satellite altimetry has been demonstrated by a series of altimeters of increasing precision flown on Skylab, Geos3, Seasat and Geosat. The Seasat altimeter in particular, has shown for the first time that spaceborne microwave altimeters are capable of obtaining global measurements of ocean topography with sufficient accuracy to be useful for oceanographic studies. Looking into the future, NASA and the French Centre National d' Etudes Spatiales (CNES), in cooperation with other national partners, have been planning the coordinated Topex/Poseidon dedicated satellite mission for observing the oceans.

The data collected from the different satellite altimeter missions have allowed for studies that led to substantial improvement in our knowledge of the gravity field of the earth, the shape of the oceanic geoid, ocean tides, current structure and oceanic behavior, crustal structure, solid earth dynamics and others. All these studies have produced a large volume and variety of scientific literature. One could mention, for example, three special issues of the Journal of Geophysical Research (Vol. 84, B8, 1979 on Geos3; Vols. 87, C5, 1982 and 88, C3, 1983 on Seasat); Oceanography from Space, Marine Science (Vol. 13, 1981); Marine Geodesy (Vol. 8, 1984); and the Journal of Astronautical Sciences (Vol. 28, Oct.-Dec. 1980, on orbit determination for Seasat). Three comprehensive reviews of the work published in the USA alone from 1975 to date have been made by Stanley (1979), Marsh (1983), and Douglas et al. (1987), while a substantial number of publications is contained in the proceedings of a number of international symposia.

From the very early days of Geos3 it has been clear that altimetric measurements of the oceans have many sources of error which are a complex function of position and scale. The most important of these errors were the ones associated with the orbit determination of the satellite and the altimeter itself. Continuous technological improvements have substantially improved the precision of the altimeter (10 cm noise for Seasat and even lower for future missions) so that altimeter noise is not considered as a serious error source anymore. The orbit determination related errors result from

the inability to accurately compute the radial component of the orbit at the time of the altimeter observation. This radial error is due primarily to errors in the tracking to the satellite, incomplete tracking, and errors in the modeling of the gravity field, air drag and solar radiation pressure.

By far, the major component of the radial orbit error is due to the gravity field errors. Gravity field models and tracking of the 70's have resulted in radial errors of about 5 meters for Geos3. With the implementation of the GEM9 gravity field and use of altimeter observations, radial errors were reduced to the 2 meter level (Lerch et al., 1979). A similar improvement has been reported for the Seasat orbits. The first calculations of the radial component of the Seasat orbits had an error of about 5 meters which was reduced to about 1.5 meters in the ephemeris that was used for the generation of the Geophysical Data Records. This error was further reduced to about 70 cm in the early 1980's (Lerch et al., 1982).

The ephemeris accuracies for both Geos3 and Seasat provided accuracies of the sea surface that were prohibitive for many investigations, such as determination of sea surface topography and of an accurate oceanic geoid that can be used together with terrestrial data, for the computation of high degree and order gravity fields. So both Geos3 and Seasat observations needed to be analysed to reduce the radial error. New procedures were developed, ranging from fits of the altimetric surfaces to some long wavelength geoid computed from a satellite derived gravity model, to crossover analysis and optimal filtering. For the Seasat data analysis the most dominant method was the one that used crossover discrepancies as observables. The radial error, being recognized of long wavelength nature, was modeled either by a bias and tilt, or by a Fourier series of some low frequencies. These types of analyses have reduced the radial error to a reported level of 20-30 cm (e.g. Rowlands, 1981). Further combination with adjusted Geos3 data has produced accurate and detailed maps of the ocean surface (Marsh et al., 1984, Rapp, 1985, 1986). Additionally the adjusted Seasat data with the combination of the GEML2 gravity field (Lerch et al., 1985a) have produced the first qualitative maps of the long wavelength permanent sea surface topography and ocean circulation (Tai and Wunsch, 1983, 1984, Douglas et al., 1984, Engelis, 1983,1985).

Recently it has been recognized that in order to efficiently remove the radial errors from altimeter data, a more analytical modeling of these errors is necessary. Such a motivation was initiated by the early work of Anderle and Hoskins (1977) who showed that the errors are not random in nature but geographically correlated. Subsequent studies by Colombo (1984) and Wagner (1985) made use of the Lagrangian perturbation theory to derive expressions for the radial errors. These studies were followed by works of Tapley and Rosborough (1985), Rosborough (1986), Pisacane (1986), Mazzega (1986) and Tai and Fu (1986). Wunsch and Gaposchkin (1980),

Wagner (1986) and Marshall (1985) have proposed ways to simultaneously determine the permanent sea surface topography, improve the geoid and reduce the radial error. They have all used simulations to demonstrate the potential of their methods.

The present study basically treats the same problem i.e., to analytically represent the orbit error due to the geopotential and describe its characteristics. Furthermore it attempts to optimally separate the long wavelength sea surface topography from the geoid at comparable wavelengths, while reducing the orbit error. This study has been independent and in parallel to most of the above mentioned investigations. A rather substantial use of Colombo's results (Colombo, 1984) has been made and some of his notation is adopted. Some errors in his derivations have also been identified and corrected. This study extends the formulation to represent the geoid error and sea surface topography in a Lagrangian form. A Fourier series expression with respect to time and a geographic representation with respect to geocentric latitude and longitude are also developed for all the quantities. Then matrix expressions are developed and variances of the radial distances and the geoid as well as their error correlations are computed. The analytical formulation also allows for the development of observation equations to solve for parameters representing the gravity field and the sea surface topography.

In a more detailed outline, this report is structured as follows. Chapter 2 makes a summary on the usefullness and applications of satellite altimetry as well as on solutions attempted in the past to remove the radial orbit errors.

In Chapter 3 the linearized mathematical model to be used for the determination of the sea surface topography and the reduction of the orbit errors is developed.

The detailed modeling of the radial orbit errors, geoid undulation errors and sea surface topography is made in Chapters 4, 5 and 6. Chapter 4 starts with the necessary background on the Lagrangian perturbation theory and the definition of a reference orbit to develop linear expressions for the radial error. An extensive validation to assess the accuracy of the theory is made by comparison with numerically integrated orbits. In Chapter 5 alternative equations of the radial error are developed. More specifically, a Fourier series expression with respect to time and a geographic representation with respect to geocentric latitude and longitude are computed, as well as expressions contained in Wagner (1985) and Rosborough (1986). Numerical "estimates" of the radial error and its properties for a Seasat orbit are then provided by assuming potential coefficient "errors" that are generated by differencing two satellite derived gravity fields. Chapter 6 analyzes the geoid undulation errors and sea surface topography along the lines of the previous Chapters and points out differences and similarities with the radial errors.

All these models are used in Chapter 7 to derive matrix expressions for all quantities and compute variances for radial distances and geoid undulations as well as their error correlations. This covariance propagation is made using the full covariance matrix of a gravity field. Numerical estimates on the accuracies of the radial distances for Seasat arcs are presented both along the subsatellite tracks and on a geographic grid.

The simultaneous determination of the sea surface topography and the reduction of the radial errors using altimeter data is addressed in Chapter 8. Problems involved with the estimation are identified and crossover discrepancies, in addition to sea surface heights, as well as prior information for the parameters are used to improve the solution. A simulated solution for a three day Seasat arc is made to demonstrate the potential of the method if it is to be used with real altimeter data.

In Chapter 9 conclusions from this investigation are drawn and recommendations for further work are given.

CHAPTER II

DESCRIPTION AND APPLICATIONS OF SATELLITE ALTIMETRY

2.1 Introduction

Satellite altimetry can provide the height of the sea surface relative to a reference ellipsoid. This height is a function of ocean variability and the geoid. Typically the geoid varies by up to a hundred meters relative to a reference ellipsoid with wavelengths ranging from a few to thousands of kilometers. Superimposed on the geoid are variations due to ocean dynamics. These effects are much smaller in amplitude than the geoid having magnitudes on the order of 1-2 meters. Both quantities are very important for geophysical and oceanographic studies. Therefore, before proceeding to the description and applications of satellite altimetry, a short discussion on geophysical and oceanographic uses of the geoid and ocean variability is appropriate.

Knowledge of the oceanic geoid is very useful in geophysics, since one can infer information on seafloor topography, rigidity of the lithosphere and mantle convection. Changes in the shape of the geoid with maximum wavelengths of a few hundred kilometers are primarily caused by changes in the seafloor topography. Seamounts are particularly prominent, producing changes in the geoid from several centimeters to ten meters over distances of tens of kilometers. Thus, detailed and accurate maps of the geoid are needed to reveal the existence of seamounts. At longer wavelengths, variations of the geoid combined with other information (seismic and geochemical) can give information about the strength and thermal properties of the lithosphere. Finally the regional features of the geoid are attributable to deeper structures below the lithosphere and are related to mantle convection and other processes.

Knowledge of the signature in the sea surface due to ocean dynamics and external forces is important because it can lead to the determination of the ocean circulation. Theory and observations have shown that to a first order of approximation, the large scale motion of the sea is geostrophic. Assuming a geostrophic balance and hydrostatic equilibrium, the equations of motion for the oceans at any depth can be developed. These equations can be solved using salinity and temperature observations from ships and considering a reference surface to be known. Such a reference surface can very well be the geoid, so its deviations from the sea surface (sea surface

topography) as well as the ocean surface velocities need to be known both spatially on a worldwide basis, and temporally over a long period of time (Coleman, 1981).

The sea surface variations are composed of flows with different scales both spatially and temporally. The long wavelength spatial variations are basically time independent (stationary SST) and are attributed to the major oceanic currents. Time variations of SST are primarily of mesoscale spatial nature (eddies). Finally there are a number of smaller scale higher frequency phenomena such as internal waves, tides, tsunamis and others. These phenomena are not geostrophically balanced and are not part of the circulation itself.

For several decades oceanographers have been trying to determine the sea surface topography and ocean circulation. Problems in these determinations are primarily due to the inability of determining a reliable reference surface and due to the shipboard data sampling, since existing observations are taken sporadically over different periods of time and so they do not represent a homogeneous behavior of the oceans over an extended period of time. The most recent estimates of ocean circulation and sea surface topography have been computed by Levitus (1982).

2.2 Satellite Altimetry

The principle of using an altimetric system for earth related studies is fairly simple. A radar microwave altimeter onboard a satellite measures its distance to the ocean surface. If the geocentric distance of the satellite is also known at the epoch of observation, then the height of the sea surface with respect to a geocentric reference ellipsoid is (Gopalapillai, 1974)

$$h = r - \rho - r_E - \frac{r_E}{8}\left(1 - \frac{r_E}{r}\right) e^4 \sin^2 2\phi_s \qquad (2.1)$$

where ρ is the nadir distance from the center of mass of the satellite to the sea surface, h is the ellipsoidal height of the sea surface and r_E, r are the geocentric distances of the ellipsoid and the satellite respectively. The last term in equation (2.1) is a correction that accounts for the non colinearity of the geocentric distance r and the nadir distance ρ. It is a function of the eccentricity e of the reference ellipsoid and the geodetic latitude ϕ_s of the satellite position.

The nadir distance, ρ, from the center of mass of the satellite to the ocean surface is provided by the altimeter observation. Each altimeter observation is the outcome of considerable preprocessing of the raw measurement of the altimeter. The fundamental measurement

is obtained from the round trip travel time, Δt, required for an electromagnetic pulse, transmitted by the onboard electronics and emitted from the altimeter antenna, to reach the ocean surface, return back to the antenna and be detected and recorded by the onboard electronics. Sensor related corrections must be applied before the travel times are converted to distances (Hancock et al., 1980). These distances have further to be corrected for biases, reference to the center of mass of the satellite, relativistic effects and atmospheric propagation delays (Tapley et al., 1982). The latter can be separated into tropospheric and ionospheric effects. The retarding effects of the troposphere amount to about 2.5 meters with the dominant portion coming from the dry component. This effect can be modeled to the 1-2 cm level, using surface pressure measurements. The maximum correction due to the wet tropospheric delays is 40 cm. These delays have rapid changes so the best way to correct for them is to include a scanning multichannel microwave radiometer (SMMR) on board the satellite that can measure the error caused by the pulse delays due to the water vapor. Ionospheric effects on the other hand can be computed to the 3 cm level by using a model compiled from independent data (Lorell et al., 1982) or by using a dual frequency altimeter. After these corrections are made, individual altimeter measurements can be averaged (over a couple of seconds) to produce one observation which is regarded to have an error being mostly white noise. Additional "in flight" calibration of the altimeter is needed (Kolenkiewicz and Martin, 1982; Marsh and Williamson, 1982) to assure that no bias exists in the altimeter observations.

The Seasat instrumentation included a single frequency radar altimeter and a five frequency microwave radiometer. The reported accuracy of the observations was 10 cm for measurements averaged over a 1 sec interval. The footprint of each observation had an average width of 7 km along the satellite track on the surface of the earth. The Geosat altimeter is basically an improved version of the Seasat technology providing an accuracy of 5 cm after a 1 sec averaging. The Topex/Poseidon satellite is expected to carry instruments from both NASA and CNES. The NASA instruments include an advanced dual frequency radar altimeter and a three frequency microwave radiometer. After the necessary calibrations, the altimeter observations are expected to have an accuracy of 2 cm after averaging over a 3 sec interval which corresponds to an average footprint of 20 km along the satellite track. The CNES altimeter is an experimental single frequency solid state altimeter. It is expected to operate only 5% of the satellite lifetime at regular intervals and provide observations with an accuracy of 4 cm after similar averaging (Stewart et al., 1986).

The geocentric distance, r, of the satellite is determined from the computed ephemeris which is obtained by a high precision orbit determination process. The determination of the precise ephemeris involves the adjustment of the initial position of the satellite and several other parameters representing mainly coefficients of non

conservative forces. This adjustment minimizes in the least square sense the differences between the tracking data and the corresponding values that are computed using known station coordinates and comprehensive force models for the earth's geopotential, lunisolar attraction, air drag, solar radiation pressure, earth tides, earth albedo, relativistic effects and others. The parameters to be adjusted are usually estimated at short intervals of a few days. Based on the initial positions and velocities for each interval, the orbits are then computed using a numerical integration of the force models. The solution is iterated until convergence.

There are several errors involved in the determination of the precise ephemeris, associated with the observations to the satellite and the force models. Observation errors include errors in the tracking data, imperfect refraction corrections, errors in the station coordinates, and non global tracking data, both spatially and temporally. Tracking of altimeter satellites is usually done by laser ranging, Unified S-Band (USB) radiometry, and Doppler. For the Seasat satellite, laser tracking data had accuracies of 10 cm and 50 cm for the Goddard Space Flight Center (GSFC) and the Smithsonian Astrophysical Observatory (SAO) lasers, respectively. The USB range rate data had a precision of 0.1 mm/sec with an accuracy degraded by atmospheric effects. Finally the Doppler data, collected by the Department of Defense, had a precision of 10 cm at 30 sec integration intervals in range difference measurements. Spatial coverage was sparse for the laser data and almost global for the USB and Doppler data (Tapley and Born, 1980).

The Topex/Poseidon satellite will have four modes of tracking. The NASA instruments of tracking, onboard the satellite, will be a laser retroreflector, a Tranet Beacon and a Global Positioning System experimental receiver. The CNES instrument is a radiometric tracking system using a one way Doppler system, called Doris, that receives signals transmitted from the ground. The primary tracking will be provided by the Defense Mapping Agency Tranet network and is expected to provide single pass radial accuracies of 13 cm. Laser tracking will be used primarily for the altimeter calibration and the satellite ephemeris validation. The observational accuracy of the laser ranging will be 2-5 cm. The Doris and GPS systems are expected to provide radial accuracies of 10 cm (Stewart et al., 1986).

The most dominant errors in the precise ephemeris are due to gravity field modeling errors. Gravity field errors propagate into errors in the estimation of the initial state vector of the satellite and errors along the computed orbits from numerical integration. These errors have a variety of signatures and are systematic both spatially and temporally. As it will be seen later on, they are primarily of very long wavelength nature. Air drag and solar radiation pressure errors are smaller than gravity field errors. For altimetric satellites though they can be significant. The reason is that due to the complexity of their shape, the accurate modeling of the surface forces

acting on them is extremely difficult and so , only approximations are used in the modeling. Partial compensation for those approximations is made by adjusting, together with the initial state vector, the coefficients representing air drag and solar radiation pressure.

Satellite derived gravity field models are being computed since the early 1960's and are continuously improved. Their improvement is reflected in the improvement of the accuracies in the computations of the radial distance to altimetric satellites. Based on prelaunch knowledge of the gravity field and other forces, the error in the first calculations of the radial component of the Seasat orbits was about 5 m. After tailoring the gravity field with Seasat laser and USB tracking data and some Geos3 altimeter data, the error was reduced to about 1.5 m. This gravity field, PGSS3, was further improved with the incorporation of Seasat altimeter data to produce the PGSS4 gravity field, which gave a radial orbit error of about 70 cm (Lerch et al., 1982). In order to meet the 10 cm requirements for radial position accuracies for the Topex/Poseidon mission, a new effort is currently underway at GSFC and the University of Texas at Austin to compute a very accurate gravity field. Preliminary solutions have led to the generation of the GEM-T1 field (Marsh et al., 1986b) which yields orbit accuracies much higher than any of the previous fields. Further improvement is underway since this model is expected to provide accuracies of 20-25 cm (ibid) for the Topex/Poseidon orbits.

Considering the observational errors, $\Delta\rho$, and the errors in the determination of the geocentric distance of the satellite, Δr, equation (2.1) becomes (after neglecting the correction term)

$$h = r_c - \rho_{obs} - r_E + \Delta r - \Delta\rho \qquad (2.2)$$

where ρ_{obs} is the actual altimeter observation and r_c is the computed geocentric distance. The sea surface heights, on the other hand, can be written as

$$h = N + \zeta + \zeta_t + \tau + w \qquad (2.3)$$

where N is the geoid undulation, ζ is the stationary SST, ζ_t are the time variations of SST, τ are the solid earth and ocean tides and w are other motions of the oceans like wind driven waves and others. With the implication of (2.2), (2.3) becomes

$$r_c - \rho_{obs} - r_E + \Delta r - \Delta\rho = N + \zeta + \zeta_t + \tau + w \qquad (2.4)$$

or, considering that $h_c = r_c - \rho_{obs} - r_E$

$$h_c = N + \zeta + \zeta_t + \tau + w - \Delta r + \Delta\rho \qquad (2.5)$$

where h_c are the "observed" sea surface heights. Estimates of geoid undulations in (2.5) can be computed by using a set of potential coefficients up to a certain degree and order. Then

$$h_c = N_o + \Delta N^c + \Delta N^o + \zeta + \zeta_t + \tau + w - \Delta r + \Delta\rho \qquad (2.6)$$

where N_o is the computed undulation, ΔN^c is the undulation error due to errors in the modeled gravity field (commission error) and ΔN^o is the undulation signal that is not modeled from the given field (omission error). Setting

$$\Delta h = h_c - N_o \qquad (2.7)$$

equation (2.6) becomes

$$\Delta h = \Delta N^c + \Delta N^o + \zeta + \zeta_t + \tau + w - \Delta r + \Delta\rho \qquad (2.8)$$

where Δh are the so called residual sea surface heights that can be used in stationary SST determinations.

Of all the quantities contained in the observed sea surface heights, the geoidal undulations have by far the largest magnitude with a maximum of about 100 meters and a global root mean square variation of about 30 meters. They are primarily of long wavelength nature (over 90% of the geoid signature is at wavelengths longer than 1000 km). High frequency variations with wavelengths down to 10 - 20 km and amplitudes ranging from several centimeters to tens of meters do exist (Rapp, 1985). The stationary SST, as shown by oceanographic evidence, is also of long wavelength nature with additional high frequency contributions in energetic regions of the oceans. The time variations of SST and the tides are mesoscale phenomena while the orbit errors are long wavelength.

For oceanographic applications, mesoscale SST variations can be determined by differencing repeat altimeter tracks. Any long wavelength signatures in these differences are attributed to long wavelength orbit errors and can be easily removed (Cheney et al., 1983). On the contrary, as shown from equation (2.8), the determination of the stationary SST requires the knowledge of an accurate geoid (very small ΔN^c and ΔN^o) and the effective reduction of the orbit errors.

For geophysical applications and particularly for studying the local features of the oceans (e.g. seamounts) the long wavelength small oceanographic signal in equation (2.5) can be treated as noise since it does not have any effect in the high frequency spectrum of the geoid. This is not always true for the radial error as it can be seen later on and so it must be removed. For the determination of an accurate geoid at longer wavelengths the separation of the geoid from the stationary SST and the reduction of radial error become critical since both quantities have signatures in comparable wavelengths.

So the problem in satellite altimetry is a combined one requiring the simultaneous determination of both the geoid and stationary SST while reducing the radial error. The observables that can be used for this purpose are the sea surface heights which are linearly related to all the above quantities.

2.3 Existing Solutions of the Combined Altimetric Problem

Solutions to the combined altimetric problem that have been attempted in the past have focused on the reduction of the radial errors and the determination of a time averaged sea surface. Then, from that adjusted sea surface, together with the implementation of an independent satellite derived gravity model, estimates of the stationary SST were derived.

The method that has been primarily used for the determination of the radial errors is the minimization in the least square sense, of the crossover discrepancies observed at the intersections of the ascending and descending groundtracks of the satellite. These discrepancies do not contain any geoid and stationary SST information. They only represent radial errors and SST time variations as well as the time variable part of mismodeling of quantities such as tides. In using the crossover discrepancies it was assumed that the radial error is independent in ascending and descending arcs. So minimization of the discrepancies would also effectively minimize the radial error.

Based on the above principle for the solution, several techniques have been developed. In one technique followed by Rowlands (1981) for the Seasat sea surface heights, the Seasat arcs were broken into short arcs bounded by the ocean boundaries. For each of the short arcs, modeling of the radial errors was made by a bias and a tilt or only by a bias depending on the length of the arc. In order to remove the time variations of SST, repeating arcs from the repeat era of Seasat were averaged and used for the adjustment. In order to provide a reference for the solution an arc of 35 minutes of length in the Atlantic Ocean was held fixed. Then a global adjustment of the averaged arcs was made to reduce the crossover discrepancies from 1.5 meters to 0.28 meters. The adjusted arcs were then held fixed to adjust the arcs of the non repeat era of the satellite in regional

solutions.

Similar solutions, with small variations of the above technique, were made by Cloutier (1981), Marsh and Cheney (1982), and Marsh et al., (1982, 1986a). In Marsh et al. (1986a) the ocean surface was divided into small diamond shaped regions. Then minimization of the crossover discrepancies between the arcs within those regions was made to solve for the radial error that was modeled as a single bias for each arc. The resulting surfaces were then used to create a unique surface by adjusting the biases and tilts among these surfaces. All these solutions that use the crossover discrepancies as observables, although they have improved the estimates of the sea surface, are subject to several problems. The most important one as will be seen later on, is that the radial error has a component that is common to both ascending and descending arcs and cancels out during the generation of the crossover discrepancies. Therefore it cannot be removed during the crossover adjustment and so it exists in the adjusted sea surface. Additionally all the error along the arcs that are held fixed propagates to the adjusted surface. Finally all the effects like mismodeling of tides and SST time variations (in the non repeat arcs) alias the solution.

An alternative technique for removal of the radial error is the one that uses the residual sea surface heights as observables (see equation 2.8). The radial error, being recognized of long wavelength nature, is modeled by a Fourier series of low frequencies. Then, a solution for the Fourier coefficients yields corrections to the radial distance and eventually to the ocean surface. The potential of such a method to improve the satellite ephemeris was demonstrated by Goad et al., (1980) who also recognized limitations of the method because of aliasing due to the long wavelength geoid undulation commission errors and the existence of the oceanic effects. A similar solution was also used by Rapp (1979) who used the residual sea surface heights, in combination with crossover discrepancies to adjust the Geos3 data.

Since the Seasat ground tracks are not dense enough to allow for the detailed mapping of the sea surface, as is needed for geophysical applications, the combination of Geos3 and Seasat sea surface heights was made, using basically the same procedures and considering all the crossovers created between the ascending and descending arcs of the two satellites (Liang, 1983, Marsh et al., 1984). These combinations created high resolution maps of the sea surface and the gravity field of the oceans (Rapp, 1985, 1986) but they also introduced additional problems such as across track high frequency residual errors that can be easily detected in the maps. These residual errors are due to the fact that the non modeled part of the orbit error has different magnitudes in Geos3 and Seasat, resulting in a signature of long wavelength nature along track but of a high frequency nature across track.

The adjusted Seasat sea surface heights have been used to determine the stationary SST. In order to model the geoid recent satellite derived gravity models were used and residual sea surface heights were computed. These models have accuracies that only allow for the determination of very long wavelength stationary SST. Using the GEML2 gravity field, estimates of the stationary SST with wavelengths on the order of 3000 km and longer have been computed by Engelis (1985), Tai and Wunsch (1983, 1984) and Douglas et al., (1984) that agree quite well with oceanographic estimates at least qualitatively.

CHAPTER III

FORMULATION OF THE SOLUTION

3.1 Introduction

To overcome the problems that arise from the empirical solutions of the combined altimeter problem, a more general solution has to be made, involving the simultaneous determination of the geoid, stationary SST and other ocean effects and the reduction of radial errors. In order to do that, a mathematical model relating all quantities has to be developed, in which the dynamic properties of the orbit are to be considered. The basic equation that relates all quantities of interest is obtained from (2.1) and (2.3)

$$h = r - \rho - r_E = N + \zeta + \zeta_t + \tau + w \qquad (3.1)$$

In the context of this study which concentrates on the determination of the stationary SST, the sea surface time variations and the tides will be omitted from equation (3.1). This could in principle be a justifiable omission since sea surface variations can be determined independently (Cheney et al., 1983). Furthermore, the major ocean tides are obtained by contemporary ocean tidal charts, which are believed to be reasonably good (Schwiderski, 1980) although direct evidence for this is limited to data from tidal stations scattered widely along the coasts and islands. Recently a new procedure has been developed to also determine the minor tidal constituents by using a linear interpolation on the admittance function of the major ocean tides (Christodoulidis et al., 1986). Finally solid earth tides are considered to be known much better than ocean tides at present. So (3.1) reduces to

$$h = r - \rho - r_E = N + \zeta \qquad (3.2)$$

3.2 Mathematical Model

It is well known that the state of a satellite at any epoch t can be represented by a six dimensional vector $\bar{s}$, where three of the components of $\bar{s}$ represent the position and the other three the velocity of the satellite. Then $\bar{s}_I$ is the initial state vector

corresponding to the beginning of the orbit which usually coincides with the time origin. Let $\bar{p}$ be an n-dimensional vector of parameters associated with the various forces acting on the satellite and $\bar{q}$ be an m-dimensional vector representing all other non force model parameters. Then any observation, f, to the satellite is generally a nonlinear function of those parameters

$$f = f(\bar{s}(\bar{p}), \bar{q}) \tag{3.3}$$

where f has a functional dependence on the parameters $\bar{p}$ through the state vector $\bar{s}$. The task in orbit determination is to solve equation (3.3) for the state vector and/or the parameters. Since this is a nonlinear problem, initial values $\bar{p}_o$, $\bar{q}_o$ for the parameters as well as an approximate state vector $\bar{s}_o$ are required for its linearization. Then a Taylor series expansion gives

$$f = f_o + \frac{\partial f}{\partial \bar{s}} \Delta\bar{s} + \frac{\partial f}{\partial \bar{q}} \Delta\bar{q} \tag{3.4}$$

where f_o is the computed observation from (3.3) using the given approximate values, and $\Delta\bar{s}$, $\Delta\bar{p}$, $\Delta\bar{q}$ are small corrections to the state vector and the parameters. The corrections $\Delta\bar{s}$ and $\Delta\bar{p}$ are interrelated through the functional relationship $\bar{s}(\bar{p})$. As a matter of fact the state $\bar{s}$ of the satellite has a nonlinear dependence on the force parameters $\bar{p}$ as well as on the initial state $\bar{s}_I$ as follows

$$\bar{s} = \bar{s}(\bar{s}_I, \bar{p}) \tag{3.5}$$

and so small variations $\Delta\bar{s}_I$ and $\Delta\bar{p}$ result in small errors of the state vector

$$\Delta\bar{s} = \frac{\partial \bar{s}}{\partial \bar{s}_I} \Delta\bar{s}_I + \frac{\partial \bar{s}}{\partial \bar{p}} \Delta\bar{p} \tag{3.6}$$

where the partials represent matrices with elements the derivatives of the state at any time with respect to all components of $\bar{s}_I$ and $\bar{p}$ respectively. Substituting (3.6) into (3.4) we obtain

$$f = f_o + \frac{\partial f}{\partial \bar{s}} \frac{\partial \bar{s}}{\partial \bar{s}_I} \Delta\bar{s}_I + \frac{\partial f}{\partial \bar{s}} \frac{\partial \bar{s}}{\partial \bar{p}} \Delta\bar{p} + \frac{\partial f}{\partial \bar{q}} \Delta\bar{q} \tag{3.7}$$

Equation (3.7) is the general linearized mathematical model that relates any satellite observation with the initial state vector, the force field and the other parameters. The partials $\partial f/\partial \bar{s}$ and $\partial f/\partial \bar{q}$ are to be computed on the approximate orbit $\bar{s}_o$ using the initial values $\bar{p}_o$, $\bar{q}_o$ of the parameters. The partials $\partial \bar{s}/\partial \bar{s}_I$ are the solutions of the variational equations and they compose the so called state transition matrix. Equation (3.7) can be solved in the least squares sense to determine the initial state vector and any parameters of interest. The adjusted parameters are then used to integrate the equations of motion and determine the satellite state vector at any epoch. The solution is iterated until convergence.

Equation (3.7) can be used to set up the mathematical model for the solution of the combined altimeter problem. The basic observable in this case is the distance ρ between the sea surface and the satellite. From (3.2) we have

$$\rho = r - h - r_E \tag{3.8}$$

Neglecting for the moment the dependence of h on the parameters $\bar{p}$ and using (3.7) for ρ, we obtain

$$\rho = r_o + \frac{\partial r}{\partial \bar{s}} \frac{\partial \bar{s}}{\partial \bar{s}_I} \Delta \bar{s}_I + \frac{\partial r}{\partial \bar{s}} \frac{\partial \bar{s}}{\partial \bar{p}} \Delta \bar{p} + \frac{\partial r}{\partial \bar{q}} \Delta \bar{q} - h - r_E \tag{3.9}$$

where $\dfrac{\partial \rho}{\partial (\cdot)} = \dfrac{\partial r}{\partial (\cdot)}$

has been used. Since the radial orbit error in altimetric satellites is ou the order of a few meters and is primarily of long wavelength nature, equation (3.9) is a good linear approximation of the corresponding non linear equation of the type (3.3) when the initial values r_o, $\bar{s}_o$, $\bar{p}_o$, $\bar{q}_o$ are the ones that have been computed (r_o, $\bar{s}_o$), or used ($\bar{p}_o$, $\bar{q}_o$) in a precise orbit determination process. A solution of equation (3.9) can then be considered as a second step to a two step solution of the combined altimeter problem. In the first step, the satellite observations (laser ranges, USB range rates and Doppler range differences), a very accurate gravity field, surface force models, a tidal model and a set of station coordinates are used to provide estimates of the radial distance r, the initial state vector $\bar{s}_I$ and surface force parameters $\bar{p}$. In the second step the altimeter observations are used, together with r and $\bar{s}_I$, to improve the gravity field and the surface force parameters and to provide a more accurate sea surface.

For the purpose of this study we neglect the parameters representing the surface forces. Then the force parameters $\bar{p}$ represent only the potential coefficients of the gravity field. Considering also that there is no explicit relationship of the observables with the parameters $\bar{q}$, we obtain

$$\rho = r_o + \frac{\partial r}{\partial \bar{s}} \frac{\partial \bar{s}}{\partial \bar{s}_I} \Delta \bar{s}_I + \frac{\partial r}{\partial \bar{s}} \frac{\partial \bar{s}}{\partial \bar{p}} \Delta \bar{p} - h - r_E \qquad (3.10)$$

The implementation of the stationary SST and geoid undulations in equation (3.10) can be made by using (3.2). The use of a reference gravity field for the geoid undulations gives

$$h = N_o + \frac{\partial N}{\partial \bar{p}'} \Delta \bar{p}' + \Delta N^o + \frac{\partial \zeta}{\partial \bar{p}_T} \Delta \bar{p}_T - r_E \qquad (3.11)$$

where $\bar{p}'$ is an n-dimensional vector containing potential coefficients of the reference gravity field, ΔN^o are the omission errors and $\bar{p}_T$ is a k-dimensional vector containing parameters of the stationary SST. For the SST representation a spherical harmonic expansion is also adopted although it has not been established yet that this is the best representation. A reference field could in principle be used for the stationary SST, using oceanographically derived estimates. But since its magnitude is on the order of 1-2 meters no such reference is necessary. Combination of (3.10) and (3.11) gives

$$\rho = r_o - N_o + \frac{\partial r}{\partial \bar{s}} \frac{\partial \bar{s}}{\partial \bar{s}_I} \Delta \bar{s}_I + \frac{\partial r}{\partial \bar{s}} \frac{\partial \bar{s}}{\partial \bar{p}} \Delta \bar{p} - \frac{\partial N}{\partial \bar{p}'} \Delta \bar{p}' - \frac{\partial \zeta}{\partial \bar{p}_T} \Delta \bar{p}_T - \Delta N^o - r_E \qquad (3.12)$$

A very important aspect of equation (3.12) is the choice of the reference gravity field for the geoid undulations. The efficient mapping of the geoid requires a high degree and order gravity field model. This is in contrast with the satellite perturbations which are only sensitive, due to satellite altitude, to gravitational variations that can be described by a relatively low degree field. In principle one can use an existing high degree reference field (e.g., Rapp and Cruz, 1986) so that the omission errors are small and solve for corrections to that field. This choice though can be impractical computationally and certainly will not provide good high degree estimates since altimetric observations are only taken over the oceans. So unless some combination with terrestrial gravity data is made, any attempted solution will seriously suffer from leakage effects. On the other hand high degree solutions can be obtained by techniques like satellite to

satellite tracking which are global in nature. So for the solution of (3.12), the reference field that is adopted for the undulations can be the same as the one used for the orbit determination. In such a case the omission error can be quite large and some special filtering has to be made to the residual sea surface heights Δh to remove it. This filtering will also remove all the stationary SST signature with harmonic degrees greater than the maximum degree of the reference gravity field. More details on the geoid representation, the omission errors and their removal are contained in Chapter 6. Assuming that ΔN^o can be effectively removed, (3.12) can be written as

$$\rho = \rho_o + \frac{\partial r}{\partial \bar{s}} \frac{\partial \bar{s}}{\partial \bar{s}_I} \Delta \bar{s}_I + \left[\frac{\partial r}{\partial \bar{s}} \frac{\partial \bar{s}}{\partial \bar{p}} - \frac{\partial N}{\partial \bar{p}}\right] \Delta \bar{p} - \frac{\partial \zeta}{\partial \bar{p}_T} \Delta \bar{p}_T \qquad (3.13)$$

where $\rho_o = r_o - N_o - r_E$ (3.14)

In terms of the residual sea surface heights equation (3.13) is written as

$$\Delta h + \frac{\partial r}{\partial \bar{s}} \frac{\partial \bar{s}}{\partial \bar{s}_I} \Delta \bar{s}_I + \left[\frac{\partial r}{\partial \bar{s}} \frac{\partial \bar{s}}{\partial \bar{p}} - \frac{\partial N}{\partial \bar{p}}\right] \Delta \bar{p} - \frac{\partial \zeta}{\partial \bar{p}_T} \Delta \bar{p}_T = 0 \qquad (3.15)$$

Equations (3.13) and (3.15) are the basic mathematical models of the combined altimeter problem. In order to be able to solve for the corrections $\Delta \bar{s}_I$, $\Delta \bar{p}$ and $\Delta \bar{p}_T$, the functional representation of the radial orbit error, undulation error and stationary SST has to be developed. This modeling will give insight into the properties of the above quantities and their correlations and will provide the observation equations for the solution. After the corrections are estimated the same models can be used to compute the radial orbit error, undulation error and stationary SST to provide a solution for the combined altimeter problem. These models will be developed in detail in Chapter 4, 5, and 6.

CHAPTER IV

ANALYSIS OF RADIAL ORBIT ERRORS

4.1 The Satellite Orbit

The state of a satellite at any epoch can be defined in a Cartesian coordinate system with origin at the center of mass of the earth. The x axis of such a system points towards the vernal equinox and the z axis is directed towards the celestial pole at some fundamental mean epoch. The y axis is perpendicular to the xz plane so as to form a right handed orthogonal system. This Cartesian coordinate system is semi-inertial since it is accelerated, together with the earth, from external gravitational attractions of the sun, the moon and other planets. In practice the orientation of this system is defined from quasi-stellar radio sources while its origin is defined by satellite orbit dynamics. An alternative but equivalent system can be defined if agreed upon values of precession and nutation are adopted. In such a system the z axis coincides with the spin axis of the earth that is consistent with the adopted nutation theory, the x axis is directed towards the vernal equinox and the xy plane is perpendicular to the z axis and defines the equator of the earth. The Cartesian formulation does not lend itself to any singularites in describing the state of a satellite and is very convenient in developing the equations of motion and integrating them. Alternative formulations also exist that are better suited to describe properties of the orbit. The most common one, that makes, the description of a satellite orbit particularly simple, is the formulation in Keplerian elements. The Keplerian elements define an ellipse that has one focus at the geocenter and is always tangent to the true orbit. That is why the ellipse is called an instantaneous or osculating ellipse and the corresponding elements instantaneous or osculating elements.

The size and shape of the ellipse are defined by the semimajor axis, a, and the eccentricity, e, while its orientation with respect to the Cartesian system is defined by the inclination, i, the right ascension of the ascending node, Ω, and the argument of perigee, ω. The position of the satellite on the osculating ellipse is specified by the true anomaly, f, or equivalently by the eccentric anomaly, E, that is related to the mean anomaly, M, by Kepler's equation

$$M = E - e\sin E \qquad (4.1)$$

which is a transcendental equation in E and can be solved iteratively given M and e. The six Keplerian elements are equivalent to the rectangular components of position and velocity. They have the advantage, with the exception of the mean anomaly, that their variation in time is much smaller than the variation of the rectangular coordinates. The rate of change of the mean anomaly on the osculating ellipse can be approximated by the mean motion, n, which according to Kepler's third law, is

$$n = \frac{d}{dt} M(t) = (\mu a^{-3})^{\frac{1}{2}} \tag{4.2}$$

where μ is the product of the universal constant of gravitation, G, times the mass of the earth and the atmosphere, M_e.

The motion of the satellite can be traced on the surface of the earth by the so called groundtrack of the satellite which is the line connecting all the subsatellite points. The satellite orbit can be tuned so as to form a periodically repeating groundtrack. This type of orbit is called a frozen orbit, and is used in altimetric missions. Altimeter satellites are placed in orbits of small eccentricity to keep the distance to the ocean surface always close to the optimum range of the onboard instruments. They are also put high to reduce air drag, but sufficiently low to have short orbital periods and finely spaced groundtrack. Their inclination is chosen so that most of the oceans are sampled. These requirements result in orbits with an altitude of about 1000 km, a small eccentricity ($e \approx 0.001$) and inclinations larger than 60°. The orbital periods are all close to 100 minutes or about 14 revolutions per day.

The relationships between the rectangular coordinates, the Keplerian elements and the geographic coordinates of the groundtrack will be used later on in this study and are given in Appendix A. A detailed description of the orbital geometry can be found in Kaula (1966).

4.2 Equations of Motion

The Newtonian equations of motion for the center of mass of a satellite in an inertial coordinate system can be written

$$\ddot{\bar{r}} = \bar{P} \tag{4.3}$$

which is a set of three second order differential equations of the position vector $\bar{r}$. $\bar{P}$ is the total acceleration vector and contains

accelerations due to the gravitational field of the earth, third body attractions, aerodynamic forces, solar radiation pressure, thrusting of the spacecraft rockets, attitude control system corrections and others. If we consider only the gravitational acceleration of the earth then P is the gradient of the gravitational potential and (4.2) becomes

$$\ddot{\underline{r}} = \nabla V \tag{4.4}$$

In order to express the equations of motion from rectangular coordinates to Keplerian elements the three second order equations have to be transformed to six first order equations. This transformation is made by Lagrange and is described in Kaula (1966). The Lagrangian equations of motion are

$$\frac{da}{dt} = \frac{2}{na}\frac{\partial F}{\partial M}$$

$$\frac{de}{dt} = \frac{1-e^2}{na^2e}\frac{\partial F}{\partial M} - \frac{(1-e^2)^{1/2}}{na^2e}\frac{\partial F}{\partial \omega}$$

$$\frac{di}{dt} = \frac{\cos i}{na^2(1-e^2)^{1/2}\sin i}\frac{\partial F}{\partial \omega} - \frac{1}{na^2(1-e^2)^{1/2}\sin i}\frac{\partial F}{\partial \Omega}$$

$$\frac{d\omega}{dt} = -\frac{\cos i}{na^2(1-e^2)^{1/2}\sin i}\frac{\partial F}{\partial i} + \frac{(1-e^2)^{1/2}}{na^2e}\frac{\partial F}{\partial e} \tag{4.5}$$

$$\frac{d\Omega}{dt} = \frac{1}{na^2(1-e^2)^{1/2}\sin i}\frac{\partial F}{\partial i}$$

$$\frac{dM}{dt} = -\frac{1-e^2}{na^2e}\frac{\partial F}{\partial e} - \frac{2}{na}\frac{\partial F}{\partial a}$$

where the forcing function F is

$$F = \frac{\mu}{2a} + R \tag{4.6}$$

The function R is known as the disturbing function and contains all the terms of the gravitational potential V except the zero degree term.

Inserting (4.6) in (4.5) we obtain the same form of equations, with F replaced by R, except for the last equation that becomes

$$\frac{dM}{dt} = n - \frac{1-e^2}{na^2e}\frac{\partial R}{\partial e} - \frac{2}{na}\frac{\partial R}{\partial a} \tag{4.7}$$

Equations (4.5) and (4.7) have the general form

$$\dot{\bar{s}} = \dot{\bar{s}}(\bar{s}, \bar{p}) \tag{4.8}$$

where the dependency on $\bar{s}$ is straightforward while the dependency on $\bar{p}$ is given through the disturbing function R. Obviously small variations in $\bar{p}$ result in small errors in the rates of the Keplerian elements

$$\Delta\dot{\bar{s}} = \frac{\partial\dot{\bar{s}}}{\partial\bar{p}}\Delta\bar{p} \tag{4.9}$$

4.3 The disturbing function

The disturbing function R which is equal to the gravitational potential V without the zero degree term, is a time invariant function in an earth-fixed geocentric coordinate system. It has the very well known form (Heiskanen and Moritz, 1967)

$$R = \frac{\mu}{r}\sum_{\ell=2}^{\infty}\left(\frac{a_e}{r}\right)^{\ell}\sum_{m=0}^{\ell}(\bar{C}_{\ell m}\cos m\lambda + \bar{S}_{\ell m}\sin m\lambda)\bar{P}_{\ell m}(\sin\phi) \tag{4.10}$$

where r,ϕ,λ are geocentric distance, latitude and longitude in an earth fixed equatorial system, a_e is the semimajor axis of the earth, $\bar{C}_{\ell m}$ and $\bar{S}_{\ell m}$ are the fully normalized potential coefficients and $\bar{P}_{\ell m}(\sin\phi)$ are the fully normalized associated Legendre functions. A more compact expression for the disturbing function can be obtained by considering the surface spherical harmonics which can be written in the form

$$\bar{Y}_{\ell ma}(\phi,\lambda) = \sum_{a=0}^{1}\bar{P}_{\ell m}(\sin\phi)\cos(m\lambda - \frac{\pi}{2}a) \tag{4.11}$$

Then (4.7) becomes

$$R = \frac{GM}{r} \sum_{\ell=2}^{\infty} \left(\frac{a_e}{r}\right)^{\ell} \sum_{m=0}^{\ell} \sum_{a=0}^{1} \bar{C}_{\ell ma}\, \bar{Y}_{\ell ma}(\phi, \lambda) \tag{4.12}$$

where $\bar{C}_{\ell m0} = \bar{C}_{\ell m}$ and $\bar{C}_{\ell m1} = \bar{S}_{\ell m}$

The disturbing function R, in order to be used in equations (4.5), has to be transformed from the earth fixed coordinate system to an inertial coordinate system. This is a transformation that has been carried out in detail by Kaula (1966). The expression for the disturbing function R in terms of osculating Keplerian elements is

$$R = \frac{\mu}{a} \sum_{\ell=2}^{\infty} \left(\frac{a_e}{a}\right)^{\ell} \sum_{m=0}^{\ell} \sum_{p=0}^{\ell} F_{\ell mp}(i) \sum_{q=-\infty}^{\infty} G_{\ell pq}(e)\, S_{\ell mpq}(\omega, M, \Omega, \theta) \tag{4.13}$$

where

$$S_{\ell mpq} = \begin{bmatrix} C_{\ell m} \\ -S_{\ell m} \end{bmatrix}_{\ell-m \text{ odd}}^{\ell-m \text{ even}} \cos[(\ell-2p+q)M + (\ell-2p)\omega + m(\Omega-\theta)]$$

$$+ \begin{bmatrix} S_{\ell m} \\ C_{\ell m} \end{bmatrix}_{\ell-m \text{ odd}}^{\ell-m \text{ even}} \sin[(\ell-2p+q)M + (\ell-2p)\omega + m(\Omega-\theta)] \tag{4.14}$$

and $F_{\ell mp}(i)$ are the inclination functions, $G_{\ell pq}(e)$ are the eccentricity functions and θ is the Greenwich sidereal angle. A more compact form given by Colombo (1984) is

$$R = \frac{\mu}{a} \sum_{\ell=2}^{\infty} \sum_{m=0}^{\ell} \sum_{a=0}^{1} \left(\frac{a_e}{a}\right)^{\ell} C_{\ell ma} \sum_{p=0}^{\ell} \sum_{q=-\infty}^{\infty} F_{\ell mp}(i)\, G_{\ell pq}(e)\, C_{\ell mpqa}(\omega, M, \Omega, \theta) \tag{4.15}$$

where

$$C_{\ell mpqa} = \cos\{(\ell-2p+q)M + (\ell-2p)\omega + m(\Omega-\theta) - \frac{\pi}{2}[a + \frac{1}{2}(1-(-1))^{\ell-m}]\} \tag{4.16}$$

Equations (4.13) through (4.16) are expressed with respect to unnormalized coefficients. Similar expressions can be obtained if the fully normalized potential coefficients and the normalized inclination functions are used. The summation limit for the harmonic degree ℓ, being infinity in theory, is in practice limited to a rather low value. Indeed, due to the altitude attenuation factor $(a_e/a)^\ell$ the higher the harmonic degree of a spherical harmonic coefficient, the lesser its effect on the potential and the gravitational acceleration acting on the satellite. It turns out that for a satellite with an altitude of about 1000 km the series for R can be truncated at $\ell_{max} \cong 40$.

4.3.1 Inclination and Eccentricity functions

The inclination functions $F_{\ell mp}(i)$ are the result of a transformation of the Legendre functions from a plane parallel to the equator to a plane coinciding with the orbit plane. The expression for computing the inclination functions is (Kaula, 1966)

$$F_{\ell mp}(i) = \sum_t \frac{(2\ell-2t)!}{t!(\ell-t)!(\ell-m-2t)!2^{2\ell-2t}} (\sin i)^{\ell-m-2t}$$

$$\cdot \sum_{s=0}^{m} \binom{m}{s} \cos^s i \sum_c \binom{\ell-m-2t+s}{c} \binom{m-s}{p-t-c} (-1)^{c-k} \qquad (4.17)$$

where k is the integer part of $(\ell-m)/2$, t is summed from 0 to the lesser of p or k, and c is summed over all values making the binomial coefficients non zero.

This series representation of the inclination functions makes their computation quite costly or even impossible, due to hardware limitations, when the maximum harmonic degree is high. An efficient method to compute the inclination functions for practically any maximum harmonic degree has been developed by Goad (1987). This method uses the fact that the inclination functions (and their derivatives) are the Fourier coefficients of a series of values of surface spherical harmonics along a great circle of inclination i, and therefore uses a Fast Fourier Transform algorithm to recover their values. The method is stable, does not rely on short or long-period characteristics of the surface harmonics and does not require large amounts of computer resources even at degrees 180 and higher. An alternative technique that uses recurence relations has been developed by Kostelecky (1985). The technique is very efficient in computation time but requires large amounts of computer memory.

The eccentricity functions, also known as Hansen coefficients, are needed to substitute r and f by a, M and e to obtain the final expression (4.12) for the disturbing function. Expressions for the

eccentricity functions are very complicated and can be found in Kaula (1966). For small eccentricities these functions become proportional to $e^{|q|}$ so for nearly circular orbits ($e < 0.005$) one usually retains only terms of $q = -1, 0, 1$ in the summation of equation (4.12). For small eccentricities the following approximations are valid

$$G_{\ell p o} = 1 + 0(e)$$

$$G'_{\ell p o} \approx \frac{G_{\ell p o - 1}}{e}$$

$$G_{\ell p \pm 1} = 0 + 0(e) \qquad (4.18)$$

$$G'_{\ell p 1} \approx \frac{3\ell - 4p + 1}{2}$$

$$G'_{\ell p -1} \approx \frac{-\ell + 4p + 1}{2}$$

where G' denotes the derivative of G with respect to e. The efficient computation of the eccentricity functions and their derivatives is being implemented by Goad (1987) in a method similar to the one for the inclination functions.

4.4 The Radial Orbit Error

From equation (3.13) the radial orbit error Δr can be expressed as

$$\Delta r = \frac{\partial \bar{r}}{\partial \bar{s}} \frac{\partial \bar{s}}{\partial \bar{s}_I} \Delta \bar{s}_I + \frac{\partial r}{\partial \bar{s}} \frac{\partial \bar{s}}{\partial \bar{p}} \Delta \bar{p} \qquad (4.19)$$

where the partial derivatives of r and $\bar{s}$ are to be taken along the precise orbit that is computed during the first step of the solution. Equation (4.19) can also be written as

$$\Delta r = \Delta r_I + \Delta r_G \qquad (4.20)$$

where

$$\Delta r_G = \frac{\partial r}{\partial \bar{s}} \frac{\partial \bar{s}}{\partial \bar{p}} \Delta \bar{p} \tag{4.21}$$

$$\Delta r_I = \frac{\partial r}{\partial \bar{s}} \frac{\partial \bar{s}}{\partial \bar{s}_I} \Delta \bar{s}_I \tag{4.22}$$

are the errors of direct gravitational origin and errors due to initial state vector errors. The explicit form of the radial orbit errors, of either origin, with respect to Keplerian element errors can be obtained by considering that the radial distance is

$$r = a(1-e\cos E) \tag{4.23}$$

Expanding E as a function of M, we get, to the order of e^3 (Smart, 1977)

$$\cos E = (1-\frac{1}{8}e^2)\cos M - \frac{1}{2}e\cos 2M + \frac{3}{8}e^2\cos 3M \tag{4.24}$$

So

$$r = a(1-e\cos M) + O(e^2) \tag{4.25}$$

Then an error in a, e, M of either gravitational origin or due to the initial state vector will result in an error in the radial distance

$$\Delta r = \frac{\partial r}{\partial \bar{s}} \Delta \bar{s} = \Delta a(1-e\cos M) - a\Delta e\cos M + ae\Delta M\sin M \tag{4.26}$$

or

$$\Delta r = \Delta a - (a\Delta e+e\Delta a)\cos M + ae\Delta M\sin M \tag{4.27}$$

In the following, the radial orbit error from both initial state and gravitational origin will be analyzed.

4.5 The Radial Orbit Error of Gravitational Origin

4.5.1 Linearized Equations of Motion

The equations of motion of the type (4.8) or equivalently of the type (4.4) can be numerically integrated with a suitable integration technique. A description of several numerical integration techniques that are used for this purpose is contained in Cappellari et al., (1976). Equations (4.8) can also be integrated analytically by considering the following linearization

$$\dot{\bar{s}} = \dot{\bar{s}}(\bar{s}_o) + \frac{\partial \dot{\bar{s}}}{\partial \bar{s}} \int \dot{\bar{s}}(\bar{s}_o)\, dt \qquad (4.28)$$

where $\bar{s}_o$ is a vector of approximate elements defining a reference orbit. The first term in equation (4.28) can be analytically integrated using the linearized Lagrangian perturbation theory. Let $\bar{s}_1$ be this first order approximation to the osculating elements

$$\bar{s}_1 = \int \dot{\bar{s}}(\bar{s}_o)\, dt \qquad (4.29)$$

Then the second term of (4.28) can, in principle, be also analytically integrated to provide the second order terms representing the coupling effects between the Keplerian elements. This analytical integration technique with different variations regarding the completeness in the representation of the disturbing function and the choice of variables (Keplerian, Delaunay, etc.) has been used in the past by Kozai (1959), Brouwer (1959), Brouwer and Clemence (1961), Kaula (1966) and others. But even with the incorporation of second order coupling effects, the accuracies with which the satellite state vector was computed were rather limited and so the analytical method has been replaced by numerical integration techniques.

For the solution of the combined altimeter problem the quantities of interest are the small potential coefficient corrections giving rise to radial orbit errors on the order of 1-2 meters. For such magnitudes the linearized theory is expected to be quite accurate and is the one that is applied in this study. Consistent with the linearization of (4.8), (4.9) becomes

$$\Delta\dot{\bar{s}} = \frac{\partial \dot{\bar{s}}}{\partial \bar{p}} \Delta\bar{p} = \frac{\partial \dot{\bar{s}}(\bar{s}_o)}{\partial \bar{p}} \Delta\bar{p} + \frac{\partial \dot{\bar{s}}}{\partial \bar{s}} \frac{\partial \bar{s}_1}{\partial \bar{p}} \Delta\bar{p} \qquad (4.30)$$

or

$$\Delta\dot{\bar{s}} = \Delta\dot{\bar{s}}(\bar{s}_o) + \frac{\partial\dot{\bar{s}}}{\partial\bar{s}}\,\Delta\bar{s}_1 \tag{4.31}$$

where

$$\Delta\bar{s}_1 = \int \frac{\partial\dot{\bar{s}}(\bar{s}_o)}{\partial\bar{p}}\,\Delta\bar{p}dt = \frac{\partial\bar{s}_1}{\partial\bar{p}}\,\Delta\bar{p} \tag{4.32}$$

is the first approximation to the Keplerian element errors computed on the reference orbit $\bar{s}_o$. Then (4.31) is integrated to

$$\Delta\bar{s} = \Delta\bar{s}_1 + \int \frac{\partial\dot{\bar{s}}}{\partial\bar{s}}\,\Delta\bar{s}_1 dt \tag{4.33}$$

Substituting into (4.21) we obtain

$$\Delta r_G = \frac{\partial r}{\partial\bar{s}}\,\Delta\bar{s}_1 + \frac{\partial r}{\partial\bar{s}}\int \frac{\partial\dot{\bar{s}}}{\partial\bar{s}}\,\Delta\bar{s}_1 dt \tag{4.34}$$

Note that the partials $\partial r/\partial\bar{s}$ still need to be taken on the precise orbit. The first term in (4.34) represents the first order approximation of Δr_G while the second term accounts for second order effects which arise from the interactions of the first order errors with all the potential coefficient terms. Before we proceed to the determination of the detailed expressions for the first and second order terms of the radial orbit error, the reference orbit $\bar{s}_o$ has to be defined.

4.5.2 The Reference Orbit

The major force acting on the satellite is the one due to the central force field of the earth. In such a field the satellite follows an elliptical orbit that obeys the three laws of Kepler. The size, shape and orientation of this ellipse are fixed and described by Keplerian elements that have no variations in time. Because the earth's potential is not represented by only a zero degree term additional forces acting on the satellite make it depart from its normal orbit. The largest of those forces is due to the equatorial bulge of the earth which can be described by the (2,0) term of the gravitational field. The time independent part of the equations of motion, considering only the central force and equatorial bulge of the

earth are given by Kaula (1966)

$$\frac{da}{dt} = 0$$

$$\frac{de}{dt} = 0$$

$$\frac{di}{dt} = 0$$

$$\frac{d\omega}{dt} = -\frac{3nJ_2a_e^2}{4(1-e^2)^2a^2}\,[1-5\cos^2 i] \tag{4.35}$$

$$\frac{d\Omega}{dt} = -\frac{3nJ_2a_e^2}{2(1-e^2)^2a^2}\cos i$$

$$\frac{dM}{dt} = n + \frac{3nJ_2a_e^2}{4(1-e^2)^{3/2}a^2}\,(3\cos^2 i-1)$$

where J_2 is the dynamic form factor of the earth. Then the resulting orbit will have the following elements

$$a_o(t) = a_o$$

$$e_o(t) = e_o$$

$$i_o(t) = i_o$$

$$\omega_o(t) = \omega_o + \dot{\omega}(t-t_o) \tag{4.36}$$

$$\Omega_o(t) = \Omega_o + \dot{\Omega}(t-t_o)$$

$$M_o(t) = M_o + \dot{M}(t-t_o)$$

where $(a_o, e_o, i_o, \omega_o, \Omega_o, M_o)$ are the time invariant or mean Keplerian elements and t_o is the time at the beginning of the orbit. Equations

(4.36) define an ellipse that is gradually changing with a secular motion. Its variations are a steady slow turning of the orbit plane due to a secular change in Ω (precession of the line of nodes), a rotation of the major axis in the orbit plane about the geocenter due to a secular change in ω (precession of the argument of perigee) and a slight departure from Kepler's third law given by equation (4.2).

In order to use equations (4.36) to define the reference orbit, the mean Keplerian elements need to be determined. One method that has been used by Brouwer (1959) and Kozai (1966) is the following: since the largest periodic perturbations are the ones due to J_2, a good approximation to the mean elements can be obtained if the J_2 periodic perturbations are computed and subtracted from the initial elements $\bar{s}_I$ that are given from the orbit adjustment. These perturbations are computed in Appendix B. Then the mean values of the semimajor axis and the eccentricity, for example, are

$$a_o = a - \frac{3}{2} J_2 \frac{a_e^2}{a} \sin^2 i \cos 2(\omega+M) \tag{4.37}$$

$$e_o = e - J_2 \left(\frac{a_e}{a}\right)^2 \left[\frac{7}{8} \sin^2 i \cos(3M+2\omega) + \frac{3}{8} \sin^2 i \cos(M+2\omega) \right. \tag{4.38}$$

$$\left. + \left(\frac{3}{2} - \frac{9}{4} \sin^2 i\right) \cos M \right]$$

where the elements on the right hand side are the initial elements.

A more accurate determination of the mean elements can be obtained when a precise numerically integrated orbit is available for a time period that is an integer multiple of the periods of all orbital perturbations. The mean elements (a_o, e_o, i_o) and the mean rates ($\dot{M}$, $\dot{\omega}$, $\dot{\Omega}$) can be determined by averaging the computed osculating elements and rates over the time span for which the orbit is computed. Then (M_o, ω_o, Ω_o) are the mean values such that they give the best fits to the corresponding osculating elements in the sense $\bar{s}_o + \dot{\bar{s}}(t-t_o) \approx \bar{s}$. This approach of determining the mean elements has the advantage, over the previous one, that in addition to the periodic effects due to J_2, it also removes all the periodic effects due to the other terms of the geopotential. Additionally the secular rates contain all the secular (from all even zonal terms and not only from J_2) and very long period effects. In reality the two procedures are almost identical since the perturbations, other than from J_2, are quite small and so the resulting mean elements are almost the same. This will be seen in Section 4.7 where a numerical validation of the theory developed in the present Chapter will be made.

For altimetric orbits, which are almost circular, the determination of the mean elements becomes more complicated. For such orbits the position of the perigee cannot be easily defined. As a result, variations in both the argument of perigee and mean anomaly are markedly non linear, while the eccentricity variations are not sinusoidal anymore. The perigee does not precess but oscillates about a mean value of ±90° (Cook, 1966). It turns out that the mean anomaly has similar variations, so the total variations of (ω+M) behave well and can be easily determined. The mean elements e and ω can be computed using the theory developed by Cook who used the following non singular transformation

$$\xi = e\cos\omega$$
$$\eta = e\sin\omega \qquad (4.39)$$

Cook has determined perturbations in ξ and η using the zonal only field and concluded that there are no perturbations of zonal origin in e and ω when these elements are equal to

$$\omega_o = \frac{\pi}{2} \qquad (4.40)$$

$$e_o = \frac{c}{k} \qquad (4.41)$$

where

$$c = n \sum_{\ell=3}^{\ell_{max}} J_\ell \left(\frac{a_e}{a}\right)^\ell \frac{(\ell-1)}{\ell(\ell+1)} P_{\ell 1}(o) P_{\ell 1}(\cos i) \qquad (4.42)$$

$$k = -\frac{3}{4} n J_2 \left(\frac{a_e}{a}\right)^2 (1-5\cos^2 i) \qquad (4.43)$$

ℓ_{max} being the maximum harmonic degree of the summation which is only over odd degrees. $P_{\ell 1}(\cos i)$ are the associated Legendre functions given by

$$P_{\ell 1}(\cos i) = \frac{\sin i}{2^\ell} \sum_t \frac{(2\ell-2t)!(-1)^t}{(\ell-1-2t)!(\ell-t)!t!} (\cos i)^{\ell-1-2t} \qquad (4.44)$$

the summation over t being from 0 to $(\ell-1)/2$.

This type of orbit with $\omega_0 = \pi/2$ and e_0 given by (4.41), (4.42) and (4.43) is the orbit that is desirable in satellite altimetry since it has the property of forming a very precisely repeating groundtrack. In reality $\dot{\omega}$ is very close to zero but not equal to it. For small values of $\dot{\omega}$ the mean values of e and ω can still be computed using Cook's theory.

In the particular application of the combined altimeter problem the following reference orbit will be used. The mean values i_0, ω_0, Ω_0, M_0 are identical to the initial values; a_0, e_0 are computed by equations (4.37) and (4.41); $\dot{M}$ and $\dot{\Omega}$ are computed by (4.35) and $\dot{\omega}$ is computed by (4.35) supplemented by the effect of all odd zonal harmonics (consistent with Cook's theory). It turns out (see Section 4.7) that such a reference orbit is very close to the one computed by averaging the osculating elements of a precise ephemeris.

4.5.3 First Order Radial Orbit Error

From (4.34) the first order radial orbit error is

$$\Delta r_{G1} = \frac{\partial r}{\partial \bar{s}} \Delta \bar{s}_1 \tag{4.45}$$

and written explicitly

$$\Delta r_{G1} = \Delta a_1 - (a\Delta e_1 + e\Delta a_1)\cos M + ae\Delta M_1 \sin M \tag{4.46}$$

where a, e, M are the osculating elements given by the precise ephemeris and Δa_1, Δe_1, ΔM_1 are computed analytically using the linearized perturbation theory. Expression (4.46) is valid in the general case of an elliptic orbit. For nearly circular orbits though like the altimetric ones, Δe_1 and ΔM_1 cannot be computed unless the non singular transformation (4.39) (applied for the errors) is used to compute Δe_1 and $\Delta \omega_1$. Then by computing $\Delta \omega_1 + \Delta M_1$ the errors ΔM_1 can also be obtained. This transformation can be avoided by introducing the variable

$$u = e\cos M \tag{4.47}$$

which is also a non singular variable and can be computed analytically (Lerch, 1986). Then its differential

$$\Delta u = \Delta e \cos M - e \Delta M \sin M \tag{4.48}$$

is also a non singular variable and can be computed analytically on the reference orbit. Considering that a and Δa_1 are also non singular, the first order radial orbit error of (4.46) can be approximated by

$$\Delta r_{G1} = \Delta a_1 - (a_o \Delta e_1 + e_o \Delta a_1) \cos M_o(t) + a_o e_o \Delta M_1 \sin M_o(t) \tag{4.49}$$

which is a non singular expression for the first order radial orbit error although the individual errors Δe_1 and ΔM_1 are not. Equation (4.49) provides the radial orbit errors of the precise ephemeris, computed approximately on the reference orbit. Tests on the accuracy of (4.49) are to be made in Section 4.7.

To compute Δa_1, Δe_1, ΔM_1 the rates $\Delta \dot{a}$, $\Delta \dot{e}$, $\Delta \dot{M}$ need to be integrated, in the sense

$$\Delta \bar{s}_1(t) = \int_o^{\Delta t} \Delta \dot{\bar{s}}(t) dt \tag{4.50}$$

where $\Delta t = t - t_o$

The rates $\Delta \dot{a}$, $\Delta \dot{e}$, $\Delta \dot{M}$ are computed on the reference orbit using equations (4.5) and (4.15), with (4.15) being applied for the potential coefficient corrections $\Delta C_{\ell ma}$. Dropping the subscript "o" of the mean elements for simplicity, we obtain the following expressions for the rates

$$\Delta \dot{a}(t) = -\sum_{\ell mpqa} \Delta C_{\ell ma} \, \tilde{a}_{\ell mpq} \sin(\dot{\psi}_{\ell mpq} t + \psi_{\ell mpqa_o}) \tag{4.51}$$

$$\Delta \dot{e}(t) = -\sum_{\ell mpqa} \Delta C_{\ell ma} \, \tilde{e}_{\ell mpq} \sin(\dot{\psi}_{\ell mpq} t + \psi_{\ell mpqa_o}) \tag{4.52}$$

$$\Delta \dot{M}(t) = \sum_{\ell mpqa} \Delta C_{\ell ma} \, \tilde{M}_{\ell mpq} \cos(\dot{\psi}_{\ell mpq} t + \psi_{\ell mpqa_o}) \tag{4.53}$$

where

$$\tilde{a}_{\ell mpq} = \frac{2\mu}{na^2}\left(\frac{a_e}{a}\right)^{\ell} F_{\ell mp}(i)G_{\ell pq}(e)(\ell-2p+q) \qquad (4.54)$$

$$\tilde{e}_{\ell mpq} = \frac{\mu}{na^3 e}\left(\frac{a_e}{a}\right)^{\ell} F_{\ell mp}(i)G_{\ell pq}(e)[(1-e^2)^{1/2}(\ell-2p+q) - (\ell-2p)](1-e^2)^{1/2} \qquad (4.55)$$

$$\tilde{M}_{\ell mpq} = \frac{\mu}{na^3}\left(\frac{a_e}{a}\right)^{\ell} F_{\ell mp}(i)\left[-\frac{1-e^2}{e}\frac{\partial G_{\ell pq}(e)}{\partial e} + 2(\ell+1)G_{\ell pq}(e)\right] \qquad (4.56)$$

$$\dot{\psi}_{\ell mpq} = (\ell-2p+q)\dot{M} + (\ell-2p)\dot{\omega} + m(\dot{\Omega}-\dot{\theta}) \qquad (4.57)$$

$$\psi_{\ell mpqa_o} = (\ell-2p+q)M_o + (\ell-2p)\omega_o + m(\Omega_o-\theta_o) - \frac{\pi}{2}\left[a+\frac{1}{2}(1-(-1)^{\ell-m})\right] \qquad (4.58)$$

In the above equations $\dot{\psi}_{\ell mpq}$ describes the frequency of each particular summation term, and $\psi_{\ell mpqao}$ gives the corresponding phase. Each frequency is a linear combination of the following frequency components: the orbital frequency $\dot{\omega} + \dot{M}$ (one cycle per revolution), the apsidal frequency $\dot{\omega}$ of a complete revolution of the perigee and the frequency $\dot{\Omega}-\dot{\theta}$ of a complete rotation of the earth with respect to the precessing orbital plane. One such rotation is called a nodal day.

Equations (4.51) - (4.53) are sinusoidal oscillations with time independent amplitudes frequencies and phases. These equations are generally valid for a short time period because of the orbital decay due to surface forces that can change the overall characteristics of the orbit. Of extreme importance is the correct determination of the reference orbit since errors in this orbit can substantially distort the computed frequencies and phases. On the contrary, the amplitudes are not very sensitive to such errors. From equations (4.54) - (4.57) and the definition of the eccentricity functions we can conclude that the major contribution to the semimajor axis error arises with $q = 0$ while for the eccentricity and mean anomaly such contribution is given from terms involving $q \neq 0$. Since altimetric orbits are almost circular, truncation of the series at $q = \pm 1$ is adequate.

When the frequencies $\dot{\psi}_{\ell mpq}$ are different from zero each term of the summations in (4.51) - (4.53) can be normally integrated as a cosine or sine function. The total integrated effect is then

$$\Delta a_1(t) = \sum_{\ell mpqa} \Delta C_{\ell ma} \frac{\tilde{a}_{\ell mpq}}{\dot{\psi}_{\ell mpq}} \cos(\dot{\psi}_{\ell mpq}\Delta t + \psi_{\ell mpqa_o}) - \Delta a_o \qquad (4.59)$$

$$\Delta e_1(t) = \sum_{\ell mpqa} \Delta C_{\ell ma} \frac{\tilde{e}_{\ell mpq}}{\dot{\psi}_{\ell mpq}} \cos(\dot{\psi}_{\ell mpq}\Delta t + \psi_{\ell mpqa_o}) - \Delta e_o \qquad (4.60)$$

$$\Delta M_1(t) = \sum_{\ell mpqa} \Delta C_{\ell ma} \frac{\tilde{M}_{\ell mpq}}{\dot{\psi}_{\ell mpq}} \sin(\dot{\psi}_{\ell mpq}\Delta t + \psi_{\ell mpqa_o}) - \Delta M_o \qquad (4.61)$$

where the summations are over the indices that do not make $\psi_{\ell mpq} = 0$. Δa_o, Δe_o, ΔM_o are the quantities computed at $\Delta t = 0$ to make $\Delta a_1(t_o) = \Delta e_1(t_o) = \Delta M_1(t_o) = 0$. This is physically meaningful because errors in the forcing function cannot affect the orbit instantly. They only accumulate with the evolution of time.

Substitution of (4.59) - (4.61) into (4.49) gives the periodic part of the first order approximation of the radial orbit error. After applying trigonometric identities to the resulting products of cosines and sines we obtain

$$\begin{aligned}\Delta r^P_{G1}(t) = \sum_{\ell mpqa} \Delta C_{\ell ma} \Big[& A^o_{\ell mpq} \cos(\dot{\psi}_{\ell mpq}\Delta t + \psi_{\ell mpqa_o}) \\ & + A^1_{\ell mpq} \cos(\dot{\psi}_{\ell mp(q+1)}\Delta t + \psi_{\ell mp(q+1)a_o}) \\ & + A^{-1}_{\ell mpq} \cos(\dot{\psi}_{\ell mp(q-1)}\Delta t + \psi_{\ell mp(q-1)a_o}) \Big] \\ & - \Delta a_o + (e_o\Delta a_o + a_o\Delta e_o)\cos M_o(t) - a_o e_o \Delta M_o \sin M_o(t) \end{aligned} \qquad (4.62)$$

where

$$A^o_{\ell mpq} = \frac{\tilde{a}_{\ell mpq}}{\dot{\psi}_{\ell mpq}}$$

$$A^{1}_{\ell mpq} = -\frac{1}{2\dot{\psi}_{\ell mpq}}\left[e_o\tilde{a}_{\ell mpq} + a_o\tilde{e}_{\ell mpq} + a_o e_o\tilde{M}_{\ell mpq}\right] \qquad (4.63)$$

$$A^{-1}_{\ell mpq} = -\frac{1}{2\dot{\psi}_{\ell mpq}}\left[e_o\tilde{a}_{\ell mpq} + a_o\tilde{e}_{\ell mpq} - a_o e_o\tilde{M}_{\ell mpq}\right]$$

and

$$\dot{\psi}_{\ell mp(q\pm 1)} = \dot{\psi}_{\ell mpq} \pm \dot{M} \qquad (4.64)$$

with a similar expression for $\psi_{\ell mp(q\pm 1)a0}$. From (4.62) it becomes obvious that each component of the disturbing function produces, in addition to an error component of frequency ψ, an excitation modulated by ±M (or by 1 cy/rev). The contribution at frequency ψ is given by the semimajor axis errors while the modulated components are a result of errors in the eccentricity and mean anomaly. So any long period effects in these two elements will produce an error with a frequency close to 1 cy/rev. On the contrary, errors close to 1 cy/rev will produce long wavelength errors as well as errors with a frequency close to 2 cy/rev. In addition to these periodic terms the radial orbit error contains a constant bias and a 1 cy/rev terms. These two error components are a function of all the potential coefficient terms. This is in contrast to the periodic errors that are functions of particular degrees and orders giving rise to corresponding frequencies.

4.5.4 Resonant Effects

When the disturbing function has a frequency that is identical or very close to one of the eigenfrequencies of the homogeneous partial differential equations that correspond to the equations of motion (4.4), then resonance occurs. Simply stated, resonance occurs whenever the satellite is subjected repeatedly to the same force field resulting into large very long wavelength oscillations or even a secular change in the satellite motion. A secular change is called perfect resonance while the long period oscillations are called deep or shallow resonances.

A resonance appears in the form of zero divisors (perfect resonance) or small divisors (deep or shallow resonance) in the solution of the linear equations of the type (4.51) - (4.53). The existence of small divisors though does not imply that the perturbations have any infinite or wild behavior, but the fact that the analytical solutions break down. In order to see what particular conditions create resonant effects, equation (4.57) has to be written

as

$$\dot{\psi}_{\ell mpq} = (\ell-2p+q)(\dot{\omega}+\dot{M}) - q\dot{\omega} + m(\dot{\Omega}-\dot{\theta}) \qquad (4.65)$$

This equation becomes zero for all even zonal terms for which q = 0 and p = $\ell/2$. All those terms produce secular changes (perfect resonance) in the Keplerian elements and their errors. Long period perturbations on the other hand (deep resonance) are produced by the odd zonal terms for which p = $(\ell+1)/2 \pm 1$ and q = ± 1. Then $\dot{\psi}_{\ell mpq} = \pm\dot{\omega}$. Since $\dot{\omega} \approx$ 1-2 degrees per day these perturbations have periods of about 200 days and large amplitudes. Another case in which resonance occurs is when the frequencies involved in (4.65) become locked together. In other words when the orbital frequency $(\dot{\omega}+\dot{M})$ is related to the nodal frequency $(\dot{\Omega}-\dot{\theta})$ by a simple integer ratio. When this happens the satellite passes through the same geographic region and is subjected to the same gravitational features, resulting into a gradual accumulation of the corresponding perturbations that have a frequency equal to $q\dot{\omega}$. When either q or $\dot{\omega}$ are equal to zero then there is a perfect resonance ($\dot{\omega}$ = 0 is the resonant constraint for frozen altimeter orbits). When $q\dot{\omega}$ is different from zero then there is a deep resonance.

In reality $\dot{\omega}$ can never be identical to zero, or even be kept very close to zero throughout the satellite lifetime because the orbit drifts with time. This constraint can only be maintained if small corrections are applied to the orbit by firing rockets onboard the spacecraft. Furthermore, the orbital and nodal frequencies can never be perfectly locked together because of interactions with periodic perturbations and the surface force effects. So instead of perfect and deep resonances we have the so called shallow resonances which occur when the orbital frequency and the nodal frequency are very close in forming an integer ratio. As an example of shallow resonances consider a satellite with an orbital frequency of 14.3 cy/day. Then the first shallow resonance occurs at m = 14 (primary shallow resonance for which $\dot{\psi}_{\ell mpq} \approx$ 0.3 cy/day) the second at m = 28-29 (secondary shallow resonance) and so on.

Next in importance to perfect, deep and shallow resonances are the effects of the terms with $\ell-2p+q = 0$ and $m \neq 0$. Then the frequency reduces to $-q\dot{\omega} + m(\dot{\Omega}-\dot{\theta})$ which can never become zero since all perturbations of importance have a $q < 2$ in nearly circular orbits. This frequency becomes small for small values of m. And since m multiplies the nodal frequency the corresponding terms are called m-dailies.

The resonant effects in the Keplerian elements can be seen by examining equations (4.51) - (4.56). It is obvious that Δa_1 is not affected by secular and long period effects of zonal origin and by the m-dailies because in all cases $\ell-2p+q = 0$ and so (4.54) becomes zero.

Secular changes occur only in ΔM_1 while long period effects of zonal origin and m-dailies occur in both Δe_1, ΔM_1. Shallow resonances occur in all Δa_1, Δe_1, ΔM_1. Long period effects due to shallow resonances and m-dailies can generally be computed in a normal way using the theory as described in the previous Section. The secular changes in ΔM_1 can be computed by direct integration of (4.53) considering $\dot{\psi}_{\ell mpq} = 0$. Then

$$\Delta M^r(t) = \sum_{\ell} \Delta C_{\ell_o o} \tilde{M}_{\ell_o \frac{\ell_o}{2}} \Delta t \tag{4.66}$$

where ℓ is even. For long period perturbations of zonal origin and for a small integration period (i.e. about 7-10 days) the oscillations in $\Delta\dot{e}$ and $\Delta\dot{M}$ expressed by (4.52) and (4.53) can be approximated by a linear trend. Then these equations can be integrated to

$$\Delta e^r(t) = \sum_{\ell} \Delta C_{\ell_o o} \tilde{e}_{\ell_o \frac{\ell \pm 1}{2} \mp 1} \Delta t \cos\omega_o \tag{4.67}$$

$$\Delta M^r(t) = \sum_{\ell} \Delta C_{\ell_o o} \tilde{M}_{\ell_o \frac{\ell \pm 1}{2} \mp 1} \Delta t \sin\omega_o \tag{4.68}$$

where ℓ is odd. Note that for a longer integration period a quadratic term should be included to account for the non linear effect of the long period oscillation. The general form of the equations (4.66), (4.67) and (4.68) is

$$\Delta e^r(t) = \tilde{e}^r \Delta t \tag{4.69}$$

$$\Delta M^r(t) = \tilde{M}^r \Delta t \tag{4.70}$$

where

$$\tilde{e}^r = -\sum_{\ell mpqa} \Delta C_{\ell ma} \tilde{e}_{\ell mpq} \sin\psi_{\ell mpqa_o} \tag{4.71}$$

$$\tilde{M}^r = \sum_{\ell mpqa} \Delta C_{\ell ma} \tilde{M}_{\ell mpq} \cos\psi_{\ell mpqa_o} \tag{4.72}$$

These equations are more general than the previous ones, because they can be used to compute any type of resonance that may occur and not only the ones of zonal origin. This can be done by establishing a threshold while computing $\dot{\psi}_{\ell mpq}$ and then using the above equations for all combinations of ℓ, m, p, q that give rise to $\dot{\psi}_{\ell mpq}$ smaller than the threshold. Since a resonance can also occur in the semimajor axis a similar equation for Δa^r has to be included. Δa^r as well as $\Delta\omega^r$ (which is to be used in the next section) are given by

$$\Delta a^r(t) = \tilde{a}^r \Delta t \tag{4.73}$$

$$\Delta\omega^r(t) = \tilde{\omega}^r \Delta t \tag{4.74}$$

where

$$\tilde{a}^r = -\sum_{\ell mpqa} \Delta C_{\ell ma} \tilde{a}_{\ell mpq} \sin\psi_{\ell mpqa_o} \tag{4.75}$$

$$\tilde{\omega}^r = \sum_{\ell mpqa} \Delta C_{\ell ma} \tilde{\omega}_{\ell mpq} \cos\psi_{\ell mpqa_o} \tag{4.76}$$

with

$$\tilde{\omega}_{\ell mpq} = -\frac{\mu}{na^3} \frac{\frac{\partial F_{\ell mp(i)}}{\partial i} G_{\ell pq}(e)}{\tan i(1-e^2)^{\frac{1}{2}}} \tag{4.77}$$

Equation (4.77) can be obtained by substituting the forcing function into the equation of motion (4.5) for $\dot{\omega}$.

Using (4.69), (4.70) and (4.73) in (4.49) the first order radial orbit error due to resonant terms is

$$\Delta r_{G1}^r(t) = \tilde{a}^r \Delta t - (a_o \tilde{e}^r + e_o \tilde{a}^r) \Delta t \cos M_o(t)$$

$$+ a_o e_o \tilde{M}^r \Delta t \sin M_o(t) \tag{4.78}$$

which contains a linear trend and a 1 cy/rev component with an amplitude linearly increasing with time. This type of error is also zero at $t = t_o$.

4.5.5 Second Order Radial Orbit Error

In the previous sections the first order radial orbit error has been computed. In these computations it has been assumed that the Keplerian elements that are used as arguments in equations (4.59) - (4.61) are the mean elements which are time independent and contain no errors. In reality these elements are the osculating elements and have perturbations that interact with the computed errors to produce second order effects. These second order errors in the radial distance are

$$\Delta r_{G2} = \frac{\partial r}{\partial \bar{s}} \int \frac{\partial \dot{\bar{s}}}{\partial \bar{s}} \Delta \bar{s}_1 dt \tag{4.79}$$

Since (4.79) involves the interaction of the singular elements e, M with their first order errors Δe_1, ΔM_1 the non singular transformation (4.47) has to be applied. Then (4.79) becomes

$$\Delta r_{G2} = \frac{\partial r}{\partial \bar{s}'} \int \frac{\partial \dot{\bar{s}}'}{\partial \bar{s}} \Delta \bar{s}_1 dt \tag{4.80}$$

where

$$\bar{s}' = (a,u) = (a, e\cos M) \tag{4.81}$$

Since the errors $\Delta \bar{s}_1$ are generally small, all the interactions with the perturbed elements $\bar{s}'$ will be negligible with the exception of the resonant errors which accumulate with time, and the constant error in the semimajor axis. The latter one can be quite important because of its interaction with the mean motion n through Kepler's third law. Then, using (4.81) we can write (4.80) as follows

$$\Delta r_{G2} = -(1-u) \int \frac{\partial \dot{a}}{\partial a} \Delta a_o dt + a \int \frac{\partial \dot{u}}{\partial a} \Delta a_o dt$$

$$+ (1-u) \int \frac{\partial \dot{a}}{\partial e} \tilde{e}^r \Delta t dt - a \int \frac{\partial \dot{u}}{\partial e} \tilde{e}^r \Delta t dt$$

$$+ (1-u) \int \frac{\partial \dot{a}}{\partial M} \tilde{M}^r \Delta t dt - a \int \frac{\partial \dot{u}}{\partial M} \tilde{M}^r \Delta t dt$$

$$+ (1-u) \int \frac{\partial \dot{a}}{\partial \dot{\omega}} \tilde{\omega}^r \Delta t dt - a \int \frac{\partial \dot{u}}{\partial M} \tilde{\omega}^r \Delta t dt \qquad (4.82)$$

Equation (4.82) is computed in Appendix C. The computation has been made separately for the coupling effects of the semimajor axis and the variable, u, so that their individual second order effects can be determined. These individual effects are given by equations (C.17) and (C.37), while their combined effect on the radial distance is given by (C.38). All the integrations have been made on the reference orbit.

From (C.17) we observe that the largest second order contribution in the semimajor axis is an oscillation with a frequency of 2 cy/rev and an amplitude linearly increasing with time. A similar error with a smaller amplitude exists in the variable, u. These two errors have a different sign so the resulting error in the radial distance is largely reduced. Another oscillation with a frequency of 1 cy/rev and an amplitude linearly increasing with time is the result of the interaction of the constant bias with the mean motion. These two components of the radial orbit error are the following

$$\Delta r_{G2} \cong a_o e_o \left[\frac{3}{2} \frac{n}{a_o} \Delta a_o\right] \Delta t \sin M_o(t)$$

$$- \frac{1}{2} a_o J_2 \left(\frac{a_e}{a_o}\right)^2 \left[\frac{3}{2} \frac{n}{a_o} \Delta a_o + \tilde{M}^r + \tilde{\omega}^r\right] \Delta t \sin^2 i \sin 2[M_o(t) + \omega_o(t)]$$

(4.83)

The magnitude of the oscillations in (4.83) is clearly dependent on the satellite specifications and on the errors of the gravity field that is used for the orbit determination. The quantities Δa_o, $\tilde{M}^r$, $\tilde{\omega}^r$ can become very small when an accurate gravity field is used. Additionally since they do not have any periodic behavior they can be removed rather easily during the orbital adjustment by comparing the computed orbit with the observations. Care should be exercised in this type of removal because if the observations are not globally distributed and accurate, the removal of these quantities will not be efficient. In the context of this study we will assume that no such removal is made.

4.6 The Radial Orbit Error Due to Initial State Vector Error

The initial state vector that is computed from the least squares fit of the various force models to the satellite observations, contains errors arising from errors in the force models (and primarily the gravity field), and errors in the station coordinates and tracking to the satellite. When the initial state vector is used for the orbit integration, its errors propagate into the computed orbit. This error propagation in terms of the radial distance is given by equation (4.22)

$$\Delta r_I = \frac{\partial r}{\partial \bar{s}} \frac{\partial \bar{s}}{\partial \bar{s}_I} \Delta \bar{s}_I \tag{4.84}$$

The analytical determination of Δr_I is possible along the lines developed so far in this Chapter. Using equation (4.28) the osculating elements $\bar{s}$ can be written

$$\bar{s} = \bar{s}_o + \bar{s}_1 + \bar{s}_2 \tag{4.85}$$

where $\bar{s}_o$ is the vector of the mean elements, $\bar{s}_1$ is given by (4.29) and $\bar{s}_2$ represents the second order coupling effects between the different harmonic terms and is equal to

$$\bar{s}_2 = \int \frac{\partial \dot{\bar{s}}}{\partial \bar{s}} \bar{s}_1 dt \tag{4.86}$$

Since $\bar{s}_1$ and $\bar{s}_2$ are computed using the mean elements $\bar{s}_o$ which are determined from the initial elements $\bar{s}_I$, all three terms of (4.85) are affected by errors $\Delta\bar{s}_I$. Then

$$\Delta r_I = \frac{\partial r}{\partial \bar{s}} \left[\frac{\partial \bar{s}_o}{\partial \bar{s}_I} + \frac{\partial \bar{s}_1}{\partial \bar{s}_I} + \frac{\partial \bar{s}_2}{\partial \bar{s}_I} \right] \Delta \bar{s}_I \tag{4.87}$$

The last partial representing effects of the order of J_2^2 is about three orders of magnitude smaller than the other two partials and since $\Delta\bar{s}_I$ is generally small, this last term is not expected to have any significance and therefore it can be dropped. As it is described in section (4.5.2) the mean elements are usually computed by removing the J_2 perturbations from the initial elements, or by averaging the osculating elements, whenever available. In both cases the errors of the initial elements propagate directly into the computed mean elements. So the partial $\partial\bar{s}_o/\partial\bar{s}_I$ is

$$\frac{\partial \bar{s}_n}{\partial \bar{s}_I} = I + O(J_2) \tag{4.88}$$

where I is a unit matrix. Computing also the derivatives $\partial r/\partial \bar{s}$ on the reference orbit we obtain for the first part of (4.87)

$$\Delta r_{I1} = \Delta a_I - (a_o \Delta e_I + e_o \Delta a_I)\cos M_o(t) + a_o e_o \Delta M_I \sin M_o(t) \tag{4.89}$$

The errors Δr_{I1} have an identical form to the errors in (4.62) that are functions of the constants of integration Δa_o, Δe_o and ΔM_o. They both have a constant part and a 1 cy/rev part but with different signs. So initial state vector errors can either reduce or enhance the constant and 1 cy/rev errors of gravitational origin.

The second part of (4.87) can be written as

$$\Delta r_{I2} = \frac{\partial r}{\partial \bar{s}} \int \frac{\dot{\partial \bar{s}}}{\partial \bar{s}_I} \Delta \bar{s}_I dt \tag{4.90}$$

which is identical to equation (4.79) describing the second order effects of gravitational origin. So equation (4.90) can be determined in a similar way by introducing the transformation (4.81). Then the only initial error that can produce any effect of significance is the one in the semimajor axis. Using the equations in Appendix C for Δa_I we obtain

$$\Delta r_{I2} = -a_o e_o \left[\frac{3}{2} \frac{n}{a_o} \Delta a_I\right] \Delta t \sin M_o(t)$$

$$+ \frac{1}{2} a_o J_2 \left(\frac{a_e}{a}\right)^2 \left[\frac{3}{2} \frac{n}{a_o} \Delta a_I\right] \Delta t \sin^2 i \sin 2(M_o(t) + \omega_o(t)) \tag{4.91}$$

which again is of the same form with the corresponding error of gravitational origin. The interaction of Δa_I with the other terms other than J_2 are negligible as long as Δa_I is small.

4.7 Validation of the Theory for Errors of Gravitational Origin

Throughout this Chapter the complete theory for the modeling of the radial orbit error has been developed, and formulas providing the first order and second order effects of the error have been computed. It remains to be seen how accurate this formulation is, so

that it can be used for real applications.

The validation of the theory aims primarily at the assessment of the accuracy of the computed first and second order radial error. As a by product one can obtain estimates on the accuracy of the determination of the reference orbit and on the accuracy in the computation of the semimajor axis error Δa and the error $a\Delta u$ of the scaled non singular variable au. Furthermore, it can be shown that individual errors Δe and ΔM are indeed non estimable from the theory.

To make the validation, two numerically integrated orbits were provided to us by NASA, Goddard Space Flight Center (Klosko, private communication, 1986). These orbits were computed for a six day Seasat arc at 2 minute intervals using the GEM10B (Lerch et al., 1981) and GEM9 gravity fields and the same initial state vector. Both fields were used up to harmonic degree 10 so that to facilitate the computations. The satellite state vectors for the two orbits were initially in terms of rectangular coordinates and velocities. So they have been transformed into Keplerian elements using the transformation described in Appendix A. The initial elements used for the generation of both orbits are given in Table 1.

Table 1

Initial State Vector Used for the GEM10B and GEM9 Numerically Integrated Orbits.

Epoch	780923
Semimajor Axis	7177305.511 m
Eccentricity	0.00086
Inclination	108:0077
R.A. of Asc. Node	160:9817
Arg.of Perigee	0:0
Mean Anomaly	0:0

For the determination of the mean elements the time averages of a, e, i as well as the average rate of Ω have been computed using the GEM9 ephemeris and are shown in Table 2. Individual mean rates of ω and M could not be computed because of the erratic behavior of these elements which are singular for almost circular orbits. Instead, the rate of the total argument $\omega + M$, which is a well defined quantity was determined and is also shown in Table 2.

The mean elements have also been computed using the analytic formulation. The mean semimajor axis was computed by (4.37) and the eccentricity by (4.41). The mean inclination is not computed because

of the small variations observed in the ephemeris of the GEM9 orbit. For the computation of the rates $\dot{\omega}$, $\dot{\Omega}$, and $\dot{M}$, equations (4.35), providing the J_2 secular perturbations, have been used. The computation of $\dot{\omega}$ has been repeated including the secular and long period perturbations from all zonal coefficients with no change in the result. The mean elements a, e and rates $\dot{\omega}$, $\dot{M}$, $\dot{\omega} + \dot{M}$, $\dot{\Omega}$ are also shown in Table 2.

Table 2

Mean Elements and Rates Computed by Numerical Averaging and Analytical Methods.

Element	Averaging	Analytical
a	7168889.259 m	7168980.740 m
e	0.0008	0.00084
i	108.017	—
$\dot{\omega}$	—	-1:727/day
$\dot{M}$	—	5146:699/day
$\dot{\omega} + \dot{M}$	5144:966/day	5144:972/day
$\dot{\Omega}$	2:053/day	2:044/day

From Table 2 we can see the excellent agreement between the two methods in all the estimates. The agreement in the mean rate $\dot{\omega} + \dot{M}$ indicates that the individual rates are also correct. From Tables 1 and 2 it turns out that, with the exception of the semimajor axis the mean elements and the mean rates can be very well approximated by their initial values and the rates computed from J_2, respectively. Note that for the computation of M the mean semimajor axis has to be used.

The GEM10B and GEM9 numerically integrated orbits were differenced to generate "errors" in the semimajor axis, the scaled variable au, and the radial distance. These errors are shown in Figures 1, 3, 5 while their amplitude spectra, computed by a Fast Fourier Transform technique, are shown in Figures 2, 4, 6. From these figures we can see that the radial orbit error can reach magnitudes of about 3-4 meters with the major error being at 1 cy/rev. Additional energy is found in the frequencies around the 1 cy/rev frequency primarily due to the m-dailies, while practically no energy exists above 3 cy/rev. The 1 cy/rev error comes from $a\Delta u$ since there is no 1 cy/rev error in Δa. The RMS error Δr is 1.74 meters. The error Δa on the other hand has a constant bias of -1.007 meters and an RMS value of 1.33 meters. As it can be seen from Figures 1 and 2, Δa is increasing in time with an apparent 2 cy/rev frequency of large amplitude. Additional frequencies as high as 5

cy/rev with smaller amplitudes do exist. All these errors are largely reduced when Δa is merged with $a\Delta u$ to create the radial orbit error Δr.

The errors Δa, $a\Delta u$ and Δr have also been computed analytically using the differences GEM10B - GEM9 up to degree 10 as potential coefficient errors. The first order equations (4.59), (4.62) and (4.78) have initially been used. First order results indicate that the summation part of (4.62) does not give rise to any errors at frequencies of 0, 1, and 2 cy/rev. The constant bias and 1 cy/rev errors come exclusively from the last terms of (4.62). Additional 1 cy/rev errors with a time dependent amplitude arise from the long period errors in eccentricity which build up to about 70 cm after six days. On the contrary the secular and long period effects of mean anomaly errors are negligible (3 mm after six days).

The first remarkable agreement of the first order results with the numerical ones is that the constant bias has a value of -1.009 meters which differs from its true value by only 2 mm. In a more detailed comparison it is seen that the first order theory is able to model all the frequencies including the 1 cy/rev terms of constant amplitude with a remarkable accuracy. Indeed the discrepancies from the numerical results have systematic patterns of 1 and 2 cy/rev with time dependent amplitudes, which are characteristic of the second order effects as seen from equation (4.83). With these effects included, the agreement in the semimajor axis is excellent. The maximum discrepancy is 5 cm and the RMS discrepancy is 1.5 cm. These discrepancies are shown in Figure 7 while their amplitude spectrum is shown in Figure 8. This spectrum shows frequencies at 1, 2 and 3 cy/rev with a maximum amplitude of 8 mm.

On the contrary the agreement in terms of the radial orbit error is not as good. From Figures 9 and 10 we can see that there is still a systematic discrepancy at 1 cy/rev with time dependent amplitude and an RMS value of 20 cm. Superimposed is a discrepancy of daily frequency and small magnitude. It turns out that the 1 cy/rev discrepancy is equal to $(n/a)\Delta a_0 \Delta t \sin M$ which implies that the first term of (4.83) should be three times smaller than it is given. This systematic discrepancy is of unknown nature and more investigation is needed to resolve it. If we account for this correction, the overall discrepancy in Δr has an RMS value of 1.2 cm with a maximum value of 5 cm.

The comparison between the two sets of errors has shown that the analytic formulation can provide a very accurate modeling of the radial orbit error and can be used to form the detailed observation equations. Indeed errors in the theory (with the exception of the error in (4.83)) are expected to be smaller than 1 cm when the theory is applied for future altimetric missions, like the Topex/Poseidon mission, since the radial orbit errors are also expected to be quite smaller than the simulated errors used in this comparison.

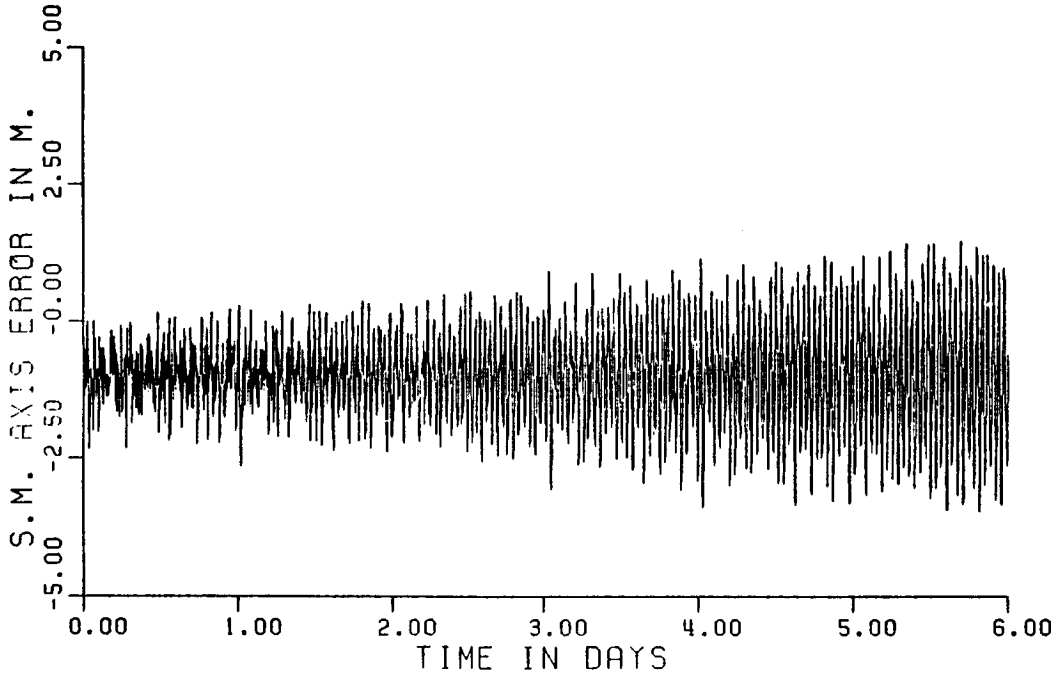

Figure 1. Semimajor Axis Error Computed by Differencing Two Numerically Integrated Orbits Based on GEM9 and GEM10B to Harmonic Degree 10.

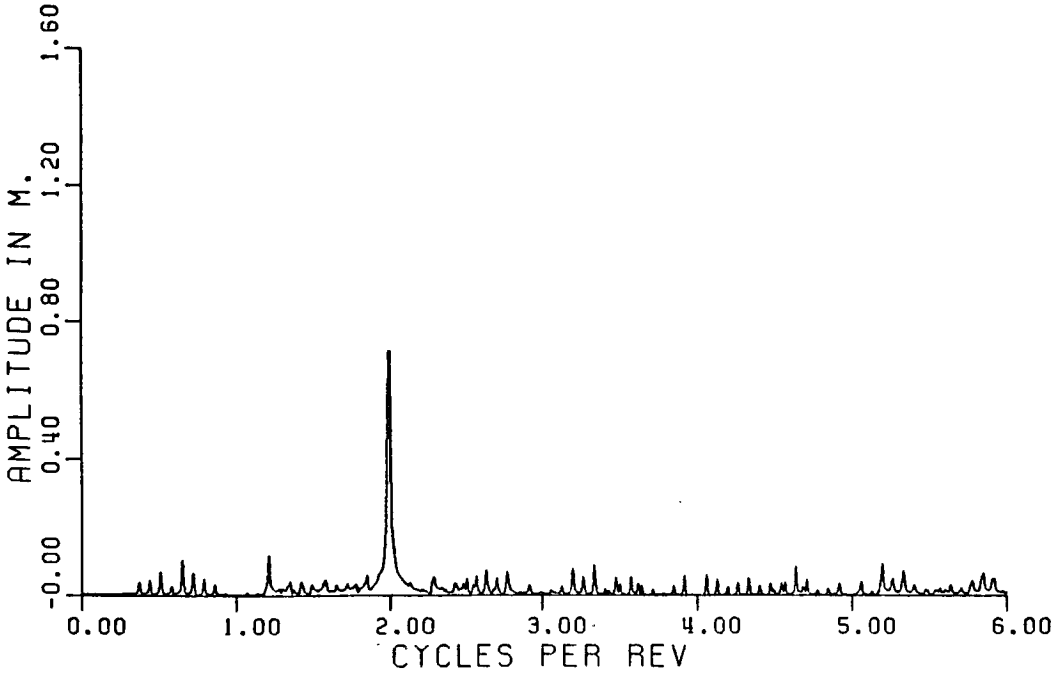

Figure 2. Amplitude Spectrum of Semimajor Axis Error.

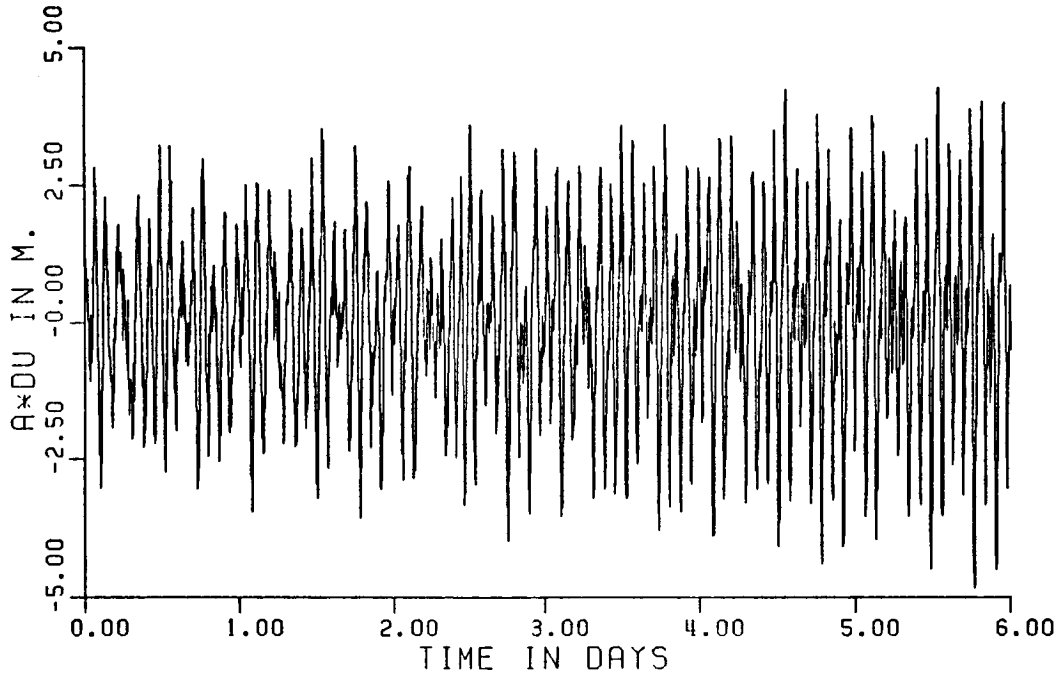

Figure 3. Error in the Non Singular Variable au Computed by Differencing Two Numerically Integrated Orbits Based on GEM9 and GEM10B to Harmonic Degree 10.

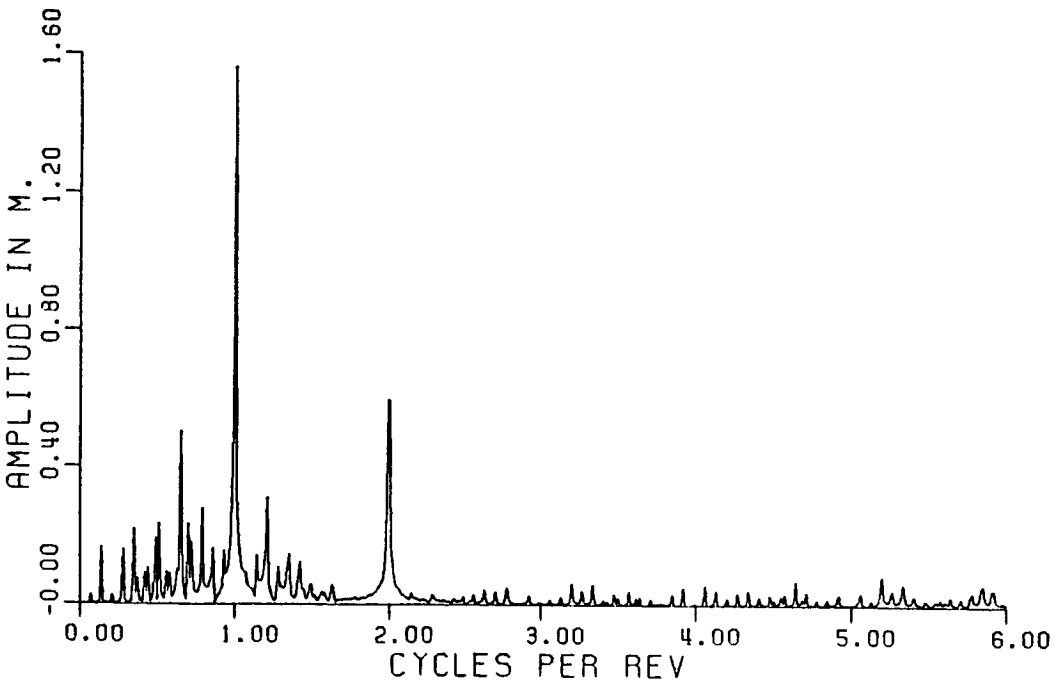

Figure 4. Amplitude Spectrum of the Error in the Non Singular Variable au.

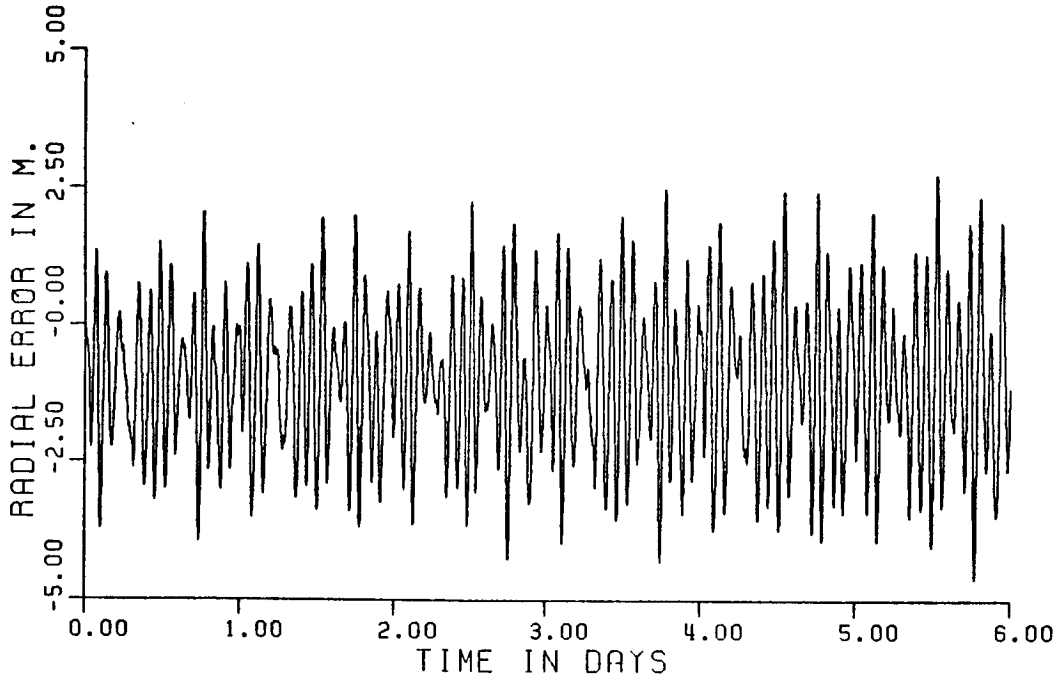

Figure 5. Radial Orbit Error Computed by Differencing Two Numerically Integrated Orbits Based on GEM9 and GEM10B to Harmonic Degree 10.

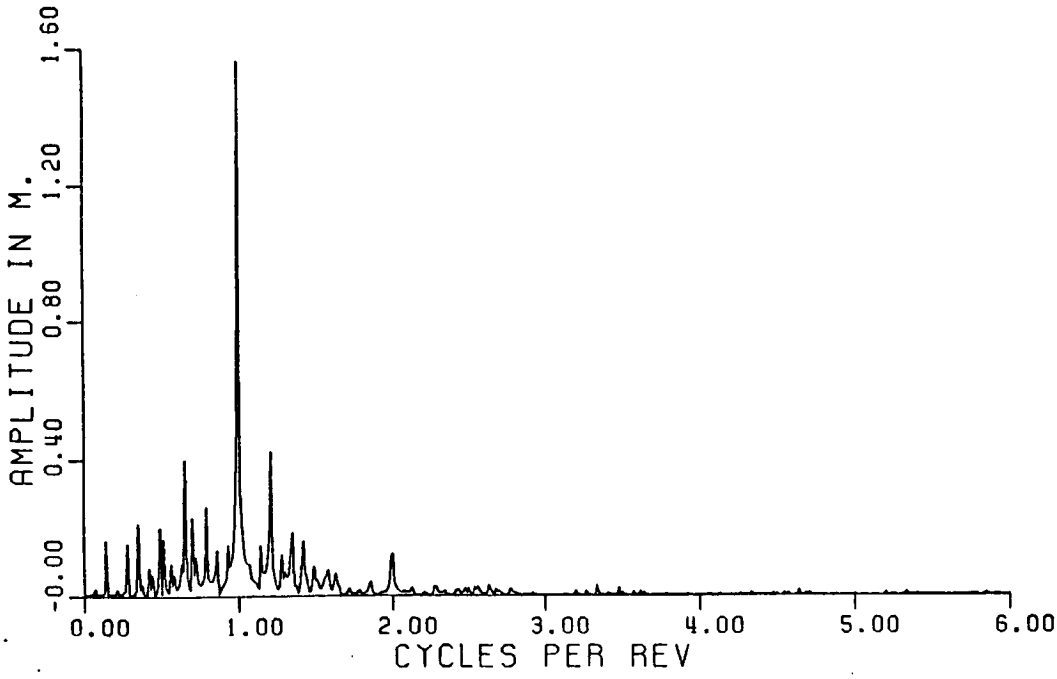

Figure 6. Amplitude Spectrum of Radial Orbit Error.

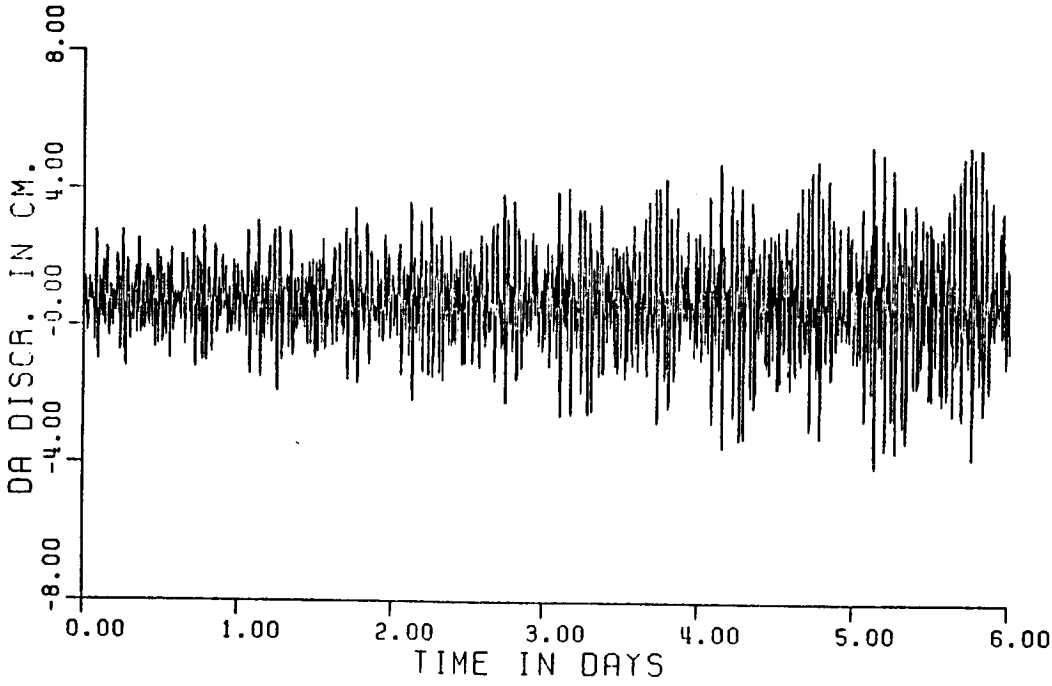

Figure 7. Discrepancies in the Computation of the Semimajor Axis Error Using the Numerical and Analytical Methods.

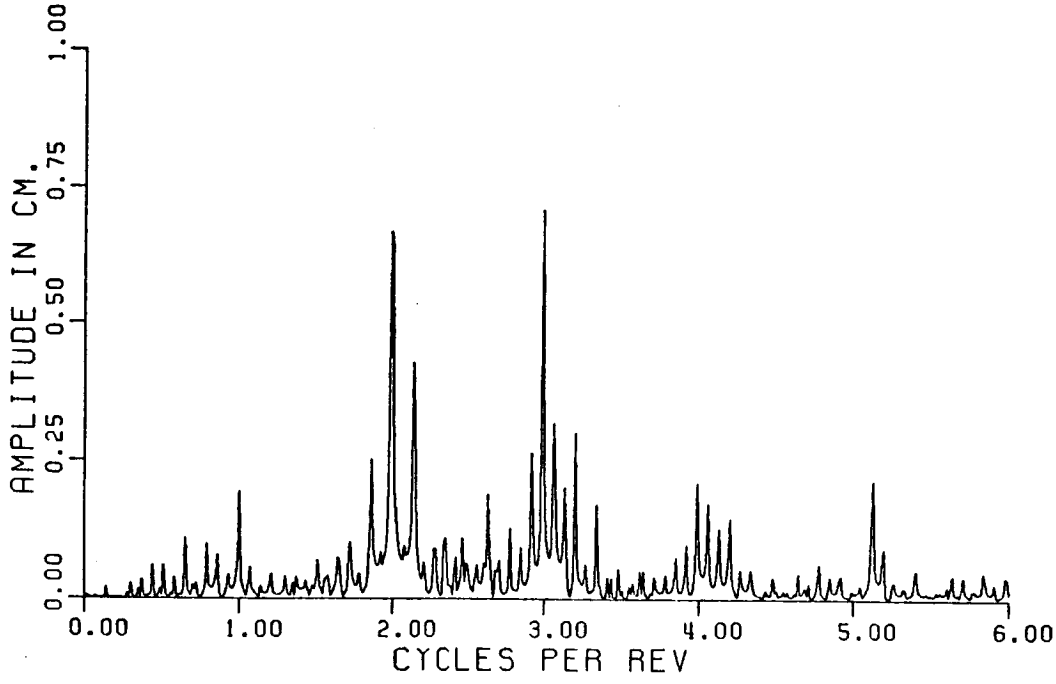

Figure 8. Amplitude Spectrum of the Discrepancies in the Computation of the Semimajor Axis Error.

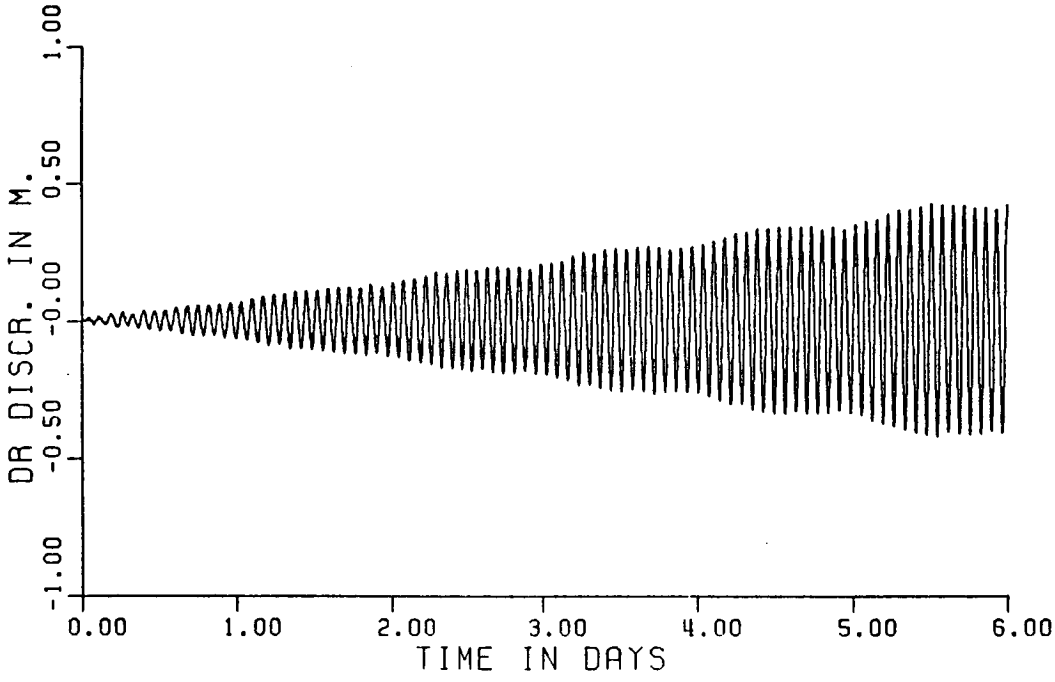

Figure 9. Discrepancies in the Computation of the Radial Orbit Error Using the Numerical and Analytical Methods.

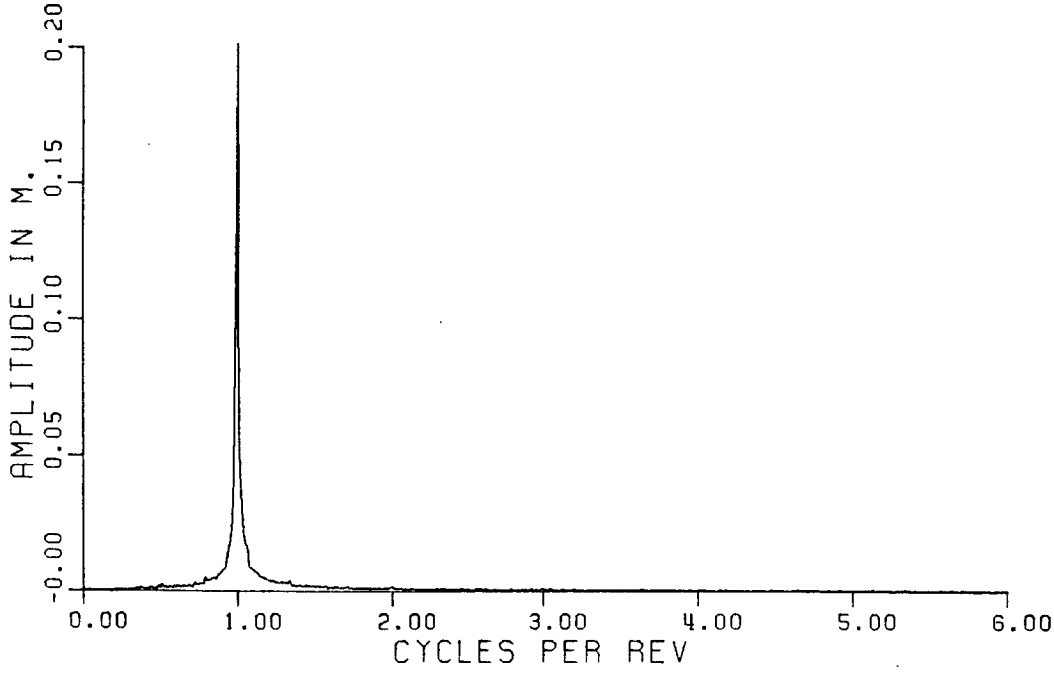

Figure 10. Amplitude Spectrum of the Discrepancies in the Computation of the Radial Orbit Error.

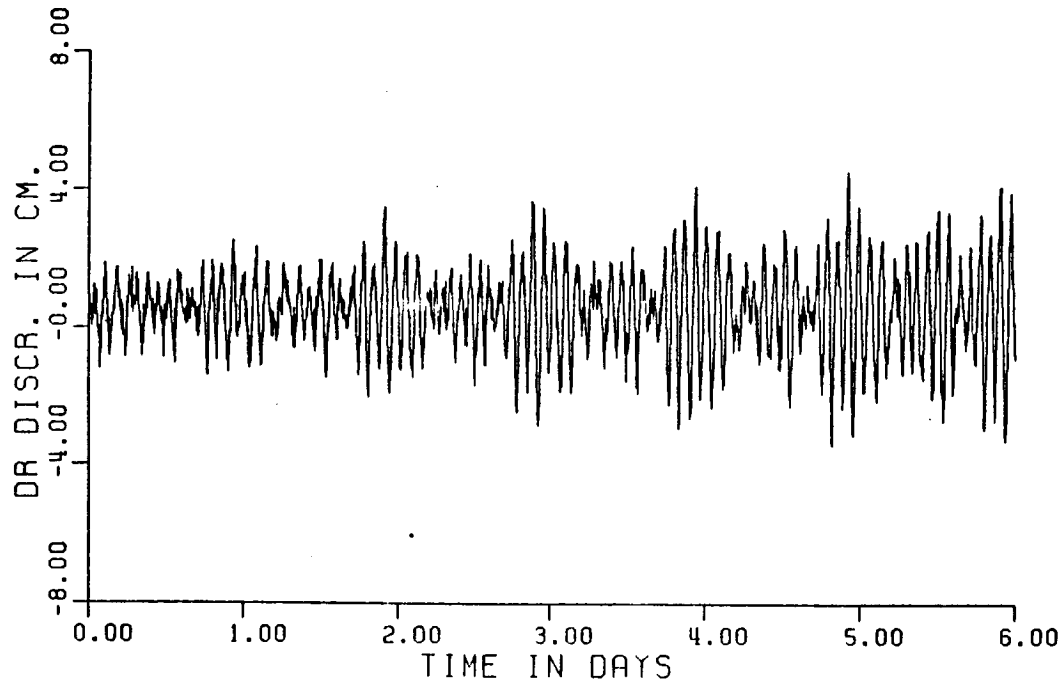

Figure 11. Discrepancies in the Computation of the Radial Orbit Error After Additional Empirical Correction Has Been Applied.

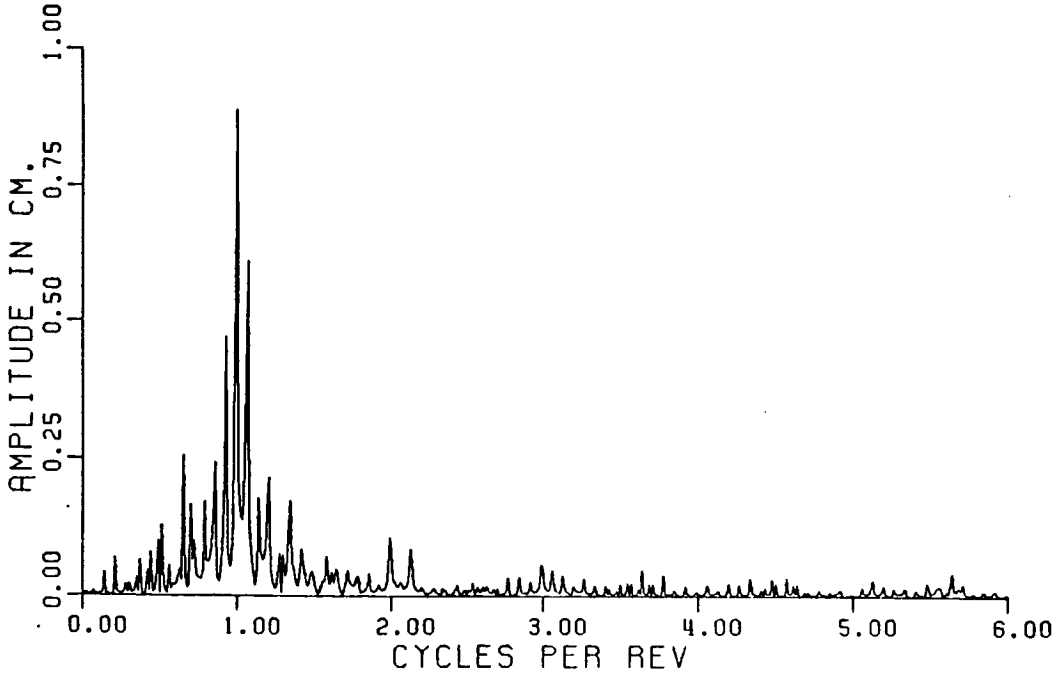

Figure 12. Amplitude Spectrum of the Discrepancies in the Computation of the Radial Orbit Error After Additional Empirical Correction has been Applied.

CHAPTER V

ALTERNATIVE EXPRESSIONS OF THE RADIAL ORBIT ERROR

5.1 Introduction

In the previous Chapter the complete formulation leading to detailed equations for the orbit error has been developed. These equations, given a set of potential coefficient errors and initial state vector errors, are able to provide the radial orbit error over a short period of time. Closer examination of them reveals some properties of the error, like the strong 1 cy/rev term arising from all potential coefficient errors, the linear time dependence of the amplitude of the error arising from resonant terms and the constant bias and others. Computation of individual summation terms can even reveal information about the contribution of specific degrees and orders to the error. Additionally it can be seen that different combinations of ℓ, m, p, q produce oscillations of the same frequency and phase but of different amplitudes. Finally the geographic location of the subsatellite point at a particular epoch for which the radial error is computed, can be found by simply converting the Keplerian elements at epoch to spherical coordinates.

This type of formulation though does not lend itself to a systematic analysis of the properties of the orbit error. Furthermore its implementation on the computer is quite expensive. So transformations of these equations are necessary. One such transformation involves the grouping of all terms that produce the same frequencies to create a Fourier series expression. Then the frequency content of the error can be easily determined. Furthermore, the cumulative contributions by degree and order are easier to compute. Another formulation that can be obtained involves the systematic transformation of the orbit error from the inertial coordinate system to an earth fixed system. This formulation allows for the determination of the geographic patterns of the error.

In this Chapter the Fourier series formulation and the geographic representation of the orbit error are going to be developed. Then some numerical results using a set of "known" potential coefficient errors will be given for both methods. Finally some alternative forms for the orbit error used by other investigators will be derived.

5.2 Fourier Series Formulation

5.2.1 Determination of the Fourier Frequencies

The frequency of each individual term contributing to the orbit error is defined by equation (4.65)

$$\dot{\psi}_{\ell mpq} = (\ell-2p+q)(\dot{M}+\dot{\omega}) - q\dot{\omega} + m(\dot{\Omega}-\dot{\theta}) \qquad (5.1)$$

The integers ℓ, m, p, q can be any combination of integers in the ranges defined by

$$\begin{aligned} \ell &= [2, \ell_{max}] \\ m &= [0, \ell] \\ p &= [0, \ell] \\ q &= [-1, 1] \end{aligned} \qquad (5.2)$$

where ℓ_{max} is the maximum harmonic degree for which the satellite shows any sensitivity to the gravity field. The range of q has been restricted to only three values for the case of near circular orbits.

In (5.1) the most dominant term in characterising the frequency content is $(\ell-2p+q)$ $(\dot{M}+\dot{\omega})$ or k cy/rev. The second largest term is $m(\dot{\Omega}-\dot{\theta})$ or about -m/14.3 cy/rev while $q\dot{\omega}$ is very small and can be neglected. Considering the range of variation of p and q a certain harmonic degree ℓ will generate frequencies in the range $[-\ell-1,\ell+1]$ cy/rev. Allowing also for the modulation by $\pm\dot{M}$ this range becomes $[-\ell-2,\ell+2]$ giving a total of $(2\ell+5)$ different frequencies separated by 1 cy/rev. Around each of these frequencies there is a number of other frequencies generated by the terms $m(\dot{\Omega}-\dot{\theta})$. So we can view the frequency spectrum of the orbit error for a particular degree as being composed by $(2\ell+5)$ distinct frequency bands 1 cy/rev apart, each of them containing m different frequencies separated by $(\dot{\Omega}-\dot{\theta})$ or 1/14.3 cy/rev. The total number of frequencies is $(\ell+1)(2\ell+5)$. Obviously some frequencies belonging to different bands and to different orders can become identical or have a very small separation.

It turns out that for all harmonic degrees there are always combinations of p and q that generate the same frequency. In other words harmonic coefficients of different degrees and same order are lumped together in the same frequencies. The total number of frequencies generated by a gravity field up to ℓ_{max} is $(\ell_{max}+1)(2\ell_{max}+5)$ while the maximum positive and negative frequencies

are

$$\dot{\psi}_{max}^{+} = (\ell_{max}+2) \text{ cy/rev}$$

$$\dot{\psi}_{max}^{-} = [-(\ell_{max}+2) - \ell_{max}/14.3] \text{ cy/rev} \qquad (5.3)$$

It is of interest and very important to investigate what combinations of ℓ, p, q give rise to waves of the same frequency band. For m=0 we have three possible combinations of ℓ, p, q that provide the same frequency, k. Denoting by i = (-1,0,1) the modulations (-M,0,M), these combinations are

$$\ell-2p+q = k \qquad \text{for } i = 0 \qquad (5.4)$$

$$\ell-2p+q+1 = k \qquad \text{for } i = 1 \qquad (5.5)$$

$$\ell-2p+q-1 = k \qquad \text{for } i = -1 \qquad (5.6)$$

All the possible values of p and q for a particular ℓ that satisfy these equations are given in Table 3 .

Table 3

Combinations Between ℓ, p, q that generate a frequency k.

modulation	ℓ-k even	ℓ-k odd
	p,q	p,q
i = 0	$\frac{\ell-k}{2}$, 0	$\frac{\ell+1-k}{2}$, 1 $\frac{\ell-1-k}{2}$, -1
i = 1	$\frac{\ell+2-k}{2}$, 1 $\frac{\ell-k}{2}$, -1	$\frac{\ell+1-k}{2}$, 0
i = -1	$\frac{\ell-k}{2}$, 1 $\frac{\ell-2-k}{2}$, -1	$\frac{\ell-1-k}{2}$, 0

From Table 3 it can be seen that each degree ℓ has either four or five components contributing to the same frequency k, depending on whether ℓ-k is odd or even. Obviously the minimum harmonic degree ℓ that can give rise to a frequency k is given by

$$\ell^{i}_{min} = \begin{cases} \max(|k|-1,m,2) & \text{for } i=0 \\ \max(|k|-2,m,2) & i=1 \\ \max(|k|,m,2) & i=-1 \end{cases} \qquad (5.7)$$

Using the above Table and equations (5.4) - (5.7) a frequency of km cy/rev can be defined and written as

$$\dot{\psi}_{km} = k(\dot{M}+\dot{\omega}) + m(\dot{\Omega}-\dot{\theta}) \qquad (5.8)$$

5.2.2. Determination of the Fourier Coefficients

As it is shown in Chapter 4 the radial orbit error is basically composed of a constant bias, a 1 cy/rev term with constant and time dependent amplitudes, a 2 cy/rev term with time dependent amplitudes and a sum of many periodic terms containing all the frequencies as defined in Section 5.2.1. The first three terms are trivial to bring into a Fourier series form. The summation part of (4.62) can be rewritten as

$$\Delta r = \sum_{k} \sum_{m} \Delta r_{km} \qquad (5.9)$$

where

$$\Delta r_{km} = \sum_{i} \sum_{\ell^{i}_{min}} \sum_{p,q} A^{i}_{\ell mpq} \cos(\dot{\psi}_{km}\Delta t + \psi_{\ell mpqai_o}) \qquad (5.10)$$

which shows that a wave of frequency km is a sum of waves of the same frequency with amplitudes and phases that are generally not identical. So in order to form the main wave of frequency km all the components with different phases have to be combined. From (4.16) we obtain

$$\psi_{\ell mpqai_o} = (\ell-2p+q+i)M_o + (\ell-2p)\omega_o + m(\Omega_o-\theta_o) + C \qquad (5.11)$$

where

$$C = -\frac{\pi}{2}\left[a+\frac{1}{2}(1-(-1)^{\ell-m})\right] \qquad (5.12)$$

Depending on whether ℓ-k is even or odd, the combinations of ℓ,p,q as shown in Table 3 lead to the following different phases that are shown in Table 4 for m=0.

Table 4

Phases for p,q from Table 3 that generate a frequency k.

modulation	ℓ-k even	ℓ-k odd
	p,q	p,q
i = 0	$k(M_o+\omega_o) + C$	$k(M_o+\omega_o) + C - \omega_o$ $k(M_o+\omega_o) + C - \omega_o$
i = 1	$k(M_o+\omega_o) + C - 2\omega_o$ $k(M_o+\omega_o) + C$	$k(M_o+\omega_o) + C - \omega_o$
i = -1	$k(M_o+\omega_o) + C$ $k(M_o+\omega_o) + C + 2\omega_o$	$k(M_o+\omega_o) + C + \omega_o$

Table 4 shows that the individual phases are all composed by a common phase which is shifted by integer multiples of ω_o. Denoting by

$$\psi_{kmo} = k(M_o+\omega_o) + m(\Omega_o-\theta_o) \qquad (5.13)$$

the phases of equation (5.11) become

$$\psi_{\ell mpqai_o} = \psi_{kmo} + C + j\omega \qquad (5.14)$$

where j takes values in the range [-2,2] consistent with Tables 3 and

4. After some manipulation equation (5.10) becomes

$$\Delta r_{km} = \sum_{\ell} \sum_{a} \Delta C_{\ell ma} \left[A_{km\ell} \cos(\dot{\psi}_{km} \Delta t + \psi_{kmo} + C) + B_{km\ell} \sin(\dot{\psi}_{km} \Delta t + \psi_{kmo} + C) \right] \tag{5.15}$$

where

$$A_{km\ell} = A_{km\ell_o} + A_{km\ell_1} \cos\omega_o + A_{km\ell_2} \cos 2\omega_o \tag{5.16}$$

$$B_{km\ell} = B_{km\ell_1} \sin\omega_o + B_{km\ell_2} \sin 2\omega_o \tag{5.17}$$

and

$$A_{km\ell_o} = \begin{cases} A^{o}_{\ell_m \frac{\ell-k}{2} o} + A^{1}_{\ell_m \frac{\ell-k}{2} -1} + A^{-1}_{\ell_m \frac{\ell-k}{2} 1} & \ell-k \text{ even} \\ 0 & \ell-k \text{ odd} \end{cases}$$

$$A_{km\ell_1} = \begin{cases} 0 \\ A^{o}_{\ell_m \frac{\ell-1-k}{2} -1} + A^{o}_{\ell_m \frac{\ell+1-k}{2} -1} + A^{1}_{\ell_m \frac{\ell+1-k}{2} o} + A^{-1}_{\ell_m \frac{\ell-1-k}{2} o} \end{cases} \tag{5.18}$$

$$B_{km\ell_1} = \begin{cases} 0 \\ -A^{o}_{\ell_m \frac{\ell-1-k}{2} -1} + A^{o}_{\ell_m \frac{\ell+1-k}{2} -1} + A^{o}_{\ell_m \frac{\ell+1-k}{2} o} - A^{-1}_{\ell_m \frac{\ell-1-k}{2} o} \end{cases}$$

$$A_{km\ell_2} = \begin{cases} A^{1}_{\ell_m \frac{\ell+2-k}{2} 1} + A^{-1}_{\ell_m \frac{\ell-k-2}{2} -1} \\ 0 \end{cases}$$

$$B_{km\ell_2} = \begin{cases} A^{1}_{\ell_m \frac{\ell+2-k}{2} 1} - A^{-1}_{\ell_m \frac{\ell-k-2}{2} -1} \\ 0 \end{cases}$$

The coefficients in these equations are obtained from (4.63). In equation (5.15) the summation over ℓ starts from ℓ_{min} = max(|k|-2,m,2), which is the lower bound of equations (5.7), so that to account for the coefficients $A^{1}{}_{\ell mpq}$. Obviously the coefficients $A^{0}{}_{\ell mpq}$ are zero for ℓ_{min}, while the coefficients $A^{-1}{}_{\ell mpq}$ are zero for both ℓ_{min} and $(\ell_{min}+1)$.

For the final transformation of equation (5.15), to bring it into a Fourier series form, we have to use (5.12) for the constant C, write the summation over 'a' explicitly, and apply some trigonometric identities. Then equation (5.15) becomes

$$\Delta r_{km} = C_{km}\cos\dot{\psi}_{km}\Delta t + S_{km}\sin\dot{\psi}_{km}\Delta t \tag{5.19}$$

where

$$C_{km} = D_{km}\cos\psi_{kmo} + E_{km}\sin\psi_{kmo} \tag{5.20}$$

$$S_{km} = E_{km}\cos\psi_{kmo} - D_{km}\sin\psi_{kmo} \tag{5.21}$$

with

$$D_{km} = \sum_{\ell} \begin{cases} D_{km\ell} & \ell-m \text{ even} \\ -E_{km\ell} & \ell-m \text{ odd} \end{cases} \tag{5.22}$$

$$E_{km} = \sum_{\ell} \begin{cases} E_{km\ell} & \ell-m \text{ even} \\ D_{km\ell} & \ell-m \text{ odd} \end{cases} \tag{5.23}$$

and

$$D_{km\ell} = \Delta C_{\ell m} A_{km\ell} - \Delta s_{\ell m} B_{km\ell} \tag{5.24}$$

$$E_{km\ell} = \Delta S_{\ell m} A_{km\ell} + \Delta C_{\ell m} B_{km\ell} \tag{5.25}$$

Equation (5.18) can also be written in terms of its amplitude and phase

$$\Delta r_{km} = A_{km}\cos(\dot{\psi}_{km}\Delta t - \psi_{km}) \tag{5.26}$$

where the amplitude at frequency km is

$$A_{km} = (C_{km}^2 + S_{km}^2)^{1/2} \tag{5.27}$$

and the phase is

$$\psi_{km} = \tan^{-1}\frac{S_{km}}{C_{km}} \tag{5.28}$$

Then the total radial error representing the summation part of (4.62) can be written in either of the two equivalent forms

$$\Delta r = \sum_k \sum_m (C_{km}\cos\dot{\psi}_{km}\Delta t + S_{km}\sin\dot{\psi}_{km}\Delta t) \tag{5.29}$$

or

$$\Delta r = \sum_k \sum_m A_{km}\cos(\dot{\psi}_{km}\Delta t - \psi_{km}) \tag{5.30}$$

The bias and 1 cy/rev terms in (4.62) become

$$\Delta r_o = -\Delta a_o \tag{5.31}$$

$$\Delta r_1 = C_1\cos\dot{M}\Delta t + S_1\sin\dot{M}\Delta t \tag{5.32}$$

or $\Delta r_1 = A_1\cos(\dot{M}\Delta t - \bar{M})$

where

$$C_1 = (e_o\Delta a_o + a_o\Delta e_o)\cos M_o + e_o a_o \Delta M_o \sin M_o \tag{5.33}$$

$$S_1 = -(e_o\Delta a_o + a_o\Delta e_o)\sin M_o + e_o a_o \Delta M_o \cos M_o \tag{5.34}$$

$$A_1 = (C_1^2+S_1^2)^{1/2} \tag{5.35}$$

$$\bar{M} = \tan^{-1} \frac{S_1}{C_1} \tag{5.36}$$

while similar expressions exist for the oscillations with amplitudes that increase with time.

Equations (5.29) or (5.30) are very convenient to compute various statistics of the periodic orbit error. More specifically the amplitude spectrum is readily obtained by the amplitudes A_{km} while the average power by degree, order, or cumulative, over the period of the orbit can be easily computed. The average power for a Fourier series in general, is defined by

$$P = \frac{1}{T} \int_0^T \left[\sum_i (a_i \cos\dot{x}_i t + b_i \sin\dot{x}_i t)\right]^2 dt \tag{5.37}$$

where T is the integration limit and is chosen such that it is longer than the period corresponding to any $\dot{x}_i \pm \dot{x}_j$ that is formed after the expansion of the square of the series. Integration of (5.37) leads to

$$P = \frac{1}{2} \sum_i (a_i^2+b_i^2) \tag{5.38}$$

Based on (5.38) the RMS orbit error over a period longer than the period corresponding to any frequency $\dot{\psi}_{km} \pm \dot{\psi}_{\ell j}$ will be

$$||\Delta r||^{1/2} = \left[\frac{1}{2} \sum_{km} (C_{km}^2+S_{km}^2)\right]^{1/2} \tag{5.39}$$

Restricting the summation to be only over k, we can have the RMS orbit error by order

$$||\Delta r||_m^{1/2} = \left[\frac{1}{2} \sum_k (C_{km}^2+S_{km}^2)\right]^{1/2} \tag{5.40}$$

Finally the RMS orbit error by degree, after some manipulation, becomes

$$\|\Delta r\|_{\ell}^{\frac{1}{2}} = \left[\frac{1}{2}\sum_{km}(A^2_{km\ell}+B^2_{km\ell})(\Delta C^2_{\ell m}+\Delta S^2_{\ell m})\right]^{\frac{1}{2}} \qquad (5.41)$$

By breaking (5.41) even further, one can obtain the RMS effect for any individual degree and order. This effect is summed only over k that has a $k_{min} = \ell$ and takes both positive and negative values absolutely greater or equal to k_{min}.

5.2.3. Numerical Results

In this section, some numerical estimates of the radial error, its frequency content and its statistics will be given. These numerical estimates will be computed based on the orbit characteristics of the Seasat satellite and a set of "known" potential coefficient errors up to harmonic degree 36. This harmonic degree is chosen because the sensitivity of Seasat to gravity field perturbations of higher harmonics is negligible, with the possible exception of some resonant terms.

To create the potential coefficient errors the half differences between the GEM10B and GRIM3L1 (Reigber et al., 1985) gravity models were used. Both these fields are given complete to degree and order 36 and have been independently derived, although not from entirely independent data. They are both produced by combining satellite observations, surface gravity measurements and altimeter data. Their greatest differences are, the larger number of satellites used in the GEM10B solution and the more recent data used in the GRIM3L1 solution, particularly the laser tracking data of Lageos and the Seasat altimeter data. Both of these fields should represent reasonable global models of the earth's gravity field, so their differences, divided by two, could be a possible realization of their errors.

The radial orbit error has been computed for the first six day arc of Seasat satellite, using equations (4.62), (4.78) and (4.83) and is shown in Figure 13. It may be seen that the most dominant features of the error are, the 1 cy/rev effects, as well as the daily terms. Note also the gradual increase of the error with time, that is due primarily to the eccentricity resonant errors and second order effects.

The error for the same six day arc has also been computed using the Fourier series equations (5.16) - (5.29). The agreement between the two methods is at the 1 mm level, indicating that the Fourier series is equally accurate to the original error expression. After this consistency check, the Fourier series equations were used to generate the radial orbit errors for all six day arcs of Seasat. The results indicate that the periodic part of the first order error (equation 5.29) is practically the same for all the arcs. Its variations from arc to arc is on the order of 1-2 cm in individual values. The RMS error

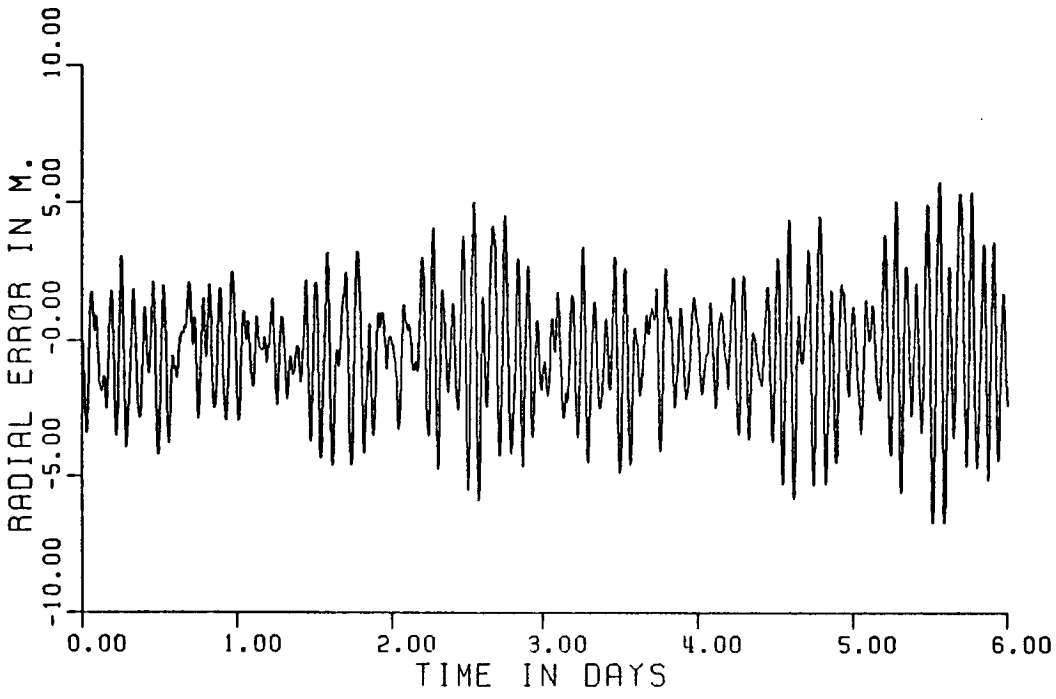

Figure 13. Seasat Radial Orbit Error Computed Analytically Using the GEM10B - GRIM3L1 Half Differences as Potential Coefficient Errors.

for any of the arcs is 1.65 meters as computed by (5.39). The amplitude spectrum of the error, up to 6 cy/rev, for the first Seasat arc (and for all arcs) is shown in Figure 14. In this Figure we observe that most of the energy of the error is below 2 cy/rev. Tests have shown that the total energy of the error above 6 cy/rev is about 5 mm. It can be seen that there is no energy at the 1 cy/rev frequency arising from implemetation of (5.29). The same is true for the zero frequency and the 2 cy/rev frequency. This is partly due to the fact that the zonal terms (that give rise to these frequencies) are very small, and partly because the sensitivity of the spectrum at that frequency is extremely small. This sensitivity has been computed by assuming a uniform potential coefficient error, of $5 \cdot 10^{-9}$, for all degrees and orders. This spectrum is shown in Figure 15, where indeed there is almost no radial error at those frequencies.

The constant term and the 1 cy/rev error have been computed by (5.31) - (5.36) and are clearly dependent on the particular arc for which they are computed. The magnitudes of these two types of errors are shown in Table 5 for all the arcs of Seasat. As it can be seen, both errors have significant variations from arc to arc. The 1 cy/rev error is the dominant error for all arcs. Using these values and the RMS periodic error of 1.65 m, the total RMS error for each arc has been computed and is shown in Table 5.

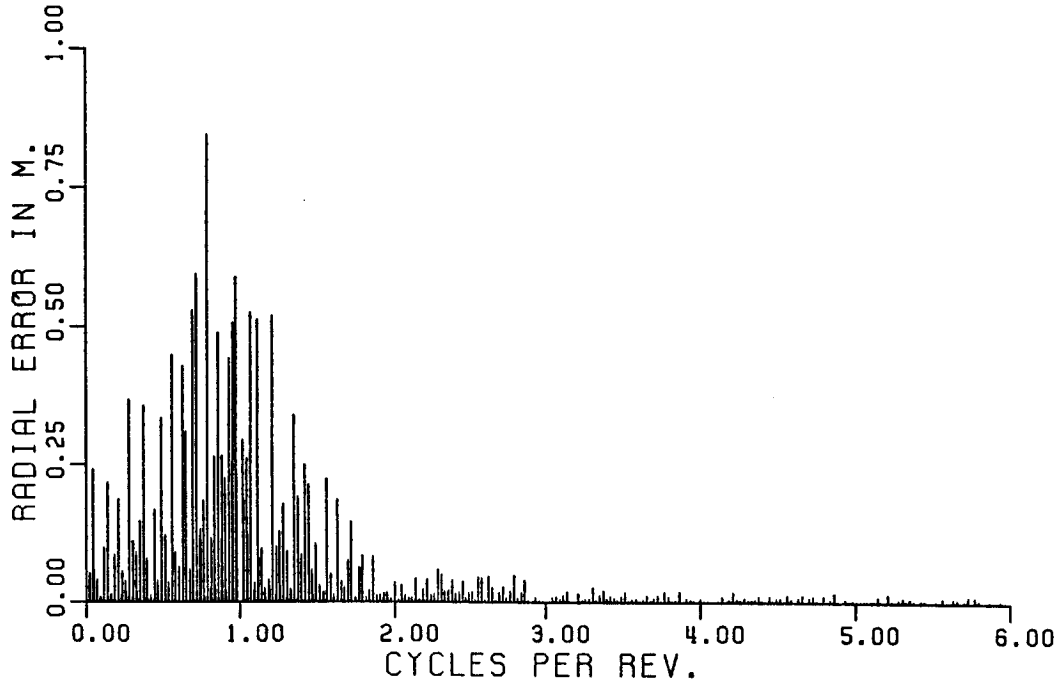

Figure 14. Amplitude Spectrum of Seasat Radial Orbit Error Using the GEM10B - GRIM3L1 Half Differences as Potential Coefficient Errors.

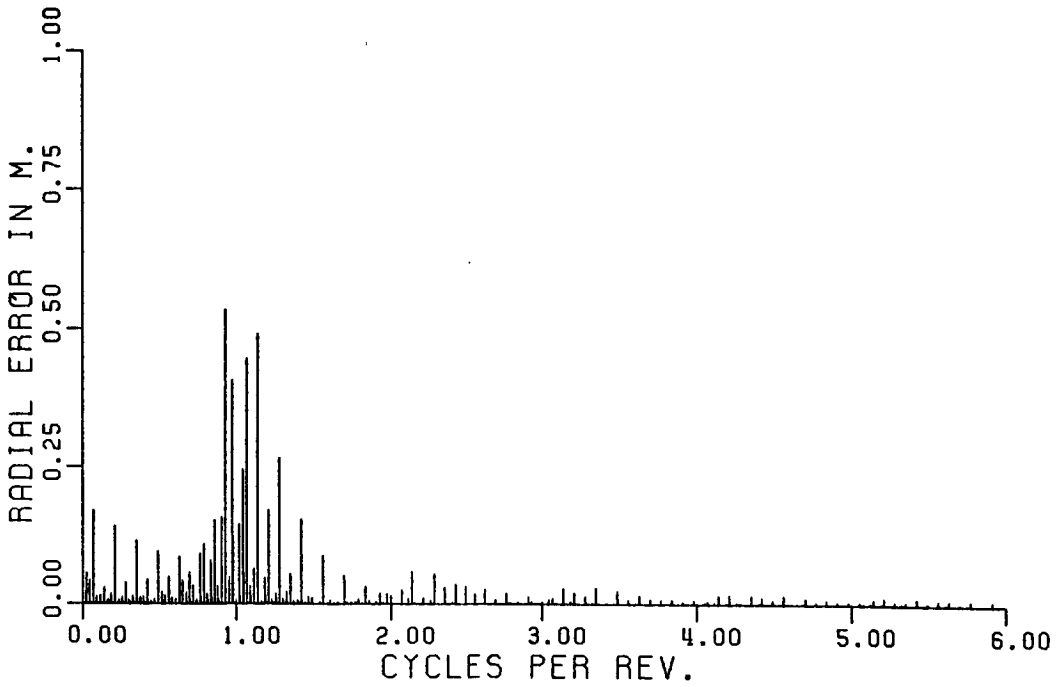

Figure 15. Amplitude Spectrum of Seasat Radial Orbit Error Using a Uniform Potential Coefficient Error of $5 \cdot 10^{-9}$.

Table 5

Constant, 1 cy/rev and Total RMS Radial Orbit Error for Seasat Arcs Using the GEM10B - GRIM3L1 Half Differences as Potential Coefficient Errors.

Seasat Arc	Constant	1 cy/rev	Total RMS
1	0.33 m	0.79 m	1.78 m
2	-0.44	1.58	2.05
3	0.57	2.37	2.43
4	-0.43	2.96	2.70
5	-0.18	3.35	2.90
6	-0.51	2.05	2.27
7	-0.07	1.30	1.90
8	-0.16	1.03	1.82
9	-0.47	2.59	2.52
10	0.75	2.68	2.63
11	1.10	3.63	3.25
12	0.09	2.68	2.52

Using equations (5.40) and (5.41) the RMS values by harmonic degree, harmonic order and individual degrees and orders have also been computed. The RMS errors by order for the (GEM10B - GRIM3L1)/2 errors and the uniform errors are shown in Figures 16 and 17. From both Figures we can see the higher sensitivity of the errors to harmonic order 1 (daily errors), to orders 14, 15, and 16 (primary shallow resonance) and to order 29 (secondary shallow resonance). Comparing the two Figures we can see the definite large discrepancies of the GEM10B and GRIM3L1 gravity fields between orders 5 to 12. Additional conclusions can be obtained from the RMS errors by degree, by comparing Figures 18 and 19. More specifically, there is a much higher sensitivity of the error to odd degrees, for degrees below the primary shallow resonance, and there is a change in sensitivity for degrees between resonant degrees. Again it becomes clear that the GEM10B and GRIM3L1 fields have large discrepancies in degrees 5 to 12. Table 6 containing the RMS errors for individual degrees and orders shows basically the same type of information.

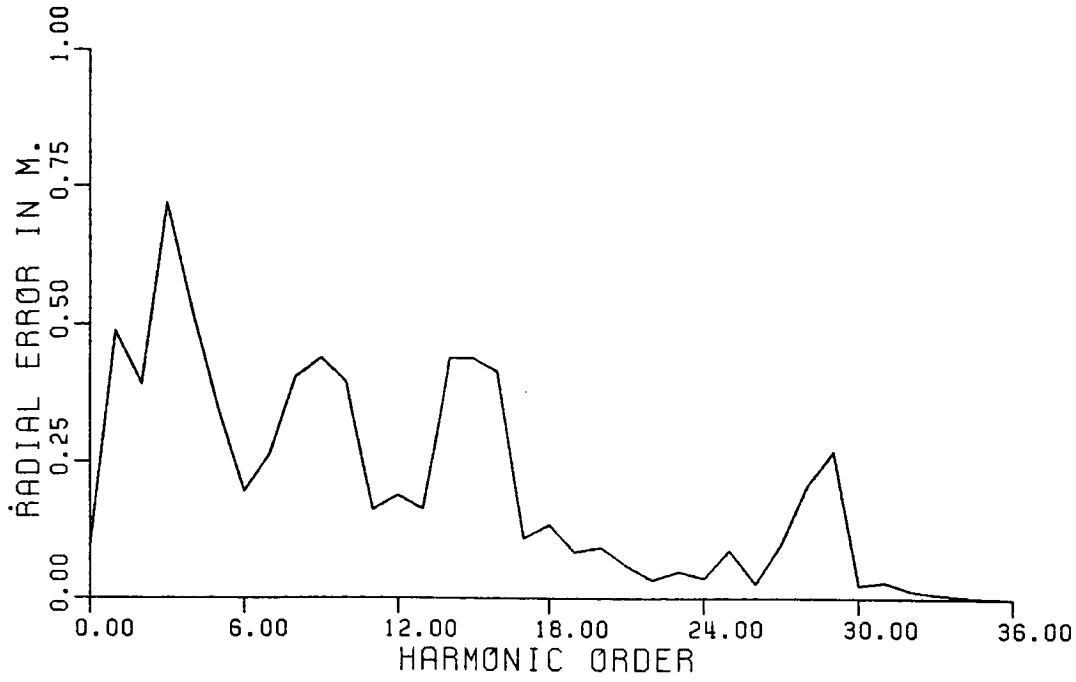

Figure 16. RMS Seasat Radial Orbit Error by Harmonic Order Using the GEM10B-GRIM3L1 Half Differences as Potential Coefficient Errors.

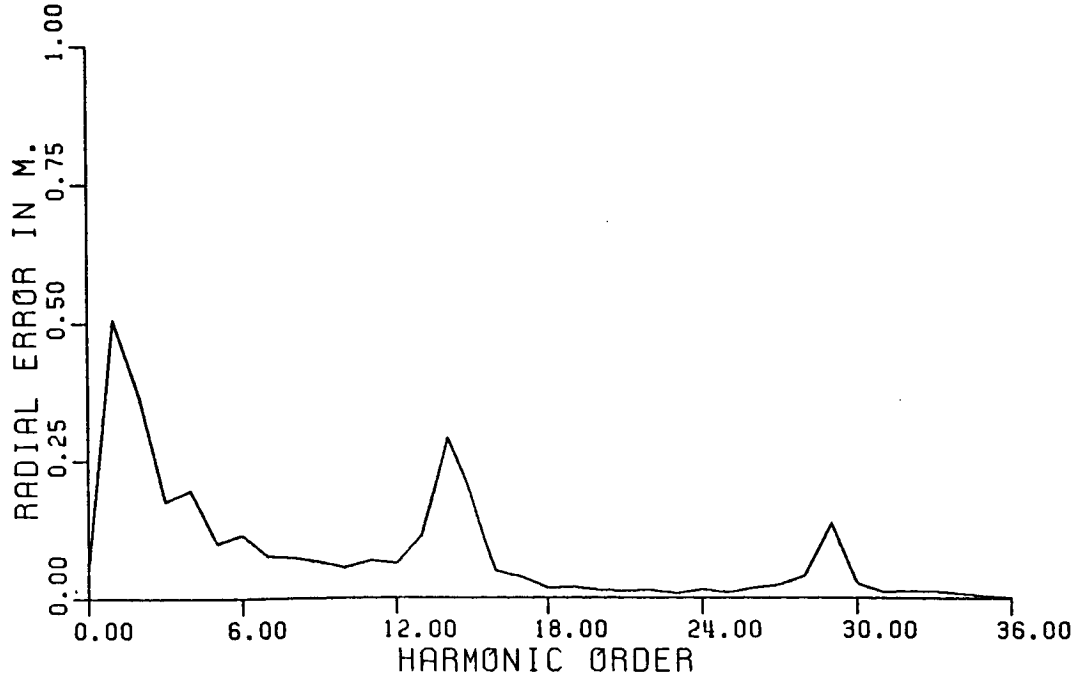

Figure 17. RMS Seasat Radial Orbit Error by Harmonic Order Using a Uniform Potential Coefficient Error of $5 \cdot 10^{-9}$.

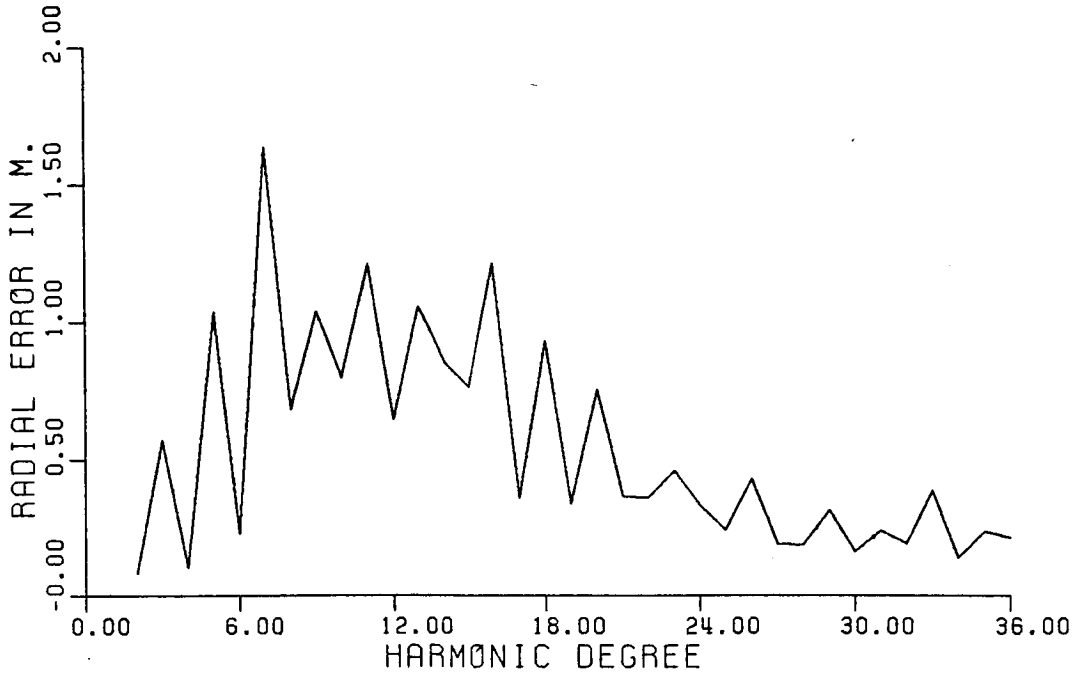

Figure 18. RMS Seasat Radial Orbit Error by Harmonic Degree Using the GEM10B-GRIM3L1 Half Differences as Potential Coefficient Errors.

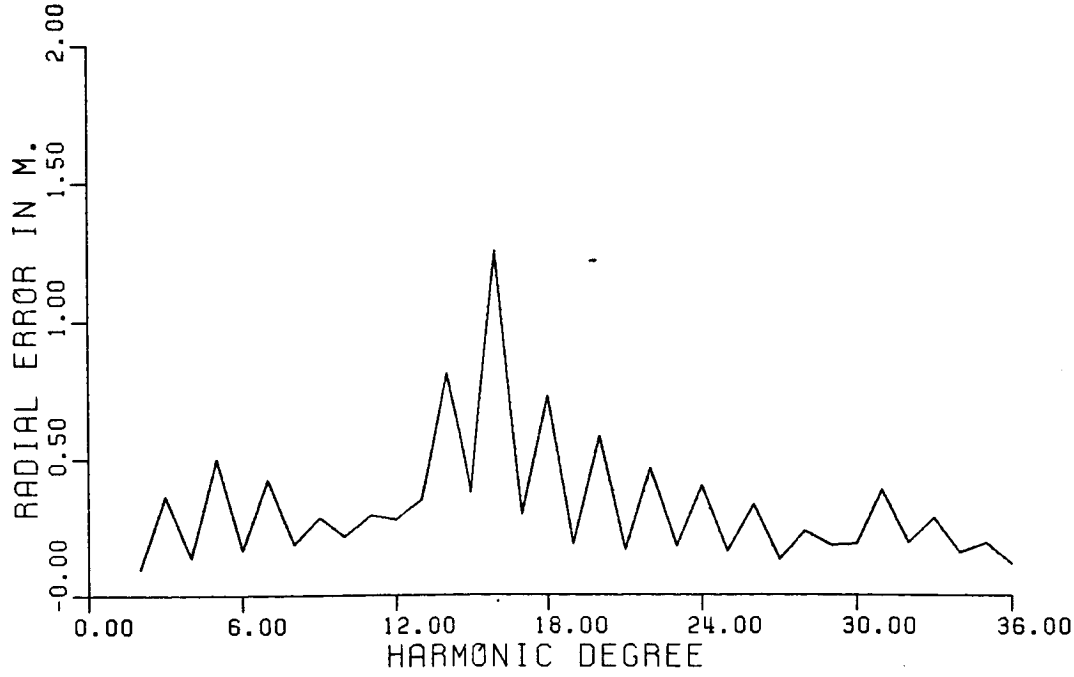

Figure 19. RMS Seasat Radial Orbit Error by Harmonic Degree Using a Uniform Potential coefficient Error of $5 \cdot 10^{-9}$.

Table 6

RMS of Seasat Radial Orbit Error for Each Coefficient Degree and Order Using the GEM10B - GRIM3L1 Half Differences as Potential Coefficient Errors. Units are in Centimeters

	0	1	2	3	4	5	6	7	8	9	10	11	12	13	14	15	16	17	18	19	20
2	2	0	7																		
3	0	24	33	38																	
4	0	7	1	4	5																
5	0	65	34	57	25	37															
6	1	15	8	12	5	2	6														
7	1	118	75	70	14	37	16	10													
8	3	16	4	24	14	16	2	21	53												
9	1	33	47	54	31	37	27	13	21	25											
10	3	2	36	2	46	4	7	27	21	30	25										
11	0	60	76	5	57	16	6	10	19	21	15	11									
12	0	8	9	9	9	3	1	3	14	31	3	34	37								
13	0	87	38	32	14	7	14	2	4	17	9	9	2	3							
14	0	11	4	13	8	10	2	17	6	19	57	8	1	9	51						
15	0	68	3	5	8	23	3	7	13	2	6	4	2	2	2	10					
16	0	15	0	9	1	7	3	4	6	12	10	14	10	13	104	39	30				
17	0	15	23	4	5	1	5	3	1	6	0	3	0	0	2	15	4	8			
18	2	4	8	5	6	5	3	2	3	10	13	3	2	35	51	47	43	2	8		
19	0	13	20	3	17	1	1	1	4	3	3	1	1	1	1	4	7	3	8	1	
20	4	1	4	1	3	2	4	3	7	2	1	7	12	38	49	24	15	14	17	6	0
21	0	28	4	1	14	1	0	0	2	2	2	1	1	0	3	4	3	2	3	11	8
22	2	3	1	4	0	1	3	3	5	1	3	3	6	10	16	17	3	6	4	10	13
23	0	42	6	8	4	2	1	1	0	0	0	0	1	1	3	5	0	0	1	3	1
24	0	0	0	1	0	4	0	4	1	3	1	1	2	13	19	18	3	8	3	1	3
25	0	21	2	4	0	1	0	4	0	1	0	0	0	0	2	1	0	0	1	4	4
26	0	0	0	1	1	2	0	2	0	1	0	2	1	7	24	32	4	5	2	2	0
27	0	6	7	4	0	2	0	4	0	2	0	0	0	0	1	1	1	0	1	1	1
28	0	0	1	0	1	1	1	0	1	1	1	3	0	5	5	13	6	2	3	1	0
29	0	2	12	0	1	0	0	0	0	0	0	1	0	0	0	1	1	0	2	0	0
30	1	0	1	0	0	0	0	0	1	1	2	1	2	5	6	9	0	3	0	1	0
31	0	2	6	1	0	0	0	0	0	0	1	0	0	0	0	1	0	0	0	0	0
32	0	0	0	0	1	0	0	0	0	0	0	0	3	1	15	5	5	1	0	1	0
33	0	6	2	1	0	2	0	0	0	0	0	0	0	0	1	1	0	0	0	1	0
34	0	0	0	0	0	0	0	0	0	0	1	0	1	0	12	2	1	0	0	0	0
35	0	10	0	2	0	1	0	0	0	0	0	0	0	0	0	0	1	0	0	0	0
36	0	0	0	0	0	0	0	0	0	0	0	0	0	1	20	4	1	0	0	0	0

	21	22	23	24	25	26	27	28	29	30	31	32	33	34	35	36
21	2															
22	7	2														
23	4	5	1													
24	3	3	2	0												
25	1	1	4	2	2											
26	1	0	0	4	0	0										
27	0	0	2	2	12	1	4									
28	1	1	1	1	1	0	0	0								
29	1	1	5	2	3	7	8	23	9							
30	1	0	0	1	0	0	0	7	1	0						
31	0	0	1	2	4	1	10	14	12	0	0					
32	0	1	0	0	0	0	0	0	5	1	0	0				
33	0	1	0	0	1	2	1	3	37	4	2	0	0			
34	0	1	0	0	0	0	0	0	0	2	3	1	0	0		
35	0	0	1	0	0	1	2	12	15	1	3	2	1	0	0	
36	0	0	0	0	0	0	0	0	2	0	0	0	1	0	0	0

5.3 Approximate Expressions of the Radial Error for a Near Circular Orbit

The equations for the radial orbit error that have been derived in Chapter 4 and in the previous sections are general equations involving no approximations except for the truncation of the series containing the eccentricity functions to q = ±1 in the Fourier series form. The general expression for the Fourier series for any order of eccentricity can be easily computed by extending the Tables 3 and 4 to account for the higher orders. Then equations (5.16), (5.17), and (5.18) can also be extended accordingly.

In this section simpler forms for equations (4.62) and (5.29) will be obtained, using the explicit values of $G_{\ell pq}(e)$ as given by equation (4.18) for small eccentricities, and recognizing that Δa is primarily sensitive to terms containing $G_{\ell p0}(e)$ while Δe, ΔM are sensitive to terms containing $G_{\ell p\pm1}(e)$. A notation consistent with equation (4.13) will be adopted. Based on the above we obtain

$$\Delta a_{\ell mp0} = na\left(\frac{a_e}{a}\right)^{\ell} F_{\ell mp} \frac{2(\ell-2p)}{\dot{\psi}_{\ell mp0}} S_{\ell mp0} \tag{5.42}$$

$$\Delta e_{\ell mp\pm1} = n\left(\frac{a_e}{a}\right)^{\ell} F_{\ell mp} \left[\frac{3\ell-4p+1}{2\dot{\psi}_{\ell mp1}} S_{\ell mp1} + \frac{-\ell+4p+1}{2\dot{\psi}_{\ell mp-1}} S_{\ell mp-1}\right] \tag{5.43}$$

$$\Delta M_{\ell mp\pm1} = -\frac{\mu}{e}\left(\frac{a_e}{a}\right)^{\ell} F_{\ell mp}\left[\frac{-\ell+4p+1}{2\dot{\psi}_{\ell mp-1}} \bar{S}_{\ell mp-1} + \frac{3\ell-4p+1}{2\dot{\psi}_{\ell mp1}} \bar{S}_{\ell mp1}\right] \tag{5.44}$$

In these equations $S_{\ell mpq}$ is

$$S_{\ell mpq} = S_{\ell mpq}(\Delta t) - S_{\ell mpq}(o) \tag{5.45}$$

and has the functional form given by (4.14). $\bar{S}_{\ell mpq}$ is the integrated $S_{\ell mpq}$ with respect to its argument, it has the form

$$\bar{S}_{\ell mpq} = \begin{Bmatrix} \Delta C_{\ell m} \\ -\Delta S_{\ell m} \end{Bmatrix} \sin[(\ell-2p+q)M + (\ell-2p)\omega + m(\Omega-\theta)]$$

$$- \begin{Bmatrix} \Delta S_{\ell m} \\ \Delta C_{\ell m} \end{Bmatrix} \cos[(\ell-2p+q)M + (\ell-2p)\omega + m(\Omega-\theta)] \qquad (5.46)$$

and is equal to

$$\bar{S}_{\ell mpq} = \bar{S}_{\ell mpq}(\Delta t) - \bar{S}_{\ell mpq}(o) \qquad (5.47)$$

Using (5.42) - (5.44) in (4.46) and neglecting the term $e\Delta a$ we obtain

$$\Delta r_{\ell mp} = an\left(\frac{a_e}{a}\right)^{\ell} F_{\ell mp}\left[\frac{2(\ell-2p)}{\dot{\psi}_{\ell mpo}} S_{\ell mpo}\right.$$

$$+ \frac{4p-3\ell-1}{2\dot{\psi}_{\ell mp1}} \left(S_{\ell mp1}\cos M + \bar{S}_{\ell mp1}\sin M\right)$$

$$\left. + \frac{4p-\ell+1}{2\dot{\psi}_{\ell mp-1}} \left(S_{\ell mp-1}\cos M - \bar{S}_{\ell mp-1}\sin M\right)\right] \qquad (5.48)$$

Then using (5.45) and (5.47) and the equalities

$$S_{\ell mp1}(\Delta t)\cos M + \bar{S}_{\ell mp1}(\Delta t)\sin M = S_{\ell mpo}(\Delta t)$$

$$S_{\ell mp-1}(\Delta t)\cos M + \bar{S}_{\ell mp-1}(\Delta t)\sin M = S_{\ell mpo}(\Delta t) \qquad (5.49)$$

$$S_{\ell mp1}(o)\cos M + \bar{S}_{\ell mp1}(o)\sin M = S_{\ell mpo}(o)\cos\dot{M}\Delta t + \bar{S}_{\ell mpo}(o)\sin\dot{M}\Delta t$$

$$S_{\ell mp-1}(o)\cos M - \bar{S}_{\ell mp-1}(o)\sin M = S_{\ell mpo}(o)\cos\dot{M}\Delta t - \bar{S}_{\ell mpo}(o)\sin\dot{M}\Delta t$$

we obtain for the periodic first order radial orbit error the following expression

$$\Delta r_{G1} = \Delta r_p - \Delta r_o - \Delta r_1 \tag{5.50}$$

with

$$\Delta r_p = \sum_{\ell mp} \left[A_{\ell mp} + B_{\ell mp} + C_{\ell mp}\right] S_{\ell mpo}(\Delta t) \tag{5.51}$$

$$\Delta r_o = \sum_{\ell mp} A_{\ell mp} S_{\ell mpo}(o) \tag{5.52}$$

$$\Delta r_1 = \sum_{\ell mp} \left[(B_{\ell mp} + C_{\ell mp}) S_{\ell mpo}(o) \cos\dot{M}\Delta t + (B_{\ell mp} - C_{\ell mp}) \bar{S}_{\ell mpo}(o) \sin\dot{M}\Delta t\right] \tag{5.53}$$

where

$$\begin{aligned} A_{\ell mp} &= J_{\ell mp} \frac{2(\ell-2p)}{\dot{\psi}_{\ell mpo}} \\ B_{\ell mp} &= J_{\ell mp} \frac{4p-3\ell-1}{2\dot{\psi}_{\ell mp1}} \\ C_{\ell mp} &= J_{\ell mp} \frac{4p-\ell+1}{2\dot{\psi}_{\ell mp-1}} \end{aligned} \tag{5.54}$$

$$J_{\ell mp} = an\left(\frac{a_e}{a}\right)^{\ell} F_{\ell mp}(i)$$

Equations (5.50) – (5.54) provide an expression for the radial orbit error that is equivalent to (4.62) when the eccentricity is small. These equations have also been computed by Rosborough (1986).

The Fourier series representation of Δr_p can be easily obtained. First the summation of the constant quantities $A_{\ell mp}$, $B_{\ell mp}$, $C_{\ell mp}$ is rearranged by setting $k = \ell - 2p$ and summing over m, k. The sum of these quantities for any ℓ, m, p is

$$A_{\ell mp} + B_{\ell mp} + C_{\ell mp} = J_{\ell mp}\left[\frac{2k}{\dot{\psi}} - \frac{\ell+2k+1}{2(\dot{\psi}+\dot{M})} + \frac{\ell-2k+1}{2(\dot{\psi}-\dot{M})}\right] \tag{5.55}$$

which is equal to

$$A_{\ell mp} + B_{\ell mp} + C_{\ell mp} = J_{\ell mp}\left[\frac{1}{n}\,\frac{(\ell+1)\beta - 2k}{\beta(\beta^2-1)}\right] \tag{5.56}$$

with $\beta = \dfrac{\dot{\psi}}{\dot{M}}$

Using (5.54) for $J_{\ell mp}$ and (4.14) for $S_{\ell mpo}$ and separating the individual phases from the corresponding frequency arguments in the cosines and sines we obtain

$$\Delta r_p = \sum_{k=-\ell_{max}}^{\ell_{max}} \sum_{m=o}^{\ell_{max}} \sum_{\ell=\ell_{min}}^{\ell_{max}} H_{\ell km}\left[C_{\ell km}\cos\dot{\psi}_{km}\Delta t + S_{\ell km}\sin\dot{\psi}_{km}\Delta t\right] \tag{5.57}$$

where

$$H_{\ell km} = a\left(\frac{a_e}{a}\right)^{\ell} F_{\ell m \frac{\ell-k}{2}}\,\frac{\beta(\ell+1)-2k}{\beta(\beta^2-1)} \tag{5.58}$$

$$C_{\ell km} = \begin{pmatrix}\Delta C_{\ell m}\\ -\Delta S_{\ell m}\end{pmatrix}\cos\psi_{kmo} + \begin{pmatrix}\Delta S_{\ell m}\\ \Delta C_{\ell m}\end{pmatrix}\sin\psi_{kmo} \tag{5.59}$$

$$S_{\ell km} = \begin{pmatrix}\Delta S_{\ell m}\\ \Delta C_{\ell m}\end{pmatrix}\cos\psi_{kmo} - \begin{pmatrix}\Delta C_{\ell m}\\ \Delta S_{\ell m}\end{pmatrix}\sin\psi_{kmo} \tag{5.60}$$

The summation in ℓ is made over the harmonic degrees that have the same parity with k. The minimum harmonic degree is given by

$$\ell_{min} = \max(|k|,\ 2,\ m+\mathrm{mod}(|k|-m,2)) \tag{5.61}$$

Equation (5.57) is identical to the one given by Wagner (1985). This equation becomes singular when $\dot{\psi}_{km}=0$ due to resonance with harmonics of order $m\neq 0$ or when $\dot{\psi}_{km}=1$ cy/rev due to secular and long period effects in the mean anomaly and eccentricity arising from even and odd zonal errors. As it is mentioned in Chapter 4 the first type of resonance is not likely to occur for a short arc while the second type of resonance is computed from equations (4.66), (4.67), (4.68) and (4.78). Expressions for these resonant terms, more in the line of this section can be obtained by simply using the specific values of $\tilde{e}^r$ and $\tilde{M}^r$ contained in these equations, and the eccentricity functions as given by (4.18). For the particular case of near zero eccentricities long period effects in the mean anomaly cannot be computed since this formulation breaks down. The resonant effects $e\Delta M^r(t)$ though can be obtained. Making these substitutions we have

$$\Delta e^r(t) = \sum_{\ell_{odd}} n\left(\frac{a_e}{a}\right)^{\ell} F_{\ell_0 \frac{\ell-1}{2}}(\ell-1)\Delta C_{\ell_0}\cos\omega_0 \qquad (5.62)$$

$$e\Delta M^r(t) = \sum_{\ell_{odd}} n\left(\frac{a_e}{a}\right)^{\ell} F_{\ell_0 \frac{\ell-1}{2}}(\ell-1)\Delta C_{\ell_0}\sin\omega_0$$

$$\sum_{\ell_{even}} ne\left(\frac{a_e}{a}\right)^{\ell} F_{\ell_0 \frac{\ell}{2}} \frac{(\ell+1)(\ell-4)}{2} \Delta C_{\ell_0} \qquad (5.63)$$

For the computation of the second term of $e\Delta M^r(t)$ the approximate equality

$$G'_{\ell \frac{\ell}{2}_0}(e) \approx \frac{\ell(\ell+1)}{2} e \qquad (5.64)$$

has been used. From equation (5.63) it becomes obvious that the odd zonal errors have a much greater effect than the even zonal errors, since each of the latter is multiplied by the eccentricity.

5.4 Geographic Representation of the Radial Orbit Error

The equations that have been developed so far describe the temporal characteristics of the radial orbit error in an inertial coordinate system. These results are important for understanding the nature of the orbit error and its evolution in time as well as for computing appropriate statistics. Of equal importance is the understanding of the spatial behavior of the orbit error, both along

and across the subsatellite tracks. A systematic analysis of the spatial behavior of the error requires the functional transformation of the Keplerian elements to geographic coordinates in an earth fixed system. Such transformation can be viewed as the inverse Lagrange transformation where now the $S_{\ell mpq}$ functions have to be transformed into functions of geographic dependence. In order to do that the orbital geometry of the satellite has to be considered. From Kaula (1966, p.32) we have the following relationships between Keplerian elements and the geocentric coordinates of the subsatellite points.

$$\Omega-\theta = \lambda - (a-\Omega) \tag{5.65}$$

$$\cos(a-\Omega) = \frac{\cos(\omega+f)}{\cos\phi} \tag{5.66}$$

$$\sin(a-\Omega) = \frac{\sin(\omega+f)\cos i}{\cos\phi} \tag{5.67}$$

$$\sin(\omega+f) = \frac{\sin\phi}{\sin i} \tag{5.68}$$

$$\cos(\omega+f) = \pm\left(1-\frac{\sin^2\phi}{\sin^2 i}\right)^{\frac{1}{2}} \tag{5.69}$$

where a is the right ascension of the subsatellite point. In equation (5.69), the plus sign corresponds to an ascending arc (ω+f is in the first or fourth quadrant) and the minus sign corresponds to a descending arc (ω+f is in the second or third quadrant).

5.4.1. First Order Periodic Radial Orbit Error

For the implementation of the above equations in one of the expressions developed so far for the first order periodic radial orbit error, the true anomaly f has to be approximated by the mean anomaly M. This is acceptable for nearly circular orbits like the altimetric ones, where the eccentricity can be assumed to be zero. Consistent with this approximation, the expression of the first order periodic radial orbit error that has to be used is the approximation that is given by equations (5.50) - (5.54). As it will be seen the desired transformation of these equations becomes exact. The same cannot be true when higher orders of eccentricity are also considered because of the additional term $-q\dot{\omega}$ that enters the $S_{\ell mpq}$ functions. Then the radial orbit error of higher orders becomes time dependent

without a strict relation to geographic location.

The quantity that has to be transformed in equation (5.51) is $S_{\ell mpo}$. Using (5.65) we obtain

$$S_{\ell mpo} = \begin{pmatrix} \Delta C_{\ell m} \\ -\Delta S_{\ell m} \end{pmatrix} \cos[(\ell-2p)(M+\omega) + m\lambda - m(a-\Omega)]$$

$$+ \begin{pmatrix} \Delta S_{\ell m} \\ \Delta C_{\ell m} \end{pmatrix} \sin[(\ell-2p)(M+\omega) + m\lambda - m(a-\Omega)] \qquad (5.70)$$

Applying trigonometric identities and setting for simplicity

$$\ell-2p = k$$

$$M+\omega = v \qquad (5.71)$$

$$a-\Omega = u$$

we obtain

$$S_{\ell mpo} = \left[\begin{pmatrix} \Delta C_{\ell m} \\ -\Delta S_{\ell m} \end{pmatrix} \cos(kv-mu) + \begin{pmatrix} \Delta S_{\ell m} \\ \Delta C_{\ell m} \end{pmatrix} \sin(kv-mu) \right] \cos m\lambda$$

$$+ \left[\begin{pmatrix} \Delta S_{\ell m} \\ \Delta C_{\ell m} \end{pmatrix} \cos(kv-mu) - \begin{pmatrix} \Delta C_{\ell m} \\ -\Delta S_{\ell m} \end{pmatrix} \sin(kv-mu) \right] \sin m\lambda \qquad (5.72)$$

The next step in the transformation is to express the cosine and sine of multiple arcs with respect to single arcs. This computation is made in Appendix D. Then

$$\cos(kv-mu) = \sum_{s=o}^{|k|} \sum_{t=o}^{m} \begin{pmatrix} |k| \\ s \end{pmatrix} \begin{pmatrix} m \\ t \end{pmatrix} (-1)^{\beta} \cos^{|k|-s} v \, \sin^{s} v \, \cos^{m-t} u \, \sin^{t} u \qquad (5.73)$$

where s,t have the same parity and

$$\beta = \begin{cases} \frac{3s+t}{2} & k>0 \\ \frac{s+t}{2} & k<0 \end{cases} \tag{5.74}$$

$$\sin(kv-mu) = \sum_{s=0}^{|k|} \sum_{t=0}^{m} \binom{|k|}{s} \binom{m}{t} (-1)^c \cos^{|k|-s} v \sin^s v \cos^{m-t} u \sin^t u \tag{5.75}$$

where s,t have different parities and

$$c = \begin{cases} \frac{3s+t+1}{2} & k>0 \\ \frac{s+t+1}{2} & k<0 \end{cases} \tag{5.76}$$

Using (5.66) - (5.69) in (5.73) and (5.75) we obtain

$$\cos(kv-mu) = (\pm 1)^{|k|+m} \frac{1}{\cos^m \phi} \sum_s \sum_t \binom{|k|}{s} \binom{m}{t} (-1)^\beta \cdot \left(1 - \frac{\sin^2\phi}{\sin^2 i}\right)^{\frac{|k|+m-s-t}{2}} \left(\frac{\sin\phi}{\sin i}\right)^{s+t} \cos^t i \tag{5.77}$$

$$\sin(kv-mu) = (\pm 1)^{|k|+m+1} \frac{1}{\cos^m \phi} \sum_s \sum_t \binom{|k|}{s} \binom{m}{t} (-1)^c \cdot \left(1 - \frac{\sin^2\phi}{\sin^2 i}\right)^{\frac{|k|+m-s-t}{2}} \left(\frac{\sin\phi}{\sin i}\right)^{s+t} \cos^t i \tag{5.78}$$

where β, c are given by (5.74) and (5.76) and s,t have the same parity in (5.77) and a different parity in (5.78). In a more compact form we write

$$\cos(kv-mu) = (\pm 1)^{|k|+m} Q_{\ell mp}(\phi) = (\pm 1)^{\ell-m} Q_{\ell mp}(\phi) \tag{5.79}$$

$$\sin(kv-mu) = (\pm 1)^{|k|+m} R_{\ell mp}(\phi) = (\pm 1)^{\ell-m+1} R_{\ell mp}(\phi) \qquad (5.80)$$

where the exponents of (±1) have been changed based on the fact that k and ℓ have always the same parity. Obviously $Q_{\ell mp}$ is symmetric and $R_{\ell mp}$ is antisymmetric with respect to the equator. Substituting these quantities in (5.72) and taking the appropriate potential coefficient errors, depending on whether ℓ-m is even or odd, we get

$$S_{\ell mpo} = Q_{\ell mp}(\Delta C_{\ell m}\cos m\lambda + \Delta S_{\ell m}\sin m\lambda)$$

$$-(\pm R_{\ell mp})(\Delta C_{\ell m}\sin m\lambda - \Delta S_{\ell m}\cos m\lambda) \qquad (5.81)$$

when ℓ-m is even, and

$$S_{\ell mpo} = R_{\ell mp}(\Delta C_{\ell m}\cos m\lambda + \Delta S_{\ell m}\sin m\lambda)$$

$$\pm Q_{\ell mp}(\Delta C_{\ell m}\sin m\lambda - \Delta S_{\ell m}\cos m\lambda) \qquad (5.82)$$

when ℓ-m is odd. Combining (5.81) and (5.82) we finally obtain

$$S_{\ell mpo} = \tilde{Q}_{\ell mp}(\Delta C_{\ell m}\cos m\lambda + \Delta S_{\ell m}\sin m\lambda)$$

$$\pm \tilde{R}_{\ell mp}(\Delta C_{\ell m}\sin m\lambda - \Delta S_{\ell m}\cos m\lambda) \qquad (5.83)$$

where

$$\tilde{Q}_{\ell mp} = \begin{cases} Q_{\ell mp} & \ell-m \text{ even} \\ R_{\ell mp} & \ell-m \text{ odd} \end{cases} \qquad (5.84)$$

$$\tilde{R}_{\ell mp} = \begin{cases} -R_{\ell mp} & \ell-m \text{ even} \\ Q_{\ell mp} & \ell-m \text{ odd} \end{cases} \tag{5.85}$$

Then Δr_p of equation (5.51) becomes

$$\Delta r_p(\phi,\lambda) = \sum_{\ell mp} \left(A_{\ell mp} + B_{\ell mp} + C_{\ell mp}\right) \left[\tilde{Q}_{\ell mp}\left(\Delta C_{\ell m}\cos m\lambda + \Delta S_{\ell m}\sin m\lambda\right)\right.$$

$$\left. \pm \tilde{R}_{\ell mp}\left(\Delta C_{\ell m}\sin m\lambda - \Delta S_{\ell m}\cos m\lambda\right)\right] \tag{5.86}$$

Consistent with equation (5.69), the plus sign corresponds to an ascending arc and the minus sign to a descending arc. So it becomes obvious that Δr_p is composed of a mean error that is common to both ascending and descending arcs and by a variable error of the same magnitude and different sign depending on the direction of the arc. Furthermore there is no dependence of Δr_p on the actual epoch of the orbit integration and on the initial position of the satellite. Both components of Δr_p are only dependent on the geocentric coordinates of the subsatellite tracks and the elements a_o, i_o, $\dot{\omega}$, $\dot{M}$ and $\dot{\Omega}$ that are used to compute the quantities $A_{\ell mp}$, $B_{\ell mp}$, $C_{\ell mp}$, $Q_{\ell mp}$ and $R_{\ell mp}$. Since these elements are not expected to change appreciably between weekly arcs, the error Δr_p is fixed in space throughout the satellite lifetime. The spatial variation in Δr_p is specified by the behavior of the functions $Q_{\ell mp}$, $R_{\ell mp}$ and the cosines and sines of the longitudes. The same property has been numerically observed in equations (4.62) and (5.29).

The constant term Δr_o of equation (5.52) can be written

$$\Delta r_o(\phi_o,\lambda_o) = \sum_{\ell mp} A_{\ell mp}\left[\tilde{Q}_{\ell mp}(\phi_o)\left(\Delta C_{\ell m}\cos m\lambda_o + \Delta S_{\ell m}\sin m\lambda_o\right)\right.$$

$$\left. + j\tilde{R}_{\ell mp}(\phi_o)\left(\Delta C_{\ell m}\sin m\lambda_o - \Delta S_{\ell m}\cos m\lambda_o\right)\right] \tag{5.87}$$

where (ϕ_o,λ_o) are the geocentric coordinates of the subsatellite point at the beginning of the arc, and j takes the values 1 and -1 depending whether the arc starts ascending or descending.

To transform Δr_1 of equation (5.53), we need to use the equalities

$$S_{\ell mpo}(o)\cos\dot{M}\Delta t + \bar{S}_{\ell mpo}(o)\sin\dot{M}\Delta t = S_{(\ell+1)mpo}(o)\cos(M+\omega)$$

$$+ \bar{S}_{(\ell+1)mpo}(o)\sin(M+\omega)$$

$$S_{\ell mpo}(o)\cos\dot{M}\Delta t - \bar{S}_{\ell mpo}(o)\sin\dot{M}\Delta t = S_{(\ell-1)mpo}(o)\cos(M+\omega) \tag{5.88}$$

$$- \bar{S}_{(\ell-1)mpo}(o)\sin(M+\omega)$$

where the approximation $\dot{\omega}\Delta t=0$ has been used, to obtain

$$\cos\dot{M}\Delta t \cong \cos(\omega+M-\omega_o-M_o) \tag{5.89}$$

and similarly for $\sin M\Delta t$. $\bar{S}_{\ell mpo}$ can be transformed similar to $S_{\ell mpo}$ to give

$$\bar{S}_{\ell mpo} = \tilde{Q}_{\ell mp}(\Delta C_{\ell m}\sin m\lambda - \Delta S_{\ell m}\cos m\lambda)$$

$$-(\pm\tilde{R}_{\ell mp})(\Delta C_{\ell m}\cos m\lambda + \Delta S_{\ell m}\sin m\lambda) \tag{5.90}$$

Then, from (5.53), (5.68), (5.69), (5.83) and (5.90) we obtain

$$\Delta r_1(\phi,\phi_o,\lambda_o) = \frac{\sin\phi}{\sin i}\sum_{\ell mp}[W^1_{\ell mp}(\phi_o)(\Delta C_{\ell m}\cos m\lambda_o + \Delta S_{\ell m}\sin m\lambda_o)$$

$$+ jW^2_{\ell mp}(\phi_o)(\Delta C_{\ell m}\sin m\lambda_o - \Delta S_{\ell m}\cos m\lambda_o)]$$

$$\pm\left(1-\frac{\sin^2\phi}{\sin^2 i}\right)^{1/2}\sum_{\ell mp}[W^3_{\ell mp}(\phi_o)(\Delta C_{\ell m}\sin m\lambda_o - \Delta S_{\ell m}\cos m\lambda_o)$$

$$+ jW^4_{\ell mp}(\phi_o)(\Delta C_{\ell m}\cos m\lambda_o + \Delta S_{\ell m}\sin m\lambda_o)] \tag{5.91}$$

with

$$W^1_{\ell mp}(\phi_o) = -B_{\ell mp}\,\tilde{R}_{(\ell+1)mp}(\phi_o) + C_{\ell mp}\,\tilde{R}_{(\ell-1)mp}(\phi_o)$$

$$W^2_{\ell mp}(\phi_o) = B_{\ell mp}\,\tilde{Q}_{(\ell+1)mp}(\phi_o) - C_{\ell mp}\,\tilde{Q}_{(\ell-1)mp}(\phi_o) \qquad (5.92)$$

$$W^3_{\ell mp}(\phi_o) = B_{\ell mp}\,\tilde{R}_{(\ell+1)mp}(\phi_o) + C_{\ell mp}\,\tilde{R}_{(\ell-1)mp}(\phi_o)$$

$$W^4_{\ell mp}(\phi_o) = B_{\ell mp}\,\tilde{Q}_{(\ell+1)mp}(\phi_o) + C_{\ell mp}\,\tilde{Q}_{(\ell-1)mp}(\phi_o)$$

Equations (5.87) and (5.91) give the geographic representation of the constant bias and the 1 cy/rev error. Δr_0 is constant spatially while Δr_1 is independent of longitude but has a variation with latitude. It is composed of a mean error and a variable error. The mean error becomes maximum at the nothernmost and southernmost latitudes where the variable error becomes zero. On the contrary the mean error becomes zero at the equator, where the variable error is maximum.

Both the constant bias and the 1 cy/rev error are dependent on the geocentric coordinates of the subsatellite point at the beginning of the arc, computed from M_o, ω_o, Ω_o, and θ_o. These quantities are expected to vary appreciably between arcs, so for every arc these two types of errors have different magnitudes. Superimposed on the arc independent error Δr_p they provide the total first order periodic error for each arc. The total error is very close to zero in the region surrounding the initial point (ϕ_o, λ_o), and the maximum error is in the region with longitude difference of about 180°.

The geographic representation of the first order periodic error due to coefficient errors given by the half differences GEM10B - GRIM3L1 has been computed using (5.86), (5.87) and (5.91) for all Seasat arcs. Implementation of these equations on a global scale is quite expensive in computer time, primarily because the latitude dependent functions $Q_{\ell mp}$, $R_{\ell mp}$ and the equations themselves have to be computed for every subsatellite point. An alternative way is to compute the error on a regular grid and then to interpolate to any subsatellite point to compute the actual error. It turns out that computation on a 1° grid can provide interpolated estimates of the error that are quite reliable. More specifically the discrepancies between the interpolated estimates and the corresponding values computed by (4.62) have a maximum value of about 10 cm in the northern and southern latitudes, where the error variation is quite

rapid, and are generally on the order of 1-2 cm in the equatorial regions.

The error for the first Seasat arc is shown in Figures 20 and 21. Figure 20 shows the error in the ascending arcs while Figure 21 shows the error in the descending arcs. Both Figures have been created using a 5° grid with a contour interval of 50 cm. Examining these Figures we can observe that the spatial variation of the radial orbit error is quite complex. Consistent with the results from the analysis of the temporal characteristics of the error, we observe a long wavelength along track variation. The across track variation though is quite erratic and is by no means of long wavelength nature. This is obviously due to the fact that spatially adjacent tracks are substantially separated in time and so they have different magnitudes in their errors. In some geographic regions this across track variability is quite smooth while in others there is a rapid change of even 7 meters within distances of 1000 km. The minimum error in the ascending arcs is in the equatorial region close to India and is very close to zero. This is expected, because the initial integration point of the arc is in that region (ϕ = -11.97, λ = 101.85) and so the error should indeed be zero. The maximum error is in the region west of the United States with a magnitude of about -5 meters. On the contrary, the descending arcs have a maximum error of 4 meters in the region of the initial integration point and a minimum error, very close to zero, in the region of the maximum ascending error. Similar patterns of the error, with more or less the same magnitude can be observed in maps of the errors in all the other arcs of Seasat. The minima and maxima are of course shifted depending on where the initial subsatellite point for each arc is located, but the overall characteristics are the same.

5.4.2. Resonant, Second Order and Initial State Vector Induced Error

To complete the representation of the radial orbit error in terms of geographic coordinates the 1 cy/rev and 2 cy/rev components from resonant and second order effects as well as the initial state vector errors, have to be expressed with respect to (ϕ,λ).

Starting with (4.89) for Δr_{I1} we transform cosM and sinM as follows

$$\cos M = \cos(M+\omega)(\cos\omega_o - \dot{\omega}\Delta t\sin\omega_o) + \sin(M+\omega)(\sin\omega_o + \dot{\omega}\Delta t\cos\omega_o) \tag{5.93}$$

$$\sin M = -\cos(M+\omega)(\sin\omega_o + \dot{\omega}\Delta t\cos\omega_o) + \sin(M+\omega)(\cos\omega_o - \dot{\omega}\Delta t\sin\omega_o) \tag{5.94}$$

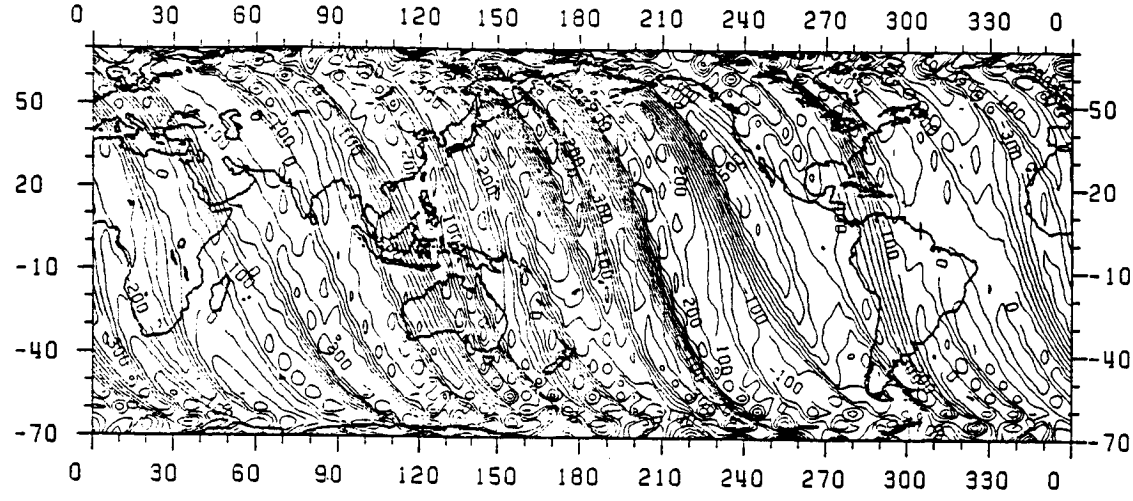

Figure 20. Radial Orbit Error of Ascending Seasat Arcs Using the GEM10B-GRIM3L1 Half Differences as Potential Coefficient Errors. C.I. = 50 cm.

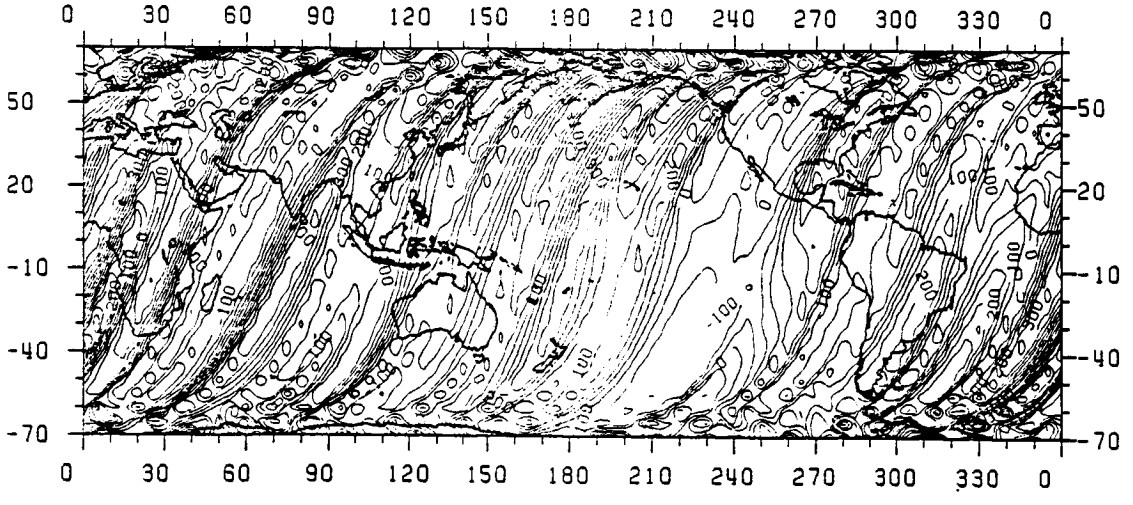

Figure 21. Radial Orbit Error of Descending Seasat Arcs Using the GEM10B-GRIM3L1 Half Differences as Potential Coefficient Errors. C.I. = 50 cm.

Since $\dot{\omega}$ is generally small and the initial state vector errors are also small, the time dependent terms can be dropped. Then, using (5.68) and (5.69) we have

$$\Delta r_{I1} = \Delta a_I + \frac{\sin\phi}{\sin i}(-a\Delta e_I \sin\omega_o + ae\Delta M_I \cos\omega_o)$$

$$\pm \left(1 - \frac{\sin^2\phi}{\sin^2 i}\right)^{\frac{1}{2}} (-a\Delta e_I \cos\omega_o - ae\Delta M_I \sin\omega_o) \qquad (5.95)$$

which demonstrates that the initial state first order error has a behavior identical to the constant bias and the 1 cy/rev error of gravitational origin.

For the resonant terms, we can use (5.62) and (5.63) in (4.78) and neglect $\tilde{a}^r$, to obtain

$$\Delta r^r_{G1}(t) = A_1 \Delta t \cos(\omega_o + M) + A_2 \Delta t \sin M \qquad (5.96)$$

where

$$A_1 = an \sum_{\ell\,odd} \left(\frac{a_e}{a}\right)^{\ell} F_{\ell_o \frac{\ell-1}{2}} (\ell-1)\Delta C_{\ell_o} \qquad (5.97)$$

$$A_2 = -aen \sum_{\ell\,even} \left(\frac{a_e}{a}\right)^{\ell} F_{\ell_o \frac{\ell}{2}} \frac{(\ell+1)(\ell-4)}{2} \Delta C_{\ell_o} \qquad (5.98)$$

Using (5.92) and

$$\cos(\omega_o + M) = \cos(\omega + M) + \dot{\omega}\Delta t \sin(\omega + M) \qquad (5.99)$$

we obtain

$$\Delta r^r_{G1}(t) = (A_1 + A_2 \sin\omega_o - A_2 \cos\omega_o \dot{\omega}\Delta t)\Delta t \cos(\omega + M)$$

$$+ (A_1\dot{\omega}\Delta t - A_2\cos\omega_0 + A_2\sin\omega_0\dot{\omega}\Delta t)\Delta t\sin(\omega+M) \qquad (5.100)$$

where now the terms in $\dot{\omega}\Delta t^2$ are not necessarily negligible, depending on the magnitudes of A_1 and A_2. Using (5.68) and (5.69)

$$\Delta r^r_{G1}(\phi,t) = \frac{\sin\phi}{\sin i}(A_1\dot{\omega}\Delta t - A_2\cos\omega_0 + A_2\sin\omega_0\dot{\omega}\Delta t)\Delta t$$

$$\pm \left[1 - \frac{\sin^2\phi}{\sin^2 i}\right]^{1/2}(A_1 + A_2\sin\omega_0 - A_2\cos\omega_0\dot{\omega}\Delta t)\Delta t \qquad (5.101)$$

So the resonant induced errors are not strictly a function of geocentric coordinates (ϕ,λ). They also depend on the time elapsed from the beginning of the arc, in a non linear fashion. They are independent of longitude and they contain a mean error and a variable error. Unless the coefficients A_1 and A_2 are very small (which imply extremely accurate zonal coefficients) they can reach appreciable magnitudes with the evolution of time. Examining A_1 and A_2 in (5.97), (5.98) it is expected that the major contribution of the error will be from the terms containing A_1 (resonant errors in eccentricity due to odd zonal errors). These errors depend on the initial position through ω_0.

The second order effects of gravitational and initial state origin can be computed in an almost identical way. The 1 cy/rev term of Δr_{G2} in (4.83) as well as the corresponding term of Δr_{I2} in (4.91) can be easily transformed by setting A_1 of (5.97) equal to zero and A_2 to be equal to A_2' where

$$A_2' = \frac{3}{2}\frac{n}{a}(\Delta a_I - \Delta a_0) \qquad (5.102)$$

and evaluating (5.101) with $A_1 = 0$ and A_2'

$$\Delta r^1_{G2,I2}(\phi,t) = \frac{\sin\phi}{\sin i}(-A_2'\cos\omega_0 + A_2'\sin\omega_0\dot{\omega}\Delta t)\Delta t$$

$$\pm \left[1 - \frac{\sin^2\phi}{\sin^2 i}\right]^{1/2}(A_2'\sin\omega_0 - A_2'\cos\omega_0\dot{\omega}\Delta t)\Delta t \qquad (5.103)$$

C-2

The final transformation involves the 2 cy/rev terms of (4.83) and (4.91). This is a straightforward transformation giving

$$\Delta r^2_{G2,I2}(\phi,\lambda) = \pm\left(1-\frac{\sin^2\phi}{\sin^2 i}\right)^{\frac{1}{2}} \frac{\sin\phi}{\sin i} A_3 \Delta t \qquad (5.104)$$

where

$$A_3 = -aJ_2 \left(\frac{a_e}{a}\right)^2 \left[\frac{3}{2}\frac{n}{a}(\Delta a_0 - \Delta a_I) + \tilde{M}^r + \tilde{\omega}^r\right]\sin^2 i \qquad (5.105)$$

This type of error is also dependent only on latitude and on time in a linear fashion. It is independent of the initial position and it has only a variable component which becomes zero both at the northern and southern latitudes as well as at the equator.

5.3.3. Observability of the Radial Orbit Error from Crossover Discrepancies

Having been able to understand the spatial behavior of the radial orbit error, it is now straightforward to assess its observability from crossover discrepancies. This assessment is quite important, because, as it is mentioned in Chapter 2, crossover discrepancies have been the primary observable in the reduction of the orbit error in altimeter data from Geos3, Seasat and currently Geosat. Adjusted sea surface heights have been used to create global mean sea surfaces and estimates of the sea surface topography. These surfaces obviously contain all radial orbit errors that are not observable from crossovers.

If we assume that all the signal in a crossover discrepancy is due to radial orbit errors then we can write

$$\Delta r_D = \Delta r(t_1) - \Delta r(t_2) \qquad (5.106)$$

where t_1 represents the time of the ascending crossing and t_2 the time of the descending crossing. For simplicity it is also assumed that the crossing occurs between arcs of the same integration period. Then the discrepancy using the first order periodic error will be

$$\Delta r_D = 2\Delta r^v_p - 2\Delta r^v_1 - 2\Delta r^v_{I1} \qquad (5.107)$$

where 'v' refers to the variable part of the various error components. The part of the error that cancels out during the differencing is

$$\Delta r^c = \Delta r_p^c - \Delta r_o - \Delta r_i^c + \Delta a_I + \Delta r_I^c \qquad (5.108)$$

where 'c' refers to the mean geographic error. It is composed of a constant bias ($\Delta a_I - \Delta r_o$), of a latitude dependent function ($\Delta r_f^c - \Delta r_f$) and the periodic function Δr_p^c which is both latitude and longitude dependent.

The spatial signatures of both the mean and variable parts of the first order periodic error of gravitational origin are shown in Figures 22 and 23 respectively. These maps are constructed using the same potential coefficient errors as before and plotted on a 5° grid with a 50 cm contour interval. We can observe that both types of errors have quite an erratic variation with individual values ranging from about -3 meters to 2 meters. They both have the same regional characteristics although with different magnitudes. These characteristics follow the directions of the subsatellite tracks and are prominent in regions of rapid across track variations of either ascending or descending arcs (compare with Figures 20 and 21). The particular patterns of these errors may very well change in shape and or locations with a different choice of potential coefficient errors and of course with a different initial integration point.

Obviously, in a crossover adjustment, Δr^c cannot be observed and remains intact in the adjusted surface. Judging from Figure 23 this error can be substantial and can affect the computation of the stationary SST and geophysical investigations even on a local basis. This situation becomes worse when we consider the time dependent errors. The variable part of these errors is primarily a function of the crossing latitude and the crossing time differences (t_1-t_2) while the part that cancels out is simply $\Delta r_T(t_1)$ (T denotes all the time dependent errors and t_1 is assumed to be smaller than t_2). This type of error may very well create a high frequency across track signature in the mean radial error, because spatially neighbouring crossovers may belong to pairs of arcs that are widely separated in time, resulting into large variations in small spatial distances.

The dependency of the mean error on each particular arc can create additional problems when crossovers between different arcs are formed. Then, each crossover discrepancy (considering for simplicity only Δr_{G1}) is

$$\Delta r_D = 2\Delta r_p^v - \Delta r_o^{ij} - \Delta r_i^{cij} - (\Delta r_i^{vi} + \Delta r_i^{vj}) \qquad (5.109)$$

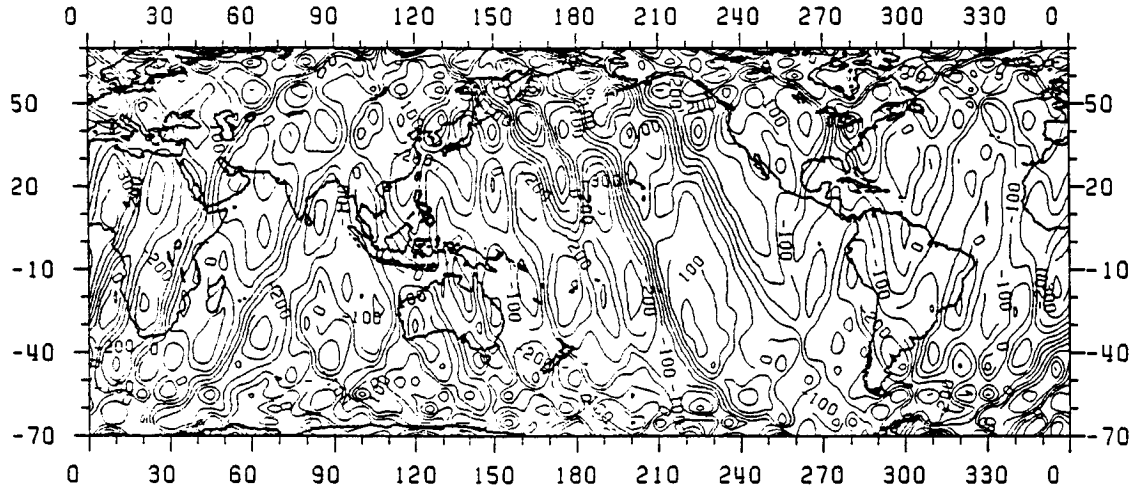

Figure 22. Mean Radial Error of a Seasat Arc Using the GEM10B-GRIM3L1 Half Differences as Potential Coefficient Errors. C.I. = 50 cm.

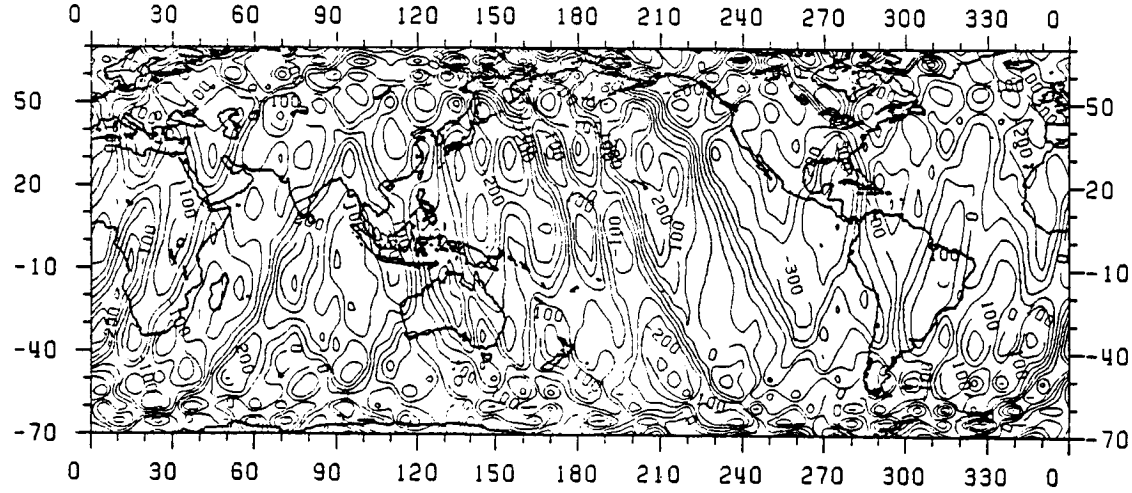

Figure 23. Variable Radial Error of a Seasat Arc Using the GEM10B-GRIM3L1 Half Differences as Potential Coefficient Errors. C.I. = 50 cm.

with additional terms for the initial state errors and the time dependent errors. In (5.109) i and j denote the two different weekly arcs, and ij denotes the difference of the corresponding mean errors, which are generally not the same from arc to arc (see Table 5). The unobserved part of the error will be

$$\Delta r^c = \Delta r_p^c - \min(\Delta r_o^i, \Delta r_o^j) - \min(\Delta r_1^{ci}, \Delta r_1^{cj}) \qquad (5.110)$$

with additional elements for initial state induced errors. Formation of several crossovers in a small geographic area between several arcs (there are twelve weekly arcs for Seasat) will create a surface of unobserved error that has high frequency signature in both the along and across track directions. The magnitude of this signature clearly depends on the differences of the mean errors in the various arcs. The incorporation of the time dependent errors makes the situation even worse. Further study needs to be made for particular patterns of this error where crossovers between different weekly arcs are considered.

An additional error in the geometric adjustment of the crossover discrepancies arises from the fact that one arc of about 30-40 minutes of length is kept fixed so that to remove the singularities existing in the adjustment. Then the error in this arc (both the mean and variable parts) remains unaltered and propagates through all the crossing arcs, which in turn propagate the resulting error to all the parallel arcs in an unpredictable way.

These types of problems are expected to have occured in all determinations of mean sea surfaces (e.g., Rapp, 1986). The problems are enhanced when data from both Geos3 and Seasat satellites are combined, since mean errors in the two types of orbits are expected to differ appreciably. The resulting geographic mean error has clearly a high frequency signature that can be easily detected in the detailed maps of the sea surface and the gravity field that have been produced (ibid, 1986).

In terms of potential coefficient corrections it can be seen in the equations that all degrees and orders are partly unobservable from crossover discrepancies. More particularly the observability of the zonal coefficients is zero from the variable part of Δr_p and is very small in the constant and 1 cy/rev parts since all the coefficients are lumped together. The observability of the potential coefficient corrections increases with increasing order.

CHAPTER VI

ANALYSIS OF GEOID UNDULATION ERRORS AND STATIONARY SST

In Chapters 4 and 5 the complete analysis of the radial orbit error was made and formulas expressing the error in a Lagrangian form, in a Fourier series form and a geographic representation, were developed. Furthermore, the theory has been tested for its accuracy and numerical results were given. A similar analysis can be made for the geoid undulation errors and the stationary SST. Since both quantities are expressed as a spherical harmonic expansion on a sphere, this analysis is common for both of them. Some differences between the two quantities exist and will be pointed out. The spherical harmonic expansion of the geoid undulations is

$$N = \frac{\mu}{r\gamma} \sum_{\ell=2}^{\infty} \left(\frac{a_e}{r}\right)^{\ell} \sum_{m=0}^{\ell} \left(\bar{C}^{*}_{\ell m} \cos m\lambda + \bar{S}_{\ell m} \sin m\lambda\right) \bar{P}_{\ell m}(\sin\phi) \qquad (6.1)$$

where (ϕ,λ,r) are the geocentric coordinates of the computation point, γ is the normal gravity on the reference ellipsoid, $\bar{P}_{\ell m}$ are the fully normalized associated Legendre functions and $\bar{C}^{*}_{\ell m}$, $\bar{S}_{\ell m}$ are the normalized coefficients of the disturbing potential. The $\bar{C}^{*}_{\ell m}$ coefficients are related to the potential coefficients by

$$\bar{C}^{*}_{\ell m} = \bar{C}_{\ell m} - \bar{C}^{ref}_{\ell m} \qquad (6.2)$$

with all $\bar{C}_{\ell m}{}^{ref}$ being equal to zero except for the even degree zonals. The summation from ℓ=2 in (6.1) implies that the reference ellipsoid is a geocentric ellipsoid having the same mass as the earth. The geoid undulations can be computed using potential coefficients of some gravity field model that is determined either from satellite data or from terrestrial and altimetrically derived gravity anomalies. As it is stated in Chapter 3 a satellite derived gravity field provides only the long wavelength undulation signatures. On the contrary, use of a detailed (1°x1° or even finer grid) set of gravity anomalies can provide potential coefficients of high degree and order which in turn can be used to compute high frequency undulations. Specific high degree models that have been computed are the OSU81 up to degree

180 (Rapp, 1981) and OSU86F up to degree 360 (Rapp and Cruz, 1986). Use of any of those models can provide undulation estimates which are related to the true undulations by

$$N = N_o + \Delta N^c + \Delta N^o \qquad (6.3)$$

where N_o are the computed undulations, ΔN^c are the commission errors and ΔN^o are the omission errors. Estimates from the OSU86F field which is complete to degree 360 (although with some degree of smoothing in degrees higher than 180) indicate that the undulations up to harmonic degree 36 have an RMS magnitude of 30.43 meters with an omission error of 1.58 meters and a commision error of 79 cm. Undulations up to harmonic degree 180, on the other hand, have an RMS magnitude of 30.47 meters, an omission error of 23 cm and a commission error of 1 meter. This indicates that about 95 percent of the undulation signal is at wavelengths corresponding to harmonic degrees smaller than 36, while more than 99 percent of the signal is contained in degrees smaller than 180. These commission and omission errors are approximate estimates and are based on the assumption that there is no signal above degree 360 and that the accuracy estimates of the field are reliable. In reality the omission errors are expected to be slightly higher because of the smoothing of the field above degree 180 and the omission errors of the field itself, which though on the average should be quite small.

The omission errors are obviously expressed by equation (6.1) with the summation over ℓ being from $\ell_{max} + 1$ to infinity. The commission errors can be written

$$\Delta N^c = \frac{\mu}{r\gamma} \sum_{\ell=2}^{\ell_{max}} \left(\frac{a_e}{r} \right)^{\ell} \sum_{m=o}^{\ell} \left(\Delta \bar{C}_{\ell m} \cos m\lambda + \Delta \bar{S}_{\ell m} \sin m\lambda \right) \bar{P}_{\ell m}(\sin\phi) \qquad (6.4)$$

where $\Delta \bar{C}_{\ell m}$ and $\Delta \bar{S}_{\ell m}$ are the potential coefficient errors. Equation (6.4) can provide the commission errors at the groundtrack of a satellite if the geocentric coordinates of the subsatellite points are given. These coordinates are given in the Geophysical Data Records and are computed from the fully perturbed state vector of the satellite.

In order to be able to express (6.4) in an inertial coordinate system with respect to Keplerian elements, a transformation of the surface spherical harmonics on the orbital plane has to be applied. Then

$$\Delta N^c = \frac{\mu}{r\gamma} \sum_{\ell=2}^{\ell_{max}} \left(\frac{a_e}{r} \right)^{\ell} \sum_{m=0}^{\ell} \sum_{a=0}^{1} \Delta C_{\ell ma} \sum_{p=0}^{\ell} F_{\ell mp}(i)$$

$$\cdot \cos[(\ell-2p)(\omega+f) + m(\Omega-\theta) + C] \qquad (6.5)$$

where C is given by (5.12) and i, ω, f, Ω, are the osculating elements of the satellite with groundtracks ϕ and λ. Note that (6.5) is given with respect to unnormalized coefficients for consistency with the developments made so far. In order to obtain an expression consistent with the ones for the radial orbit error (equation 4.62 or 5.29), a circular orbit approximation and a linearization in the context of section 4.5.1 are necessary. Considering also that the magnitudes of the potential coefficient errors are small, a spherical earth approximation can be made. Then (6.5) reduces to

$$\Delta N^c = R \sum_{\ell} \sum_{m} \sum_{a} \Delta C_{\ell ma} \sum_{p} F_{\ell mp}(i) \cos[(\ell-2p)(M+\omega) + m(\Omega-\theta) + C] \qquad (6.6)$$

where now i, ω, M and Ω take values on the reference orbit and can be computed from equations (4.36). A test on the effect of these approximations on the computation of ΔN^c was made by using the half differences of GEM10B - GRIM3L1 as potential coefficient errors. First, equation (6.4) was used to compute ΔN^c along the subsatellite points of the first six day Seasat arc at two minute intervals. This error is plotted in Figure 24. It has an RMS magnitude of 1.15 meters with maximum values on the order of 9 meters. The commission error was also computed using (6.6). The RMS discrepancy with the "true" values is 10 cm with a maximum discrepancy of about 70 cm. The discrepancies between the two sets occur because of the linearization that is used in ω, M and Ω, resulting in computing the undulation error not at the correct coordinates but at a location implied by the secularly changing ω, M and Ω. This level of agreement indicates that equation (6.6) cannot be used to model the commission undulation errors. These effects have to be modeled using equation (6.4).

Although equation (6.6) cannot be used for modeling purposes, it is very useful in investigating the frequency content of the undulation errors. For this investigation equation (6.6) has to be rearranged through an analysis similar to the one in section 5.3. Setting $k = \ell-2p$ and reordering the summations we obtain

$$\Delta N = R \sum_{k=-\ell_{max}}^{\ell_{max}} \sum_{m=0}^{\ell_{max}} \sum_{\ell=\ell_{min}}^{\ell_{max}} \sum_{a=0}^{1} \Delta C_{\ell ma} F_{\ell m \frac{\ell-k}{2}}(i) \cos(\dot{\psi}_{km} \Delta t + \psi_{kmo} + C)$$

(6.7)

where $\dot{\psi}_{km}$ and ψ_{kmo} are defined in (5.8) and (5.13) respectively, ℓ_{min} is given by (5.61) and the summation in ℓ is over degrees that have the same parity with k. After some trigonometric operations we obtain

$$\Delta N^c = \sum_{km} \left[a_{km} \cos\dot{\psi}_{km}\Delta t + b_{km} \sin\dot{\psi}_{km}\Delta t \right] \tag{6.8}$$

where

$$a_{km} = R \sum_{\ell}^{kpar} F_{\ell_m \frac{\ell-k}{2}}(i) \left[\begin{pmatrix} \Delta C \\ -\Delta S \end{pmatrix}_{\ell_m} \cos\psi_{kmo} + \begin{pmatrix} \Delta S \\ \Delta C \end{pmatrix}_{\ell_m} \sin\psi_{kmo} \right] \tag{6.9}$$

$$b_{km} = R \sum_{\ell}^{kpar} F_{\ell_m \frac{\ell-k}{2}}(i) \left[\begin{pmatrix} \Delta S \\ \Delta C \end{pmatrix}_{\ell_m} \cos\psi_{kmo} - \begin{pmatrix} \Delta C \\ -\Delta S \end{pmatrix}_{\ell_m} \sin\psi_{kmo} \right] \tag{6.10}$$

or, in terms of amplitudes and phases

$$\Delta N^c = \sum_{km} A_{km} \cos(\dot{\psi}_{km}\Delta t - \psi_{km}) \tag{6.11}$$

where

$$A_{km} = \left(a_{km}^2 + b_{km}^2 \right)^{1/2} \tag{6.12}$$

$$\psi_{km} = \tan^{-1} \frac{b_{km}}{a_{km}} \tag{6.13}$$

Equations (6.8) - (6.10) provide the Fourier series representation of the undulation commission errors. The frequencies are again expressed in terms of cy/rev and the phases are computed based on the mean elements ω_o, M_o, Ω_o of the satellite arc. Equations (6.8) - (6.10) have a similarity with the corresponding equations (5.57) - (5.59) for the zero order periodic radial error. The actual spectral signatures of the two quantities though are expected to differ appreciably, due to the damping factor applied to the inclination functions in equation (5.58), causing the frequencies that are close to zero and 1 cy/rev to have large amplitudes, and higher frequencies to have small amplitudes, as shown in Figure 15.

The amplitude spectrum of the commission error is shown in Figure 25 up to 6 cy/rev. It is observed that this error has a more or less flat spectrum with the exception of the integer cy/rev frequencies that have no energy. It turns out that the higher frequencies do not die out as in Figure 15 but they have energies up to 36 cy/rev, which is the maximum frequency defined when using a field up to harmonic degree 36. The RMS errors by degree and order have also been computed and shown in Figures 26 and 27 respectively. Both Figures show distinct differences from the corresponding Figures 16 and 18. Figure 26 shows that indeed the GEM10B and GRIM3L1 models have large coefficient discrepancies at degrees 6 to 12.

As discussed in Chapter 3 the modeling of the undulation errors up to a high degree is not practical and does not yield an accurate solution for potential coefficient recovery since residual sea surface heights can only be obtained in the oceans. So the same gravity field that is used for the orbit integration is also used for the computation of the reference undulations. It has also been clear that such a field, being of low degree and order (ℓ_{max} = 36) yields a large omission error that coexists in the residual sea surface heights together with the radial orbit errors, the commission undulation errors and other effects. This omission error is on the order of 1.58 meters (as computed using OSU86F). The frequency content of the omission error can be determined by equations of the type (6.8) - (6.10). These equations have been implemented using the OSU86F potential coefficients from degree 37 to 180. The maximum degree 180 is chosen because of the practical difficulty in computing the inclination functions for degrees higher than 180 even with the extremely fast method derived by Goad (1987). It turns out that the omission errors have a substantial effect both in the lower part of the spectrum (k<36 cy/rev) as well as in the higher part (k>36 cy/rev). The RMS magnitudes of both these effects are shown in Table 7.

The higher frequency omission undulation errors of 1.20 meters can in principle be filtered out by applying a low pass filtering to the sea surface heights with a cutoff frequency of 36 cy/rev. This filtering is expected to have problems close to the ocean boundaries, where the profiles become discontinuous. The lower frequency effects of 1.04 meters are more serious because they cannot be separated from the commission errors since all degrees of a particular order are lumped together to generate one frequency. Furthermore additional frequencies lower than 36 cy/rev are generated from harmonics of higher orders. Both these lower frequency errors can be reduced by modeling the higher degree undulations errors using a high degree and order gravity field (i.e. OSU86F) and removing these undulations from the residual sea surface heights. This removal will introduce commission errors due to the uncertainties of the high degree field. These errors have been computed based on the standard deviations of the OSU86F field up to degree 180 and are shown in Table 7. We can

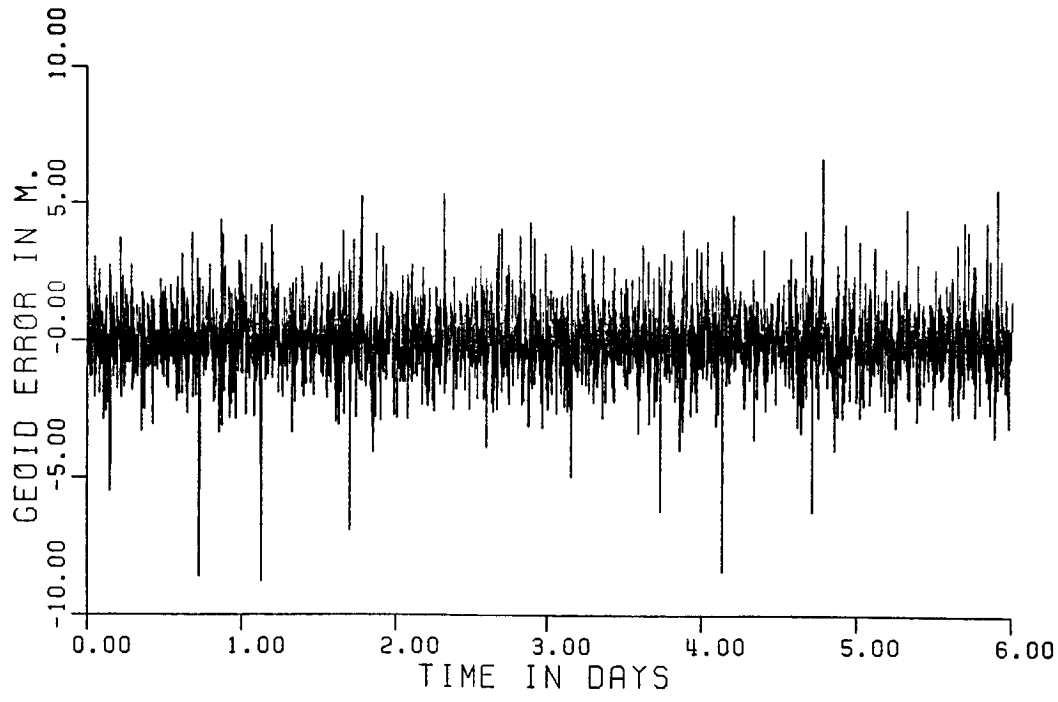

Figure 24. Along Track Geoid Undulation Error Using the GEM10B - GRIM3L1 Half Differences as Potential Coefficient Errors.

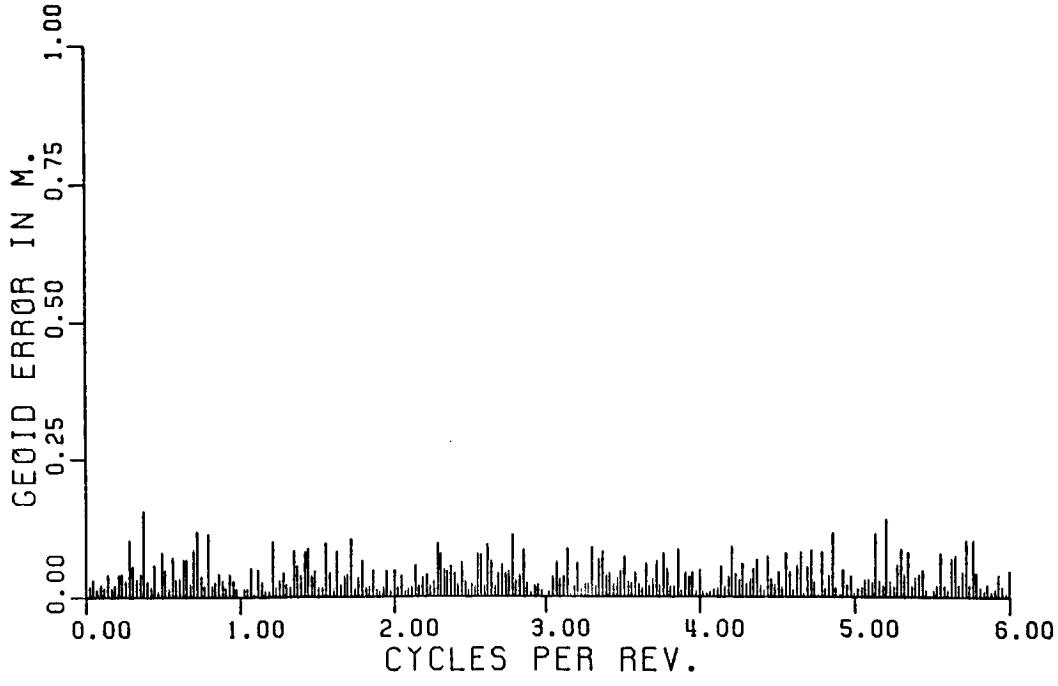

Figure 25. Amplitude Spectrum of Geoid Undulation Error Using the GEM10B - GRIM3L1 Half Differences as Potential Coefficient Errors.

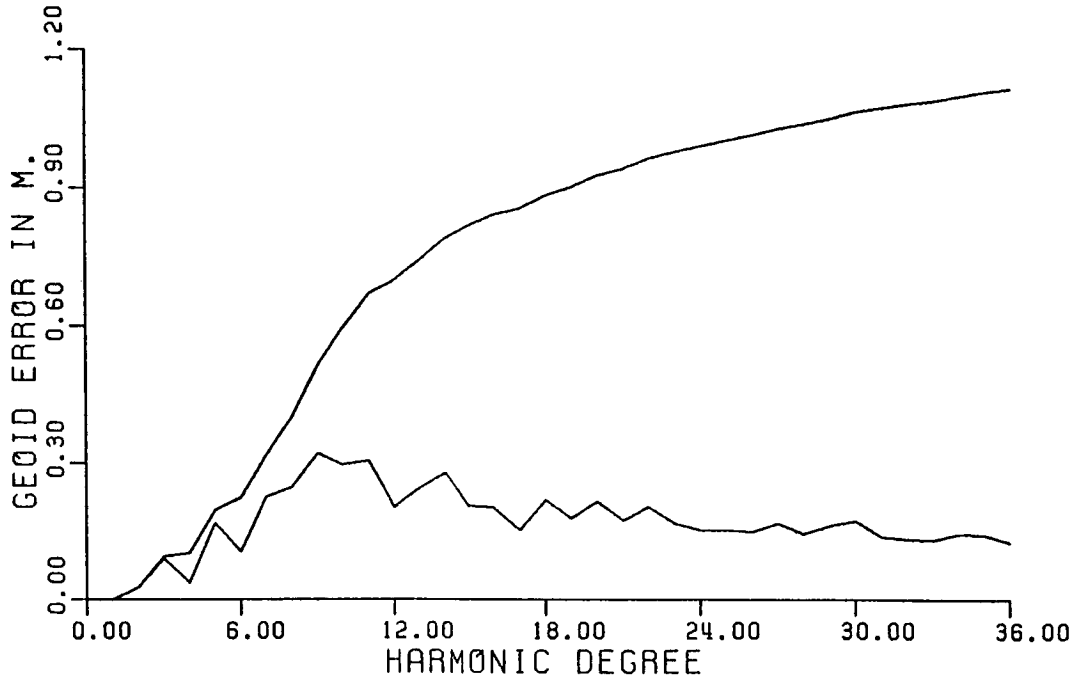

Figure 26. RMS Geoid Undulation Error by Harmonic Degree and Cumulative, Using the GEM10B - GRIM3L1 Half Differences as Potential Coefficient Errors.

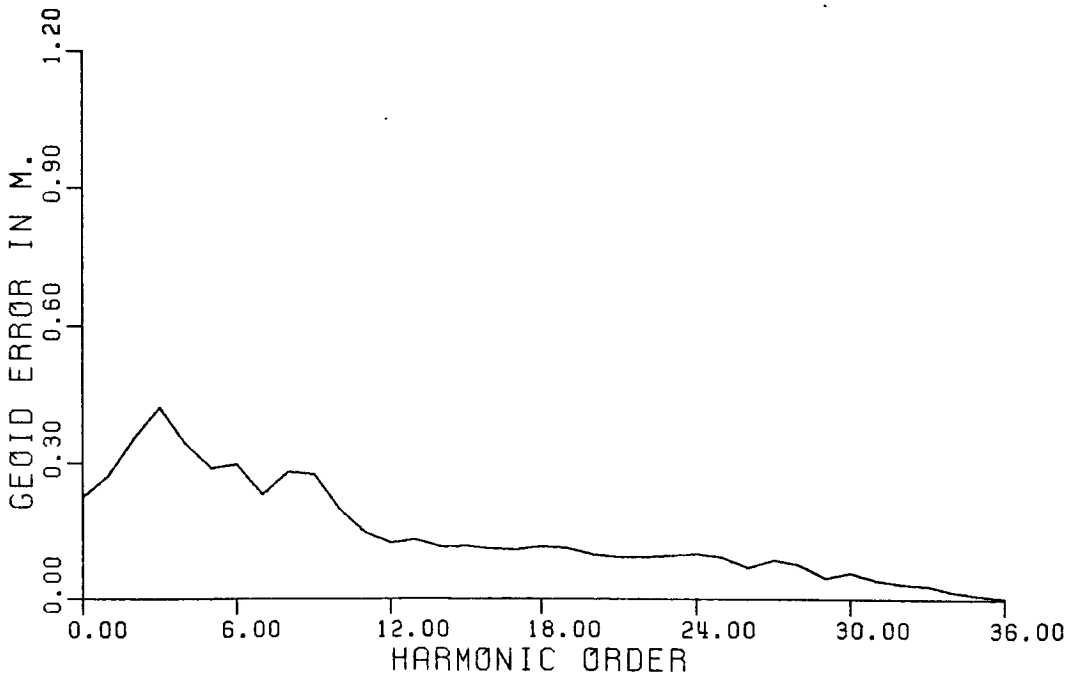

Figure 27. RMS Geoid Undulation Error by Harmonic Order Using the GEM10B - GRIM3L1 Half Differences as Potential Coefficient Errors.

see that the errors both at high and low parts of the spectrum are substantially reduced. A low pass filtering is still needed to remove the high frequency errors. The side effects due to the profile discontinuities are now expected to be much smaller. The error of 32 cm at the low frequencies is expected to affect the estimated potential coefficient corrections and the stationary SST coefficients. A quantitative estimate of this effect though has not been obtained. Further study is needed in this matter.

Table 7

RMS Geoid Undulation Omission Errors for a Gravity Field up to $\ell_{max} = 36$ as Computed from the OSU86F Field and Its Standard Deviations to $\ell_{max} = 180$

Frequency	Signal	Error
k < 36 cy/rev	1.04 m	0.32 m
k > 36 cy/rev	1.20	0.48
Total	1.58	0.60

A similar analysis with the preceding one for the undulation errors, can be made for the stationary SST. The stationary SST can be viewed as a function that is zero on land and takes specific values in the oceans. Furthermore it can be approximated as being a function on a sphere with the mean radius of the earth. Then the periodic part of the stationary SST can be expanded into surface spherical harmonics

$$\zeta = R \sum_{\ell=1}^{\infty} \sum_{m=0}^{\ell} \left(\bar{C}_{\ell m_T} \cos m\lambda + \bar{S}_{\ell m_T} \sin m\lambda \right) \bar{P}_{\ell m}(\sin\phi) \qquad (6.14)$$

where $\bar{C}_{\ell m_T}$, $\bar{S}_{\ell m_T}$ are the spherical harmonic coefficients of the stationary SST on a sphere of radius R. The zero degree term, if any, is not present in (6.14) because it is absorbed by the mean earth ellipsoid that is used as a reference for the geoid undulations. This is consistent with the definition of the oceanic geoid which requires that the average SST be zero as sampled globally in oceanic regions. A more detailed discussion on the definition of the oceanic geoid and how the mean earth ellipsoid can be defined in the presence of the stationary SST is contained in Engelis (1985). Contrary to (6.1) equation (6.14) contains a first degree term which arises from the depression of the sea surface, relative to the geoid, in the southern hemisphere. This depression is caused by the strong circumpolar currents.

The transformation of (6.14) into a Fourier series form follows the same steps and has the same problems with the one leading to equations (6.8) - (6.10). But now ℓ=1 is also included giving rise to a 1 cy/rev signature, in contrast to undulation errors that do not have any 1 cy/rev effects. Modeling of the stationary SST in the context of the combined altimeter problem has the same problems regarding the omission errors. Solution up to degree 36 introduces aliasing effects into frequencies up to 36 cy/rev arising from higher degree harmonics. The higher frequency signature due to those harmonics will be filtered out together with the higher frequency undulation errors.

CHAPTER VII

COVARIANCE ESTIMATION OF RADIAL DISTANCES AND GEOID UNDULATIONS BASED ON A GEOPOTENTIAL COVARIANCE

7.1. Introduction

The numerical example that was worked out in Chapters 5 and 6 has provided error estimates for both the radial distances (for a Seasat orbit) and undulations. These error estimates, although they are realistic and may indeed be a possible choice of errors that might occur, they are only based on an arbitrary set of numbers representing potential coefficient errors. In reality, errors in existing gravity field models are unknown. The only available information in some of these models is the estimates of their variances and, for even fewer of them, their error correlations. So the only information that one can infer about the errors of the radial distances and undulations is of statistical nature. Using the covariance matrix of a gravity field model one can compute variances and error correlations of the above quantities and of their frequency components by

$$\Sigma = G\Sigma_{cs}G^{T} \tag{7.1}$$

where Σ_{cs} is the covariance matrix of potential coefficients and G is the Jacobian that can be computed in a straightforward manner, since all the models developed so far are linear with respect to potential coefficients.

Since the orbital specifications that have been used so far in this study are the ones of the Seasat orbits as computed from the PSSS4 gravity field, it was decided to also use its covariance matrix to retain a consistency throughout the study. This will also provide some accuracy estimates for computed orbits that have already been used for the computation of mean sea surfaces (e.g. Marsh et al., 1986a). As discussed in Chapter 2, the PGSS4 gravity field is given complete to degree and order 36 and has been determined from the combination of the PGSS3 gravity field with a set of Seasat altimeter data. Such a tailoring of the field to the Seasat characteristics led to the computation of orbits with a reported RMS error of 70 cm (Lerch et al., 1982) which was based on the computed RMS crossover discrepancy of two 6 day Seasat arcs.

For the computation of reliable accuracy estimates and error correlations of both the orbit and the geoid an appropriate scaling of the covariance matrix has to be made. Such scaling is common practice for the most recent GEM models (Lerch et al., 1985) but has not been applied on the PGSS4 matrix. For the purposes of this study the PGSS4 covariance is scaled up by a factor of 10. This scaling being uniform in all degrees and orders is suboptimum and may result into erroneous accuracy estimates. But since the primary purpose of this study is to demonstrate the ability of analytic techniques to model and eventually determine the radial orbit error, the very accurate scaling of the covariance matrix is not that critical at this stage.

In the next sections the accuracies of the radial distances and undulations as well as their error correlations are going to be computed both with respect to time and in their geographical representation. For the temporal representation the Fourier series expression is going to be used since it is more efficient and economical than the Lagrangian form. The Fourier series expression will also enable us to compute accuracies of individual frequencies and their correlations as well as the accuracies of the radial distances by degree and order. It should be noted that secular and second order effects are not going to be computed. The geographic representation on the other hand will provide the accuracy estimates of ascending and descending arcs as well as statistical estimates of the parts of the orbit error that are observed or non observed in crossover discrepancies.

7.2. Covariance Propagation Using the Fourier Series Approach

For the efficient computation of (7.1) the Fourier series expression has first to be converted in a matrix form. Equation (5.19) can be written as follows

$$\Delta r_{km} = \left|\cos\dot{\psi}_{km}\Delta t \;\; \sin\dot{\psi}_{km}\Delta t\right| \left|\begin{matrix} C_{km} \\ S_{km} \end{matrix}\right| \tag{7.2}$$

where

$$\left|\begin{matrix} C_{km} \\ S_{km} \end{matrix}\right| = \left|\begin{matrix} \cos\psi_{km} & \sin\psi_{km} \\ -\sin\psi_{km} & \cos\psi_{km} \end{matrix}\right| \left|\begin{matrix} D_{km} \\ E_{km} \end{matrix}\right| \tag{7.3}$$

From (5.24) and (5.25) D_{km}, E_{km} can be written

$$D_{km} = \sum_{\ell_{min}} \left(P_{km\ell}\Delta C_{\ell m} - Q_{km\ell}\Delta S_{\ell m}\right) \tag{7.4}$$

$$E_{km} = \sum_{\ell_{min}} \left(Q_{km\ell}\Delta C_{\ell m} + P_{km\ell}\Delta S_{\ell m}\right) \tag{7.5}$$

where

$$P_{km\ell} = \begin{pmatrix} A_{km\ell} \\ -B_{km\ell} \end{pmatrix}_{\ell-m\ \text{odd}}^{\ell-m\ \text{even}} \tag{7.6}$$

$$Q_{km\ell} = \begin{pmatrix} B_{km\ell} \\ A_{km\ell} \end{pmatrix}_{\ell-m\ \text{odd}}^{\ell-m\ \text{even}} \tag{7.7}$$

$$\ell_{min} = \max(|k|-2,\ m,\ 2) \tag{7.8}$$

and $A_{km\ell}$, $B_{km\ell}$ are given by (5.16) and (5.17). In a matrix form we have

$$D_{km} = \begin{vmatrix} P_{km\ell_{min}} & \cdots & P_{km\ell_{max}} & \vdots & -Q_{km\ell_{min}} & \cdots & -Q_{km\ell_{max}} \end{vmatrix} \begin{vmatrix} \Delta C_{\ell_{min}m} \\ \vdots \\ \Delta C_{\ell_{max}m} \\ \cdots\cdots \\ \Delta S_{\ell_{min}m} \\ \vdots \\ \Delta S_{\ell_{max}m} \end{vmatrix} \tag{7.9}$$

with a similar expression for E_{km}. In a more compact notation

$$D_{km} = \left| P_{km} - Q_{km} \right| \left| \begin{matrix} \Delta C_m \\ \Delta S_m \end{matrix} \right| \tag{7.10}$$

$$E_{km} = \left| Q_{km} - P_{km} \right| \left| \begin{matrix} \Delta C_m \\ \Delta S_m \end{matrix} \right| \tag{7.11}$$

where P_{km}, Q_{km}, ΔC_m, ΔS_m are row and column vectors of length $\ell_{max} - \ell_{min} + 1$. The generalization for all frequencies km can be obtained in a straight-forward manner. Then the matrix equation for all the coefficients C_{km}, S_{km} can be written in the following compact form

$$\left| \begin{matrix} C_{km} \\ S_{km} \end{matrix} \right| = \left| \begin{matrix} \cos\psi_{km} & \sin\psi_{km} \\ -\sin\psi_{km} & \cos\psi_{km} \end{matrix} \right| \left| \begin{matrix} P^C_{km} & - Q^S_{km} \\ Q^C_{km} & P^S_{km} \end{matrix} \right| \left| \begin{matrix} \Delta C_{\ell m} \\ \Delta S_{\ell m} \end{matrix} \right| \tag{7.12}$$

where C_{km} and S_{km} are vectors of length $(2\ell_{max} + 5)(\ell_{max} + 1)$. Since the energy in the orbit error is negligible in frequencies higher than 6 cy/rev each of those vectors has a length of 481. The coefficients C_{km} and S_{km} are stored orderwise from 0 to 36 and for k starting from -6 to 6. The quantities $\cos\psi_{km}$ and $\sin\psi_{km}$ represent diagonal matrices of dimension 481x481. Each of the diagonal elements contain the cosine or sine of the phase that corresponds to that particular row. $\Delta C_{\ell m}$ and $\Delta S_{\ell m}$ are vectors containing the potential coefficient corrections. The vector $\Delta C_{\ell m}$ has $[(\ell+1)(\ell+2)/2-3]$ (or 700) elements since no zero and first degree terms are present, while the vector $\Delta S_{\ell m}$ has a length of $[\ell(\ell+1)/2-1]$ (or 665) elements since in addition no zonal terms are present. All coefficients are arranged orderwise so that to be consistent with the structure of the PGSS4 covariance matrix. Finally the matrices P^c_{km} and Q^c_{km} referring to $\Delta C_{\ell m}$ have a dimension of 481x700 and the matrices P^s_{km} and Q^s_{km} referring to $\Delta S_{\ell m}$ have a dimension of 481x665. All four of these matrices have mostly zero elements except for $(\ell_{max} - \ell_{min} + 1)$ elements per row that are non-zero and have values as given by (7.6), (7.7) and (7.9). Equation (7.12) readily provides the Jacobian (or the design matrix) of the Fourier coefficients of the radial orbit error.

To compute the covariance matrix of the Fourier coefficients we first compute the covariance matrix of the coefficients D_{km} and E_{km} for one particular combination of indices km and nj. Equation (7.1) then gives

$$\begin{vmatrix} \sigma_{D_{km,nj}} & \sigma_{DE_{km,nj}} \\ & \sigma_{E_{km,nj}} \end{vmatrix}_2 = \begin{vmatrix} P^C_{km} & -Q^S_{km} \\ Q^C_{km} & P^S_{km} \end{vmatrix}_2 \begin{Vmatrix} \Sigma_C & \Sigma_{CS} \\ \Sigma_{SC} & \Sigma_S \end{Vmatrix}_{70} \begin{Vmatrix} P^{C^T}_{nj} & Q^{C^T}_{nj} \\ -Q^{S^T}_{nj} & P^{S^T}_{nj} \end{Vmatrix}_2 \tag{7.13}$$

where the geopotential covariance of orders m and j is split into the covariance matrices Σ_C, Σ_S, Σ_{CS}, and Σ_{SC}. Then

$$\sigma_{D_{km,nj}} = P^C_{km}\Sigma_C P^{C^T}_{nj} + Q^S_{km}\Sigma_S Q^{S^T}_{nj} - P^C_{km}\Sigma_{cs} Q^{S^T}_{nj} - Q^S_{km}\Sigma_{SC} P^{C^T}_{nj} \tag{7.14}$$

$$\sigma_{E_{km,nj}} = Q^C_{km}\Sigma_C Q^{C^T}_{nj} + P^S_{km}\Sigma_S P^{S^T}_{nj} + Q^C_{km}\Sigma_{CS} P^{S^T}_{nj} + P^S_{km}\Sigma_{SC} Q^{C^T}_{nj} \tag{7.15}$$

$$\sigma_{DE_{km,nj}} = P^C_{km}\Sigma_C Q^{C^T}_{nj} - Q^S_{km}\Sigma_S P^{C^T}_{nj} - Q^S_{km}\Sigma_{SC} Q^{C^T}_{nj} + P^C_{km}\Sigma_{CS} P^{S^T}_{nj} \tag{7.16}$$

Since most of the elements in these matrix multiplications are zero it is more efficient to express these equations in a summation form over the non-zero elements. Then we obtain

$$\sigma_{D_{km,nj}} = \sum_{\ell} \sum_{i} \left[P_{km\ell} P_{nji} \sigma_{C_{\ell m,ij}} + Q_{km\ell} Q_{nji} \sigma_{S_{\ell m,ij}} - P_{km\ell} Q_{nji} \sigma_{CS_{\ell m,ij}} - Q_{km\ell} P_{nji} \sigma_{CS_{ij,\ell m}} \right] \tag{7.17}$$

$$\sigma_{E_{km,nj}} = \sum_{\ell} \sum_{i} \left[Q_{km\ell} Q_{nji} \sigma_{C_{\ell m,ij}} + P_{km\ell} P_{nji} \sigma_{S_{\ell m,ij}} + Q_{km\ell} P_{nji} \sigma_{CS_{\ell m,ij}} + P_{km\ell} Q_{nji} \sigma_{CS_{ij,\ell m}} \right] \tag{7.18}$$

$$\sigma_{DE_{km,nj}} = \sum_{\ell} \sum_{i} \left[P_{km\ell} Q_{nji} \sigma_{C_{\ell m,ij}} - Q_{km\ell} P_{nji} \sigma_{S_{\ell m,ij}} + P_{km\ell} P_{nji} \sigma_{CS_{\ell m,ij}} - Q_{km\ell} Q_{nji} \sigma_{CS_{ij,\ell m}} \right] \tag{7.19}$$

The above equations can compute the variances of the coefficients D_{km} and E_{km} when km=nj, covariances between coefficients of different k

or different n, or as computed above, covariances between coefficients of any frequency. From equations (7.17) - (7.19) we can compute the covariances of the Fourier coefficients as follows

$$\sigma_{C_{km,nj}} = \cos\psi_{km}\cos\psi_{nj}\sigma_{D_{km,nj}} + \sin\psi_{km}\sin\psi_{nj}\sigma_{E_{km,nj}} + (\cos\psi_{km}\sin\psi_{nj} + \sin\psi_{km}\cos\psi_{nj})\sigma_{DE_{km,nj}} \quad (7.20)$$

$$\sigma_{S_{km,nj}} = \sin\psi_{km}\sin\psi_{nj}\sigma_{D_{km,nj}} + \cos\psi_{km}\cos\psi_{nj}\sigma_{E_{km,nj}} - (\cos\psi_{km}\sin\psi_{nj} + \sin\psi_{km}\cos\psi_{nj})\sigma_{DE_{km,nj}} \quad (7.21)$$

$$\sigma_{CS_{km,nj}} = -\cos\psi_{km}\sin\psi_{nj}\sigma_{D_{km,nj}} + \sin\psi_{km}\cos\psi_{nj}\sigma_{E_{km,nj}} + (\cos\psi_{km}\cos\psi_{nj} - \sin\psi_{km}\sin\psi_{nj})\sigma_{DE_{km,nj}} \quad (7.22)$$

Computation of all the covariances (7.20) - (7.22) generates the covariance matrix of the Fourier coefficients. This matrix is a symmetric one and can be split into three matrices namely Σ_C, Σ_S, and Σ_{CS}, where Σ_C and Σ_S are also symmetric. Then the variance of a coefficient of frequency km and its covariances with all the other elements can be found at the $\bar{k}$ row where

$$\bar{k} = \ell_{max}(2k_{max}+1)(k_{max}+k) - \frac{(k_{max}+k)(k_{max}+k+1)}{2} + m + 1 \quad (7.23)$$

Its covariance with a particular nj Fourier coefficient is found in the column that has the following index with respect to the diagonal of the $\bar{k}$ row

$$\text{index} = \bar{n} - \bar{k} + 1 \quad (7.24)$$

where $\bar{n}$ is computed from (7.23) with n, j as arguments. The above is valid for either Σ_C or Σ_S. Since Σ_{CS} is a square matrix the elements are simply located by the indices $\bar{n}$ and $\bar{k}$. This indexing is very important in the data management aspect of the computation and usage of this matrix.

The determination of the variances of the Fourier coefficients at zero and 1 cy/rev frequencies as well as their correlations with all the other frequencies is now a trivial matter, since their Jacobian can be readily obtained from equations (5.31), (5.33), (5.34) and (4.54) - (4.61). The basic difference between this Jacobian and the one that led to equations (7.20) – (7.22) is that all its row elements are non zero since all the potential coefficient terms give rise to these frequencies. Furthermore this Jacobian is clearly arc dependent in contrast to the first one that is arc independent and representative of the accuracies of the orbit in general.

A similar reasoning exists for the resonant and second order induced errors. Accuracies and error correlations due to zonal coefficients can be easily computed using the same formulation and considering the covariances for the zonal coefficients, while all the second order effects are readily available since they are just linear functions of the constant bias Δa_o and the resonant terms.

Having the covariance matrix of the Fourier coefficients the variance of the radial distances at time Δt can be computed by using the following generalization of (7.2)

$$\Delta r = I \left| \cos\dot{\psi}_{km}\Delta t \;\; \sin\dot{\psi}_{km}\Delta t \right| \begin{vmatrix} C_{km} \\ S_{km} \end{vmatrix} \qquad (7.25)$$

where now the cosine and sine are diagonal matrices of dimension 481x481 with their elements computed for the frequencies km and a particular Δt. Obviously C_{km} and S_{km} are row vectors containing all the Fourier coefficients and I is a unit row vector. Implementation of (7.1) can then provide the variance of the radial distance at Δt. With the same reasoning we can obtain the covariance matrix of all or a subset of radial distances within an arc or among different arcs.

The computation of the statistics of the uncertainties of the radial distance is based on equations (5.37), (5.38). As a matter of fact it turns out that the equations describing the RMS estimates of the uncertainties are identical to (5.39) - (5.41), applied for the variances. Then the RMS radial orbit uncertainty is

$$\sigma_{\Delta r} = \left[\frac{1}{2} \sum_{km} \left(\sigma^2_{C_{km}} + \sigma^2_{S_{km}} \right) \right]^{1/2} \qquad (7.26)$$

The RMS uncertainty by order becomes

$$\sigma_{\Delta r_m} = \left[\frac{1}{2} \sum_k \left(\sigma^2_{C_{km}} + \sigma^2_{S_{km}}\right)\right]^{1/2} \tag{7.27}$$

while the RMS uncertainty by degree becomes

$$\sigma_{\Delta r_\ell} = \left[\frac{1}{2} \sum_{km} \left(A^2_{km\ell} + B^2_{km\ell}\right)\left(\sigma^2_{C_{\ell m}} + \sigma^2_{S_{\ell m}}\right)\right]^{1/2} \tag{7.28}$$

By breaking (7.28) even further we can obtain the RMS uncertainties for any degree and order.

The variances of the Fourier coefficients up to 6 cy/rev have been computed by implementing (7.20) - (7.22) and using the scaled PGSS4 covariance matrix up to degree 36. The corresponding spectrum of uncertainties is shown in Figure 28, while the RMS radial orbit uncertainty is computed to be 63 cm. From Figure 28 we observe that the uncertainty at 1 cy/rev is very small. All the uncertainties are practically at frequencies below 2 cy/rev. It is also seen that the frequencies very close to 1 cy/rev have very small uncertainties which are due to the tailoring of the field with the Seasat altimeter data. Recognizing that this tailoring affected primarily the harmonics above degree 20 the following test was made to understand what this effect has been. The variances of the Fourier coefficients have been recomputed using the scaled PGSS4 covariance up to degeee 20 (Solution II) and the covariance between degrees 21 and 36 (Solution III). A final variance computation used the covariances between the coefficients of degrees lower than 20 with those of degrees greater than 20 (Solution IV). It is obvious that the sum of these three computations is equal to the first computation that used the full covariance up to degree 36 (Solution I). Comparison of the individual variance components between the four solutions for all frequencies, indicates that for most of the frequencies solutions III and IV give no significant contributions. In other words the use of the scaled PGSS4 covariance up to degree 20 gives almost identical variances as with the use of the covariance complete to degree 36. An exception to the above is for four frequencies that are very close to 1 cy/rev. These frequencies contain the first harmonic order and the resonant orders 14 and 15. They are shown in Table 8. The variance components of solutions II, III, and IV for all the four frequencies are such that the total variances of solution I are very close to zero. These components are shown in Table 8.

Table 8

Variance Components of Fourier Coefficients of Seasat Radial Distances Based on the Scaled PGSS4 Covariance

Frequency	k	m	I	II	III	IV
0.929 cy/rev	1	1	0.003 m^2	0.619 m^2	0.586 m^2	-1.202 m^2
0.975	0	14	0.009	0.419	0.404	-0.814
1.045	0	15	0.005	0.109	0.107	-0.211
1.068	-1	1	0.005	0.579	0.573	-1.147
Total			0.022	1.726	1.670	-3.374

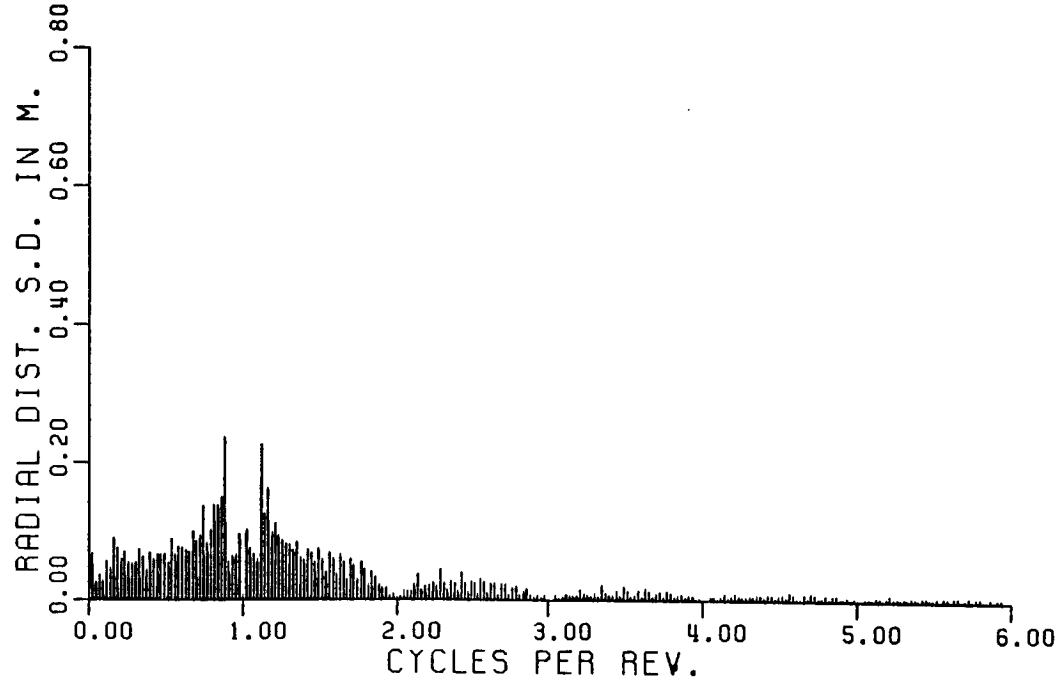

Figure 28. Spectrum of Seasat Radial Distance Standard Deviations Based on the Scaled PGSS4 Covariance.

As it can be seen from Table 8 the incorporation of the Seasat altimeter data has introduced significant correlations between coefficients of orders 1, 14 and 15 so that to produce lumped coefficients at frequencies very close to 1 cy/rev, that give an almost perfect fit to the orbit.

The RMS uncertainties of the arc dependent constant bias and 1 cy/rev effects have also been computed and are shown in Table 9 for all the six day arcs of Seasat. The total RMS uncertainty for each arc has also been computed, taking into account the arc independent RMS uncertainty of 63 cm, and is shown in Table 9.

Table 9

Constant, 1 cy/rev and Total RMS Radial Distance Standard Deviations for all Seasat Arcs Based on the Scaled PGSS4 Covariance.

Seasat Arc	Constant	1 cy/rev	Total
1	0.39 m	0.70 m	1.02 m
2	0.28	0.64	0.94
3	0.38	0.67	0.99
4	0.38	0.70	1.01
5	0.39	0.67	0.99
6	0.48	0.72	1.07
7	0.58	0.77	1.15
8	1.07	1.08	1.64
9	0.38	0.67	0.99
10	0.39	0.71	1.03
11	0.66	0.85	1.25
12	0.37	0.69	1.01

In all the arcs the 1 cy/rev error is the dominant error. It has an RMS uncertainty generally on the order of 70 cm with the exception of the eighth and eleventh arcs. The constant bias is around 40 cm with higher values for the above two arcs. No explanation for these higher uncertainties has been found. The total RMS uncertainty is on the order of 1 meter, again with the exception of the eighth and eleventh arcs. The accuracy estimates in Table 9 agree quite well with the 0.70 m accuracy estimate that was given by Lerch et al. (1982), if we consider that the latter estimate is based on the computed RMS crossover discrepancy for two 6 day arcs and that the part of the orbit error that is not observed by crossovers has almost the same magnitude with the part that is observed. So if we assume that the non observed part also provides an RMS uncertainty of 0.70 m, then the total RMS accuracy is 0.99 m which is consistent

with the estimates of Table 9. This agreement indicates that the scaling of the PGSS4 covariance by a factor of 10 could be realistic although, it is definitely a simplified one. As mentioned at the beginning of this Chapter, these accuracy estimates do not include any long wavelength zonal effects or second order effects. This should not cause any problems because these effects are expected to have been properly removed from the Seasat orbits. Additional errors arising from initial state vector errors, air drag, solar radiation pressure and other error sources are not expected to significantly change these estimates.

Additional statistics that have been computed include the arc independent RMS accuracies by degree, by order, and by degree and order. These are shown in Figures 29 and 30 and in Table 10, respectively. Figure 30 shows again the small uncertainties in orders 1, 14 and 15 which result from the use of the altimeter data. From Figure 29 we observe that the odd degrees give the largest contribution to the orbit error, together with degrees 14, 15, and 16. Note that the overall uncertainty from Figure 30 is much smaller than in Figure 29 because of the significant correlations between coefficients of different degrees and same order which are not accounted for in Figure 29. Basically the same type of information can be obtained from Table 10 where we can observe the large uncertainties of individual odd degree coefficients and primarily the ones of harmonic orders 1, 14, and 15. Again the correlations between these coefficients are not accounted for. So Figure 29 and Table 10 cannot really be used by themselves for an accuracy assessment since they provide a quite distorted estimate of the orbital accuracies.

In order to see what is the behavior of radial accuracies with respect to time, a computation was made of the variances of the radial distances for the first Seasat arc, at time intervals of 5 minutes, and using the scaled PGSS4 covariance up to degree 36. Correlations between radial distances for the first three revolutions have also been computed. To ease the computational burden, only frequencies up to 2 cy/rev have been used. The full covariance matrix of the Fourier coefficients up to that frequency as well as the variances of the constant bias and 1 cy/rev effects and their covariances with all the other frequencies have been computed for this purpose. The accuracies for the first 6 day Seasat arc are plotted in Figure 31 where we can observe the strong 1 cy/rev effect and daily and semidaily terms. Note that at the beginning of the arc the uncertainty is very close to zero and it accumulates rapidly at the 1 m level. The small error at 3 days occurs because the satellite passes through the same geographic region after that period of time and so the error is similar to the error at the initial minutes of the arc. This is another indication of the geographic correlation of the orbit error.

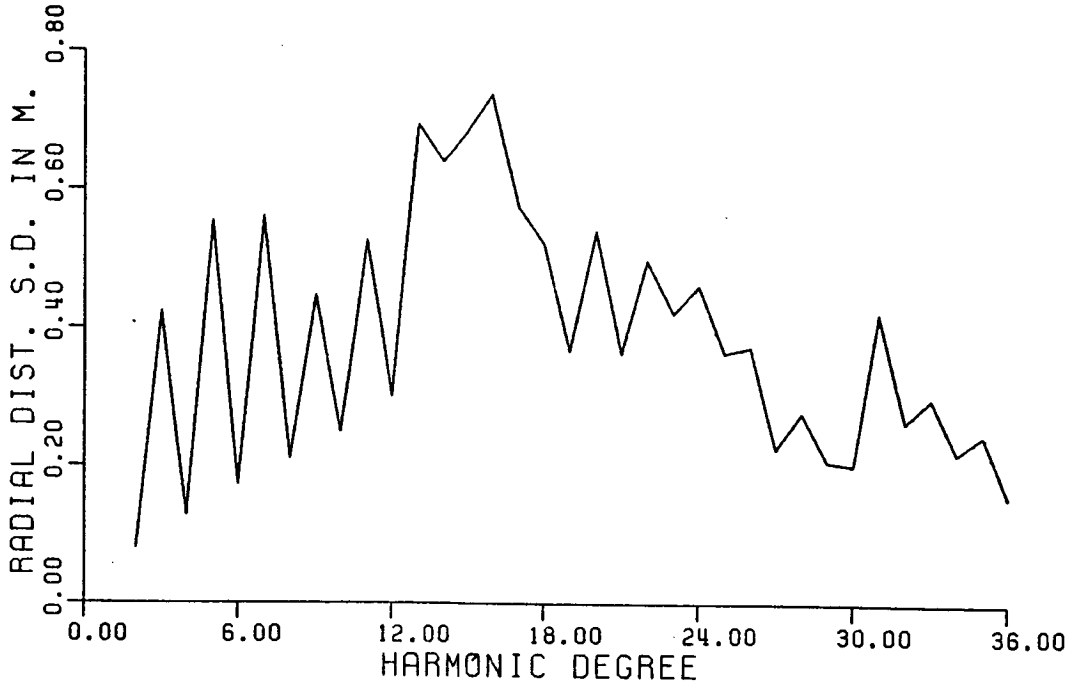

Figure 29. RMS of Seasat Radial Distance Standard Deviations by Harmonic Degree Based on the Scaled PGSS4 Covariance.

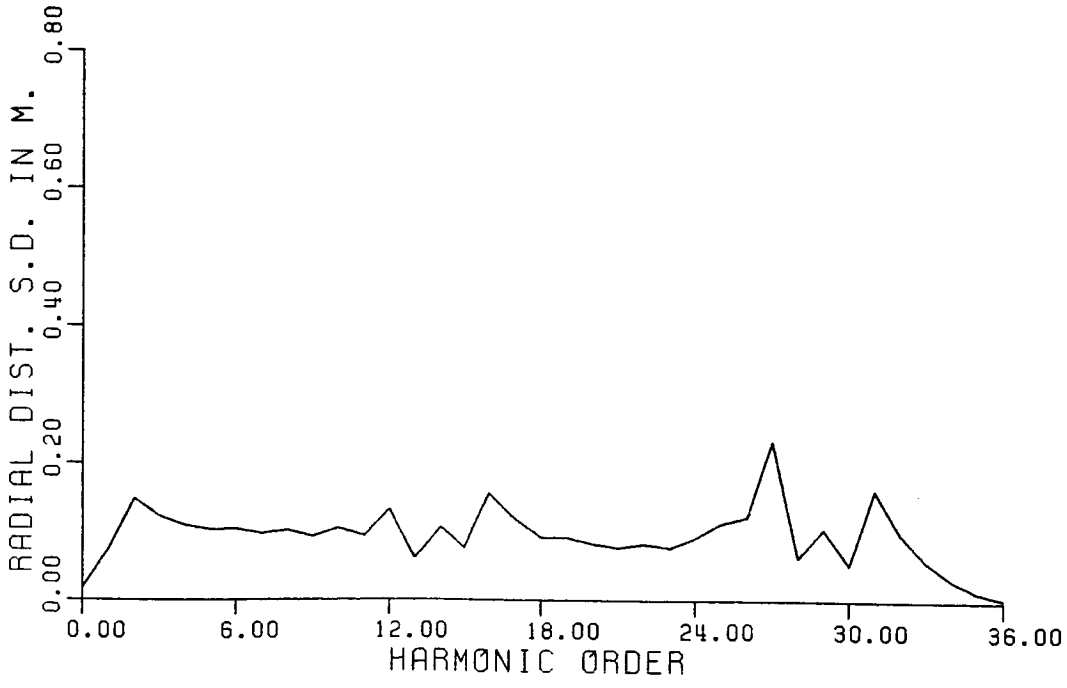

Figure 30. RMS of Seasat Radial Distance Standard Deviations by Harmonic Order Based on the Scaled PGSS4 Covariance.

Table 10

RMS of Seasat Radial Distance Standard Deviations for each Coefficient Degree and Order Based on the Scaled PGSS4 Covariance. Units are in Centimeters.

	0	1	2	3	4	5	6	7	8	9	10	11	12	13	14	15	16	17	18	19	20
2	0	3	7																		
3	1	39	13	9																	
4	0	7	3	6	7																
5	0	50	11	16	8	8															
6	1	7	3	8	3	7	9														
7	0	45	21	18	9	9	6	6													
8	2	4	8	6	6	8	5	8	10												
9	0	14	35	11	12	9	6	6	5	5											
10	2	1	10	2	8	4	8	7	7	9	11										
11	0	30	36	9	14	6	8	6	4	4	4	3									
12	1	5	7	5	7	4	8	4	9	6	10	12	14								
13	0	60	21	19	11	8	8	4	5	3	3	2	1	2							
14	0	8	2	8	3	7	5	6	7	5	10	7	12	13	56						
15	0	61	6	22	4	10	5	6	4	2	3	2	1	1	4	8					
16	1	6	3	7	2	7	2	8	4	7	7	9	10	9	53	41	14				
17	0	44	23	17	7	9	3	6	2	3	2	2	1	0	2	10	6	3			
18	1	3	6	4	5	4	4	6	4	7	5	9	8	12	30	27	17	10	5		
19	0	10	29	6	11	4	6	4	3	3	2	2	1	0	3	2	4	5	5	2	
20	1	0	6	1	5	1	5	2	5	4	6	8	7	9	32	34	9	8	7	5	2
21	0	23	20	6	9	2	6	1	4	2	2	2	1	0	1	5	4	1	4	4	4
22	1	3	3	3	4	2	4	2	5	2	6	4	8	8	34	26	10	7	3	4	4
23	0	36	8	11	5	4	3	2	3	1	2	1	1	0	1	6	1	3	3	1	4
24	0	3	0	4	1	3	1	3	3	3	5	3	7	6	36	19	10	5	4	3	2
25	0	32	1	10	1	5	1	3	1	2	1	1	1	0	2	2	2	3	1	3	2
26	0	2	1	2	1	2	0	2	1	3	2	4	5	7	29	15	8	4	3	2	2
27	0	17	6	5	3	3	1	2	0	1	0	1	0	0	2	1	2	1	2	2	1
28	0	1	1	1	1	1	1	1	1	2	1	4	2	7	19	14	5	3	2	2	1
29	0	2	6	1	3	1	1	0	1	0	0	0	0	0	0	2	1	1	1	0	1
30	0	0	1	0	1	0	1	0	1	0	1	1	2	5	12	12	3	2	1	1	1
31	0	5	11	3	6	1	4	1	3	1	2	1	1	0	0	1	1	3	2	3	3
32	0	0	1	1	2	1	2	1	3	1	5	2	8	3	15	7	8	7	3	3	3
33	0	7	4	5	2	3	2	2	2	1	1	0	1	0	0	0	2	2	1	2	1
34	0	0	0	1	0	2	0	2	1	2	3	3	6	1	13	4	8	4	3	3	1
35	0	5	1	4	0	2	0	2	0	1	0	1	0	0	0	0	2	0	1	1	1
36	0	0	0	1	0	1	0	1	0	2	0	3	2	2	8	4	6	2	3	1	1

	21	22	23	24	25	26	27	28	29	30	31	32	33	34	35	36
21	2															
22	3	1														
23	4	4	2													
24	3	3	2	0												
25	1	4	4	4	2											
26	2	1	2	2	1	0										
27	2	2	2	4	4	4	2									
28	1	1	1	1	1	0	0	0								
29	1	1	2	1	3	5	4	11	11							
30	1	0	0	0	0	0	0	1	4	0						
31	2	5	3	5	8	6	18	13	26	4	2					
32	2	2	2	1	1	1	1	0	6	2	2	0				
33	2	2	2	4	3	7	12	3	15	5	11	4	1			
34	2	1	1	1	1	1	0	0	1	1	5	3	1	0		
35	2	1	2	2	3	5	6	7	14	2	8	7	4	1	0	
36	1	1	1	1	0	0	0	0	3	0	1	3	3	2	1	0

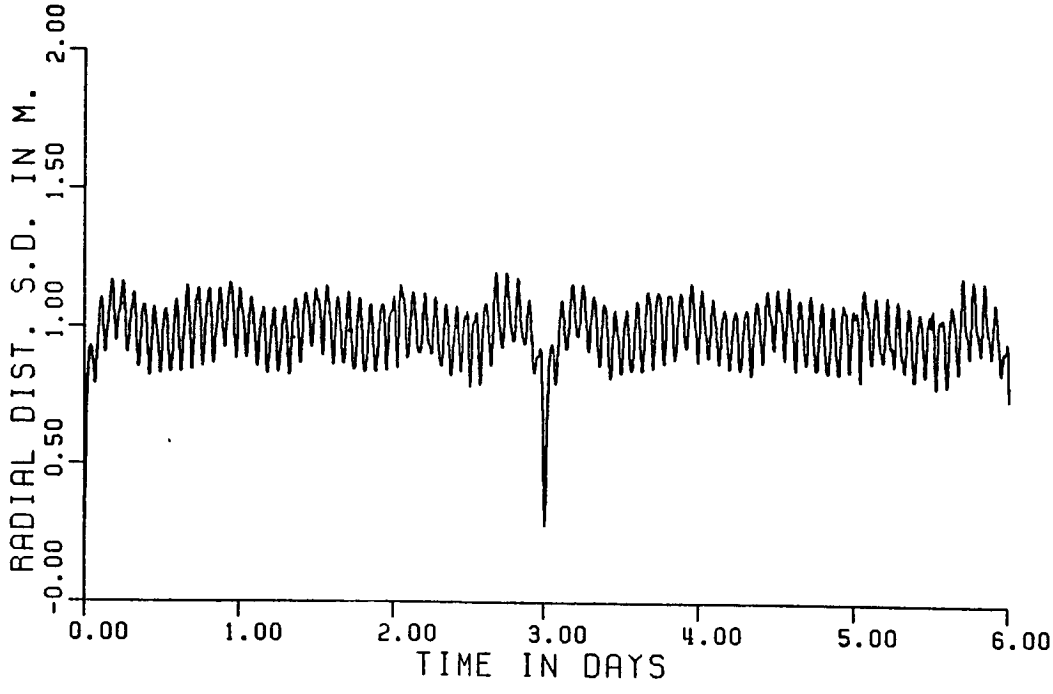

Figure 31. Seasat Radial Distance Standard Deviations Based on the Scaled PGSS4 Covariance.

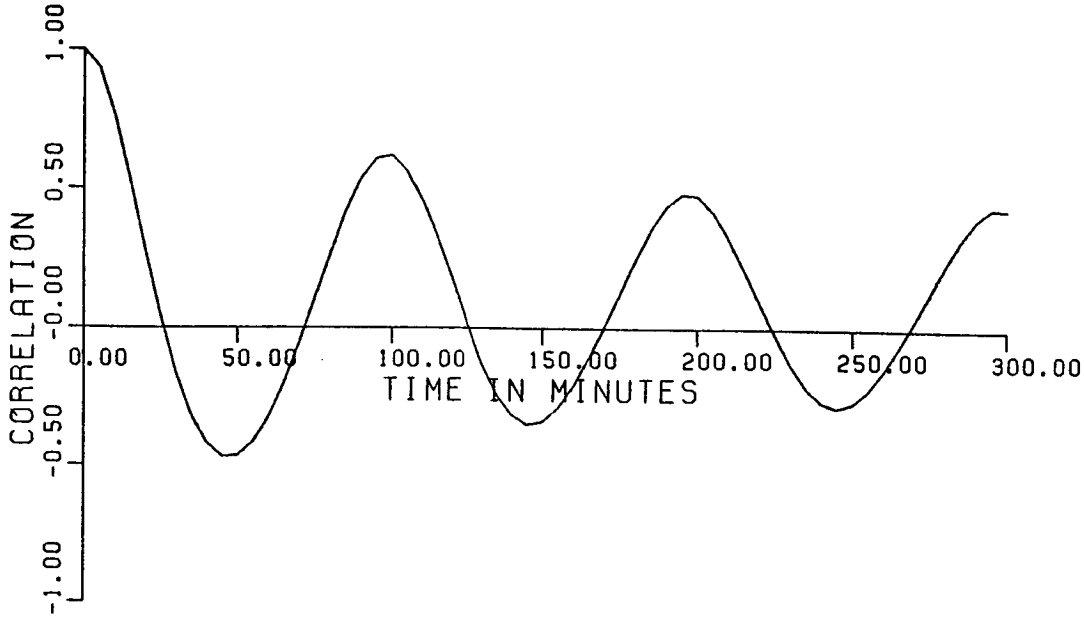

Figure 32. Error Correlations Between Seasat Radial Distances Based on the Scaled PGSS4 Covariance.

Figure 32 shows a representative correlation curve for time lags up to 300 minutes (approximately 3 revolutions). The correlation obtains a maximum negative value of about 0.40 after half a revolution and a local maximum positive value of about 0.70 after one revolution. This pattern continues with smaller amplitudes in the correlations, to become zero between radial distances being 1.5 days apart or equivalently differing by 180° in longitude. After that, the correlations start increasing again to become very close to 1 for a lag of 3 days. The actual magnitude of the correlations depends on the particular time that we consider as initial point for the correlation computation, but is not expected to vary appreciably.

The covariance propagation of geoid undulations can be made in an identical way to the one for the radial distances. All the equations developed so far in this section can be used for this purpose with the following changes in (7.6), (7.7), and (7.8)

$$P_{km\ell} = \begin{cases} RF_{\ell m \frac{\ell-k}{2}} & \ell-m \text{ even} \\ 0 & \ell-m \text{ odd} \end{cases} \tag{7.29}$$

$$Q_{km\ell} = \begin{cases} 0 & \ell-m \text{ even} \\ RF_{\ell m \frac{\ell-k}{2}} & \ell-m \text{ odd} \end{cases} \tag{7.30}$$

and ℓ_{min} as given by (5.61). The computations have to be made for all frequencies up to 36 cy/rev since the undulation spectrum has significant energies at the higher frequencies also. In a similar analysis the covariances of the errors in the residual sea surface heights can be obtained. In this study only the variances of the undulations and residual sea surface heights have been computed up to 6 cy/rev. The corresponding spectra are shown in Figures 33 and 34. Note again the distinctly different behavior of the radial distance (Figure 28) and undulation spectra. The residual sea surface height spectrum (without the sea surface topography signal) has amplified uncertainties at frequencies below the 1 cy/rev and smaller ones at frequencies between 1 and 2 cy/rev. This happens because the error correlations between the radial distances and undulations are positive in the first frequency band and negative in the second frequency band.

7.3. Covariance Propagation Using the Geographic Representation

Variances and covariances of radial distances and geoid undulations can also be obtained using equations (5.86), (5.87), (5.91), and (6.4). The covariance propagation in terms of geographic

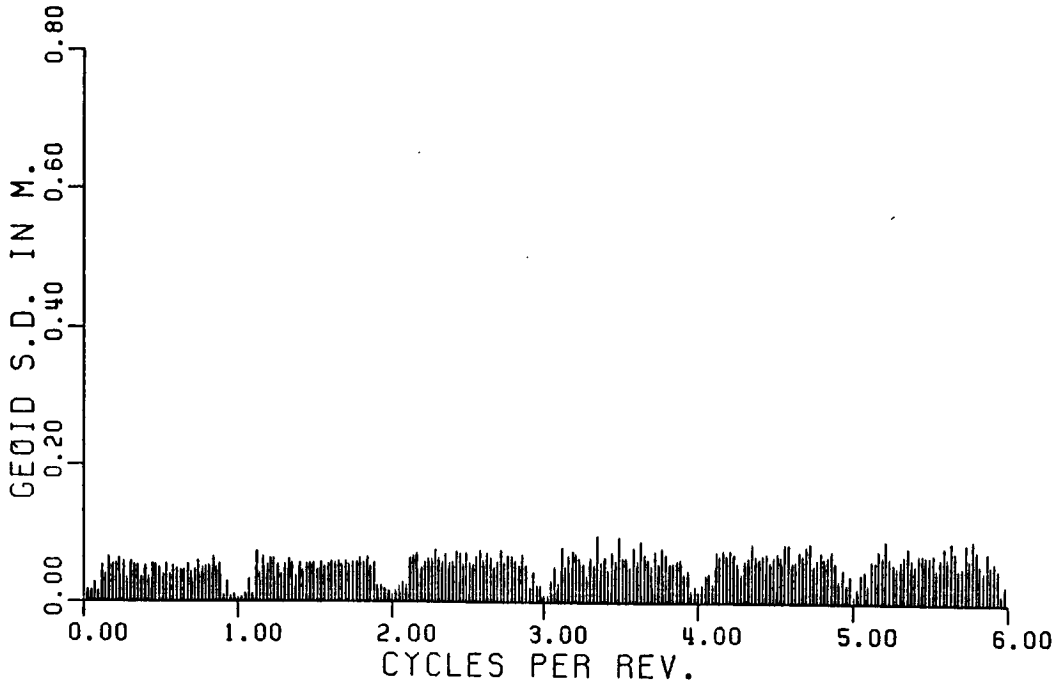

Figure 33. Spectrum of Geoid Undulation Standard Deviations Based on the Scaled PGSS4 Covariance.

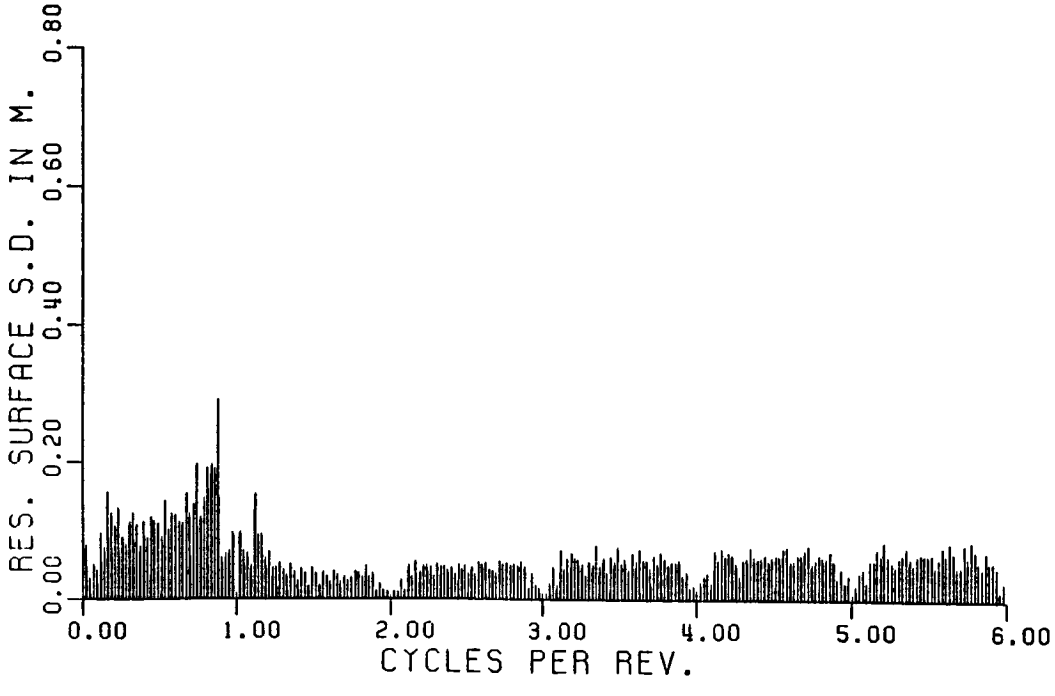

Figure 34. Spectrum of Residual Sea Surface Standard Deviations Based on the Scaled PGSS4 Covariance.

coordinates has the advantage of providing the spatial behavior of the accuracies in a satellite orbit as well as the geoid. Consistent with the computations in section 5.4 the accuracy estimation is to be done on a geographic grid. Then interpolation to the actual point of altimeter observation can provide the accuracy of the orbit at that point. As described in section 5.3.1, the first order radial orbit error of gravitational origin can be written

$$\Delta r = \Delta r^c \pm \Delta r^v \tag{7.31}$$

with

$$\Delta r^c = \Delta r^c_p - \Delta r^c_o \tag{7.32}$$

$$\Delta r^v = \Delta r^v_p - \Delta r^v_o \tag{7.33}$$

where

$$\Delta r^c_o = \Delta r_o + \Delta r^c_i \tag{7.34}$$

$$\Delta r^v_o = \Delta r^v_i \tag{7.35}$$

and c, v denote the mean and variable parts of the error respectively. Then the variances of the above quantities become

$$\sigma^2_r = \sigma^{c\,2}_r + \sigma^{v\,2}_r \pm 2\sigma^{cv}_r \tag{7.36}$$

$$\sigma^{c\,2}_r = \sigma^{c\,2}_p + \sigma^{c\,2}_o - 2\sigma^c_{po} \tag{7.37}$$

$$\sigma^{v\,2}_r = \sigma^{v\,2}_p + \sigma^{v\,2}_o - 2\sigma^v_{po} \tag{7.38}$$

$$\sigma^{cv}_r = \sigma^{cv}_p + \sigma^{cv}_o - \sigma^{cv}_{po} - \sigma^{cv}_{op} \tag{7.39}$$

To compute all the variances and covariances in equations (7.36) - (7.39) requires some tedious algebraic manipulations. Here only the final expressions for each of these quantities are going to be given. To simplify the notation we denote

$$A^c_{\ell m} = \sum_p \left(A_{\ell mp} + B_{\ell mp} + C_{\ell mp}\right)\tilde{Q}_{\ell mp}(\Phi) \tag{7.40}$$

$$A^{v}_{\ell m} = \sum_{p}\left(A_{\ell mp} + B_{\ell mp} + C_{\ell mp}\right)\tilde{R}_{\ell mp}(\phi) \tag{7.41}$$

$$B^{1}_{\ell m} = \sum_{p} A_{\ell mp}\, \tilde{Q}_{\ell mp}(\phi_o) \tag{7.42}$$

$$B^{2}_{\ell m} = i \sum_{p} A_{\ell mp}\, \tilde{R}_{\ell mp}(\phi_o) \tag{7.43}$$

$$C^{1c}_{\ell m} = \sum_{p} W^{1}_{\ell mp}\ (\phi_o) \tag{7.44}$$

$$C^{2c}_{\ell m} = i \sum_{p} W^{2}_{\ell mp}\ (\phi_o) \tag{7.45}$$

$$C^{1v}_{\ell m} = \sum_{p} W^{3}_{\ell mp}\ (\phi_o) \tag{7.46}$$

$$C^{2v}_{\ell m} = i \sum_{p} W^{4}_{\ell mp}\ (\phi_o) \tag{7.47}$$

$$A_{\ell m} = \left(B^{1}_{\ell m} + C^{1c}_{\ell m}\frac{\sin\phi}{\sin i}\right)\cos m\lambda_o + \left(B^{2}_{\ell m} + C^{2c}_{\ell m}\frac{\sin\phi}{\sin i}\right)\sin m\lambda_o \tag{7.48}$$

$$B_{\ell m} = \left(B^{1}_{\ell m} + C^{1c}_{\ell m}\frac{\sin\phi}{\sin i}\right)\sin m\lambda_o + \left(B^{2}_{\ell m} + C^{2c}_{\ell m}\frac{\sin\phi}{\sin i}\right)\cos m\lambda_o \tag{7.49}$$

$$C_{\ell m} = \left(1 - \frac{\sin^2\phi}{\sin^2 i}\right)^{1/2}\left(C^{2v}_{\ell m}\cos m\lambda_o + C^{1v}_{\ell m}\sin m\lambda_o\right) \tag{7.50}$$

$$D_{\ell m} = \left(1 - \frac{\sin^2\phi}{\sin^2 i}\right)^{1/2}\left(C^{2v}_{\ell m}\sin m\lambda_o + C^{1v}_{\ell m}\cos m\lambda_o\right) \tag{7.51}$$

then

$$\sigma^{c^2}_{p} = \sum_{m=o}^{\ell_{max}} \sum_{\ell=\ell'}^{\ell_{max}} \Bigg[\sum_{j=m}^{\ell_{max}} \sum_{i=i'}^{\ell_{max}} \left(2-\delta_{\ell m, ij}\right) A^{c}_{\ell m} A^{c}_{ij} \cos m\lambda \cos j\lambda \sigma_{c_{\ell m, ij}}$$

$$+ \sum_{j=m}^{\ell_{max}} \sum_{i=i'}^{\ell_{max}} \left(2 - \delta_{\ell m, ij}\right) A^{c}_{\ell m} A^{c}_{ij}\ \sin m\lambda \sin j\lambda \sigma_{s_{\ell m, ij}}$$

$$+ 2 \sum_{j=1}^{\ell_{max}} \sum_{i=i'}^{\ell_{max}} A^{c}_{\ell m} A^{c}_{ij} \cos m\lambda \sin j\lambda \sigma_{cs_{\ell m, ij}} \Bigg] \tag{7.52}$$

where

$$\ell' = \max(2,m)$$

$$i' = \max(2,j)$$

$$i'' = \begin{cases} \ell' & \text{if } j=m \\ j & \text{if } j>m \end{cases} \tag{7.53}$$

$$\delta_{\ell m,ij} = \begin{cases} 1 & \text{if } i=\ell \text{ and } j=m \\ 0 & \text{otherwise} \end{cases}$$

Similarly

$$\sigma_p^{v^2} = \sum\sum\Big[\sum\sum(2-\delta_{\ell m,ij})A^v_{\ell m}A^v_{ij}\sin m\lambda\sin j\lambda\sigma_{c_{\ell m,ij}} + \sum\sum(2-\delta_{\ell m,ij})A^v_{\ell m}A^v_{ij}\cos m\lambda\cos j\lambda\sigma_{s_{\ell m,ij}} - 2\sum\sum A^v_{\ell m}A^v_{ij}\sin m\lambda\cos j\lambda\sigma_{cs_{\ell m,ij}}\Big] \tag{7.54}$$

$$\sigma_p^{cv} = \sum\sum\Big[\sum\sum\big(A^c_{\ell m}A^v_{ij}\cos m\lambda\sin j\lambda+(1-\delta_{\ell m,ij})A^v_{\ell m}A^c_{ij}\sin m\lambda\cos j\lambda\big)\sigma_{c_{\ell m,ij}} - \sum\sum\big(A^c_{\ell m}A^v_{ij}\sin m\lambda\cos j\lambda+(1-\delta_{\ell m,ij})A^v_{\ell m}A^c_{ij}\cos m\lambda\sin j\lambda\big)\sigma_{s_{\ell m,ij}} - \sum\sum\big(A^c_{\ell m}A^v_{ij}\cos m\lambda\cos j\lambda-A^v_{\ell m}A^c_{ij}\sin m\lambda\sin j\lambda\big)\sigma_{cs_{\ell m,ij}}\Big] \tag{7.55}$$

$$\sigma_o^{c^2} = \sum\sum\Big[\sum\sum\big(2-\delta_{\ell m,ij}\big)\big(A_{\ell m}A_{ij}\sigma_{c_{\ell m,ij}}+B_{\ell m}B_{ij}\sigma_{s_{\ell m,ij}}\big) + 2\sum\sum A_{\ell m}B_{ij}\sigma_{cs_{\ell m,ij}}\Big] \tag{7.56}$$

$$\sigma_o^{v^2} = \Sigma\,\Sigma\Big[\Sigma\,\Sigma(2-\delta_{\ell m,ij})(C_{\ell m}C_{ij}\sigma_{c\ell m,ij}+D_{\ell m}D_{ij}\sigma_{s\ell m,ij}) + 2\Sigma\,\Sigma\,C_{\ell m}D_{ij}\sigma_{cs\ell m,ij}\Big] \tag{7.57}$$

$$\sigma_o^{cv} = \Sigma\,\Sigma\Big[\Sigma\,\Sigma(A_{\ell m}C_{ij}+(1-\delta_{\ell m,ij})C_{\ell m}A_{ij})\sigma_{c\ell m,ij} + \Sigma\,\Sigma(B_{\ell m}D_{ij}+(1-\delta_{\ell m,ij})D_{\ell m}B_{ij})\sigma_{s\ell m,ij} + \Sigma\,\Sigma(A_{\ell m}D_{ij}+C_{\ell m}B_{ij})\sigma_{cs\ell m,ij}\Big] \tag{7.58}$$

$$\sigma_{po}^{c} = \Sigma\,\Sigma\Big[\Sigma\,\Sigma\,(A^c_{\ell m}A_{ij}\cos m\lambda+(1-\delta_{\ell m,ij})A_{\ell m}A^c_{ij}\cos j\lambda)\sigma_{c\ell m,ij} + \Sigma\,\Sigma(A^c_{\ell m}B_{ij}\sin m\lambda+(1-\delta_{\ell m,ij})B_{\ell m}A^c_{ij}\sin j\lambda)\sigma_{s\ell m,ij} + \Sigma\,\Sigma(A^c_{\ell m}B_{ij}\cos m\lambda+A_{\ell m}A^c_{ij}\sin j\lambda)\sigma_{cs\ell m,ij}\Big] \tag{7.59}$$

$$\sigma_{po}^{v} = \Sigma\,\Sigma\Big[\Sigma\,\Sigma\,(A^v_{\ell m}C_{ij}\sin m\lambda+(1-\delta_{\ell m,ij})C_{\ell m}A^v_{ij}\sin j\lambda)\sigma_{c\ell m,ij} - \Sigma\,\Sigma(A^v_{\ell m}D_{ij}\cos m\lambda+(1-\delta_{\ell m,ij})D_{\ell m}A^v_{ij}\cos j\lambda)\sigma_{s\ell m,ij} + \Sigma\,\Sigma(A^v_{\ell m}D_{ij}\sin m\lambda-C_{\ell m}A^v_{ij}\cos j\lambda)\sigma_{cs\ell m,ij}\Big] \tag{7.60}$$

$$\sigma^{cv}_{po} = \Sigma\,\Sigma\Big[\Sigma\,\Sigma\,\big(A^{c}_{\ell_m}C_{ij}\cos m\lambda+(1-\delta_{\ell_m,ij})C_{\ell_m}A^{c}_{ij}\cos j\lambda\big)\sigma_{c_{\ell_m,ij}}$$

$$+\,\Sigma\,\Sigma\big(A^{c}_{\ell_m}D_{ij}\sin m\lambda+(1-\delta_{\ell_m,ij})D_{\ell_m}A^{c}_{ij}\sin j\lambda\big)\sigma_{s_{\ell_m,ij}}$$

$$+\,\Sigma\,\Sigma\big(A^{c}_{\ell_m}D_{ij}\cos m\lambda-C_{\ell_m}A^{c}_{ij}\sin j\lambda\big)\sigma_{cs_{\ell_m,ij}}\Big] \qquad (7.61)$$

$$\sigma^{cv}_{op} = \Sigma\,\Sigma\Big[\Sigma\,\Sigma\,\big(A^{v}_{\ell_m}A_{ij}\sin m\lambda+(1-\delta_{\ell_m,ij})A_{\ell_m}A^{v}_{ij}\sin j\lambda\big)\sigma_{c_{\ell_m,ij}}$$

$$-\,\Sigma\,\Sigma\big(A^{v}_{\ell_m}B_{ij}\cos m\lambda+(1-\delta_{\ell_m,ij})B_{\ell_m}A^{v}_{ij}\cos j\lambda\big)\sigma_{s_{\ell_m,ij}}$$

$$+\,\Sigma\,\Sigma\big(A_{\ell_m}B_{ij}\sin m\lambda-A_{\ell_m}A^{v}_{ij}\cos j\lambda\big)\sigma_{cs_{\ell_m,ij}}\Big] \qquad (7.62)$$

In equations (7.54) - (7.62) all the summations are over the indices indicated in (7.52). For the uniformity of equations the quantities referring to the zonal S coefficients

$$\sigma_{S_{\ell_o,ij}} = 0$$

$$A^{v}_{\ell_o} = 0$$

have also been included. The above equations provide the variance of the radial distance at a point (ϕ, λ) as well as the variances representing the mean and variable radial errors. The same type of equations can be used to compute spatial covariances for radial distances at different geographic locations and/or between different integration arcs, by assigning the appropriate values to the latitude dependent functions, the cosines and sines of longitudes and the arc dependent functions.

The undulation variance can be computed using an equation similar to (7.52) but replacing the functions A^c by the Legendre functions. Then the residual sea surface height variance can be computed by the combination of the above equations.

A correct implementation of the equations with the complete scaled PGSS4 covariance, requires the computations to be made on at least a

1° grid. This was assessed by computing the variances on a small area and then interpolating and comparing to the results of the previous section. A global implementation though on a 1° grid becomes extremely time consuming and has not been made. It has been estimated that about 20-25 CPU hours on an IBM 3081D mainframe are required for this task even for well optimized software. For demonstration purposes computations have been made on a 5° grid using the scaled PGSS4 covariance up to degree 20. It turns out that even for that maximum degree the grid of 5° is not adequate because it does not provide accurate interpolated values, particularly in the northern and southern latitudes. Therefore the accuracy maps plotted in Figures 35-39 are only approximations to the correct accuracies. Note in all Figures that the plotted uncertainties are much higher than the uncertainties computed in the previous section where the full geopotential covariance up to degree 36 was used. Also in Figure 39 that shows the undulation accuracies we can see that the oceanic regions are represented much more accurately than the continents. Both features are yet another indication of the tailoring of the PGSS4 field with the Seasat altimeter data.

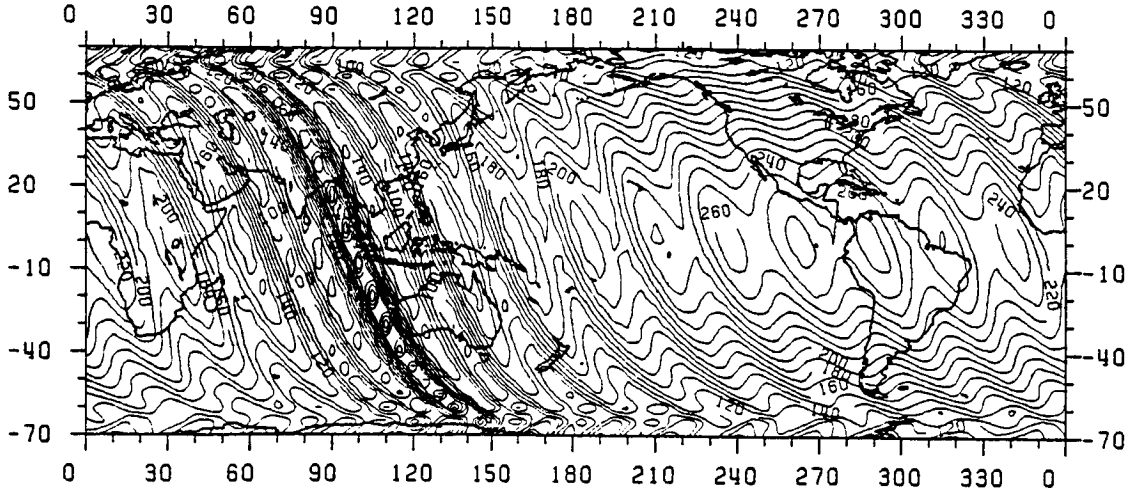

Figure 35. Standard Deviations of Radial Distances of Seasat Ascending Arcs Based on the Scaled PGSS4 Covariance to Harmonic Degree 20. C.I. = 10 cm.

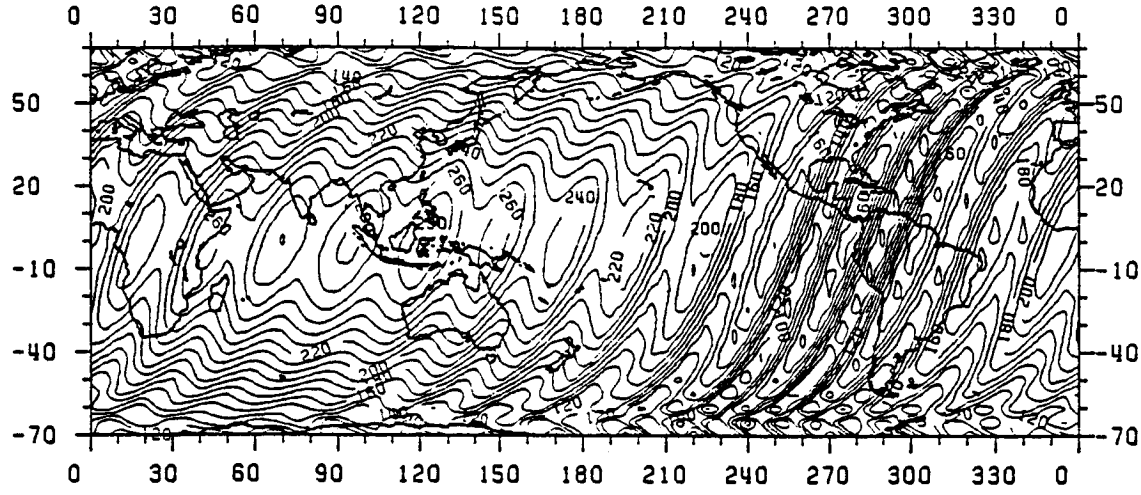

Figure 36. Standard Deviations of Radial Distances of Seasat Descending Arcs Based on the Scaled PGSS4 Covariance to Harmonic Degee 20. C.I. = 10 cm.

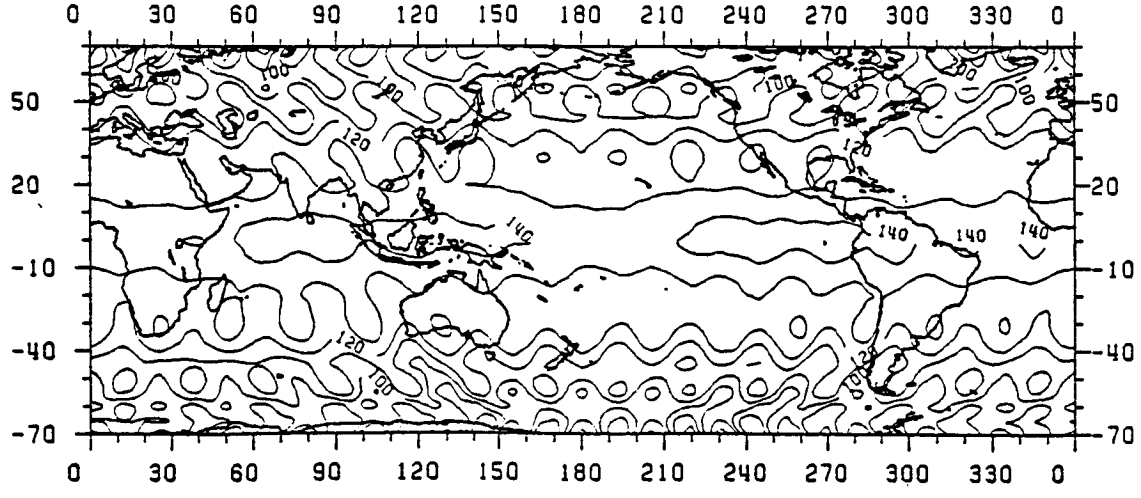

Figure 37. Standard Deviations Reflecting the Geographic Mean Error of Seasat Arcs Based on the Scaled PGSS4 Covariance to Harmonic Degree 20. C.I. = 10 cm.

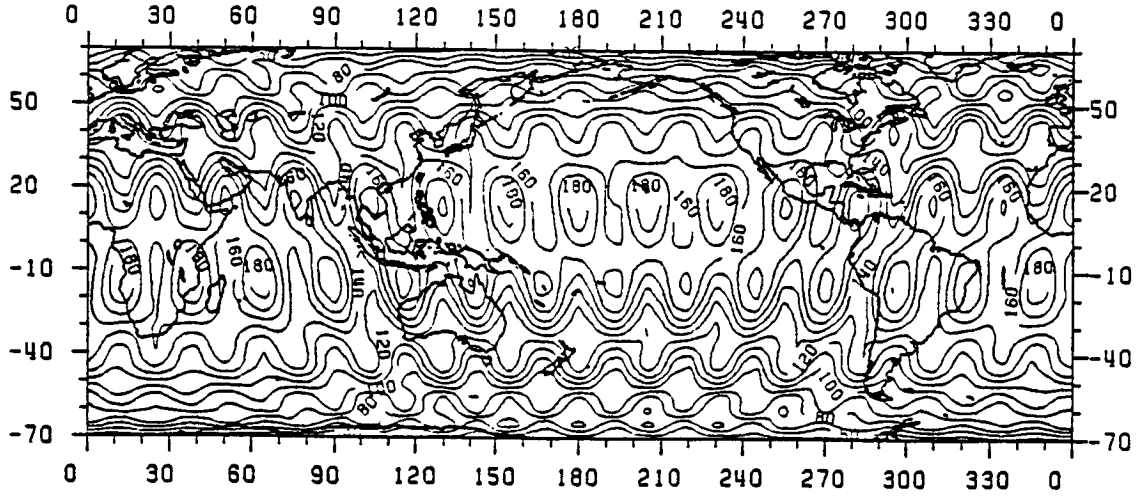

Figure 38. Standard Deviations Reflecting the Geographic Variable Error of Radial Distances of Seast Arcs Based on the Scaled PGSS4 Covariance to a Harmonic Degree 20. C.I. = 10 cm.

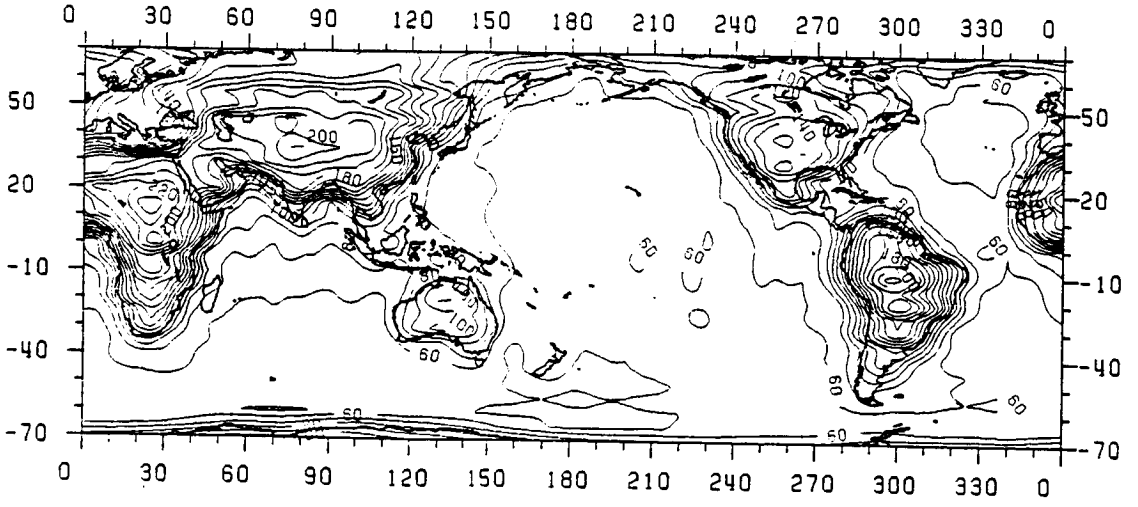

Figure 39. Geoid Undulation Standard Deviations Based on the Scaled PGSS4 Covariance to Degree 20. C.I. = 10 cm.

CHAPTER VIII

IMPROVEMENT OF THE ORBIT AND DETERMINATION OF THE STATIONARY SST

8.1. Introduction

For the solution of the combined altimeter problem the parameters Δs_I, $\Delta \bar{p}$ and $\Delta \bar{p}_T$ of equations (3.13) or (3.15) have to be optimally determined. As discussed in the previous Chapters the computation of the partials of (3.13) can be made by numerical integration for the radial distance related partials, and using equations (6.4) and (6.14) for the geoid undulations and stationary SST. Choosing to work with the analytical approach, it has been seen that the Lagrangian theory is quite accurate in modeling the radial orbit errors, and gives a considerably better insight to its properties. It has also been seen that the geographic representation of the radial error is not very accurate when it is to be implemented on a regular grid and it becomes extremely expensive for computation on a point by point basis. Furthermore, it has turned out that the Fourier series form is the most practical and economical to use without any loss of accuracy. On the contrary, undulation errors and stationary SST cannot be accurately modeled by a Fourier series expansion and equations (6.4) and (6.14) have to be implemented.

The detailed observation equations can be easily obtained by using the expressions for the Jacobian of the errors as derived in Chapter 7, complemented by the partials corresponding to the resonant and second order terms as well as the initial state vector errors. These equations are not going to be given here since this would be a repetition. Instead, problems associated with the estimability of the coefficients are going to be discussed and ways to improve it will be proposed and applied.

8.2. Problems Involved in the Estimation

From the Fourier series expressions of radial orbit error, geoid undulation error and stationary SST it is obvious that the potential coefficient corrections and the SST coefficients have several types of dependencies. More specifically the potential coefficients of all the degrees and of a particular order are linearly combined to create lumped coefficients that give rise to specific frequencies, each separated by 1 cy/rev and modulated by m cy/day. For a gravity

field up to degree and order 36 there are 77 such lumped coefficients for each order, providing a total of 2849 lumped coefficients which under ideal conditions (no other errors or SST signal, optimum sampling, etc.) can in principle provide a solution for the 1365 potential coefficients contained in the field. Even in such a case there are problems that prohibit an efficient estimation. The most serious problem arises from the considerable correlations between the potential coefficients of same order and the correlations that exist between the frequencies themselves. Furthermore due to the parity contraints in the undulation expansion (and partly in the orbit error expansion) the degrees of freedom of the system decrease substantially. Finally, as it has been seen in Chapters 5 and 6, frequencies corresponding to zonal terms do not really have any significant amplitude, resulting into low estimability of these coefficients. Coefficients of higher degree and order have a greater degree of freedom, since they are involved in linear combinations of fewer terms, and so they are expected to be better estimated. The same types of dependencies are valid for the stationary SST coefficients.

The estimability problem is further complicated by the coexistence of the three types of unknowns that give rise to the same frequencies. More specifically the initial state vector errors are fully correlated with the 1 cy/rev errors and the second order errors of gravitational origin. On the other hand, the stationary SST has the same spectrum as the combined spectrum of orbit and undulation errors at least in most of the frequencies. This can be seen from Figures 33 and 34. Some separability can be obtained only for the low frequencies (lower than 1 cy/rev). Furthermore the first degree zonal terms of the stationary SST are fully correlated with the 1 cy/rev gravitational and initial state vector errors.

Higher degree ($\ell_{max} > 36$) geoid undulation effects create additional problems. As it has been seen in Chapter 6 even if we assume that a perfect filtering of the higher frequency undulations can be obtained (with the implementation of higher degree fields and low pass filtering) there are still higher degree undulation effects that are aliased into low frequencies.

Finally the altimeter observations are not sampled globally but only in oceanic regions. This gives rise to additional errors in the coefficients to be estimated. These errors are due to leakage effects resulting from the discontinuities of the observables over land.

8.3. Conditioning of the System and Solution

To overcome the problems discussed in the previous section, or at least to improve the estimability of the unknowns, a certain conditioning has to be applied to the normal equations resulting from (3.13) or (3.15). Such conditioning can be obtained by introducing

prior information for the parameters that can be of two types. Strong prior information which translates to constraining some of the parameters that are considered to be very well known, or weak prior information, which consists of providing information about the statistical properties of the parameters.

For the potential coefficient corrections strong information can be obtained by constraining the low degree zonals which are considered to be known quite accurately. In such a case the long period effects of zonal origin, particularly in the eccentricity, have to be properly removed. Statistical information on the other hand can be provided by the covariance matrix of the gravity field that is used for the orbit generation. This matrix, being practically the major means to separate the unknowns, has to be a reliable and well scaled matrix, accurately depicting the apriori correlations of the coefficients. A similar covariance matrix can also be obtained for the initial state vector of each arc from the orbital adjustment. The stationary SST coefficients can be conditioned by use of oceanographic information. A rather mild conditioning can be obtained by using the degree variances resulting from the spherical harmonic expansion of existing SST models (e.g. Levitus, 1982). Such a spherical harmonic expansion has been carried out by Engelis (1983, 1985).

A further conditioning that can be applied to the solution is to use the crossover discrepancies as observables, so that to provide an additional type of observation equations. The mathematical model for a crossover discrepancy is

$$\rho(t_2) - \rho(t_1) = r(t_2) - h(t_2) - r(t_1) + h(t_1) = 0 \qquad (8.1)$$

where t_1 and t_2 are the times of crossing between two arcs. The convention followed in this differencing is that t_2 is greater than t_1. Such a convention allows for the easier computer implementation of the observation equations. Changing the time attributes with the corresponding indices and using (3.9) - (3.14) we obtain

$$h_2 - h_1 + \left(\frac{\partial r_2}{\partial \bar{s}_2}\frac{\partial \bar{s}_2}{\partial \bar{s}_I} - \frac{\partial r_1}{\partial \bar{s}_1}\frac{\partial \bar{s}_1}{\partial \bar{s}_I}\right)\Delta\bar{s}_I + \left(\frac{\partial r_2}{\partial \bar{s}_2}\frac{\partial \bar{s}_2}{\partial \bar{p}} - \frac{\partial r_1}{\partial \bar{s}_1}\frac{\partial \bar{s}_1}{\partial \bar{p}}\right)\Delta\bar{p} = 0 \qquad (8.2)$$

where it has been assumed that there are no time variations of the sea surface or any other time varying effects. This assumption is consistent with the development of equations (3.13) and (3.15).

Equation (8.2) models the differences of the radial orbit error at two epochs and is independent of any geoid undulation and stationary SST signature. So crossover discrepancies can in principle be used by themselves to solve for potential coefficient corrections and initial state errors, in order to correct the computed orbit. Due to the differencing though, the observability of all the lumped coefficients is reduced. This observability becomes null when the interval t_2-t_1 of the differenced sea surface heights is an integer multiple of the period of the frequency generated by each lumped coefficient. For example, the 1 cy/rev error is completely unobservable at the northernmost and southernmost latitudes where crossover discrepancies have time differences very close to multiples of one revolution. This error component is perfectly observable at the equator. This results in a reduced sensitivity of equation (8.2) to most of the parameters. In particular, zonal coefficients cannot be estimated from crossover discrepancies.

Similar to sea surface heights, crossover discrepancies also have dependencies between their parameters. Again initial state vector errors are fully correlated with the 1 cy/rev and second order gravitational errors. Furthermore, potential coefficient corrections within the same lumped coefficients are highly correlated. So, conditioning with the covariance of the field is needed to improve the estimability of the parameters. But even with the conditioning the estimated parameters are such that, although they do minimize the crossover discrepancies, they do not necessarily minimize the radial orbit error also. As can be seen in the next section, there is indeed a substantial reduction of the radial orbit error but it is not as effective as when sea surface heights are also used. Furthermore no simultaneous determination of the stationary SST coefficients can be obtained. So crossover discrepancies can be efficiently used only when combined with sea surface heights. In such a combination, crossover discrepancies can provide an excellent conditioning of the system since they do not contain any undulations or SST signature.

The observation equations for the residual sea surface heights and the crossover discrepancies have the following form respectively

$$V_1 = \left|A_P \; A_{P_T} \; A_I\right| \begin{vmatrix} \Delta\bar{p} \\ \Delta\bar{p}_T \\ \Delta\bar{s}_I \end{vmatrix} + \Delta h \qquad (8.3)$$

$$V_2 = \left|A'_P \quad A'_I\right| \begin{vmatrix} \Delta p \\ \Delta\bar{s}_I \end{vmatrix} + (h_2 - h_1) \qquad (8.4)$$

or in a more compact notation

$$V = AX + L \tag{8.5}$$

A very important aspect in forming the observation equations is the sampling of the observations. According to the sampling theorem, in order to be able to resolve frequencies up to 36 cy/rev, the residual sea surface heights have to be sampled every one minute for a time period of approximately six days (for the case of Seasat). The sampling of the crossover discrepancies is more complicated. The reason is that sampling has to be made over time differences and not the time itself. Definitely the consideration of all the crossover discrepancies is suboptimum since crossover formations are more dense in the northern and southern latitudes than in the equatorial regions and so they "observe" the gravity field in a non-homogeneous way. This irregular sampling becomes even worse when crossovers in repeat arcs are considered, so appropriate downweighting has to be applied. No quantitative investigation has been made on the sampling of the crossovers and more study is felt to be necessary.

The solution of the equations (8.5) with prior information is a typical weighted parameters least squares solution and is given by

$$\hat{X} = - (A^T P A + P_x)^{-1} A^T P L \tag{8.6}$$

where P is the weight matrix of the observations and P_x is the inverse of the prior covariance for the unknowns. In a typical solution for a six day Seasat arc there are about 2500 unknowns to be estimated, using over 10000 observations. The combination of the two data types can create singularities if both the sea surface heights h_1 and h_2 at a crossing location and the corresponding crossover discrepancy h_2-h_1 are used as observables since these three quantities are linearly dependent. When either h_1 or h_2 and h_2-h_1 are used, their error correlation has to be considered.

An additional outcome of the solution is the a posteriori covariance matrix of the parameters which can yield error estimates for the orbit, the sea surface, the stationary SST and the long wavelength geoid, as well as their error correlations.

8.4. A Simulated Solution

As discussed in the previous section, the effectiveness of the solution heavily depends on the consistency of the prior information with the unknown parameters, and on the types of observables to be used and their sampling, while additional factors like a priori accuracy of the orbit, precision of the altimeter observations and others are also quite important. So simulated solutions taking into

others are also quite important. So simulated solutions taking into account all these factors will be made to assess the optimum conditions for the setup of the solution and its sensitivity to these factors.

From the discussions made so far, it is obvious that the solution of the combined altimeter problem is computationally extremely intensive. The computer resources that are required both in terms of computing time and memory are typical of a supercomputer environment. For the purposes of software development and validation of the method it was felt that such intensive computations would be an unnecessary burden. So a computationally more relaxed setup was considered in which, simulated residual sea surface heights and crossover discrepancies up to harmonic degree 10 for a 3 day Seasat arc were used.

For the generation of the simulated "unknown" potential coefficient corrections the scaled PGSS4 covariance matrix up to degree 10 was used to create multivariate normally distributed random deviates. Using these deviates, radial orbit errors of gravitational origin (including second order effects) and undulation errors were computed every 3 minutes for the first 3 days of the first Seasat arc. No initial state vector errors were considered. The harmonic coefficients of the Levitus SST up to harmonic degree 10 were used to compute the stationary SST at the same intervals. Then, residual sea surface heights were generated by adding a 10 cm white noise to account for the altimeter noise. For the generation of crossover discrepancies, the radial orbit errors (with 10 cm white noise) were computed and differenced at the arc crossing times. The algorithm that is used to determine the crossing times as well as the geocentric latitudes and longitudes of the crossings is described in Appendix E. A similar algorithm is given in Shum (1983). The total number of observations for this 3 day Seasat arc were 984 residual sea surface heights and 1178 crossover discrepancies. For the weight matrix of the parameters, the inverses of the scaled PGSS4 covariance to degree 10 and of the degree variances of the Levitus SST field were used.

Using the above observations, three solutions were made. The first solution used both the residual sea surface heights and crossover discrepancies, the second solution used only the residual sea surface heights and the third only the crossover discrepancies. The recovered coefficients, for all three solutions, were then compared to the initial "true" coefficients. The RMS percentage discrepancies by degree and order for each of the three solutions (identified as solutions 1, 2, 3) are shown in Tables 11 and 12, together with the "true" RMS magnitudes in terms of geoid undulation corrections and stationary SST.

Table 11

RMS Magnitudes and Percentage Discrepancies by Degree Using the Scaled PGSS4 Covariance

Degree	Undulation Correction				Stationary SST		
	Magn.	Sol 1	Sol 2	Sol 3	Magn.	Sol 1	Sol 2
1					18 cm	59%	79%
2	4 cm	43%	41%	27%	22	6	12
3	7	26	24	51	9	28	36
4	6	31	45	58	7	30	33
5	9	52	53	77	7	67	68
6	12	19	30	30	14	29	21
7	12	46	53	64	10	42	46
8	13	28	31	36	7	50	49
9	18	24	24	30	5	90	83
10	13	22	37	43	3	119	155

Table 12

RMS Magnitudes and Percentage Discrepancies by Order Using the Scaled PGSS4 Covariance

Order	Undulation Correction				Stationary SST		
	Magn.	Sol 1	Sol 2	Sol 3	Magn.	Sol 1	Sol 2
0	2 cm	97%	100%	124%	30 cm	23%	23%
1	13	48	48	55	16	61	77
2	17	29	38	55	8	46	67
3	12	45	40	63	7	77	71
4	10	17	32	46	3	98	98
5	8	41	32	38	4	110	87
6	13	8	38	19	2	68	138
7	13	2	7	5	2	77	92
8	7	4	12	12	1	76	107
9	4	5	28	4	1	110	67
10	4	3	6	6	1	110	118

In an overall evaluation, the estimation of the coefficients has been satisfactory. The recovery of the potential coefficient corrections is generally better than the coefficients of the stationary SST. This is due primarily to the heavier weighting of the former ones which allows for a better decorrelation and less influence by the altimeter noise. The estimability of the potential coefficient corrections by degree is almost the same for all the degrees (discrepancies are between 20-50%). Orderwise though there is a great variation, starting from practically no estimability for the zonal terms to perfect recovery for the higher order terms. The SST coefficients being only mildly constrained are more affected by the noise. This can be seen in particular in the higher degrees and orders where the energy of SST is small and the RMS discrepancies become higher. At low degrees, and particularly the second degree, the SST coefficients are recovered very well with the exception of the first degree and order terms, which are fully correlated with the 1 cy/rev radial error.

The recovered potential coefficient corrections and SST coefficients have been used to compute radial orbit errors, commission undulation errors, crossover discrepancies, stationary SST and residual sea surface heights. All these quantities were then compared to the "true" ones over the oceanic regions. The RMS "true" magnitudes and their corresponding discrepancies are shown in Table 13 for all three solutions.

Table 13

RMS True Magnitudes and Discrepancies Using the Scaled PGSS4 Covariance

	True Magnitude	Discrepancy		
		Sol 1	Sol 2	Sol 3
Δr	111 cm	11 cm	15 cm	19 cm
ΔN	36	10	12	14
ζ	50	15	18	—
Δh	114	4	5	—
Δr_D	106	3	5	3
Δr_{asc}	88	11	14	19
Δr_{desc}	97	11	14	19

There are many conclusions that can be drawn from Table 13. Again it is obvious that the first solution that uses both types of observables provides much better estimates. In terms of the radial orbit error the recovery is at the 90% level. The recovery of undulation corrections and stationary SST is on the order of 70%.

The residual sea surface heights are perfectly recovered, although individual discrepancies of Δr, ΔN, and ζ are much higher. This is due to the correlations existing in these quantities, particularly between Δr and ΔN. The crossover discrepancies are effectively minimized although the individual errors in the ascending and descending arcs at the crossing locations have the same RMS magnitude as the RMS radial error.

The solution using only residual sea surface heights performs slightly worse than the first solution and is better than the third one that uses only crossover discrepancies as observables. In this last solution it can be seen that although the crossover discrepancies are perfectly recovered, the individual radial errors are worse than in solution 1 by a factor of 2. The undulation correction recovery has a similar degradation. The most important disadvantage of using crossover discrepancies is that the stationary SST cannot be determined simultaneously. A suboptimum solution can be obtained using methods described in Engelis (1985). Then the adjusted values of the sea surface and geoid can provide a stationary SST that would have an RMS discrepancy from the "true" values of about 25 cm.

The original error magnitudes shown in Table 13 are rather pessimistic considering that they only reflect errors up to degree 10. Nevertheless the estimation reduces these errors quite drastically. In order to see what is the degree of improvement when a more accurate gravity field is used the simulated solution was repeated using the unscaled PGSS4 covariance. The RMS magnitudes and discrepancies for all quantities are shown in Table 14.

Table 14

RMS True Magnitudes and Discrepancies Using the Unscaled PGSS4 Covariance

	True Magnitude	Discrepancy		
		Sol 1	Sol 2	Sol 3
Δr	35 cm	6 cm	7 cm	6 cm
ΔN	10	5	5	5
ζ	50	8	9	–
Δh	55	4	5	–
Δr_D	33	3	4	3
Δr_{asc}	28	6	6	6
Δr_{desc}	31	6	6	6

From Table 14 it can be seen that in this case all solutions give practically the same results although the first one is still superior. Note that use of crossover discrepancies now gives better results than the residual sea surface heights. The percentage of recovery of the errors, as compared to the previous solution, is smaller and is subject to a limit imposed by the altimeter noise. On the contrary, the stationary SST, in the presence of smaller errors, is determined much better than in the previous solution.

These simulated solutions can show the apparent requirement for a very accurate gravity field in order to efficiently compute the stationary SST from satellite altimetry. They also show that even very accurate altimeter data like the Topex/Poseidon altimeter data can further be improved. Finally they show that altimetric data from any mission even of moderate accuracies can be substantially improved and that quite reliable SST estimates can be derived. A necessary requirement is the existence of a well scaled and reliable geopotential covariance. To test the importance of this requirement several other solutions were made. In one of these solutions the PGSS4 variances were only used. In a second solution the PGSS4 covariance was slightly altered while in other ones potential coefficient errors that were completely inconsistent with the PGSS4 covariance were used. Other solutions did not use any prior information for the stationary SST. In all solutions the results were worse than the ones contained in Tables 13 and 14 and in many of them the results were unacceptable.

The "true" quantities (or a priori errors) and the discrepancies after the adjustment (a posteriori errors) as well as the Levitus and the estimated SST have also been computed on a geographic basis on a regular 5° grid. Additionally the a priori and a posteriori accuracies based on the scaled PGSS4 covariance and the estimated covariance, have been computed on the same grid. All these estimates are shown in Figures 40-61. The first conclusion is that the radial errors both for the ascending and descending arcs have been substantially reduced. Figures 40 and 41 show the substantial reduction of the error of the ascending arcs in the Pacific Ocean where errors of the order of 3.5 meters have been reduced to 16 cm. On the contrary the errors in the South Atlantic Ocean have only been reduced by a factor of two. A similar improvement exists for the descending arcs (Figures 44 and 45) where errors of about 2 meters in the South Atlantic Ocean have been reduced to about 20 cm. Figures 48 and 49 show the substantial reduction of the mean geographic error, while Figures 52 and 53 show that the variable error has been completely eliminated. Comparing Figures 41, 45, 49 and 53 it becomes obvious that the residual radial orbit errors are common to both ascending and descending arcs. The apriori and aposteriori standard deviation maps in Figures 42, 43, 46, 47, 50, 51, 54 and 55 are absolutely consistent in magnitude and shape with the maps of the corresponding errors, indicating that they can be used to obtain reliable estimates about the errors themselves.

The apriori and aposteriori geoid undulation errors are shown in Figures 56 and 57. Most of the error signature existing in Figure 56 has been eliminated. The only significant residual errors are in the Pacific Ocean with an amplitude of 20 cm and alternating sign. The standard deviation maps, shown in Figures 58 and 59, also indicate the improvement achieved from the adjustment. The determination of the stationary SST as shown in Figures 60 and 61 has also been successful. It can be seen that all the features of the apriori SST have been recovered both in shape and magnitude.

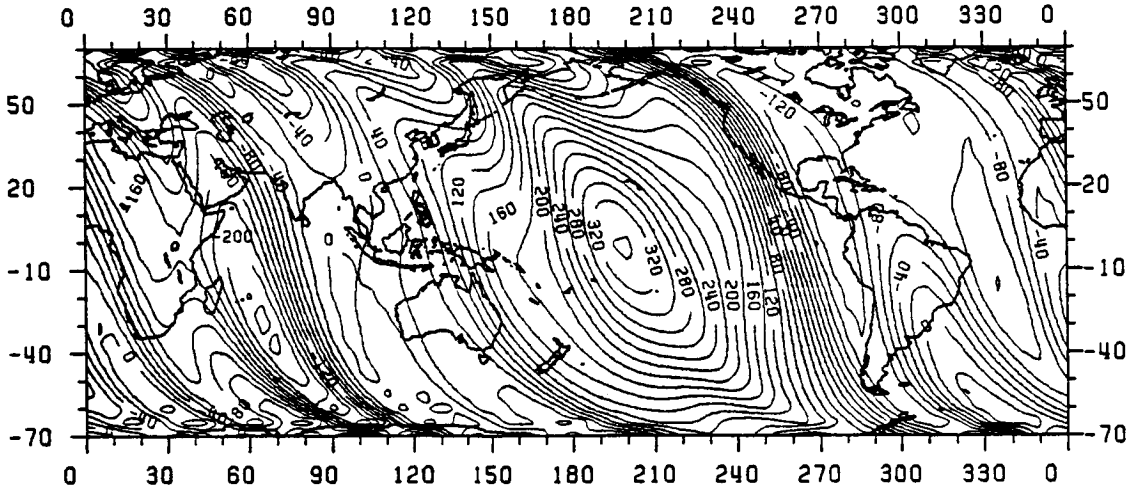

Figure 40. A Priori Radial Error of Seasat Ascending Arcs Based on Simulated Potential Coefficient Errors to Harmonic Degree 10. C.I. = 20 cm.

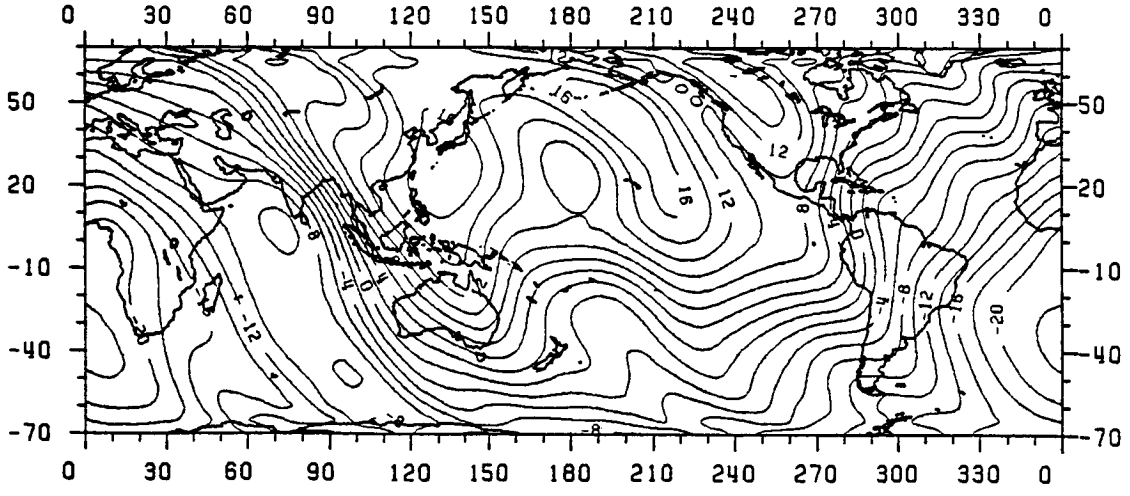

Figure 41. A Posteriori Radial Error of Seasat Ascending Arcs Based on the Discrepancies Between Simulated and Recovered Potential Coefficient Errors to Harmonic Degree 10. C.I. = 2 cm.

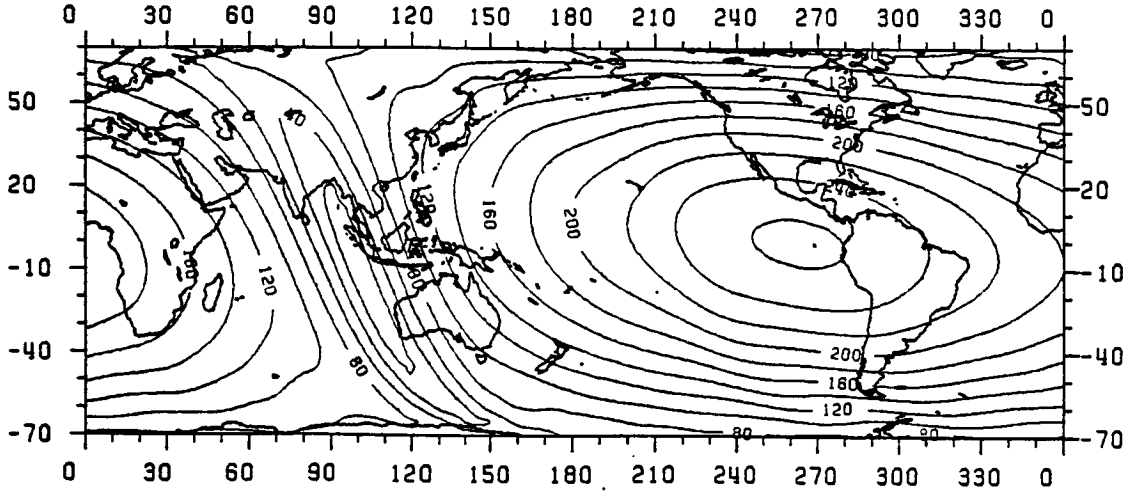

Figure 42. A Priori Standard Deviations of Radial Distances of Seasat Ascending Arcs Based on the Scaled PGSS4 Covariance to Harmonic Degree 10 . C.I. = 20 cm.

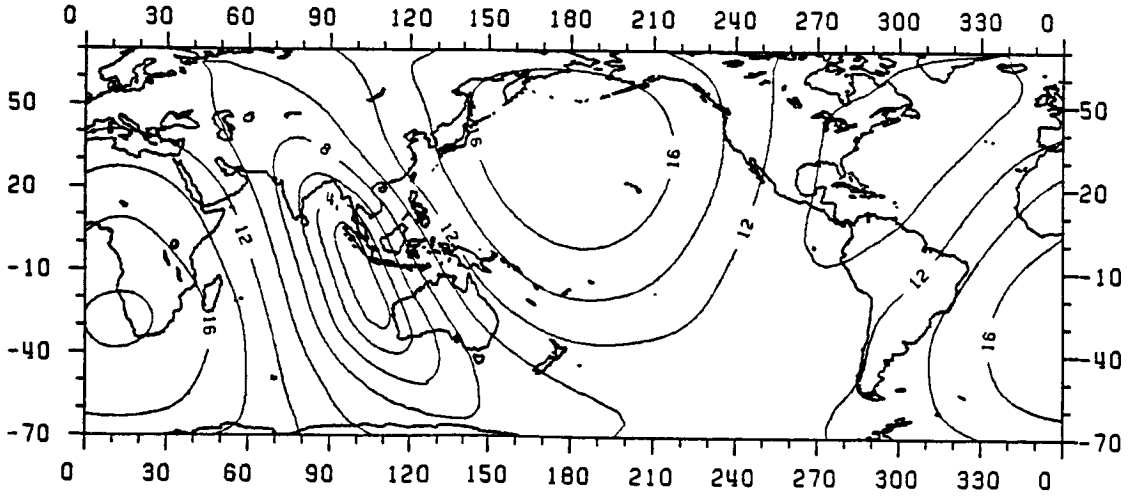

Figure 43. A Posteriori Standard Deviations of Radial Distances of Seasat Ascending Arcs Based on the Estimated Geopotential Covariance to Harmonic Degree 10. C.I. = 2 cm.

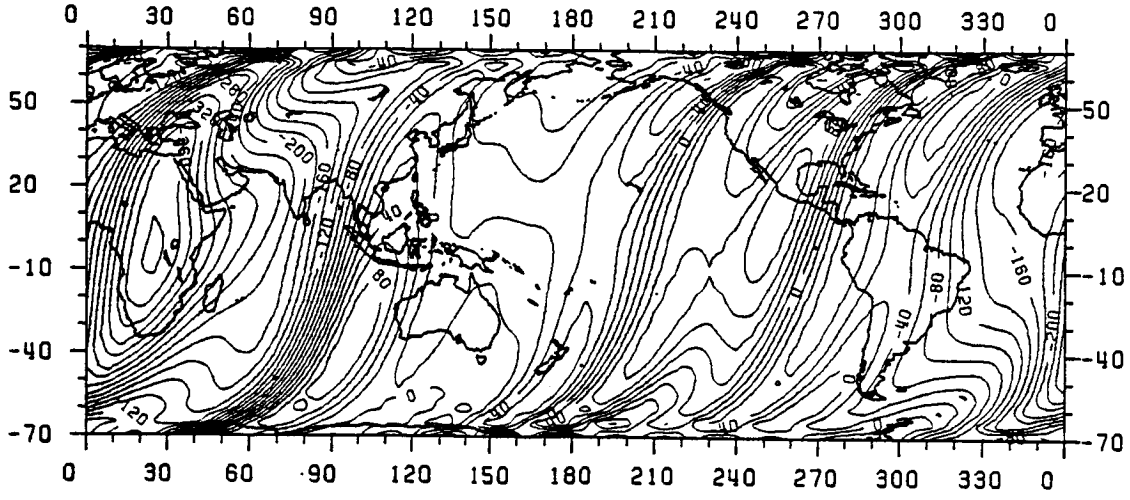

Figure 44. A Priori Radial Error of Seasat Descending Arcs Based on Simulated Potential Coefficient Errors to Harmonic Degree 10. C.I. = 20 cm.

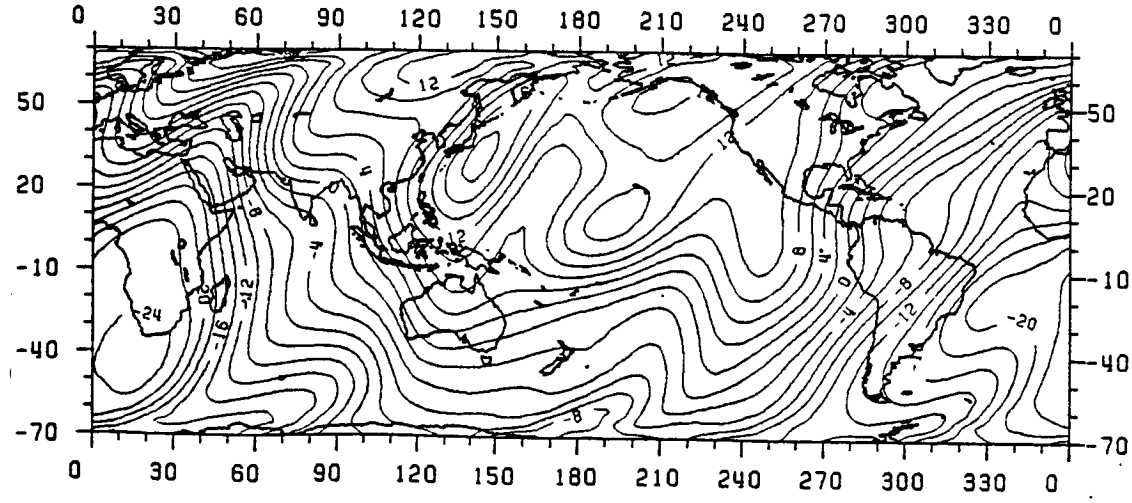

Figure 45. A Posteriori Radial Error of Seasat Descending Arcs Based on the Discrepancies Betwen Simulated and Recovered Potential Coefficient Errors to Harmonic Degree 10. C.I. = 2 cm.

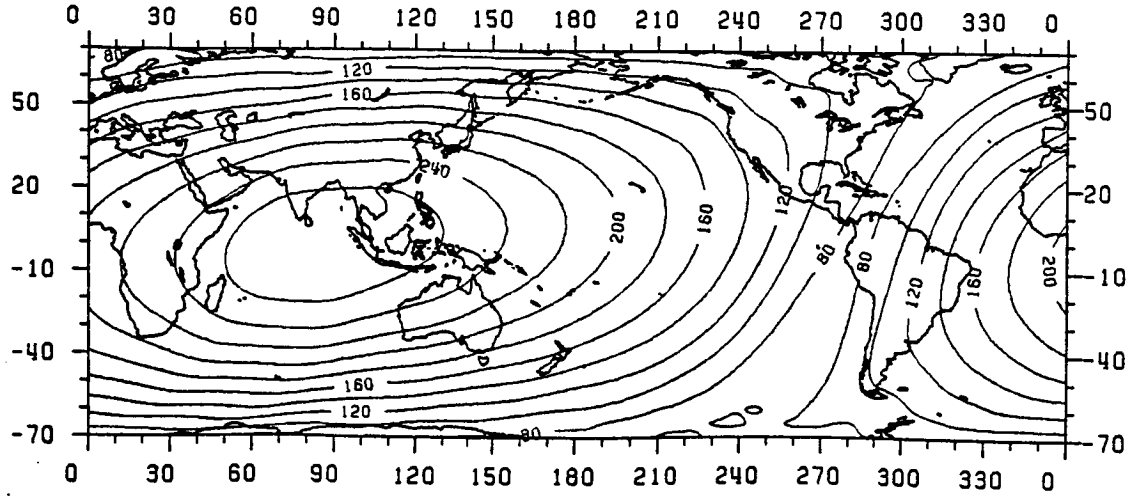

Figure 46. A Priori Standard Deviations of Radial Distances of Seasat Descending Arcs Based on the Scaled PGSS4 Covariance to Harmonic Degree 10. C.I. = 20 cm.

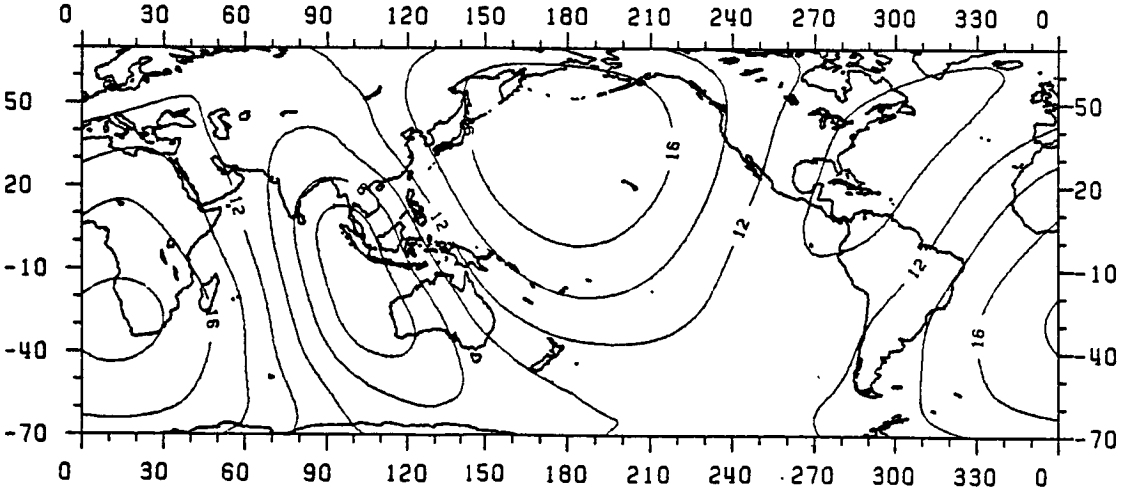

Figure 47. A Posteriori Standard Deviations of Radial Distances of Seasat Descending Arcs Based on the Recovered Geopotential Covariance to Harmonic Degree 10. C.I. = 2 cm.

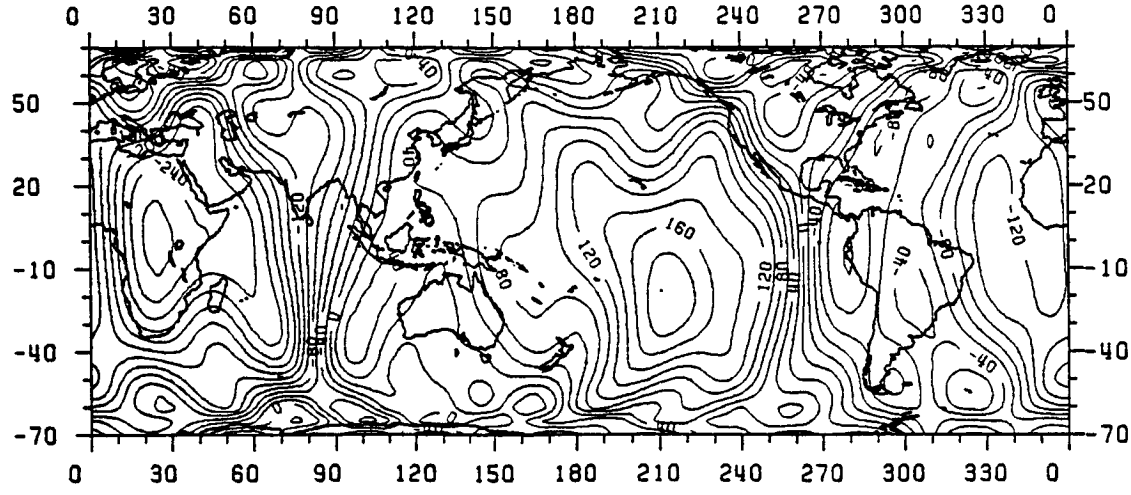

Figure 48. A Priori Mean Geographic Radial Error of a Seasat Arc Based on Simulated Potential Coefficient Errors to Harmonic Degree 10. C.I. = 20 cm.

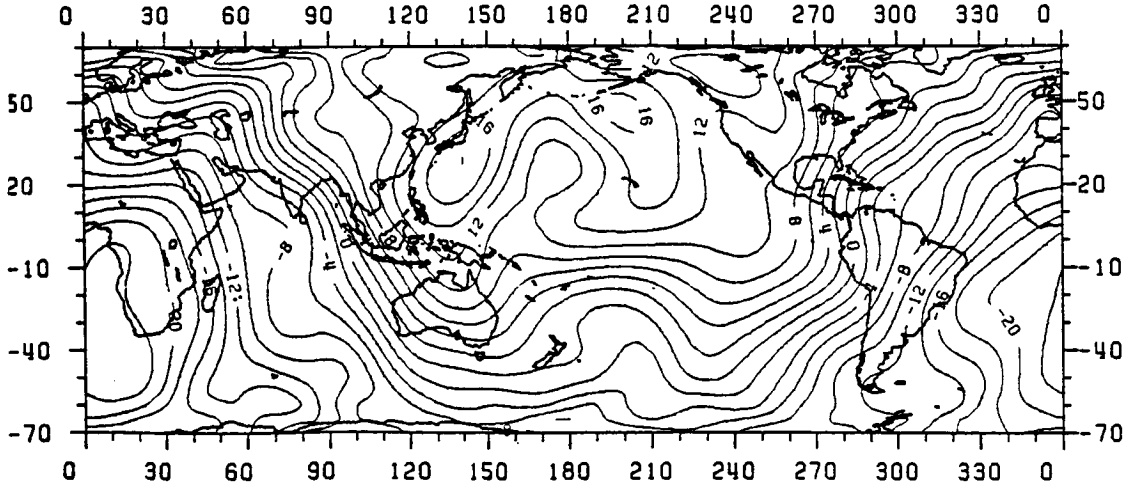

Figure 49. A Posteriori Mean Geographic Radial Error of a Seasat Arc Based on the Discrepancies Between Simulated and Recovered Potential Coefficient Errors to Harmonic Degree 10. C.I. = 2 cm.

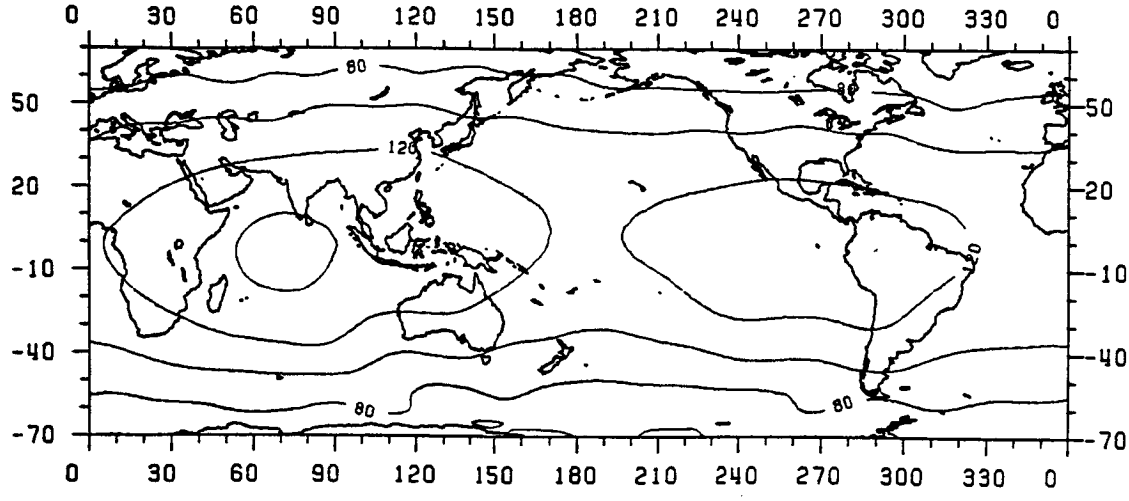

Figure 50. A Priori Standard Deviations Reflecting the Mean Geographic Radial Error of a Seasat Arc Based on the Scaled PGSS4 Covariance to harmonic Degree 10. C.I. = 20 cm.

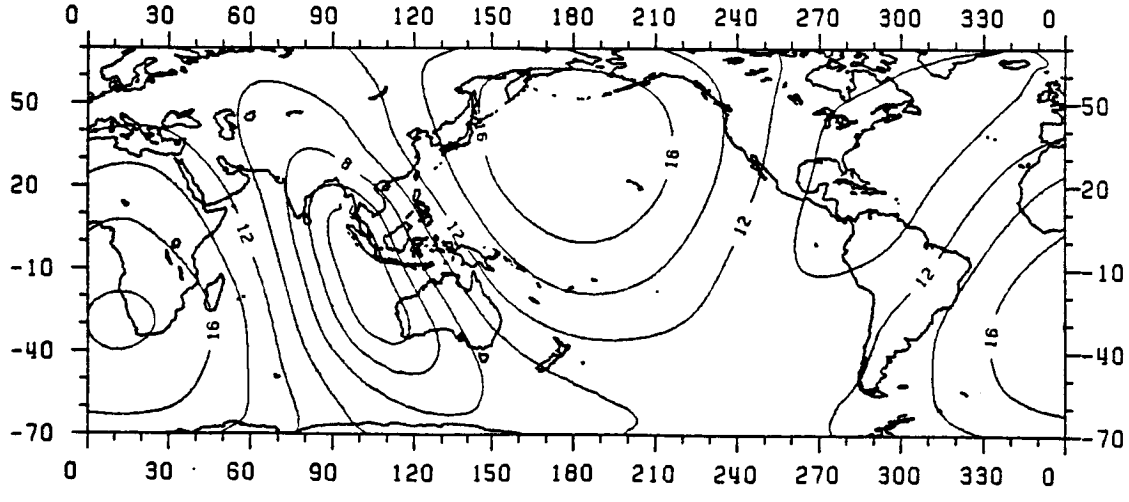

Figure 51. A Posteriori Standard Deviations Reflecting the Mean Geographic Radial Error of a Seasat Arc Based on the Recovered Geopotential Covariance to Harmonic Degree 10. C.I. = 2 cm.

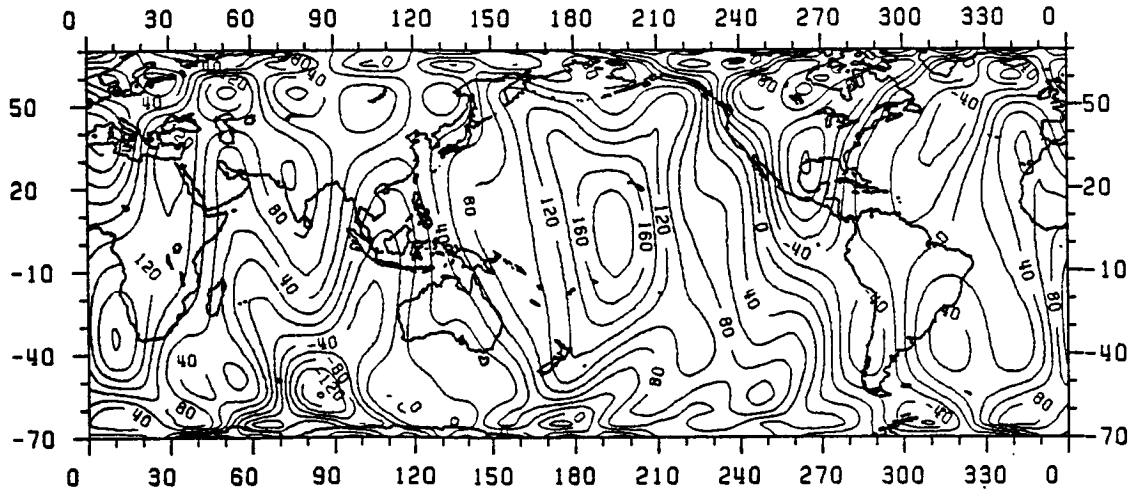

Figure 52. A Priori Variable Geographic Radial Error of a Seasat Arc Based on Simulated Potential Coefficient Errors to Harmonic Degree 10. C.I. = 20 cm.

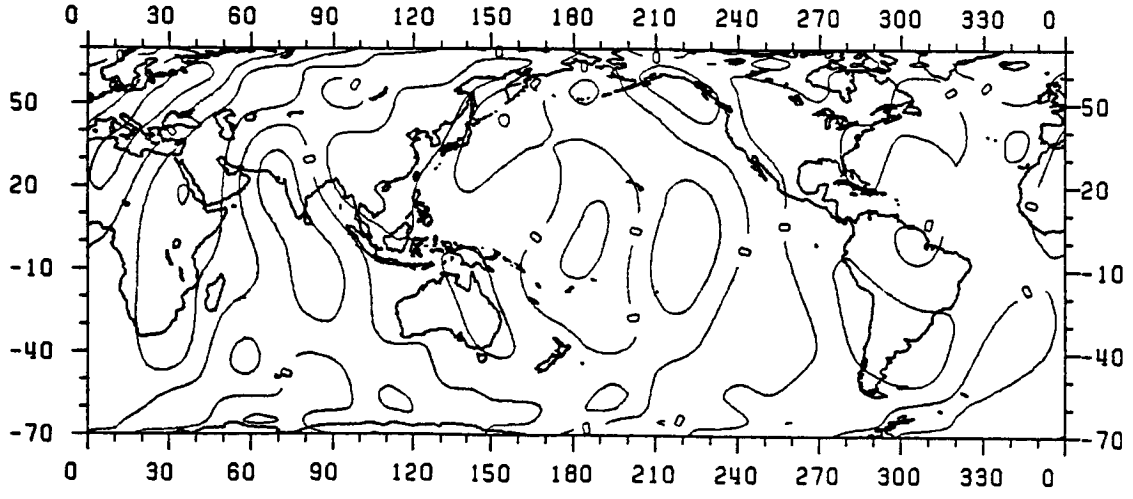

Figure 53. A Posteriori Variable Geographic Radial Error of a Seasat Arc Based on the Discrepancies Between Simulated and Recovered Potential Coefficient Errors to Harmonic Degree 10. C.I. = 2 cm.

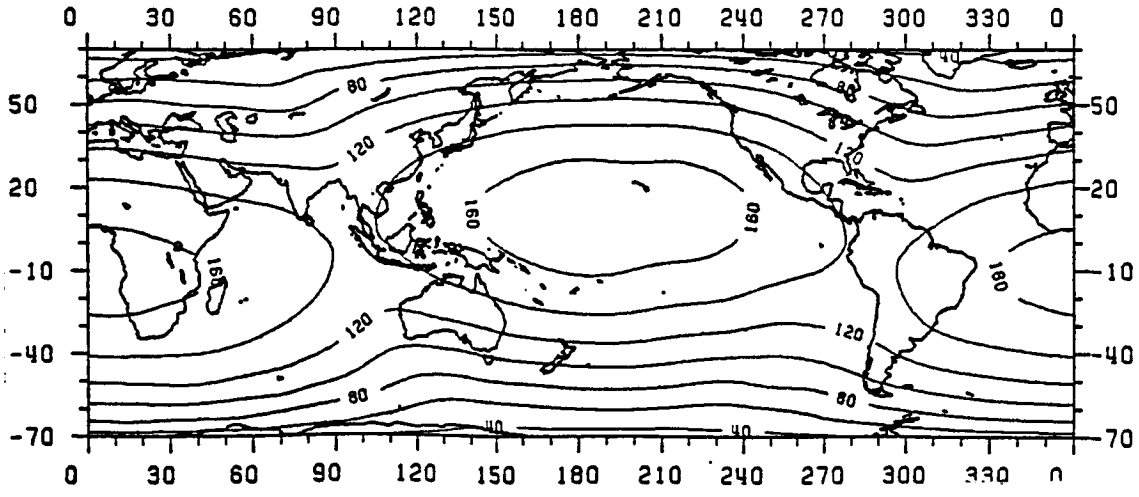

Figure 54. A Priori Standard Deviations Reflecting the Variable Geographic Radial Error of a Seasat Arc Based on the Scaled PGSS4 Covariance to Harmonic Degree 10. C.I. = 20 cm.

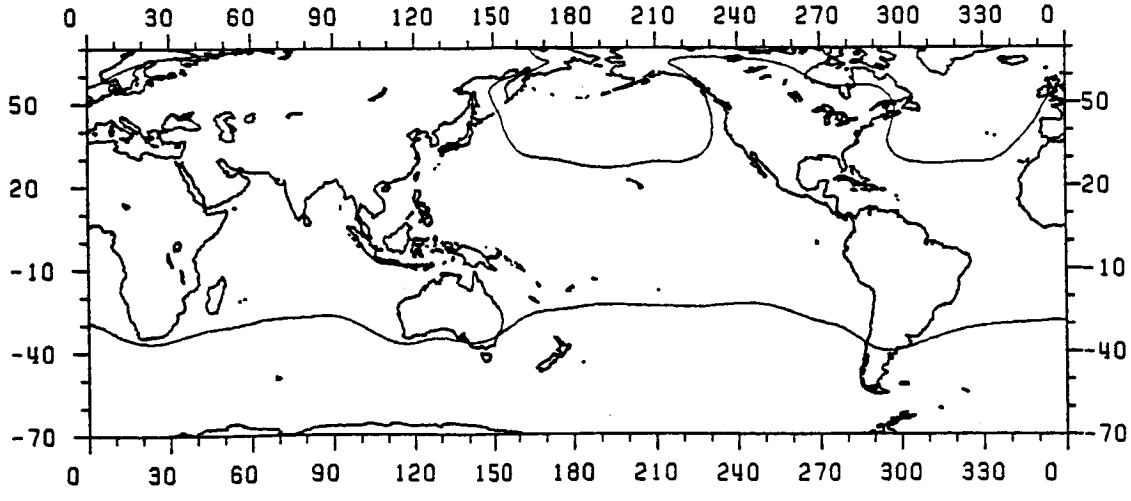

Figure 55. A Posteriori Standard Deviations Reflecting the Variable Geographic Error of a Seasat Arc Based on the Estimated Geopotential Covariance to Harmonic Degree 10. C.I. = 2 cm.

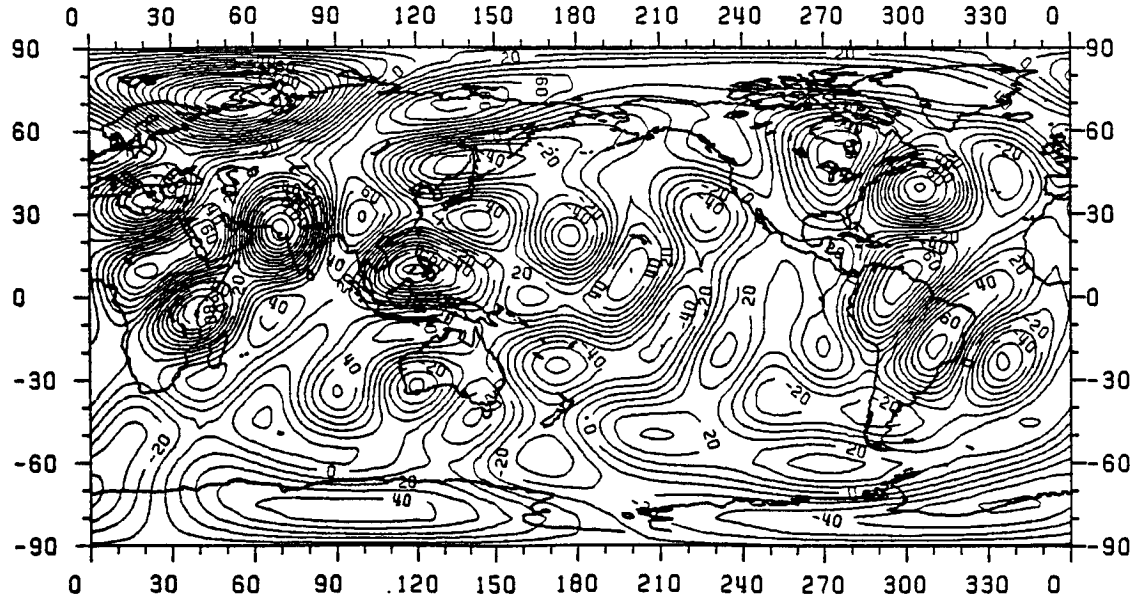

Figure 56. A Priori Geoid Undulation Errors Based on Simulated Potential Coefficient Errors to Harmonic Degree 10. C.I. = 10 cm.

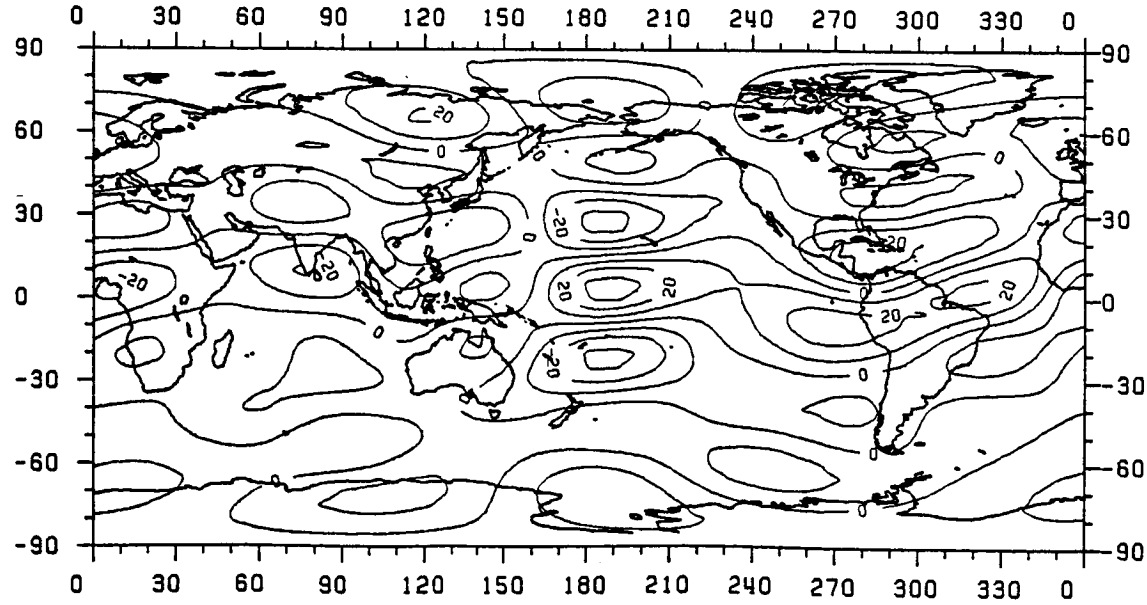

Figure 57. A Posteriori Geoid Undulation Errors Based on the Discrepancies Between Simulated and Recovered Potential Coefficient Errors to Harmonic Degree 10. C.I. = 10 cm.

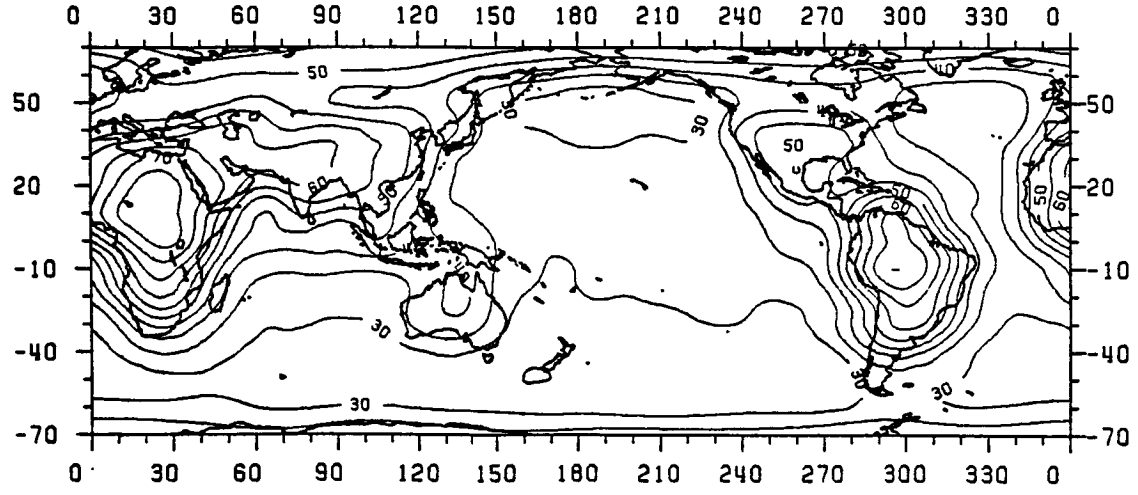

Figure 58. A Priori Standard Deviations of Geoid Undulations Based on the Scaled PGSS4 Covariance to Harmonic Degree 10. C.I. = 5 cm.

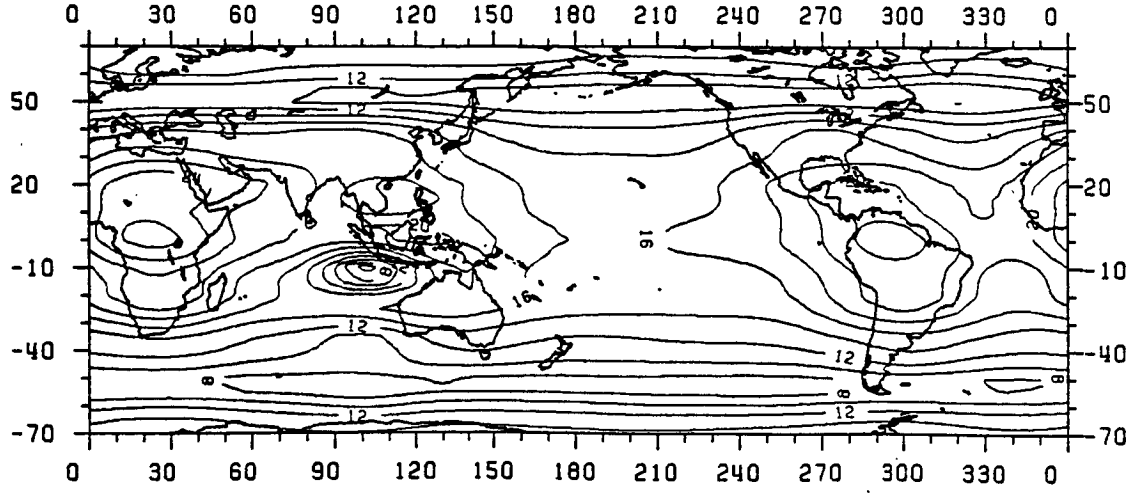

Figure 59. A Posteriori Standard Deviations of Geoid Undulations Based on the Estimated Geopotential Covariance to Harmonic Degree 10. C.I. = 2 cm.

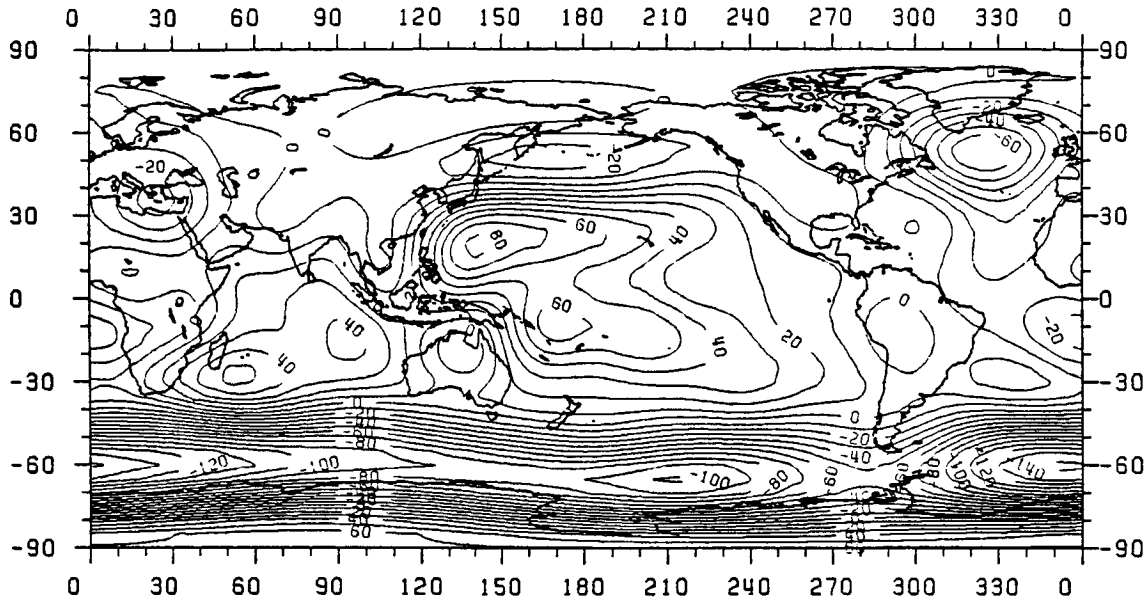

Figure 60. Stationary SST Based on the Harmonic Coefficients of the Levitus SST Model to Harmonic Degree 10. C.I. = 10 cm.

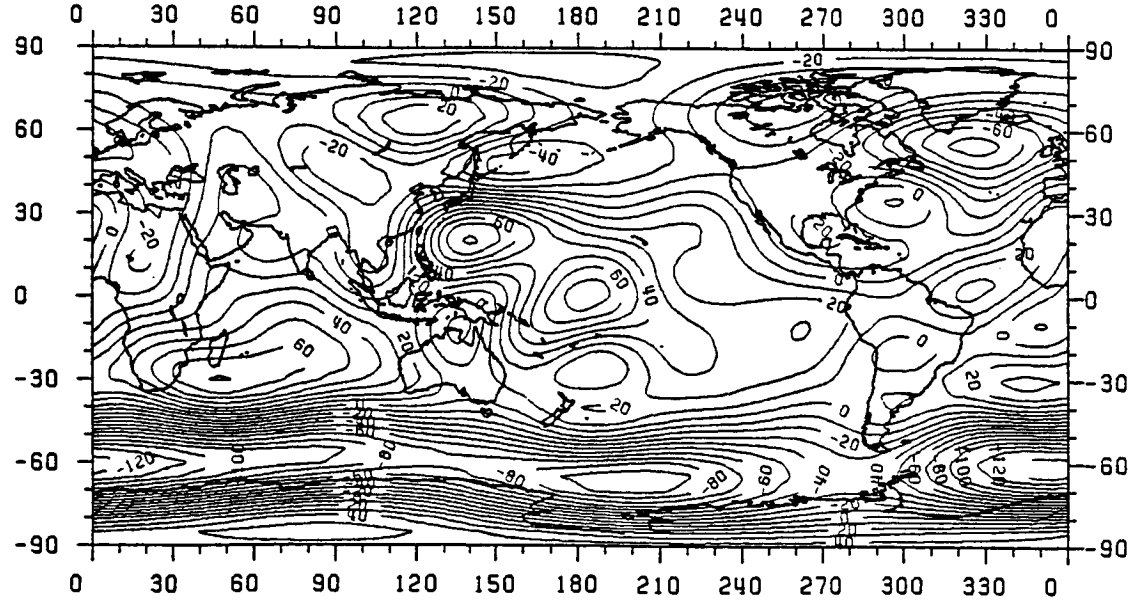

Figure 61. Stationary SST Based on the Estimated SST Coefficients to Harmonic Degree 10. C.I. = 10 cm.

CHAPTER IX

CONCLUSIONS, RECOMMENDATIONS

In this study a solution to the combined altimeter problem (as defined in Chapter 2) has been proposed. This solution differs from earlier solutions, that were of geometric nature, since it considers the dynamic properties of the satellite orbit. Sea surface heights and crossover discrepancies are used in a minimum variance solution to simultaneously determine radial orbit corrections, the sea surface and the stationary SST.

An analytical approach for modeling the radial orbit error has been adopted. Using the Lagrangian theory a linearized expression for the error, supplemented by second order effects, has been derived. A limited evaluation of this expression has shown that the analytic approach can be accurate enough to model the radial orbit error. Alternative forms have been derived, that provide a better insight into the properties of the error. It turns out that the Fourier series approach is much more convenient to use and equally accurate to the Lagrangian form. The geographic representation is valuable in showing the spatial characteristics of the radial error but is of inferior accuracy due to approximations that are necessary for its implementation.

It has been seen that the radial orbit error is of long wavelength nature. The most dominant part is at a frequency of 1 cy/rev. A constant bias and errors in frequencies very close to 1 cy/rev have also a large magnitude. Additional error of 1 and 2 cy/rev with a time dependent amplitude can also arise due to resonant conditions in the satellite orbit and due to second order effects. These time dependent errors can grow up to significant magnitudes if not properly removed during the orbital adjustment. In the space domain the radial error shows a considerable variation, that is systematic and depends on orbit specifications and the epoch of the orbit integration. It also turns out that one part of the error is common to both ascending and descending arcs while the other part is of equal magnitude but with a different sign for the two arcs. This fact is the primary reason why empirical crossover adjustments have failed to really remove the radial orbit error from the altimeter data.

In order to use the sea surface heights as observables the geoid undulations and stationary SST must be modeled. It has been seen

that modeling of these quantities with respect to time in an inertial coordinate system is not very accurate due to approximations that are involved. This formulation, although not accurate enough, can show that the spectra of undulation error and stationary SST are identical and that they both differ significantly from the one of the radial orbit error. These spectra have significant amplitudes in all the frequencies. Therefore a solution to the combined altimeter problem requires that the higher frequency signal be removed. This can be obtained by using a high degree gravity field and a low pass filtering.

For the solution of the problem, prior information is required to reduce the dependencies that exist among the parameters and improve the stability of the system. The covariance matrix of the gravity field, used for the orbit generation, and oceanographic information can be used for this purpose. A limited simulated solution has shown that the radial orbit error and the stationary SST can be effectively recovered. Statistical estimates from the solution are consistent with the simulated values.

As discussed in the introduction, the motivation and the initial stage of this research work have been based largely on investigations and conclusions obtained by Colombo (1984). A similar analysis of the radial orbit error has been made by Wagner (1985) and Rosborough (1986). Wagner has derived formulas that are identical to the ones contained in Section 5.3 and he has obtained conclusions that are very similar to the ones of the present analysis. Rosborough has made a complete analysis of the radial orbit error both in the Fourier series form and its geographic representation. He has given numerical estimates of the error for the Topex/Poseidon satellite using the differences of GEM10B and GRIM3B gravity fields as potential coefficient errors. Furthermore he has derived a formulation that leads to the computation of statistical estimates of the error. He has used the GEML2 geopotential covariance complete up to degree 20 to provide numerical results for the Topex/Poseidon radial uncertainties.

Both Wagner's and Rosborough's formulations are equivalent to the one presented here, although differences in the derivations are apparent. Neither of the two investigations has properly identified the 1 cy/rev error which is the largest error component in the determination of the radial distance to a satellite. This error component has been correctly determined in the present analysis, as seen in Section 4.7. An additional contribution of this study in the analysis of altimeter data, is the systematic development of the observation equations that lead to an optimum determination of the stationary SST and the identification of all the potential problems that are involved in such a determination. A similar estimation technique has been proposed by Wagner (1986) who has used approximate observation equations to model the residual sea surfce heights and only mild prior information to condition the unknowns. His simulated results indicate a lower estimability than the one presented in the

present simulation study.

Several problems have not been addressed in this simulation study. The first and most important one involves a more complete modeling of the radial orbit error, using a complete gravity field up to degree 36. Such a solution was not made because of large computing requirements. Based on results from the solution up to harmonic degree 10 though, it is expected that the higher degree and order potential coefficient corrections can be very well determined. An exception may be the resonant order coefficients and so more testing needs to be made.

Another problem that has to be addressed is how much the lower frequency high degree undulations contaminate the solution. This assessment can be obtained by simulating sea surface heights with the geoid undulations and stationary SST being modeled up to higher degree and order (e.g. 180). Then, using a high degree gravity field and low pass filtering the high frequency signal can be removed. The residual sea surface heights can then be used for the solution. This solution can be compared to a solution that does not contain any high degree signal. Conclusions on the contamination of the solution can then be obtained.

Another simulation test that has to be made is related to the optimum sampling of the crossover discrepancies. If all the crossover discrepancies are used, then there is an oversampling at the northern and southern regions relative to the equatorial regions. This irregular sampling results into a non uniform observability of the gravity field. An optimum sampling can be obtained by applying the sampling theory for time differences. Such an application has not been made and more investigation is necessary.

Even with all the above problems addressed, a solution of the altimeter problem as proposed in this study is oversimplified, primarily because of the incomplete modeling of the radial orbit error. As discussed in Chapter 2, radial orbit errors of smaller magnitude also arise from air drag and solar radiation pressure modeling errors. These errors affect all the Keplerian elements and primarily the mean anomaly. According to Kaula (1966) these effects are linearly dependent with time and so they closely resemble resonant and second order errors of gravitational and initial state vector origin. Further complications in the solution are expected from errors in the modeling of tides and the other sea surface variations. Finally, the modeling of the stationary SST and the prior information used are also simplified. It is expected that if more comprehensive models of the stationary SST, based on dynamic equations of motion of the oceans, are used, then a better estimability of the ocean parameters can be obtained.

Even the most comprehensive solution taking into account all these problems cannot recover high frequency stationary SST because

of the filtering that is required. These high frequency effects can be obtained in local high energetic areas by combining the recovered sea surface estimates with estimates of local detailed geoids. These detailed geoids can be computed using gravimetric methods, if accurate and dense gravity observations exist.

Based on the analysis made so far, it is expected that the analytical methods will be able to efficiently process real altimeter data. It is anticipated that the GEMT1 field, along with improved models for tides and surface forces and more accurate station coordinates will be used to compute new orbits for Seasat. These orbits will be merged with altimeter observations to provide more accurate sea surface heights. From initial tests, using the GEMT1 field, the crossover discrepancies are on the order of 70 cm (Marsh et al. 1986b) implying an accuracy of about 70 cm for the sea surface heights (assuming that the mean geographic error has the same order of magnitude as the variable geographic error). This data set, being more accurate than the PGSS4 set will have the additional advantage of being supplemented by a well scaled and accurate geopotential covariance, as the GEMT1 covariance is expected to be. Using this dataset a solution can be made, for a six day arc to obtain adjusted sea surface heights, an improved long wavelength geoid and long wavelength SST. The author anticipates a posteriori accuracies on the order of 10-15 cm or even better for all the above quantities. The solution has to be repeated for all six day arcs of Seasat. Comparison of the SST estimates between solutions can provide variability of the sea surface, while averaging of the individual solutions can provide stationary SST over the lifetime of the satellite and an even more reliable long wavelength geoid.

Application of the method to the Geosat data is expected to be rather problematic since the Geosat orbits during the Extended Repeat Mission of the satellite have accuracies on the order of 4 meters (Cheney et al., 1987). These orbits are computed using the GEM10 gravity field. With such poor orbits and with no geopotential covariance available, the only possible analysis that can be made is a crossover analysis along the lines of Chapter 8. The resulting sea surface heights are expected to have inferior accuracies as compared to the ones for Seasat. Furthermore, no stationary SST can be obtained, while the determination of SST variations might be affected by the across track high frequency variations of the orbit errors. A considerably improved analysis of the Geosat data can be obtained if the GEMT1 field is used for the orbit determination of Geosat.

For geophysical applications, that require a very detailed knowledge of the sea surface, combination of observations from different satellites can be made. The procedure described in this study can be used to independently adjust observations from different satellites and derive the ocean effects at different epochs. These effects, being generally different, have to be removed from the adjusted surfaces to provide estimates of the geoid. Since it is not

expected that the a posteriori accuracies of each individual solution will be the same, the geoid of inferior accuracy can be fitted to the one of superior accuracy to provide a more detailed and consistent surface. Such a fit can be made by a regular geometric crossover adjustment.

The activities in the area of satellite altimetry have been substantial during the last ten years and are expected to culminate with the launch of the Topex/Poseidon satellite. In view of the unprecedented accuracies that are expected from that mission, both in terms of orbit determination and altimeter observations, it is expected that comprehensive algorithms will be required for the optimum reduction and analysis of the data. In this context, the author hopes that this study has contributed in a positive way to the development of such algorithms.

LIST OF REFERENCES

Anderle, R.J., and R.L. Hoskins, Correlated Errors in Satellite Altimeter Orbits, Geophysical Research Letters, Vol. 4, pp. 421-423, 1977.

Brouwer, D., Solution of the Problem of Artificial Satellite Theory Without Drag, Astron. Journal Vol. 64, 1274, 1959.

Brouwer, D., and G.M. Clemence, Methods of Celestial Mechanics, New York Academic Press Inc., 1961.

Cappellari, J.O., C.E. Velez, and A.J. Fuchs, Mathematical Theory of the Goddard Trajectory Determination System, Goddard Space Flight Center, X-582-76-77, Greenbelt, Maryland, 1976.

Cheney, R.E., J.G. Marsh, and B.D. Beckley, Global Mesoscale Variability from Collinear Tracks of Seasat Altimeter Data, J. Geophys. Res., Vol. 88, C7, pp. 4343-4354, 1983.

Cheney, R.E., B.C. Douglas, R.W. Agreen, L.L. Miller, and D.L. Porter, Geosat Altimeter Geophysical Record (GDR) User Handbook, National Oceanic and Atmospheric Administration, National Ocean Service, Rockville, Maryland, 1987.

Christodoulidis, D.C., R.G. Williamson and S.M. Klosko, Ocean Tide Constituent Improvement for Topex, in Minutes of Topex Gravity Model Improvement Meeting, GSR-86-3, Center for Space Research, The University of Texas at Austin, 1986.

Cloutier, J.R., A New Technique for Correcting Satellite Ephemeris Errors Indirectly Observed from Radar Altimetry, Technical Report, TR-246, Naval Oceanographic Office, St. Louis, 1981.

Coleman, R., A Geodetic Basis for Recovering Ocean Dynamic Information from Satellite Altimetry, Unisurv S-19. School of Surveying, The University of New South Wales, Kensington, Australia, 1981.

Colombo, O., Altimetry, Orbits and Tides, NASA Technical Memorandum 86180, November 1984.

Cook, G.E., Perturbations of Near Circular Orbits by the Earth's Gravitational Potential, Planetary and Space Sciences, Vol. 14, pp. 433-444, 1966.

Douglas, B.C., R.W. Agreen, and D.T. Sandwell, Observing Global Ocean Circulation with Seasat Altimeter Data, Marine Geodesy, Vol. 8, 1984.

Douglas, B.C., D.D. McAdoo, and R.E. Cheney, Oceanographic and Geophysical Applications of Satellite Altimetry, Reviews of Geophysics and Space Physics, in Press, 1987.

Engelis, T., Analysis of Sea Surface Topography Using Altimeter Data, Report 343, Dept. of Geodetic Science and Surv., The Ohio State University, Columbus, 1983.

Engelis, T., Global Circulation from Seasat Altimeter Data, Marine Geodesy, Vol. 9, pp. 45-69, 1985.

Goad, C.C., An Efficient Algorithm for the Evaluation of Inclination and Eccentricity Functions, manuscripta geodaetica, Vol. 12, pp. 11-15, 1987.

Goad, C.C., B.C. Douglas and R.W. Agreen, On the Use of Satellite Altimeter Data for Radial Ephemeris Improvement, The Journal of the Astronautical Sciences, Vol. XXVIII, pp. 419-428, 1980.

Gopalapillai, S., Non Global Recovery of Gravity Anomalies from a Combination of Terrestrial and Satellite Altimetry Data, Report 210, Dept. of Geodetic Science and Surv., The Ohio State University, Columbus, 1974.

Hancock, D.W., R.G. Forsythe, and J. Lorell, Seasat Altimeter Sensor File Algorithms, IEEE Journal of Oceanic Engineering, Vol. 5, pp. 39-99, 1980.

Heiskanen, W.A. and H. Moritz, Physical Geodesy, Freeman, San Francisco, 1967.

Kaula, W.M., Theory of Satellite Geodesy, Blaisdell Publishing Co., 1966.

Kolenkiewicz, R., and C. Martin, SEASAT Altimeter Height Calibration, J. Geophys. Res., Vol. 87, pp. 3189-3198, 1982.

Kostelecky, J., Reccurence Relations for the Normalized Inclination Functions, Bull. Astron. Inst. Czechos., Vol. 36, pp. 242-246, 1985.

Kozai, Y., The Motion of a Close Earth Satellite, Astron. J. 64, 1959.

Kozai, Y., The Earth Gravitational Potential Derived from Satellite Motion, Space Science Reviews, Vol. 5, pp. 818-879, 1966.

Lerch, F.J., Gravitational Perturbation of Radial Position and Velocity for the mean Circular Satellite Orbit, Geodynamics Branch, Annual Report 1985, NASA Technical Memorandum 87801, 1986.

Lerch, F.J., S.M. Klosko, R.E. Laubscher, and G.A. Wagner, Gravity Model Improvement Using Geos-3 (GEM9 and 10), J. Geophys. Res., Vol. 84, B8, pp. 3897-3916, 1979.

Lerch, F.J., B.H. Putney, C.A. Wagner, and S.M. Klosko, Goddard Earth Models for Oceanographic Applications (GEM10B and GEM10C), Marine Geodesy, Vol. 5, No. 2, pp. 145-181, 1981.

Lerch, F.J., J.G. Marsh, S.M. Klosko, and R.G. Williamson, Gravity Model Improvement for Seasat, J. Geophys. Res., Vol. 87, C5, pp. 3281-3296, 1982.

Lerch, F.J., S.M. Klosko, G.B. Patel, and C.A. Wagner, A Gravity Model for Crustal Dynamics (GEM-L2), J. Geophys. Res., Vol. 90, B11, pp. 9301-9311, 1985a.

Lerch, F.J., S.M. Klosko, C.A. Wagner, and G.B. Patel, On the Accuracy of Recent Goddard Gravity Models, J. Geophys. Res., Vol. 90, B11, pp. 9312-9334, 1985b.

Levitus, S., Climatological Atlas of the World Ocean. Professional Paper 13. NOAA, Geophysical Fluid Dynamics Laboratory, Rockville, Maryland, 1982.

Liang, C.K., The Adjustment and Combination of Geos-3 and Seasat Altimeter Data, Report 346, Dept. of Geodetic Science and Surv., The Ohio State University, Columbus, 1983.

Lorell, J., E. Colquitt, and R.J. Anderle, Altimeter Height Correction for Ionosphere, J. Geophys. Res., Vol. 87, pp. 3207-3212, 1982.

Marsh, J.G., Satellite Altimetry, Reviews of Geophysics and Space Physics, Vol. 21, pp. 574-580, 1983.

Marsh, J.G. and R.E. Cheney, Computation of a Precise Mean Sea Surface in the Eastern North Pacific Using Seasat Altimetry, EOS Trans. AGU 63, pp. 178-179, 1982.

Marsh, J.G. and R.G. Williamson, SEASAT Altimeter Timing Bias Estimation, J. Geophys. Res., Vol. 87, pp. 3232-3238, 1982.

Marsh, J.G., T.V. Martin, and J.J. McCarthy, Global Mean Sea Surface Computation Using Geos-3 Altimeter Data, J. Geophys. Res., Vol. 87, pp. 10955-10964, 1982.

Marsh, J.G., R.E. Cheney, J.J. McCarthy, and T.V. Martin, Regional Mean Sea Surfaces Based on GEOS-3 and SEASAT Altimeter Data, Marine Geodesy, Vol. 8, pp. 385-402, 1984.

Marsh, J.G., A.C. Brenner, B.D. Beckley, and T.V. Martin, Global Mean Sea Surface Based upon the Seasat Altimeter Data, J. Geophys. Res. Vol. 91, B3, pp. 3501-3506, 1986a.

Marsh J.G., F.J. Lerch, B.H. Putney, D.C. Christodoulidis, T.L. Felsentreger, B.V. Sanchez, D.E. Smith, S.M. Klosko, T.V. Martin, E.C. Pavlis, J.W. Robbins, R.G. Williamson, O.L. Colombo, N.L. Chandler, K.E. Rachlin, G.B. Patel, S. Bhati, and D.S. Chinn, An Improved Model of the Earth's Gravitational Field GEM-T1, Goddard Space Flight Center, NASA, November 1986b.

Marshall, J.G., Determining the Ocean Circulation and Improving the Geoid from Satellite Altimetry, J. Phys. Oceanogr. Vol. 15, pp. 330-349, 1985.

Mazzega, P., How Radial Orbit Errors are Mapped in Altimetric Surfaces, J. Geophys. Res., Vol. 91, C5, pp. 6609-6628, 1986.

Pisacane, V.L., Satellite Techniques for Determining the Geopotential of Sea Surface Elevations, J. Geophys. Res., Vol. 91, C2, pp. 2365-2371, 1986.

Rapp, R.H., Geos3 Data Processing for the Recovery of Geoid Undulations and Gravity Anomalies, J. Geophys. Res., Vol. 84, B8, pp. 3784-3792, 1979.

Rapp, R.H., The Earth's Gravity Field to Degree and Order 180 Using Seasat Altimeter Data, Terrestrial Gravity Data, and other Data, Report 322, Dept. of Geodetic Science and Surv., The Ohio State University, Columbus, 1981.

Rapp, R.H., Gravity Anomalies and Sea Surface Heights from a Combined GEOS-3/SEASAT Altimeter Data Set, J. Geophys. Res., Vol. 91, B5, pp. 4867-4876, 1986.

Rapp, R.H., and J.Y. Cruz, Spherical Harmonic Expansions of the Earth's Gravitational Potential to Degree 360 Using 30′ Mean Anomalies, Report 376, Dept. of Geodetic Science and Surv., The Ohio State University, Columbus, 1986.

Reigber, C., G. Balmino, H. Müller, W. Bosch, and B. Moynot, GRIM Gravity Model Improvement Using LAGEOS (GRIM3-L1), J. Geophys. Res., Vol. 90, B11, pp. 9285-9299, 1985.

Rosborough, G.W., Satellite Orbit Perturbations Due to the Geopotential, CSR-86-1, Center for Space Research, The University of Texas at Austin, 1986.

Rowlands, D., The Adjustment of Seasat Altimeter Data on a Global Basis for Geoid and Sea Surface Height Determinations, Report 325, Dept. of Geodetic Science and Surv., The Ohio State University,

Columbus, 1981.

Schwiderski, E.W., On Charting Global Ocean Tides, Reviews of Geophysics and Space Physics, Vol. 18, pp. 243-268, 1980.

Shum, C.K., Altimeter Methods for Satellite Geodesy, CSR-83-2, Center for Space Research, The University of Texas at Austin, 1983.

Smart, W.M., Textbook on Spherical Astronomy, Cambridge University Press, Sixth edition, 1977.

Stanley, H.R., Satellite Altimetry, Reviews of Geophysics and Space Physics, Vol. 17, pp. 1418-1421, 1979.

Stewart, R., L.L. Fu, and M. Lefebvre, Science Opportunities from the Topex Poseidon Mission, JPL Publication 86-18, Pasadena, 1986.

Tai, C.K. and L.L. Fu, On Crossover Adjustment in Satellite Altimetry and its Oceanographic Implications, J. Geophys. Res., Vol. 91, C2, pp. 2549-2554, 1986.

Tai, C.K. and C. Wunsch, Absolute Measurement by Satellite Altimetry of Dynamic Topography of the Pacific Ocean, Nature, Vol. 301, pp. 408-410, 1983.

Tai, C.K. and C. Wunsch, An Estimate of Global Absolute Dynamic Topography, J. Phys. Oceanogr., Vol. 14, pp. 457-463, 1984.

Tapley, B.D. and G.H. Born, The Seasat Precision Orbit Determination Experiment, The Journal of the Astronautical Sciences, Vol. XXVIII, No. 4, Oct - Dec, 1980.

Tapley, B.D. and G.W. Rosborough, Geographically Correlated Orbit Error and its Effect on Satellite Altimetry Mission, J. Geophys. Res., Vol. 90, pp. 11817-11813, 1985.

Tapley, B.D., G.H. Born, and M.E. Parke, The SEASAT Altimeter Data and its Accuracy Assessment, J. Geophys. Res., Vol. 87, pp. 3179-3188, 1982.

Wagner, C.A., Radial Variations of a Satellite Orbit Due to Gravitational Errors: Implications for Satellite Altimetry, J. Geophys. Res., Vol. 90, B4, pp. 3027-3036, 1985.

Wagner, C.A., Accuracy Estimate of Geoid and Ocean Topography Recovered Jointly from Satellite Altimetry, J. Geophys. Res., Vol. 91, B1, pp. 453-461, 1986.

Wunsch, C. and E.M. Gaposchkin, On Using Satellite Altimetry to Determine the General Circulation of the Oceans with Application to Geoid Improvement, Reviews of Geophysics and Space Physics, Vol. 18, pp. 725-745, 1980.

APPENDIX A

SATELLITE STATE VECTOR TRANSFORMATIONS

Transformation between inertial rectangular coordinates, Keplerian elements (elliptic coordinates) and earth fixed spherical coordinates are considered.

A. Conversion from elliptic to rectangular coordinates.

A1. Use Kepler's equation

$$M = E - e\sin E \tag{A.1}$$

to compute the eccentric anomaly E

A2. Compute $\bar{q}$

$$\bar{q} = \begin{bmatrix} q_1 \\ q_2 \\ q_3 \end{bmatrix} = \begin{bmatrix} a(\cos E - e) \\ a(1-e^2)^{1/2}\sin E \\ 0 \end{bmatrix} \tag{A.2}$$

A3. Compute position vector $\bar{r}$

$$\bar{r} = \begin{bmatrix} x \\ y \\ z \end{bmatrix} = R_3(-\Omega)R_1(-i)R_3(-\omega)\bar{q} \tag{A.3}$$

A4. Compute $\dot{\bar{q}}$

$$\dot{\bar{q}} = \begin{bmatrix} \dot{q}_1 \\ \dot{q}_2 \\ \dot{q}_3 \end{bmatrix} = \frac{na}{1-e\cos E} \begin{bmatrix} -\sin E \\ (1-e^2)^{1/2}\cos E \\ 0 \end{bmatrix} \tag{A.4}$$

A5. Compute velocity vector $\dot{\bar{r}}$

$$\dot{\bar{r}} = \begin{bmatrix} \dot{x} \\ \dot{y} \\ \dot{z} \end{bmatrix} = R_3(-\Omega)R_1(-i)R_3(-\omega)\dot{\bar{q}} \tag{A.5}$$

B. Conversion from rectangular to elliptic coordinates.

B1. Compute radial distance r and tangential velocity v

$$r = |\bar{r}| = (x^2 + y^2 + z^2)^{1/2} \tag{A.6}$$

$$v = |\dot{\bar{r}}| = (\dot{x}^2 + \dot{y}^2 + \dot{z}^2)^{1/2} \tag{A.7}$$

B2. Compute angular momentum vector $\bar{h}$

$$\bar{h} = \bar{r} \times \dot{\bar{r}}$$

$$h_1 = y\dot{z} - \dot{y}z$$

$$h_2 = z\dot{x} - \dot{z}x \tag{A.8}$$

$$h_3 = x\dot{y} - \dot{x}y$$

$$h = |\bar{h}| = (h_1^2 + h_2^2 + h_3^2)^{1/2}$$

B3. Compute radial velocity $\dot{r}$

$$\dot{r} = \left(v^2 - \frac{h^2}{r^2}\right)^{1/2} \tag{A.9}$$

B4. Compute semimajor axis a and eccentricity e

$$a = \frac{rGM}{2GM - rv^2} \tag{A.10}$$

$$e = \left(1 - \frac{h^2}{GMa}\right)^{1/2} \tag{A.11}$$

B5. Compute eccentric anomaly E, true anomaly f, and mean anomaly M.

$$\cos E = \frac{a-r}{ae} \tag{A.12}$$

$$\sin E = \frac{r\dot{r}}{e(GMa)^{1/2}} \tag{A.13}$$

$$E = \tan^{-1}\left[\frac{\sin E}{\cos E}\right] \tag{A.14}$$

$$f = \tan^{-1}\left[\frac{(1-e^2)^{1/2}\sin E}{\cos E - e}\right] \tag{A.15}$$

$$M = E - e\sin E \tag{A.16}$$

B6. Compute right ascension of ascending node Ω and inclination i

$$\Omega = \tan^{-1}\left[\frac{h_1}{-h_2}\right] \tag{A.17}$$

$$i = \tan^{-1}\left[\frac{(h_1^2 + h_2^2)^{1/2}}{h_3}\right] \tag{A.18}$$

B7. Compute argument of perigee ω

$$\bar{p} = \begin{bmatrix} p_1 \\ p_2 \\ p_3 \end{bmatrix} = R_1(i)R_3(\omega)\bar{r} \tag{A.19}$$

$$\omega + f = \tan^{-1}\left[\frac{p_2}{p_1}\right] \tag{A.20}$$

$$\omega = (\omega + f) - f \tag{A.21}$$

C. Conversion from elliptic to spherical coordinates.

C1. Compute the eccentric anomaly E and true anomaly f according to (A.1) and (A.15)

C2. Compute radial distance r

$$r = a(1-e\cos E) \tag{A.22}$$

C3. Compute geocentric latitude ϕ

$$\phi = \sin^{-1}[\sin i \sin(\omega+f)] \tag{A.23}$$

ϕ is in the same quadrant as $\omega+f$ if $-\pi/2 \leq \omega+f \leq \pi/2$, otherwise in the same quadrant as $\pi - (\omega+f)$.

C.4 Compute longitude λ

$$\lambda = \sin^{-1}\left[\frac{\cos i \sin(\omega+f)}{\cos\phi}\right] + \Omega - \theta \tag{A.24}$$

where $\lambda - \Omega + \theta$ is in the same quadrant as $\mathrm{sgn}(\pi/2 - i)(\omega+f)$ for $\lambda \neq \pi/2$. When $i = \pi/2$ then $\lambda - \Omega + \theta = 0$ for $\omega+f < \pi$ and $\lambda - \Omega + \theta = \pi$ for $\omega+f \geq \pi$. (A.23) and (A.24) are the equations of the groundtrack.

APPENDIX B

PERTURBATIONS DUE TO J_2

In this Appendix perturbations in the elements a, e, M and their time derivatives due to J_2 are going to be computed. From equations (4.5) we have

$$\dot{a} = \frac{da}{dt} = \frac{2}{na}\frac{\partial F}{\partial M} \tag{B.1}$$

$$\dot{e} = \frac{de}{dt} = \frac{1-e^2}{na^2e}\frac{\partial F}{\partial M} - \frac{(1-e^2)^{1/2}}{na^2e}\frac{\partial F}{\partial \omega} \tag{B.2}$$

$$\dot{M} = \frac{dM}{dt} = -\frac{1-e^2}{na^2e}\frac{\partial F}{\partial e} - \frac{2}{na}\frac{\partial F}{\partial a} \tag{B.3}$$

The forcing function F is replaced by V_{20}

$$V_{20} = -\frac{\mu}{a} J_2 \left(\frac{a_e}{a}\right)^2 \sum_{p,q} F_{20p}(i)\, G_{2pq}(e)\, \cos[(2-2p+q)M + (2-2p)\omega] \tag{B.4}$$

Then the derivatives of V_{20} with respect to M, ω, e, a can be computed as follows

$$\frac{\partial V_{20}}{\partial M}$$

$$\frac{\partial V_{20}}{\partial M} = \frac{\mu}{a} J_2 \left(\frac{a_e}{a}\right)^2 \sum_{p,q} F_{20p}(i)\, G_{2pq}(e)\, (2-2p+q)$$

$$\cdot \sin[(2-2p+q)M + (2-2p)\omega] \tag{B.5}$$

Expanding the summation in p and q and considering that

$$F_{200}G_{20-1} = F_{202}G_{221} \tag{B.6}$$

$$F_{200}G_{200} = F_{202}G_{220} \tag{B.7}$$

$$F_{201}G_{21-1} = F_{201}G_{211} \tag{B.8}$$

$$F_{200}G_{201} = F_{202}G_{22-1} \tag{B.9}$$

we obtain

$$\frac{\partial v_{20}}{\partial M} = \frac{\mu}{a} J_2 \left(\frac{a_e}{a}\right)^2 [2F_{200}G_{20-1}\sin(M+2\omega) + 4F_{200}G_{200}\sin(2M+2\omega) + 6F_{200}G_{201}\sin(3M+2\omega) + 2F_{201}G_{21-1}\sin M] \tag{B.10}$$

Using

$$F_{200} = -\frac{3}{8}\sin^2 i \tag{B.11}$$

$$F_{201} = \frac{3}{4}\sin^2 i - \frac{1}{2} \tag{B.12}$$

$$G_{200} = 1 - \frac{5e^2}{2} \approx 1 \tag{B.13}$$

$$G_{20-1} = -\frac{e}{2} \tag{B.14}$$

$$G_{201} = \frac{7e}{2} \tag{B.15}$$

$$G_{21-1} = \frac{3e}{2} \tag{B.16}$$

the final expression for $\frac{\partial V_{20}}{\partial M}$ is

$$\frac{\partial V_{20}}{\partial M} = -\frac{\mu}{a} J_2 \left(\frac{a_e}{a}\right)^2 \left[\frac{3}{2} \sin^2 i \sin(2M+2\omega)\right.$$

$$-\frac{3}{8} e\sin^2 i \sin(M+2\omega) + \frac{63}{8} e\sin^2 i \sin(3M+2\omega)$$

$$\left. -\left(\frac{9}{4}\sin^2 i - \frac{3}{2}\right) e\sin M\right] \tag{B.17}$$

$\frac{\partial V_{20}}{\partial \omega}$

$$\frac{\partial V_{20}}{\partial \omega} = \frac{\mu}{a} J_2 \left(\frac{a_e}{a}\right)^2 \sum_{p,q} F_{20p}(i)\, G_{2pq}(e)\, (2-2p)$$

$$\sin[(2-2p+q)M + (2-2p)\omega] \tag{B.18}$$

Expanding the summation in p, q we obtain

$$\frac{\partial V_{20}}{\partial \omega} = \frac{\mu}{a} J_2 \left(\frac{a_e}{a}\right)^2 [4F_{200}G_{200} \sin(2M+2\omega)$$

$$+ 4F_{200}G_{20-1} \sin(M+2\omega) + 4F_{200}G_{201} \sin(3M+2\omega)] \tag{B.19}$$

Then

$$\frac{\partial V_{20}}{\partial \omega} = -\frac{3}{2}\frac{\mu}{a} J_2 \left(\frac{a_e}{a}\right)^2 \sin^2 i \left[\sin(2M+2\omega) - \frac{1}{2} e\sin(M+2\omega)\right.$$

$$\left. + \frac{7}{2} e\sin(3M+2\omega)\right] \tag{B.20}$$

$\frac{\partial V_{20}}{\partial e}$

$$\frac{\partial V_{20}}{\partial e} = -\frac{\mu}{a} J_2 \left(\frac{a_e}{a}\right)^2 \sum_{p,q} F_{20p}(i)\, G'_{2pq}(e)\, \cos[(2-2p+q)M + (2-2p)\omega] \tag{B.21}$$

Then

$$\frac{\partial V_{20}}{\partial e} = -\frac{\mu}{a} J_2 \left(\frac{a_e}{a}\right)^2 [2F_{200}G'_{200}\cos(2M+2\omega)$$

$$+ 2F_{200}G'_{20-1}\cos(M+2\omega) + 2F_{200}G'_{201}\cos(3M-2\omega)$$

$$+ 2F_{201}G'_{21-1}\cos M + F_{201}G'_{210}] \tag{B.22}$$

with $G_{210} = (1-e^2)^{-3/2}$ and $G'_{210} = 3e(1-e^2)^{-5/2}$ (B.23)

$$\frac{\partial V_{20}}{\partial e} = -\frac{\mu}{a} J_2 \left(\frac{a_e}{a}\right)^2 \left[\left(\frac{9}{4}\sin^2 i - \frac{3}{2}\right)e(1-e^2)^{-5/2}\right.$$

$$+ \frac{15}{4} e\sin^2 i \cos(2M+2\omega) + \frac{3}{8}\sin^2 i \cos(M+2\omega)$$

$$\left. - \frac{21}{8}\sin^2 i \cos(3M+2\omega) + \left(\frac{9}{4}\sin^2 i - \frac{3}{2}\right)\cos M\right] \tag{B.24}$$

$\frac{\partial V_{20}}{\partial a}$

$$\frac{\partial V_{20}}{\partial a} = \frac{3\mu}{a^2} J_2 \left(\frac{a_e}{a}\right)^2 \sum_{p,q} F_{20p}\, G_{2pq}\, \cos[(2-2p+q)M + (2-2p)\omega] \tag{B.25}$$

Then

$$\frac{\partial V_{20}}{\partial a} = \frac{3\mu}{a^2} J_2 \left(\frac{a_e}{a}\right)^2 \left[\left(\frac{3}{4}\sin^2 i - \frac{1}{2}\right)(1-e^2)^{-3/2}\right.$$

$$- \frac{3}{4}\sin^2 i\cos(2M+2\omega) + \frac{3}{8}e\sin^2 i\cos(M+2\omega)$$

$$\left. - \frac{21}{8}e\sin^2 i\cos(3M+2\omega) + \left(\frac{9}{4}\sin^2 i - \frac{3}{2}\right)e\cos M\right] \qquad (B.26)$$

Using (B.17), (B.20), (B.24) and (B.26) in (B.1), (B.2), (B.3) and setting $1-e^2 \approx 1$ for small eccentricities, we obtain

$$\dot{a}_{20} = -2na J_2 \left(\frac{a_e}{a}\right)^2 \left[\frac{3}{2}\sin^2 i\sin(2M+2\omega) - \frac{3}{8}e\sin^2 i\sin(M+2\omega)\right.$$

$$\left. + \frac{63}{8}e\sin^2 i\sin(3M+2\omega) - \left(\frac{9}{4}\sin^2 i - \frac{3}{2}\right)e\sin M\right] \qquad (B.27)$$

$$\dot{e}_{20} = -nJ_2 \left(\frac{a_e}{a}\right)^2 \left[\frac{3}{8}\sin^2 i\sin(M+2\omega) + \frac{21}{8}\sin^2 i\sin(3M+2\omega)\right.$$

$$\left. - \left(\frac{9}{4}\sin^2 i - \frac{3}{2}\right)\sin M\right] \qquad (B.28)$$

$$\dot{M}_{20} = nJ_2 \left(\frac{a_e}{a}\right)^2 \left[-\left(\frac{9}{4}\sin^2 i - \frac{3}{2}\right) + \frac{33}{4}\sin^2 i\cos(2M+2\omega)\right.$$

$$+ \frac{3}{8e}\sin^2 i\cos(M+2\omega) - \frac{21}{8e}\sin^2 i\cos(3M+2\omega)$$

$$\left. + \frac{1}{e}\left(\frac{9}{4}\sin^2 i - \frac{3}{2}\right)\cos M\right] \qquad (B.29)$$

where $\frac{\mu}{na^3} = n$ has been used in all three equations. In (B.29) all the terms that were multiplied by the eccentricity have been neglected.

Integration of (B.27), (B.28) and (B.29) for the periodic part of $\dot{M}_{20}$, on the reference orbit gives

$$a_{20} = 2aJ_2 \left(\frac{a_e}{a}\right)^2 \left[\frac{3}{4} \sin^2 i \cos(2M+2\omega) - \frac{3}{8} e \sin^2 i \cos(M+2\omega)\right.$$

$$\left. + \frac{63}{24} e \sin^2 i \cos(3M+2\omega) - \left(\frac{9}{4} \sin^2 i - \frac{3}{2}\right) \cos M\right] \qquad \text{(B.30)}$$

$$e_{20} = J_2 \left(\frac{a_e}{a}\right)^2 \left[\frac{3}{8} \sin^2 i \cos(M+2\omega) + \frac{7}{8} \sin^2 i \cos(3M+2\omega)\right.$$

$$\left. - \left(\frac{9}{4} \sin^2 i - \frac{3}{2}\right) \cos M\right] \qquad \text{(B.31)}$$

$$M_{20} = J_2 \left(\frac{a_e}{a}\right)^2 \left[\frac{33}{8} \sin^2 i \sin(2M+2\omega)\right.$$

$$+ \frac{3}{8e} \sin^2 i \sin(M+2\omega) - \frac{7}{8e} \sin^2 i \sin(3M+2\omega)$$

$$\left. + \frac{1}{e} \left(\frac{9}{4} \sin^2 i - \frac{3}{2}\right) \sin M\right] \qquad \text{(B.32)}$$

For the integrations the approximation $\dot{M}+\dot{\omega} = n$ has been used.

APPENDIX C

COMPUTATION OF SECOND ORDER RADIAL ORBIT ERROR

From equation (4.82) the second order radial orbit error is

$$\Delta r_{G2} = -(1-u)\int \frac{\partial \dot{a}}{\partial a}\Delta a_o dt + a\int \frac{\partial \dot{u}}{\partial a}\Delta a_o dt$$

$$+ (1-u)\int \frac{\partial \dot{a}}{\partial e}\tilde{e}^r \Delta t dt - a\int \frac{\partial \dot{u}}{\partial e}\tilde{e}^r \Delta t dt$$

$$+ (1-u)\int \frac{\partial \dot{a}}{\partial M}\tilde{M}^r \Delta t dt - a\int \frac{\partial \dot{u}}{\partial M} M^r \Delta t dt$$

$$+ (1-u)\int \frac{\partial \dot{a}}{\partial \omega}\tilde{\omega}^r \Delta t dt - a\int \frac{\partial \dot{u}}{\partial \omega}\tilde{\omega}^r \Delta t dt \qquad (C.1)$$

which can be written as

$$\Delta r_{G2} = (1-u)\Delta a_{G2} - a\Delta u_{G2} \qquad (C.2)$$

with

$$\Delta a_{G2} = I_a^a + I_e^a + I_M^a + I_\omega^a \qquad (C.3)$$

$$a\Delta u_{G2} = aI_a^u + aI_e^u + aI_M^u + aI_\omega^u \qquad (C.4)$$

First, the second order effects Δa_{G2} are going to be computed. Since the main effects in $\dot{a}$ are the ones due to J_2, $\dot{a}$ can be approximated by $\dot{a}_{2o}$ which is given by (B.27). Then the partials contained in the integrals of (C.3) are computed to be

$$\frac{\partial \dot{a}_{2o}}{\partial a} = \left(\frac{\partial \dot{a}_{2o}}{\partial a}\right)_{explicit} + \frac{\partial \dot{a}_{2o}}{\partial M}\frac{\partial M}{\partial a} = A_1 + A_2 \qquad (C.5)$$

with

$$A_1 = \frac{15}{2} nJ_2 \left(\frac{a_e}{a}\right)^2 \sin^2 i \sin(2M+2\omega) + o(e) \qquad (C.6)$$

$$A_2 = -6na\left(-\frac{3}{2}\frac{n}{a}\Delta t\right)J_2\left(\frac{a_e}{a}\right)^2 \sin^2 i \cos(2M+2\omega) + o(e) \qquad (C.7)$$

where

$$\frac{\partial M}{\partial a} \approx \frac{\partial(n\Delta t)}{\partial a} = -\frac{3}{2}\frac{n}{a}\Delta t \qquad (C.8)$$

has been used.

$$\frac{\partial \dot{a}_{2o}}{\partial e} = 2naJ_2\left(\frac{a_e}{a}\right)^2\left[\frac{3}{8}\sin^2 i \sin(M+2\omega) + \left(\frac{9}{4}\sin^2 i - \frac{3}{2}\right)\sin M - \frac{63}{8}\sin^2 i \sin(2M+2\omega)\right] \qquad (C.9)$$

$$\frac{\partial \dot{a}_{2o}}{\partial M} = \frac{\partial \dot{a}_{2o}}{\partial \omega} = -6naJ_2\left(\frac{a_e}{a}\right)^2 \sin^2 i \cos(2M+2\omega) + o(e) \qquad (C.10)$$

Having computed the partials, the integrals of equation (C.3) can be easily computed. I_a^a becomes

$$I_a^a = -\int (A_1 + A_2)\Delta a_o dt \qquad (C.11)$$

$$-\int A_1 \Delta a_o dt = \frac{15}{4} J_2 \left(\frac{a_e}{a}\right)^2 \Delta a_o \sin^2 i \cos(2M_o(t)+2\omega_o(t)) \qquad (C.12)$$

which can have an amplitude of about $3\Delta a_o$ mm for altimeter satellites and can be neglected.

$$-\int A_2 \Delta a_0 dt = 3a\left(-\frac{3}{2}\frac{n}{a}\Delta a_0 \Delta t\right) J_2 \left(\frac{a_e}{a}\right)^2 \sin^2 i \sin(2M_0(t)+2\omega_0(t)) \tag{C.13}$$

The integrals I_e^a I_M^a I_ω^a are straightforward to compute. They are equal to

$$I_e^a = 2aJ_2\left(\frac{a_e}{a}\right)^2 \tilde{e}^r \Delta t \left[\frac{3}{8}\sin^2 i \cos(M_0(t)+2\omega_0(t)) + \left(\frac{9}{4}\sin^2 i - \frac{3}{2}\right)\cos M_0(t) - \frac{63}{24}\sin^2 i \cos(3M_0(t)+2\omega_0(t))\right] \tag{C.14}$$

$$I_M^a = -3aJ_2\left(\frac{a_e}{a}\right)^2 \tilde{M}^r \Delta t \sin^2 i \sin(2M_0(t)+2\omega_0(t)) \tag{C.15}$$

$$I_\omega^a = -3aJ_2\left(\frac{a_e}{a}\right)^2 \tilde{\omega}^r \Delta t \sin^2 i \sin(2M_0(t)+2\omega_0(t)) \tag{C.16}$$

Then (C.3) becomes

$$\Delta a_{G2} = -3aJ_2\left(\frac{a_e}{a}\right)^2 \left(\frac{3}{2}\frac{n}{a}\Delta a_0 + \tilde{M}^r + \tilde{\omega}^r\right)\Delta t \sin^2 i \sin(2M_0(t)+2\omega_0(t)) + I_e^a \tag{C.17}$$

During the integrations (C.12) - (C.16) the following approximations have been used

$$\omega+M = \omega_0(t) + M_0(t) \tag{C.18}$$

and

$$\dot{\omega}+\dot{M} = n \tag{C.19}$$

The computation of Δu_{G2} requires an expression for $\dot{u}$. From (4.47) we have

$$\dot{u} = \frac{du}{dt} = \dot{e}\cos M - e\dot{M}\sin M \tag{C.20}$$

A very good approximation to $\dot{u}$ can be obtained if we approximate $\dot{e}$, e, $\dot{M}$ and M of (C.18) by the corresponding effects due to J_2. Then

$$\dot{e} \cong \dot{e}_{2o}$$

$$e = e_o + e_{2o}$$

$$\dot{M} \cong \dot{M}_o + \dot{M}_{2o} \cong n + \dot{M}_{2o} \qquad (C.20)$$

$$\cos M \cong \cos M_o(t) - M_{2o}\sin M_o(t)$$

$$\sin M \cong \sin M_o(t) + M_{2o}\cos M_o(t)$$

where M_{2o} represents only the periodic perturbations due to J_2 such that $M_o(t) = M - M_{2o}$. Similarly $\dot{M}_{2o}$ contains only the periodic rates due to J_2. Retaining the osculating value of e whenever it multiplies M_{2o} we obtain

$$\dot{u} \cong - e_o n \sin M_o(t) + \dot{e}_{2o}\cos M_o(t) - e_{2o} n \sin M_o(t)$$

$$- e\dot{M}_{2o}\sin M_o(t) - enM_{2o}\cos M_o(t) \qquad (C.21)$$

In (C.21) all the terms containing products of J_2 perturbations and/or their rates have been neglected. The values of e_{2o}, $\dot{e}_{2o}$, M_{2o} and $\dot{M}_{2o}$ can be found in Appendix B. Using these values and carrying out all the necessary operations we obtain the following form

$$\dot{u} \cong - e_o n \sin M_o(t) - \frac{5}{2} n J_2 \left(\frac{a_e}{a}\right)^2 \sin^2 i \sin(M + M_o(t) + 2\omega) \qquad (C.22)$$

Then, consistent with the approximation (C.18) we have

$$\dot{u} \cong - e_o n \sin M_o(t) - \frac{5}{2} n J_2 \left(\frac{a_e}{a}\right)^2 \sin^2 i \sin(2M_o(t) + 2\omega_o(t)) \qquad (C.23)$$

We can see that (C.23) does not contain any singular elements. As a matter of fact it is independent of the osculating eccentricity

which was cancelled out in the product eM_{2o}. Using (C.23) the partials contained in the integrals of (C.4) become

$$\frac{\partial \dot{u}}{\partial a} = U_1 + U_2 + U_3 \tag{C.24}$$

where

$$U_1 = \frac{3}{2}\frac{n}{a}e_o \sin M_o(t) \tag{C.25}$$

$$U_2 = \frac{3}{2}\frac{n^2}{a}e_o \Delta t \cos M_o(t) \tag{C.26}$$

$$U_3 \cong -5\, nJ_2 \left(\frac{a_e}{a}\right)^2 \left(\frac{3}{2}\frac{n}{a}\Delta t\right) \sin^2 i \cos(2M_o(t)+2\omega_o(t)) \tag{C.27}$$

$$\frac{\partial \dot{u}}{\partial e} = 0 \tag{C.28}$$

$$\frac{\partial \dot{u}}{\partial M} = -5\, nJ_2 \left(\frac{a_e}{a}\right)^2 \sin^2 i \cos(2M_o(t)+2\omega_o(t)) \tag{C.29}$$

$$\frac{\partial \dot{u}}{\partial \omega} = -5\, nJ_2 \left(\frac{a_e}{a}\right)^2 \sin^2 i \cos(2M_o(t)+2\omega_o(t)) \tag{C.30}$$

Having computed the partials, the computation of the integrals in (C.4) becomes straightforward. I_a^u is equal to

$$I_a^u = -a \int (U_1 + U_2 + U_3)\Delta a_o dt \tag{C.31}$$

where

$$-a \int U_1 \Delta a_o dt = 0 + O(e) \tag{C.32}$$

$$-a \int U_2 \Delta a_o dt = a e_o \left[\frac{3}{2}\frac{n}{a}\Delta a_o \Delta t\right] \sin M_o(t) \tag{C.33}$$

$$-a \int U_3 \Delta a_0 dt = \frac{5}{2} aJ_2 \left(\frac{a_e}{a}\right)^2 \left(-\frac{3}{2} \frac{n}{a} \Delta a_0 \Delta t\right) \sin^2 i \sin(2M_0(t)+2\omega_0(t)) \tag{C.34}$$

The integrals aI_M^u and aI_ω^u are

$$aI_M^u = -\frac{5}{2} aJ_2 \left(\frac{a_e}{a}\right)^2 \tilde{M}^r \Delta t \sin^2 i \sin(2M_0(t)+2\omega_0(t)) \tag{C.35}$$

$$aI_\omega^u = -\frac{5}{2} aJ_2 \left(\frac{a_e}{a}\right)^2 \tilde{\omega}^r \Delta t \sin^2 i \sin(2M_0(t)+2\omega_0(t)) \tag{C.36}$$

Then $a\Delta u_{G2}$ becomes

$$a\Delta u_{G2} = -\frac{3}{2} e_0 n \Delta a_0 \Delta t \sin M_0(t)$$

$$-\frac{5}{2} aJ_2 \left(\frac{a_e}{a}\right)^2 \left(\frac{3}{2} \frac{n}{a} \Delta a_0 + \tilde{M}^r + \tilde{\omega}^r\right) \Delta t \sin^2 i \sin(2M_0(t)+2\omega_0(t)) \tag{C.37}$$

The final expression for the second order radial orbit error given by (C.2), with the term $1-u \approx 1$, is

$$\Delta r_{G2} = \frac{3}{2} e_0 n \Delta a_0 \Delta t \sin M_0(t)$$

$$-\frac{1}{2} aJ_2 \left(\frac{a_e}{a}\right)^2 \left(\frac{3}{2} \frac{n}{a} \Delta a_0 + \tilde{M}^r + \tilde{\omega}^r\right) \Delta t \sin^2 i \sin(2M_0(t)+2\omega_0(t))$$

$$+ 2aJ_2 \left(\frac{a_e}{a}\right)^2 \tilde{e}^r \Delta t \left[\frac{3}{8} \sin^2 i \cos(M_0(t)+2\omega_0(t))\right.$$

$$\left. + \left(\frac{9}{4} \sin^2 i - \frac{3}{2}\right) \cos M_0(t) - \frac{63}{24} \sin^2 i \cos(3M_0(t)+2\omega_0(t))\right]$$

$$+ \frac{15}{4} J_2 \left(\frac{a_e}{a}\right)^2 \Delta a_0 \sin^2 i \cos(2M_0(t)+2\omega_0(t)) \tag{C.38}$$

All the above expressions are computed on the reference orbit.

APPENDIX D

MULTIPLE ANGLE TO SINGLE ANGLE TRIGONOMETRIC TRANSFORMATION

The cosine and sine of an angle kv-mu can be transformed to functions of cosines and sines of single angles v and u as follows

$$\cos(kv-mu) = \cos kv\cos mu + \sin kv\sin mu \tag{D.1}$$

$$\sin(kv-mu) = \sin kv\cos mu - \cos kv\sin mu \tag{D.2}$$

From trigonometry we generally have

$$\cos nx = \mathrm{Re}\sum_{s=0}^{n}\binom{n}{s} j^s \cos^{n-s}x \sin^s x$$

$$= \sum_{s=0}^{n'}\binom{n}{s}(-1)^{s/2}\cos^{n-s}x \sin^s x \tag{D.3}$$

where s is even and

$$n' = \begin{cases} n & \text{if } n \text{ even} \\ n-1 & \text{if } n \text{ odd} \end{cases}$$

Similarly

$$\sin nx = \mathrm{Re}\sum_{s=0}^{n}\binom{n}{s} j^{s-1}\cos^{n-s}x\sin^s x$$

$$= \sum_{s=1}^{n'}\binom{n}{s}(-1)^{\frac{s-1}{2}}\cos^{n-s}x \sin^s x \tag{D.4}$$

where s is odd and

$$n' = \begin{cases} n & \text{if } n \text{ odd} \\ n-1 & \text{if } n \text{ even} \end{cases}$$

Then the four trigonometric products of (D.1) and (D.2) are

$$\text{coskvcosmu} = \sum_{s=0}^{k'} \sum_{t=0}^{m'} \binom{k}{s} \binom{m}{t} (-1)^{\frac{s+t}{2}} F_{uv} \tag{D.5}$$

where s, t, k′, m′ are even

$$\text{sinkvsinmu} = -\sum_{s=1}^{k'} \sum_{t=1}^{m'} \binom{k}{s} \binom{m}{t} (-1)^{\frac{s+t}{2}} F_{uv} \tag{D.6}$$

where s, t, k′, m′, are odd

$$\text{sinkvsinmu} = -\sum_{s=1}^{k'} \sum_{t=0}^{m'} \binom{k}{s} \binom{m}{t} (-1)^{\frac{s+t-1}{2}} F_{uv} \tag{D.7}$$

where s, k′ are odd and t, m′ are even.

$$\text{coskvsinmu} = \sum_{s=0}^{k'} \sum_{t=1}^{m'} \binom{k}{s} \binom{m}{t} (-1)^{\frac{s+t-1}{2}} F_{uv} \tag{D.8}$$

where s, k′ are even and t, m′ are odd. In all the equations (D.5)-(D.8) F_{uv} is

$$F_{uv} = \cos^{k-s}v \sin^{s}v \cos^{m-t}u \sin^{t}u \tag{D.9}$$

Equation (D.5)-(D.8) are valid when both k and m are positive integers. When both are negative (D.5) and (D.6) remain the same while (D.7) and (D.8) change. When one integer is negative then (D.6) and (D.7) or (D.8) change. For k negative (D.6) and (D.7) become

$$\text{sinkvsinmu} = -\sum_{s=1}^{|k'|} \sum_{t=1}^{m'} \binom{|k|}{s} \binom{m}{t} (-1)^{\frac{3s+t}{2}} F_{uv} \tag{D.10}$$

$$\text{sinkvcosmu} = \sum_{s=1}^{|k'|} \sum_{t=0}^{m'} \binom{|k|}{s} \binom{m}{t} (-1)^{\frac{s+t+1}{2}} F_{uv} \tag{D.11}$$

where now F_{uv} contains the absolute value of k. Then combining (D.6), (D.10) and (D.7), (D.11) we can write for any k

$$\text{sinkvsinmu} = \sum_{s=1}^{|k|}{}' \sum_{t=0}^{m}{}' \binom{|k|}{s} \binom{m}{t} (-1)^{\beta} F_{uv} \tag{D.12}$$

$$\text{with } \beta = \begin{cases} \dfrac{3s+t}{2} & k>0 \\ \dfrac{s+2}{2} & k<0 \end{cases} \tag{D.13}$$

$$\text{sinkvcosmu} = \sum_{s=1}^{|k|}{}' \sum_{t=0}^{m}{}' \binom{|k|}{s} \binom{m}{t} (-1)^{c} F_{uv} \tag{D.14}$$

$$\text{with } c = \begin{cases} \dfrac{3s+t+1}{2} & k>0 \\ \dfrac{s+t+1}{2} & k<0 \end{cases} \tag{D.15}$$

Then equation (D.1) is written

$$\cos(kv-mu) = \sum_{s=0}^{|k|} \sum_{t=0}^{m} \binom{|k|}{s} \binom{m}{t} (-1)^{\beta} \cos^{|k|-s}v \sin^{s}v \cos^{m-t}u \sin^{t}u \tag{D.16}$$

where s, t have the same parity.

Similarly (D.2) is written

$$\sin(kv-mu) = \sum_{s=0}^{|k|} \sum_{t=0}^{m} \binom{|k|}{s} \binom{m}{t} (-1)^{c} \cos^{|k|-s}v \sin^{s}v \cos^{m-t}u \sin^{t}u \tag{D.17}$$

where s, t have different parities. Equations (D.16) and (D.17) are valid for positive m and any k.

APPENDIX E

DETERMINATION OF CROSSOVER INTERSECTIONS

As described in Chapter 8 crossover intersections occur at times t_i and t_j that correspond to particular points of the ground track with geocentric latitude ϕ and longitude λ. The determination of crossover times and geocentric coordinates can in principle be made sequentially by using the satellite ephemeris. The satellite earth fixed position at each epoch has to be compared with all the positions at following epochs so that to locate the vicinity of a crossover point. This process though is extremely time consuming and requires a lot of computer memory.

A more efficient determination can be made using an analytical approach. In such a method the secular perturbations of the satellite are used to determine approximate times and the geocentric latitude and longitude for each intersection. Then, using these approximate estimates the exact intersection times and coordinates can be found by simply using the precise ephemeris and interpolating. For the analytical determination the times and longitudes of all the equator crossings for each arc have to be known. Very accurate equator crossings can be easily obtained using the precise ephemeris. An approximation to the equator crossings can be obtained by simply considering that the argument of the satellite, when it crosses the equator, takes the value

$$(\omega + f)_n^i = [2(n - 1) + i]\pi \qquad (E.1)$$

where n is the revolution number and i indicates whether the satellite crosses the equator towards the north hemisphere (i = 0) or towards the south hemisphere (i = 1). The times of equator crossings can be found from

$$(\omega + f)_n^i = \omega_0 + f_0 + (\dot{\omega} + \dot{f})t_n^i \qquad (E.2)$$

which can be combined with (E.1) to give

$$t_{n,E}^i = \frac{[2(n-1)+i]\pi}{\dot{\omega} + \dot{f}} - \frac{\omega_0 + f_0}{\dot{\omega} + \dot{f}} \qquad (E.3)$$

where $\dot{\omega}$, f are the secular rates of the corresponding elements. In order to find the longitudes of equator crossings, we consider the following

$$\lambda = (a - \Omega) + (\Omega - \theta) \tag{E.4}$$

$$\sin(a - \Omega) = \frac{\sin(\omega+f)\cos i}{\cos\phi} \tag{E.5}$$

Then at the equator $\sin(a-\Omega) = 0$ and

$$(a - \Omega)^i_n = s[2(n-1)+i]\pi \tag{E.6}$$

where s is equal to 1 for posigrade orbits and -1 for retrograde orbits. Using (E.4) and (E.6) we obtain

$$\lambda^i_n = (\Omega_o - \theta_o) + (\dot{\Omega} - \dot{\theta})t^i_{n,E} + s[2(n-1)+i]\pi \tag{E.7}$$

Or, if we substitute for the time from (E.3)

$$\lambda^i_n = (\Omega_o - \theta_o) + [2(n-1)+i]\pi\left(s + \frac{\dot{\Omega}-\dot{\theta}}{\dot{\omega}+\dot{f}}\right) - (\omega_o + f_o)\frac{\dot{\Omega}-\dot{\theta}}{\dot{\omega}+\dot{f}} \tag{E.8}$$

When the inclination is greater than 90° (retrograde orbit) the longitude separation between two successive crossings is greater than 180°. Therefore there is always one intersection between any two north and any two south half revolutions and possibly there are two. In order to have a second intersection between any two half revolutions, k and j, the following condition needs to apply. The modulus (with respect to 180°) of the longitude separation between the k and j ascending equator crossings has to be smaller than the modulus of the longitude separation between the ascending and descending equator crossings of the k revolution. Using (E.8) the first modulus is

$$\mathrm{mod}(\Delta\lambda_{jk}, \pi) = \mathrm{mod}\left(2(j-k)\pi\,\frac{\dot{\Omega}-\dot{\theta}}{\dot{\omega}+\dot{f}}, \pi\right) \tag{E.9}$$

for $j > k$. The second modulus becomes

$$\mathrm{mod}(\Delta\lambda^{o1}_k, \pi) = \mathrm{mod}\left(\pi - \frac{\dot{\Omega}-\dot{\theta}}{\dot{\omega}+\dot{f}}, \pi\right) = -\frac{\dot{\Omega}-\dot{\theta}}{\dot{\omega}+\dot{f}} \tag{E.10}$$

Then if (E.9) is smaller than (E.10) there are two intersections between the k and j half (north or south) revolutions.

To find the longitude of a crossover intersection between any k and j revolutions in the north hemisphere the following relationship is used.

$$\lambda_{jk} = (\lambda_k^0 + \lambda_j^0 + \lambda_k^1 + \lambda_j^1)/4 \qquad \text{(E.11)}$$

if

$$\left|\frac{\lambda_k^0 + \lambda_k^1}{2} - \frac{\lambda_i^0 + \lambda_j^1}{2}\right| < \pi \qquad \text{(E.12)}$$

When the expression in (E.12) is greater than π then λ_{jk} needs to be increased by π. The equator crossing longitudes in (E.11), (E.12) need to satisfy

$$s\lambda_k^0 > s\lambda_k^1$$

$$s\lambda_j^0 > s\lambda_j^1 \qquad \text{(E.13)}$$

If this is not the case, 2π has to be added to the appropriate longitudes to satisfy (E.13). In the southern hemisphere the longitude of a crossover intersection between any k and j revolutions can be obtained by

$$\lambda_{jk} = (\lambda_k^1 + \lambda_j^1 + \lambda_{k+1}^0 + \lambda_{j+1}^0)/4 \qquad \text{(E.14)}$$

with conditions similar to the ones for (E.11) being valid. When more than one intersection (north or south) is formed between two revolutions, the longitude of the second intersection is simply offset by π from the longitude of the first one.

In order to find the time of the intersection we use

$$\tan(\omega + f) = \frac{\tan\Lambda}{\cos i} \qquad \text{(E.15)}$$

where Λ is the longitude separation between the intersection and the equator crossing immediately preceding the intersection. This longitude separation for the k revolution is

$$\Lambda_k^i = \Delta - s(\dot{\Omega} - \dot{\theta})\tau_k^i \tag{E.16}$$

where

$$\Delta = |\lambda_{jk} - \lambda_k^i| \tag{E.17}$$

is the corresponding longitude separation at time $t_{k,E}^i$. The second term of (E.16) is the additional longitude increment corresponding to the time τ_k^i that is required for the satellite to move from the equator to the intersection point. Considering the above, (E.15) becomes

$$\tan[(\dot{\omega} + \dot{f})\tau_k^i] = \frac{\tan[\Delta - s(\dot{\Omega}-\dot{\theta})\tau_k^i]}{\cos i} \tag{E.18}$$

Equation (E.18) can be solved iteratively for τ_k^i until convergence. The same determination can be made for τ_j^i. Then the crossing times t_k^i and t_j^i are

$$t_k^i = t_{k,E}^i + \tau_k^i \tag{E.19}$$

$$t_i^i = t_{i,E}^i + \tau_j^i \tag{E.20}$$

When a second crossing between two half revolutions is formed the corresponding times are

$$t_k^i = t_{k,E}^i + \tau_j^i \tag{E.21}$$

$$t_j^i = t_{j,E}^i + \tau_k^i \tag{E.22}$$

The latitude of the crossing is simply found by

$$\phi_{jk}^i = \sin^{-1}[\sin(\omega_o+f_o+(\dot{\omega}+\dot{f})t_k^i)] \tag{E.23}$$

The same value is obtained by using t_j^i instead of t_k^i. The total number of crossings that are formed from N complete revolutions is

$$M = N(N-1) + (1-s) \sum_{j=1}^{N} \sum_{k=1}^{N} \delta_{jk} \tag{E.24}$$

where

$$\delta_{jk} = \begin{cases} 1 & \text{if (E.9)} < \text{(E.10)} \\ 0 & \text{otherwise} \end{cases} \tag{E.25}$$

The analytic approach for determining the crossing locations is not very accurate for two reasons. First, the full perturbations of ω, f, Ω have to be used and not only their secular counterparts. Second, the assumption of a circular orbit, which is not valid, has been used. So the crossover solutions need to be improved by computing corrections to the analytic solutions. These corrections can be obtained by a nonlinear interpolation scheme of the precise times and coordinates taken from the precise ephemeris before and after the crossing.